STRUCTURAL AND DYNAMIC PROPERTIES OF ALPHA, OMEGA-DIBROMOALKANES AND OTHER GUEST MOLECULES IN THEIR UREA INCLUSION COMPOUNDS

Sharon Patricia Smart

A Thesis Submitted for the Degree of PhD
at the
University of St Andrews

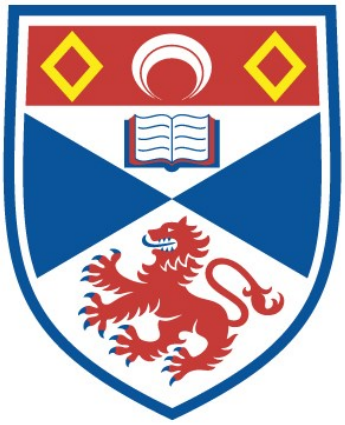

1993

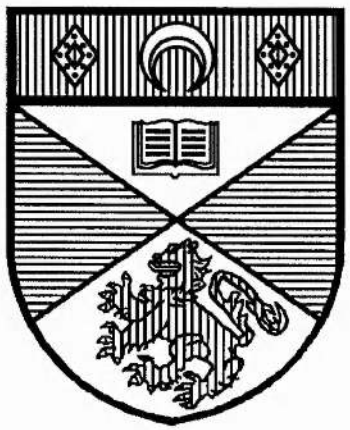

Structural and Dynamic Properties of α,ω-Dibromoalkanes and other Guest Molecules in their Urea Inclusion Compounds

A thesis presented by

SHARON PATRICIA SMART

to the

UNIVERSITY OF ST ANDREWS

in application for the degree of

DOCTOR OF PHILOSOPHY

DEPARTMENT OF CHEMISTRY

ST ANDREWS

MARCH 1993

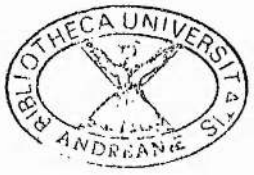

ProQuest LLC.
789 East Eisenhower Parkway
P.O. Box 1346
Ann Arbor, MI 48106 – 1346

Th B340

What we call the beginning is often the end
And to make an end is to make a beginning.

T.S. ELIOT,
Little Gidding

DECLARATIONS

(a) I, Sharon Patricia Smart, hereby certify that this thesis has been composed by myself, that it is a record of my own work, and that it has not been accepted in partial or complete fulfilment of any other degree or professional qualification.

Signed ..... Date 19/3/93

(b) I was admitted to the Faculty of Science of the University of St Andrews under Ordinance General No 12 on 2nd October 1989 and as a candidate for the degree of PhD on 1st October 1990.

Signed ... Date 19/3/93

(c) I hereby certify that the candidate has fulfilled the conditions of the Resolution and Regulations appropriate to the degree of PhD.

Signature of supervisor .....

Date 19th March 1993

COPYRIGHT

ACKNOWLEDGEMENTS

I should like to thank my supervisor, Dr Kenneth Harris, for his guidance and encouragement during my PhD - and for giving me the opportunity to spend some time in South-West France! Thanks also to the research group: Dr Abil Aliev for assistance with ^{2}H NMR, and Ali Mahdyarfar and Ian Shannon for preparing the samples of 1,8-dibromooctane/urea-d_4 and *n*-hexadecane-d_{34}/urea used for neutron scattering. For getting me started on the solid-state NMR spectrometer, I thank Dr S. Arumugam. I am grateful to the technical staff of the Chemistry Department, in particular to Jim Bews (for his ever-willing help with the Macs), Melanja Smith (for running the ^{1}H NMR spectra) and Colin Smith (glass-blowing). Thanks also to Jim Allan and his team in the Photographic Department for making up contact prints of the x-ray photos.

During my PhD, I spent five months in total at the Université de Bordeaux: I should like to thank the members of the Laboratoire de Spectroscopie Moléculaire et Cristalline for the *accueil chaleureux* they gave me - in particular, I am very grateful to Dr François Guillaume for his encouragement and interest in my work (and his patience at the beginning when I understood neither the Raman spectroscopy nor the French language! *Mais c'est en forgeant qu'on devient forgeron...*) Dr Raymond Cavagnat is also thanked for technical assistance with the Raman spectrometer.

For assistance with the neutron scattering experiments at the Institut Laue-Langevin in Grenoble, I thank Dr José Dianoux and the *responsables*. Professor Mark Hollingsworth and Dr Bernie Santasiero are thanked for collecting the diffractometric data discussed in Chapter 2. For funding, I am indebted to the SERC for a student-ship, and to the Ettie Steele Travel Fund and St Leonard's College Russell Trust for financing my visits to Bordeaux.

Finally, I should like to thank all my friends in St Andrews over the past $7\frac{1}{2}$ years for helping make my time here so enjoyable. And special thanks to my parents for their constant encouragement throughout my education.

ABSTRACT

The work described in this thesis focuses on the urea inclusion compounds of α,ω-dibromo-*n*-alkanes: $Br(CH_2)_nBr$/urea, where n=7-10. The structural and dynamic properties of the host and guest have been studied using complementary techniques.

Photographic single crystal x-ray diffraction shows that, in the regions of three-dimensional guest molecular ordering, there is a well-defined offset, Δ_g, along the channel axis, **c**, between guest molecules in adjacent channels. Δ_g is exactly one-third of the periodic repeat distance along **c** of the basic guest structure: this represents a new mode of interchannel guest ordering in urea inclusion compounds. Raman spectroscopy shows that the 'bulk' conformation of the guest molecules is the linear, *trans*, extended form, but that there is a small, but measurable, proportion of Br end-groups in the *gauche* conformation. Incoherent quasielastic neutron scattering indicates that the guest molecules undergo two motions on the picosecond time-scale, at sufficiently high temperature: translations *along* the channel axis and reorientations *about* the channel axis. These motions are successfully modelled as, respectively, continuous linear diffusion between two impermeable boundaries and uniaxial rotational diffusion in a one-fold cosine potential. Deuterium nuclear magnetic resonance spectra are shown, via simulations, to be consistent with a 180° flipping motion of the urea molecules about their C=O axes, occurring on the microsecond time-scale at room temperature. This technique also provides confirmation of guest molecular motion.

The structure of 1,6-dibromohexane/urea is found to differ from that of the other α,ω-dibromoalkane/urea inclusion compounds studied: crystal structure determination shows that it is monoclinic, and that the host and guest structures are commensurate with one another. Raman spectroscopy confirms that the Br end-groups are exclusively in the *gauche* conformation.

The urea inclusion compounds of various other guest molecules have also been investigated briefly. The complementary nature of the techniques used is crucial in establishing a complete picture of the structure and dynamics of all these compounds.

PUBLICATIONS RESULTING FROM THIS WORK

1. HARRIS KDM, SMART SP & HOLLINGSWORTH MD (1991) Structural properties of α,ω-dibromoalkane/urea inclusion compounds: a new type of interchannel guest molecule ordering, *J. Chem. Soc., Faraday Trans.*, **87**, 3423-3429.

2. SMART SP, HARRIS KDM, GUILLAUME F & EL BAGHDADI A (1992) Raman spectroscopic studies of urea inclusion compounds containing α,ω-dibromoalkane guests, *Mol. Cryst. Liq. Cryst.*, **211**, 157-166.

3. SMART SP, GUILLAUME F, HARRIS KDM, SOURISSEAU C & DIANOUX AJ (1992) Dynamic properties of α,ω-dibromoalkane guest molecules constrained within urea inclusion compounds: a neutron scattering study, *Physica B*, **180/181**, 687-690.

4. HARRIS KDM, GUILLAUME F, SMART SP, SOURISSEAU C & DIANOUX AJ (1992) Neutron scattering investigation of host molecular motion in the hexadecane/urea inclusion compound, *J. Chem. Res. (S)*, 276-277.

CONTENTS

CHAPTER 2: X-RAY DIFFRACTION STUDIES

CHAPTER 3: RAMAN SPECTROSCOPIC STUDIES

CHAPTER 1
UREA INCLUSION COMPOUNDS

1.1 INCLUSION COMPOUNDS

1.1.1 HISTORICAL BACKGROUND

Although naturally-occurring zeolites have been known since the mid-eighteenth century [Cronstedt, 1756], it was in the early nineteenth century that inclusion compounds were first studied scientifically, when Davy and Faraday prepared and analysed chlorine clathrate hydrate [Davy, 1811; Faraday, 1823]. Wöhler [1849] and Clemm [1859] prepared the first quinol clathrates; it was later proposed [Mylius, 1886] that, during crystallisation, the quinol molecules were somehow able to lock the volatile material into position without chemically combining with it. This was the first suggestion of some form of molecular imprisonment. However, it was not until after the development of x-ray diffraction techniques in the early twentieth century that the concepts of inclusion and molecular imprisonment were vindicated, when Palin and Powell solved the structure of the β-quinol clathrates [Palin & Powell, 1945 & 1947]. Indeed, it was Powell [1948] who coined the term 'clathrate' (from the Greek *clathros*, meaning cage) to describe these β-quinols; such systems are now more generally called inclusion compounds or inclusion adducts. Any molecule that can imprison another (either containing unoccupied cavities or capable of adaptation around a guest) has potential for inclusion, and interest in the field of inclusion chemistry has grown rapidly since these early studies. A brief history of inclusion chemistry is given by Powell [1984].

1.1.2 DEFINITIONS AND CLASSIFICATIONS

An inclusion compound may be defined as a system in which one species (termed the guest) is spatially confined within another species (termed the host). Inclusion compounds will be formed only with those guests which have appropriate molecular shape and volume to fit closely within the cavities of the host structure. In

addition, complementary electronic structures are sometimes necessary to provide appropriate host/guest binding sites.

Inclusion compounds may be divided into two classes, which depend on the form of the host species:

Class I: the host is a single molecule which possesses a cavity that encloses the guest species. Inclusion compounds of this class can be found both in solution and in the solid state. One example is the family of crown ethers, which have cationic guests (such as the K^+ ion) and are often used to facilitate ion transport through liquid membranes. Other examples include cyclodextrins, which have potential for enzyme modelling, and cryptates, which have wide-ranging applications involving ion separation and transport.

Class II: the host is a solid crystalline structure containing inclusion cavities in which the guest is located. The guest may be atomic, ionic or molecular. There are various types of inclusion cavity, such as isolated cages, interconnecting cages, linear non-intersecting tunnels, networks of intersecting tunnels and interlayer spaces (or a combination of these topologies). This class of inclusion compounds may be further sub-divided, by virtue of the response of the host structure when the guest species is removed:

(i) the host structure remains intact, such that the guest species may be removed and replaced. Some inclusion compounds of this type have catalytic applications, for which this facile exchange of guest species is an important feature. One example is the family of zeolites: these are microporous aluminosilicates which are widely used as catalysts, e.g. in the petroleum industry, the zeolite ZSM-5 catalyses the production of ethylbenzene from benzene and ethylene [Thomas, 1988]. Further examples of this category may be found in the historically significant family of β-quinol clathrates.

(ii) the host structure collapses on removal of the guest species. The subject of this thesis, the urea inclusion compounds, fall into this category; other examples are the inclusion compounds of thiourea, selenourea, perhydrotriphenylene, tri-*ortho*-thymotide and deoxycholic acid. The molecules which form these host structures are shown in Fig. 1.1.

Comprehensive reviews of the structure, physical properties and applications of many inclusion compounds are given by Atwood *et al* [1984]; see also Thomas & Harris [1987] and Harris [1993].

Fig. 1.1: Some host molecules which form inclusion compounds of Class II, type (ii)

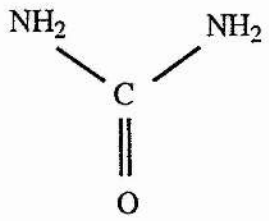

urea

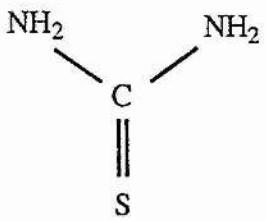

thiourea

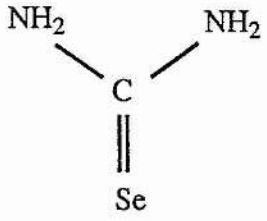

selenourea

perhydrotriphenylene

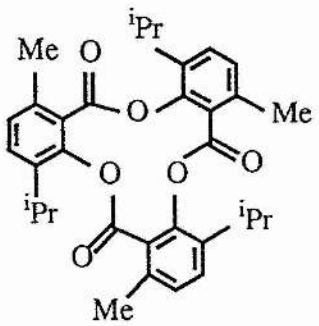

tri-*ortho*-thymotide

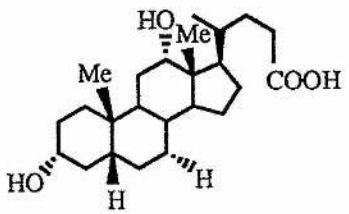

deoxycholic acid

1.2 UREA INCLUSION COMPOUNDS

1.2.1 DISCOVERY

Urea inclusion compounds (UICs) were first prepared accidentally by Bengen in 1940, when, during an analysis of milk fats using urea, he added a small quantity of *n*-octanol to prevent formation of an emulsion. He was surprised to see that crystals had formed. He repeated his experiments without the milk and later using different organic compounds (other alkanes, alcohols, carboxylic acids and esters): the resultant crystals he termed 'urea addition compounds'. He patented this discovery [Bengen, 1951 & 1953] for potential use of these compounds as a means of separating branched from straight-chain organic compounds. The first publications concerning the discovery of this new class of compounds appeared in 1949 [Bengen & Schlenk, 1949: Schlenk, 1949a; Zimmerschied *et al*, 1949]. Comprehensive studies by Schlenk [1949b] and Zimmerschied *et al* [1950] showed that these urea addition compounds belonged to the newly-discovered class of inclusion compounds. A review of the early work on UICs and other inclusion compounds is given by Montel [1955]. The discovery, formation, structure and properties of UICs are discussed more recently by Takemoto & Sonoda [1984].

1.2.2 UREA HOST STRUCTURE

The formation of urea inclusion compounds requires spatial compatibility between the space available within the urea host and the guest molecules. Therefore, before discussing the prerequisite properties for guests, we need to know the size and shape of the inclusion cavities: the urea host structure.

The urea host structure may only form in the presence of guest molecules, which act as a template for formation and serve to maintain the stability of the framework. Despite this fact, and unlike other host structures, which often depend on the identity of the guest, the urea basic host structure (as defined and discussed further in Chapter 2) is generally invariant, regardless of guest species. The urea molecules form an extended hydrogen-bonded structure containing linear, parallel channels,

within which the guest molecules are located. The effective channel diameter ranges from *ca.* 5.1 Å to *ca.* 5.9 Å [Harris, 1993]. Fig. 1.2 shows the urea basic host structure viewed along the channel axis. Because the urea molecules which make up the channel walls are arranged on a spiral around the long axis of the channel, the guest molecules are in a chiral environment: this fact suggests potential for asymmetric synthesis (see §1.2.5.2).

Single crystal x-ray diffraction studies on *n*-hexadecane/urea by Hermann & Schlenk [Schlenk, 1949b, 1950 & 1953] showed that the basic host structure is hexagonal at room temperature, with six urea molecules per unit cell, space group $P6_122$ and lattice parameters a=b=8.20 Å, c=11.1 Å. This was confirmed by Smith [1950 & 1952], who found that this structure was essentially invariant for many UICs, with lattice parameters a=b=8.24 Å, c=11.0 Å. More recently, Harris & Thomas [1990] determined diffractometrically the following lattice parameters for the basic host structure of *n*-hexadecane/urea: a=b=8.227 Å, c=11.017 Å.

The few exceptions to this urea host structure include trioxane/urea, which is similar in structure to cyclohexane/thiourea [Clément *et al*, 1974 & 1975], and UICs with very short guests, such as 1,6-dibromohexane/urea (the structure of which is discussed in Chapter 2), 1.6-diaminohexane/urea and 1,6-dicyanohexane/urea [Schlenk, 1949b; Otto, 1972] and other short-chain dinitrile/urea inclusion compounds [Hollingsworth *et al*, 1991]. Poly(ethyleneoxide)/urea also has an unusual urea host structure, which is trigonal and is thought to arise due to extensive hydrogen bonding between the host and guest species [Foxman BM & Harris KDM, unpublished work].

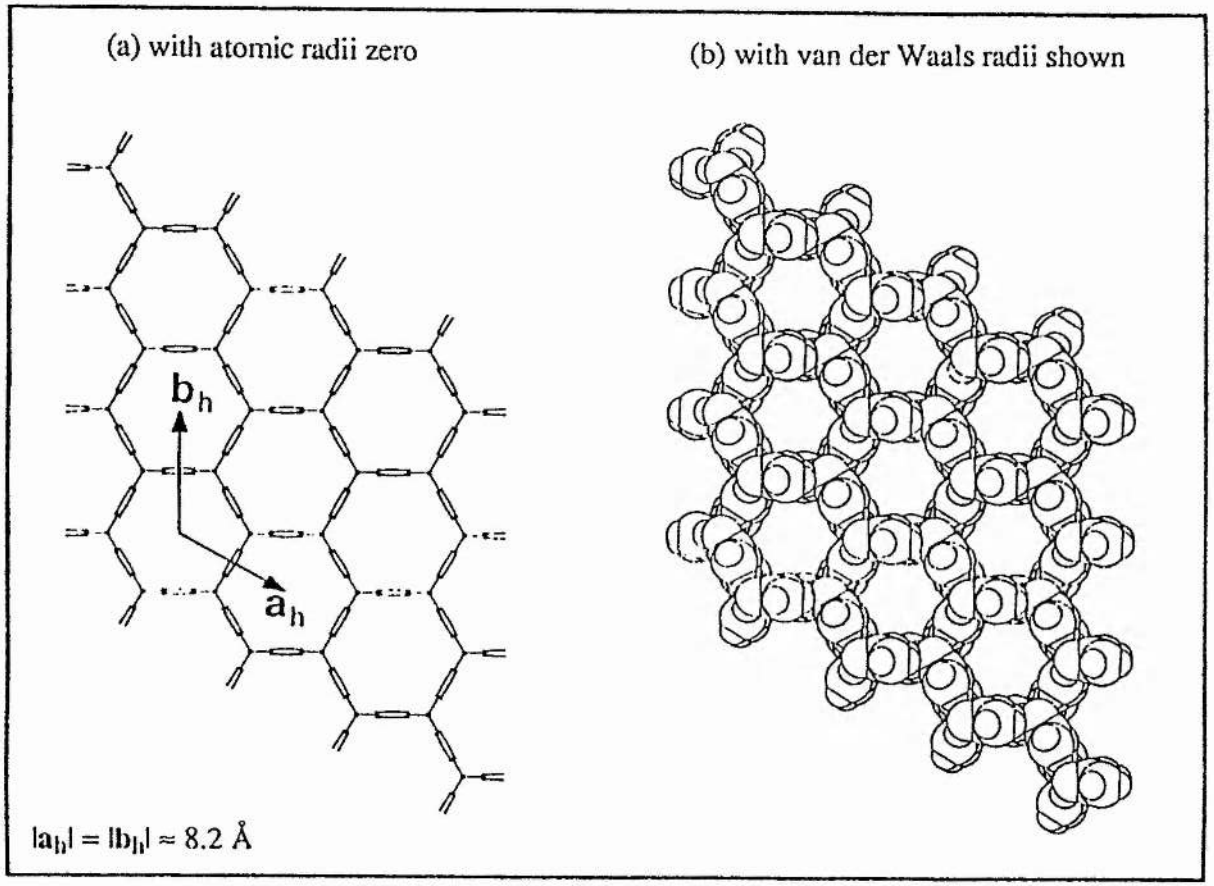

Fig. 1.2: Representation of urea basic host structure viewed along the channel axis, **c**
(For clarity, the guest molecules are not shown.) [from Harris, 1988]

1.2.3 REQUIREMENTS FOR GUESTS

Guest selectivity is governed by molecular geometry, the critical factors being (i) chain length and (ii) degree of branching.

(i) Chain length

Bengen and Schlenk found that, for *n*-alkane UICs, the main carbon chain must be a minimum of six carbon atoms long and suggested that there may also be an upper limit to chain length [Bengen & Schlenk, 1949; Schlenk, 1949b, Bengen, 1953]. This lower limit was confirmed by other workers [Fetterley, 1964], although it was generally found that *n*-hexane/urea was unstable at room temperature. Monobe and Yokoyama prepared the UIC of polyethylene of molecular weight 59 000 [Monobe & Yokoyama, 1973; Yokoyama & Monobe, 1980 & 1983], which suggests there may be no upper chain length limit for *n*-alkane guests. In practice, there is an optimal range of chain lengths. With too short a chain, the urea inclusion compound is unstable: Schlenk [1949b] suggests this is because the 'empty' van der Waals distance along the channel axis between adjacent guest molecules, which is constant for *n*-alkane guests, takes up too large a proportion of the channel for short-chain guests, and so destabilises the structure. For guest molecules of long chain length, although preparation of their UICs is possible in theory, there are problems in finding an appropriate solvent.

(ii) Degree of branching

In general, the cross-sectional diameter of the guest molecule must be less than that of the urea host channel (*ca.* 5.1-5.9 Å), so little branching is possible. Critical factors are size, number and position of substituents: very bulky or numerous substituents on a molecule will not allow it to fit into the inclusion cavities. Greater tolerance exists towards substituents at the chain ends rather than mid-chain; methyl groups at non-terminal positions are usually acceptable but not larger substituents. Carbonyl groups within the chain are acceptable. Cyclic compounds will be included only if they possess a very long aliphatic tail, which appears to confer stability

(presumably, the alkyl tail compensates the disadvantage of the bulky cyclic substituent). The destabilising influence of branching appears to be lessened for longer guest molecules.

It was found [Bengen & Schlenk, 1949; Schlenk 1949b; Bengen, 1953] that the formation of UICs with alkanes, alcohols, ethers, aldehydes, ketones, carboxylic acids and esters was possible provided the chain had at least six carbons and was unbranched or only slightly branched. Terminally halogenated compounds and carboxylic acids form UICs [Radell *et al*, 1964], as do primary thiols and terminally epoxidated chains [Radell *et al*, 1963]. The formation of UICs of aromatics and cyclic alkanes is possible provided these guest species possess long aliphatic tails, e.g. 1-phenyl-octadecane, 1-cyclohexyl-eicosane [Schiessler & Flitter, 1952]. Alkenes and alkynes of suitable length generally form UICs [Radell *et al*, 1961], although thermodynamic studies [Fetterley, 1964] show they are less stable than the corresponding *n*-alkane UICs. To summarise, Table 1.1 shows examples of guest molecules which form inclusion compounds with urea.

Co-inclusion of different types of guest is also possible. A mixture of branched and linear guests may be included more readily than the branched guest alone, or a molecule that would normally be too small for inclusion may be 'trapped' in the urea channels by the larger guest molecules. Co-inclusion of the preparation solvent is not uncommon.

Table 1.1: A selection of guest molecules which form inclusion compounds with urea

Guest Species	Examples
n-alkanes	 
terminally substituted *n*-alkanes	 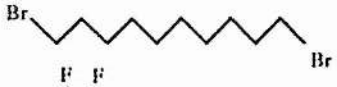
n-alkanes with small non-terminal substituents	 
cyclic alkanes and aromatics with long *n*-alkyl tails	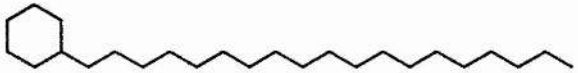 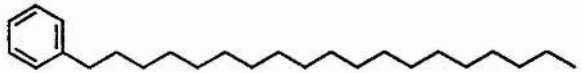
1° alcohols, 2° alcohols, thiols	  
ethers, ketones, esters, aldehydes	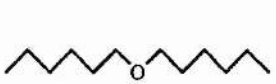 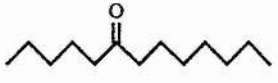 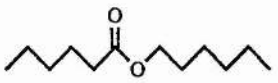 
carboxylic and dicarboxylic acids	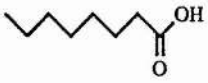 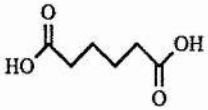
acid anhydrides, diacyl peroxides	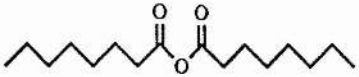 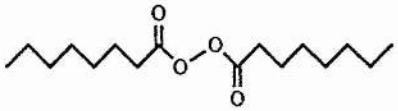
terminally or penultimately unsaturated alkenes and alkynes	 

1.2.4 PREPARATION AND PROPERTIES

1.2.4.1 Preparation

Urea inclusion compounds are usually prepared by treating a saturated methanol (or other alcohol) solution of urea with the organic guest. This may be done either at ambient temperature or at higher temperature; evaporation or cooling is normally required before UIC crystals are observed. Alternatively, the urea may be dissolved in the organic guest by heating, the inclusion compound being formed on cooling. Sometimes the UIC can be formed by pouring the liquid guest onto urea in the solid state. Decomposition of the UIC can be induced by heating: for the *n*-alkane UICs, this occurs at a temperature above the melting point of the *n*-alkane but below the melting point of urea [McAdie, 1962].

1.2.4.2 Composition and Stability

The host:guest molar ratio, which is generally non-stoichiometric, remains constant for a given guest species, regardless of method of preparation. Along a given guest homologous series, there is a linear relationship between the chain length of the guest molecule and the number of urea molecules required to enclose one molecule of guest [Schlenk, 1949b; Redlich *et al*, 1950 JACS]. A method for predicting, *ab initio*, the optimal host/guest molar ratio is given by Rennie & Harris [1992a].

The energies of formation correspond to weak van der Waals forces between the host and guest components, leading to relatively low stability [Schlenk, 1949b; Zimmerschied *et al*, 1950]. In general, ease of formation and stability of the UIC increase with the length of the main alkyl chain of the guest; UICs of volatile guests tend to decompose slowly at room temperature. The urea channels must be completely filled; they are unstable on removal of guest and recrystallise immediately [McAdie, 1962] to the 'pure' crystalline phase of urea, which has a tetragonal structure and *does not* contain empty channels.

1.2.4.3 Guest Environment

The guest molecules are densely packed within the urea channels in a predominently extended, linear, *trans*, 'zig-zag' conformation (although there is evidence that some end-groups adopt the *gauche* conformation). Rennie & Harris [1992b] have shown that, for *n*-alkane guests, $CH_3(CH_2)_nCH_3$, there is a linear relationship between the value of n and the periodic repeat distance along the channel axis of the basic guest structure. In general, if host and guest components are considered *together*, there is no overall three-dimensional ordering because these structures are incommensurate, i.e. no well-defined relationship exists between the host and guest periodicities: this concept will be defined more precisely in Chapter 2. Due to the incommensurability of the structure, successive guest molecules along a given channel are in slightly different environments with respect to the host.

1.2.4.4 Phase Transition

It was found [Pemberton & Parsonage, 1965; Parsonage & Pemberton, 1967; also Parsonage & Staveley, 1984] that the *n*-alkane UICs undergo a phase transition at a temperature that is directly related to the length of the guest molecule, provided the odd and even series of *n*-alkane guests are considered separately. This transition is similar to the 'rotator' phase transition that occurs in crystalline *n*-alkanes, although the phase transition temperatures for the UICs are lower than the corresponding rotator phase transition temperatures for the crystalline *n*-alkanes [Parsonage & Staveley, 1978]. Chatani *et al* [1977 & 1978a] have shown that the crystal symmetry of the basic host structure changes at the phase transition, from hexagonal in the high-temperature phase to orthorhombic in the low-temperature phase. There is also a significant change in motional freedom of the guest. In the high-temperature phase, the *n*-alkane guest molecules undergo rapid rotation about the channel axis [e.g. Gilson & McDowell, 1959 & 1961; Connor & Blears, 1969] and translations along the channel axis [e.g. Fukao *et al*, 1986]; these motions occur at a much slower rate in the low-temperature phase. Fukao *et al* [1990], in a study of the effects of pressure on *n*-alkane UICs,

found that the phase transition temperature increases with pressure. They also report that a pressure-induced phase transition occurs at room temperature, from hexagonal at atmospheric pressure to orthorhombic in the high-pressure phase.

1.2.5 REASONS FOR STUDYING UICS

1.2.5.1 Academic

There are numerous academic reasons for studying urea inclusion compounds, quite apart from their potential applications. It is generally very difficult to study the *n*-alkanes and their derivatives from the point of view of structure and dynamics because these molecules can adopt many conformations. However, within a urea inclusion compound, they are constrained to the essentially *trans*, planar, 'zig-zag' conformation and hence their fundamental properties are more accessible to study. These compounds thus allow study of the conformational, rotational and translational freedom of the guest molecules within a constrained environment. Such study may lead to a better understanding of how organic crystalline materials may be designed for specific uses, thus contributing to the field of crystal engineering [e.g. Desiraju, 1989]. Questions to be answered include:

(i) how do the properties and behaviour of the guest molecules change when they are placed in an inclusion environment, *vis-à-vis* the properties of the pure solid-phase guest? How restrictive is the urea host? Are the guest molecules restrained to a particular conformation?

(ii) Does the host structure respond to the presence of the guest molecules? If so, how? Does it act as a rigid tunnel or does it undergo structural perturbations?

(iii) Is there potential for either guest-guest or host-guest reactions to occur within the channels? Reactions are possible within the channels, provided that the guest molecules are constrained into a conformation favourable to subsequent reaction. Reactions may be host-guest or guest-guest (with or without some catalysing role played by the host). For example, Hollingsworth *et al* [1987] have effected the

photodecomposition of diacyl peroxides within the urea inclusion channels, as a means of studying this reaction in a constrained environment.

1.2.5.2 Applications

The selectivity of urea inclusion compounds is the basis for their chromatographic applications [Fetterley, 1964; Sybilska & Smolková-Keulemansová, 1984]. UICs have been used industrially for the separation of straight-chain alkanes from branched and cyclic organic compounds: one example is in the petroleum industry [Kobe & Domask, 1952] (although this particular application has now been usurped by zeolites). Schlenk & Holman [1950a&b] and Cason *et al* [1953] report use for separation of fatty acids. Schlenk [1952a&b, 1973a,b,c&d; also Arad-Yellin *et al*, 1984] reports use of UICs for separation of optical isomers from racemic mixtures by virtue of the chiral nature of the host structure. This property also suggests potential for asymmetric synthesis, in which the reaction between an achiral guest and the chiral host gives a chiral product. Thus it may be possible to effect stereo- or regio-specific reactions within the urea channels.

It was White [1960] who first investigated the use of UICs as hosts for addition polymerisation reactions [see also Farina, 1984]. Subsequent work in this field has been carried out by Ivanov *et al* [1964], Kawasaki *et al* [1966], Maekawa *et al* [1966], Yoshino *et al* [1967], Pohl & Hummel [1968], Matsuzaki *et al* [1968], Chatani & Kuwata [1975] and Chatani *et al* [1978b]. Such reactions give polymers of high regularity: examples include the polymerisation of vinylchloride, acrylonitrile, butadiene and pentadiene, and the co-polymerisation of acrylonitrile and ethyl acrylate.

UICs can also be used for transportation of dangerous or unstable materials that are stabilised within the UIC. Work of a fundamental nature, such as that outlined above, is indispensable for the study of many of these applications.

1.3 TECHNIQUES

1.3.1 SUITABLE TECHNIQUES

The techniques which can be used for the study of urea inclusion compounds may be divided into four broad categories: diffraction-based, spectroscopic, thermochemical and computational. These techniques are largely complementary in the information they provide.

1.3.1.1 Diffraction-Based Techniques

X-ray diffraction, which can be very informative if high-quality single crystals are available, is widely used. However, because UICs are generally incommensurate structures, structure solution may not be straightforward. Neutron powder diffraction is also possible, using the Rietveld method for structure refinement. Diffraction-based techniques probe only the average periodic properties of the structure, averaged over time and space. Study of the distribution of structural features about this average requires other techniques.

1.3.1.2 Spectroscopic Techniques

Spectroscopic techniques may be used for study at the molecular level of local structural properties and local temporal (i.e. dynamic) properties. Multinuclear magnetic resonance spectroscopy, although not as effective as diffraction for quantitative structure solution, is very instructive for study of the mobility and conformational freedom of the guest molecules. Other spectroscopic techniques include infrared, Raman, inelastic neutron-scattering, dielectric loss, electron-spin resonance, ultraviolet, photoluminescence and x-ray absorption (e.g. EXAFS). Vibrational spectroscopy allows effective study of the localised structure at the molecular level.

1.3.1.3 Thermochemical Techniques

Differential scanning calorimetry and differential thermal analysis allow study of the heat changes involved in the formation and decomposition of the UIC, and study of thermal anomalies, such as determination of phase transition temperatures.

1.3.1.4 Computational Techniques

Computer modelling can be used to predict the formation or otherwise of a UIC simply from the point of view of spatial compatibility. Monte Carlo simulations follow the evolution of a structure, so can give information on energetic properties and local structural properties; however, there is no time-scale associated with Monte Carlo simulations. In contrast, molecular dynamics simulations attach a time-scale to the motion and can be used for study of molecular motions occurring on the time-scale 10^{-12}-10^{-15} s. Molecular mechanics calculations and other computational techniques minimise the energy of the structural model and may be used for predictive purposes. Unlike experimental methods, computational techniques never suffer from practical hindrance; they also allow simultaneous study of properties of both host and guest components, and their interaction.

1.3.1.5 Other Techniques

In addition, optical microscopy can be used to verify the external morphology of the UIC. However, any technique involving use of an electron beam (e.g. high-resolution electron microscopy, electron diffraction, photoelectron spectroscopies) is precluded, because organic materials are rendered unstable both by the electron beam and by the ultra-high vacuum conditions required with electron beam techniques.

1.3.2 Complementary Features

The approaches outlined above are complementary in many respects. We can highlight this contrast for x-ray diffraction, vibrational spectroscopy and neutron techniques. The wavelength of x-radiation is in the range 10^{-8}-10^{-11} m, so is the same

order of magnitude as the interatomic bond distances (i.e. a few Å); thus, x-rays are ideal for the study of atomic and molecular structure. However, their high energy means they are unsuitable for study of dynamic properties. Conversely, the energy of visible, infrared and microwave radiation is in the range 10^0-10^4 cm^{-1} (i.e. a few meV), so is compatible with the study of molecular translations, rotations and vibrations. However, the wavelength is too long to allow study of structural properties. In contrast, suitably moderated neutrons have an energy of a few meV and a wavelength of a few Å, so may be used for the study of both the structure and the dynamics of atoms and molecules.

1.3.3 Techniques Used

In this work, four complementary experimental techniques were used: these were x-ray diffraction (XRD), Raman spectroscopy, incoherent quasielastic neutron scattering (IQNS) and ^2H nuclear magnetic resonance (NMR) spectroscopy. XRD was used to study structural properties, Raman spectroscopy to study conformational properties, neutron scattering and ^2H NMR to study dynamic properties. However, the time-scales accessible by IQNS and ^2H NMR are different: IQNS allows study of motions occurring on the timescale 10^{-10}-10^{-12} s, whereas the timescale for a ^2H NMR study is the range 10^{-3}-10^{-8} s. These techniques were chosen in order to build up a complete picture of the physicochemical properties of the UICs studied.

The choice of single crystal versus powder studies is often dictated by the quality of single crystals available. Where possible, single crystal studies are generally preferable, as they produce more specific information due to the oriented nature of the experiment. In the current work, both single crystal and powder samples were used, in keeping with the samples available and the experimental set-ups used.

1.4 OUR STUDY

1.4.1 COMPOUNDS STUDIED AND AIMS

The work described in this thesis focuses on the urea inclusion compounds of the α,ω-dibromo-*n*-alkanes, $Br(CH_2)_nBr$/urea and $Br(CH_2)_nBr$/urea-d_4, generally with n=7-10. This is the first known study of this family of guest molecules: it covers both properties of the guest and properties of the host. Other urea inclusion compounds are also investigated briefly, namely: $Br(CH_2)_nBr$/urea with n=6,11,12; $Br(CD_2)_{10}Br$/urea; $I(CH_2)_nI$/urea with n=8,10; $Cl(CH_2)_nCl$/urea with n=8,10; $Br(CH_2)_nCH_3$/urea with n=9-12; and *n*-$C_{16}D_{34}$/urea.

1.4.1.1 Properties of the Guest

Our objective was to study how various properties of these guest molecules are influenced by their inclusion environment. Specifically, we studied the structural, dynamic and conformational properties of the $Br(CH_2)_nBr$ guests, with n=7-10. The structural properties were studied by single crystal XRD, the conformational properties were studied using polarised single crystal Raman spectroscopy, and the dynamic properties were studied using IQNS of semi-oriented polycrystalline samples. In addition, guest properties of $Br(CH_2)_nBr$/urea with n=6,11,12, $I(CH_2)_{10}I$/urea, $Cl(CH_2)_{10}Cl$/urea and $Br(CH_2)_nCH_3$/urea with n=9-12 were studied using single crystal XRD. Guest properties of $Br(CH_2)_6Br$/urea, $Br(CH_2)_{11}Br$/urea, $I(CH_2)_8I$/urea and $Cl(CH_2)_8Cl$/urea were also studied by Raman spectroscopy. Guest properties of $Br(CD_2)_{10}Br$/urea were studied using ^2H NMR spectroscopy.

1.4.1.2 Properties of the Host

Although the basic hexagonal urea host structure has been studied extensively and does not change significantly with guest species, much less is know about its dynamics. Study of the motion of the host molecules of the $Br(CH_2)_nBr$/urea family, with n=7-10, was achieved using ^2H NMR spectroscopy of polycrystalline and single crystal samples. The host structure of $Br(CH_2)_6Br$/urea, which was found to differ

from hexagonal, was investigated by single crystal XRD. The host motion of n-$C_{16}D_{34}$/urea was studied by IQNS of a polycrystalline sample.

1.4.2 THESIS CHAPTERS

The current chapter has served as an introduction to urea inclusion compounds: many of the topics introduced here are explored more extensively in subsequent chapters. Each of the four experimental chapters of the thesis (Chapters 2, 3, 4 & 5) focuses on one experimental technique (XRD, Raman spectroscopy, IQNS and ^{2}H NMR spectroscopy, respectively). The theory behind each technique is outlined at the beginning of the appropriate chapter. Relevant previous work on UICs is described and the objectives of the study are examined. Our results are then presented and discussed in the light of the previous knowledge.

Chapter 6 draws together the individual conclusions reached in the experimental chapters: its aim is to present the overall state of knowledge regarding the structure and dynamics of the α,ω-dibromo-n-alkane/urea family of inclusion compounds. Some comment is also made concerning the other UICs studied. The complementary nature of the conclusions discussed in Chapter 6 highlights the value of using a combination of experimental approaches.

1.5 REFERENCES

ARAD-YELLIN R, GREEN BS, KNOSSOW M & TSOUCARIS G (1984) Enantiomeric selectivity of host lattices. In: ATWOOD JL, DAVIES JED & MACNICOL DD, Eds., Inclusion Compounds: Vol. 3. Physical Properties and Applications, Academic Press, pp 263-295.

ATWOOD JL, DAVIES JED & MACNICOL DD, Eds. (1984) Inclusion Compounds: Vol. 1. Structural Aspects of Inclusion Compounds Formed by Inorganic and Organometallic Host Lattices; Vol 2. Structural Aspects of Inclusion Compounds Formed by Organic Host Lattices; Vol. 3. Physical Properties and Applications. Academic Press.

BENGEN MF (1951) Mein Weg zu den neuen Harnstoff-Einschluß-Verbindungen, *Angew. Chem.*, **63**, 207-208.

BENGEN MF (1953) Decomposing mixtures of organic compounds [in German]. German Patent, no. 869070 (submitted 18 March 1940, Appl. O.Z. 12438): *Chem. Abs.* **48**: 11479c.

BENGEN MF & SCHLENK W (1949) Über neuartige Additionsverbindungen des Harnstoffs, *Experientia*, **5**, 200.

CASON J, SUMRELL G, ALLEN CF, GILLES GA & ELBERG S (1953) Certain characteristics of the fatty acids from the lipides of the tubercle bacillus, *J. Biol. Chem.*, **205**, 435-447.

CHATANI Y & KUWATA S (1975) Structural investigation of radiation-induced urea canal polymerisation of 1,3-butadiene, *Macromol.*, **8**, 12-18.

CHATANI Y, TAKI Y & TADOKORO H (1977) Low temperature form of urea adducts with *n*-paraffins, *Acta Crystallogr., Sect. B*, **33**, 309-311.

CHATANI Y, ANRAKU H & TAKI Y (1978a) Phase transition and structure change of urea adducts with *n*-paraffin and paraffin-type compounds, *Mol. Cryst. Liq. Cryst.*, **48**, 219-231.

CHATANI Y, YOSHIMORI K & TATSUTA Y (1978b) Several features of urea-channel polymerisation of vinyl chloride and vinyl bromide, *Polym. Prepr., Am. Chem. Soc., Div. Polym. Chem.*, **19**(2), 132-137.

CLÉMENT R, JEGOUDEZ J & MAZIERES C (1974) Transitions dans une série de clathrates de thiourée et d'urée avec encages cycliques, *J. Solid State Chem.*, **10**, 46-50.

CLÉMENT R, GOURDJI M & GUIBÉ L (1975) Etude par RMN des changements de phase et des mouvements moléculaires dans le composé d'inclusion urée-d_4-trioxane, *Mol. Phys.*, **30**, 825-838.

CLEMM A (1859) Mittheilungen aus dem chemischen Laboratorium in Gießen: I. Über Chinasäure, *Liebigs Ann. Chem. Pharm.*, **110**, 345-359.

CONNOR TM & BLEARS DJ (1969) Laboratory and rotating frame proton magnetic relaxation measurements of urea-d_4-fatty acid adducts, *Mol. Phys.*, **17**, 435-438.

CRONSTEDT AF (1756) Rön och Beskrifning: om en obekant bärg art, som kallas Zeolites [Discovery and description of a new mineral species, named zeolites], *Akad. Handl. Stockholm*, **17**, 120-123.

DAVY H (1811) The Bakerian Lecture. On some of the combinations of oxymuriatic gas and oxygene, and on the chemical relations of these principles to inflammable bodies, *Philos. Trans. R. Soc. London*, **101**, 1-35.

DESIRAJU GR, Ed. (1989) Crystal Engineering: the Design of Organic Solids, Elsevier.

FARADAY M (1823) On hydrate of chlorine, *Quart. J. Sci.*, **15**, 71-74.

FARINA M (1984) Inclusion polymerisation. In: ATWOOD JL, DAVIES JED & MACNICOL DD, Eds., Inclusion Compounds: Vol. 3. Physical Properties and Applications, Academic Press, pp 297-329.

FETTERLEY LC (1964) Organic adducts. In: MANDELCORN L, Ed., Non-Stoichiometric Compounds, Academic Press, pp 491-567.

FUKAO K, MIYAJI H & ASAI K (1986) Anharmonic vibration of *n*-paraffin molecules in urea adducts, *J. Chem. Phys.*, **84**, 6360-6368.

FUKAO K, HORIUCHI T, TAKI S & MATSUSHIGE K (1990) Phase transitions of urea adducts with *n*-paraffins under high pressure, *Mol. Cryst. Liq. Cryst.*, **180B**, 405-416.

GILSON DFR & MCDOWELL CA (1959) Molecular motion of enclathrated compounds as studied by nuclear magnetic resonance, *Nature*, **183**, 1183-1184.

GILSON DFR & MCDOWELL CA (1961) Nuclear magnetic resonance studies of urea and thiourea adducts, *Mol. Phys.*, **4**, 125-134.

HARRIS KDM (1988) Studies of urea inclusion compounds and other solids, PhD Thesis, University of Cambridge.

HARRIS KDM (1993) Molecular confinement, *Chem. Br.*, **29**, 132-136.

HARRIS KDM & THOMAS JM (1990) Structural aspects of urea inclusion compounds and their investigation by x-ray diffraction: a general discussion, *J. Chem. Soc., Faraday Trans.*, **86**, 2985-2996.

HOLLINGSWORTH MD, HARRIS KDM, JONES W & THOMAS JM (1987) ESR and x-ray diffraction studies of diacyl peroxides in urea and aluminosilicate hosts, *J. Inclusion Phenom.*, **5**, 273-277.

HOLLINGSWORTH MD, SANTASIERO BD, OUMAR-MAHAMAT H & NICHOLS CJ (1991) New series of 1:1 layered complexes of α,ω-dinitriles and urea, *Chem. Mater.*, **3**, 23-25.

IVANOV VS, SUKHIKH TA, MEDVEDEV YV, BREGER AK, OSIPOV VP & GOL'DIN VA (1964) Studies in radiation polymerisation: III. Radiation polymerisation of piperylene in the channel complexes of urea [in Russian], *Vysokomol. Soedin.*, **6**, 782-786; Engl. Transl., **6**, 856-860; *Chem. Abs.*, **61**: 5774g.

KAWASAKI M, MAEKAWA T, HAYASHI K & OKAMURA S (1966) Radiation-induced polymerisation in urea canal complexes: Part I. Radiation-induced polymerisation of acrylonitrile in urea canal complex, *J. Macromol. Chem.*, **1**, 489-506.

KOBE KA & DOMASK WG (1952) Extractive crystallisation - a new separation process: III. Practical applications, *Petroleum Refiner*, **31**(7), 125-129.

MCADIE HG (1962) Thermal decomposition of molecular complexes: 1. Urea-*n*-paraffin inclusion compounds, *Can. J. Chem.*, **40**, 2195-2203.

MAEKAWA T, KAWASAKI M. HAYASHI K & OKAMURA S (1966) Radiation-induced polymerisation in urea canal complexes: Part II. Radiation-induced polymerisation of acrylonitrile-ethyl acrylate in urea canal complex and other two-component systems, *J. Macromol. Chem.*, **1**, 507-521.

MATSUZAKI K, URYU T, OKADA M & SHIROKI H (1968) The stereoregularity of polyacrylonitrile and its dependence on polymerisation temperature, *J. Polym. Sci., Part A-1: Polym. Chem.*, **6**, 1475-1487.

MONOBE K & YOKOYAMA F (1973) Molecular association complex of urea with polyethylene: 1. Morphology of urea-polyethylene complex and polyethylene crystals obtained from the complex, *J. Macromol. Sci., Sect. B: Phys.*, **8**, 295-311.

MONTEL G (1955) Sur les composés d'insertion, *Bull. Soc. Chim. France*, 1013-1017.

MYLIUS F (1886) Zur Kenntniss des Hydrochinons und der Ameisensäure, *Ber. Bunsenges. Phys. Chem.*, **19**, 999-1009.

OTTO J (1972) Bestimmung der Wirtsstruktur von 1,4-Dichlorbutan-Harnstoff, ein Beitrag zur Bestätigung eines allgemeinen Bauprinzips für die Einschlussverbindungen des Harnstoffs und des Thioharnstoffs, *Acta Crystallogr., Sect. B*, **28**, 543-551.

PALIN DE & POWELL HM (1945) Hydrogen bond linking of quinol molecules, *Nature*, **156**, 334-335.

PALIN DE & POWELL HM (1947) The structure of molecular compounds: Part III. Crystal structure of addition complexes of quinol with certain volatile components. *J. Chem. Soc.*, 208-221.

PARSONAGE NG & PEMBERTON RC (1967) Thermal anomalies in the adducts of urea with *n*-paraffins: a theoretical treatment, *Trans. Faraday Soc.*, **63**, 311-328.

PARSONAGE NG & STAVELEY LAK (1978) Disorder in Crystals, Oxford University Press, pp 717-798.

PARSONAGE NG & STAVELEY LAK (1984) Thermodynamic studies of clathrates and inclusion compounds. In: ATWOOD JL, DAVIES JED & MACNICOL DD, Eds.. Inclusion Compounds: Vol. 3. Physical Properties and Applications, Academic Press, pp 1-36.

PEMBERTON RC & PARSONAGE NG (1965) Thermodynamic properties of (urea – hydrocarbon) adducts: Part 1. Heat capacities of the adducts of *n*-$C_{10}H_{22}$, *n*-$C_{12}H_{26}$, *n*-$C_{16}H_{34}$ and *n*-$C_{20}H_{42}$ from 12-300 K, *Trans. Faraday Soc.*, **61**, 2112-2121.

POHL HU & HUMMEL DO (1968) Quantitative IR-spektroskopische Untersuchungen der Mikrostruktur von Polyvinylchlorid, *Makromol. Chem.*, **113**, 203-214.

POWELL HM (1948) The structure of molecular compounds: Part IV. Clathrate compounds, *J. Chem. Soc.*, 61-73.

POWELL HM (1984) Introduction. In: ATWOOD JL, DAVIES JED & MACNICOL DD, Eds., Inclusion Compounds: Vol. 1. Structural Aspects of Inclusion Compounds Formed by Inorganic and Organometallic Host Lattices, Academic Press, pp 1-28.

RADELL J, CONNOLLY JW & YUHAS LD (1961) Urea inclusion compounds of alkynes, *J. Org. Chem.*, **26**, 2022-2025.

RADELL J, BRODMAN BW & BERGMANN ED (1963) Urea inclusion compounds of *n*-alkyl oxiranes and *n*-mercaptans, *Tetrahedron*, **19**, 873-877.

RADELL J, BRODMAN BW & BERGMANN ED (1964) Urea inclusion compounds of *n*-alkyl bromides and iodides, *Can. J. Chem.*, **42**, 1069-1072.

REDLICH O, GABLE CM, DUNLOP AK & MILLAR RW (1950) Addition compounds of urea and other organic substances, *J. Am. Chem. Soc.*, **72**, 4153-4160.

RENNIE AJO & HARRIS KDM (1992a) A quantitative analysis of guest periodicity in one-dimensional inclusion compounds, *J. Chem. Phys.*, **96**, 7117-7124.

RENNIE AJO & HARRIS KDM (1992b) Is the guest periodicity of $CH_3(CH_2)_nCH_3$ /urea inclusion compounds linearly dependent on n? A mathematical analysis, *Chem. Phys. Lett.*, **188**, 1-4.

SCHIESSLER RW & FLITTER D (1952) Urea and thiourea adduction of C_5-C_{42} hydrocarbons, *J. Am. Chem. Soc.*, **74**, 1720-1723.

SCHLENK W (1949a) Über aliphatische Harnstoff-Addukte, eine neue Kategorie von Additionsverbindungen, *Angew. Chem.*, **61**, 447.

SCHLENK W (1949b) Die Harnstoff-Addition der aliphatischen Verbindungen, *Liebigs Ann. Chem.*, **565**, 204-240.

SCHLENK W (1950) Die neuen Harnstoff-Additionsverbindungen, *Angew. Chem.*, **62**, 299-301.

SCHLENK W (1952a) Trennung von optischen Antipoden über Komplexverbindungen ohne Zuhilfenahme asymmetrischer Moleküle, *Experientia*, **8**, 337-338.

SCHLENK W (1952b) The fractionation of ozokerites and the separation of optical isomers. Two examples of the applicability of inclusion compounds to analytical problems, *Analyst*, **77**, 867-873.

SCHLENK W (1953) Die Struktur der Harnstoff-Additionsverbindungen, *Acta Crystallogr.*, **6**, 670.

SCHLENK W (1973a) Das asymmetrische Einschlußgitter des Harnstoffs: I. Racemattrennung, *Liebigs Ann. Chem.*, 1145-1155.

SCHLENK W (1973b) Das asymmetrische Einschlußgitter des Harnstoffs: II. Konfigurativ stetige Gitterzuordnung der Gastmoleküle, *Liebigs Ann. Chem.*, 1156-1178.

SCHLENK W (1973c) Das asymmetrische Einschlußgitter des Harnstoffs: III. Konfigurativ nicht-stetige Gitterzuordnung der Gastmoleküle, *Liebigs Ann. Chem.*, 1179-1194.

SCHLENK W (1973d) Das asymmetrische Einschlußgitter des Harnstoffs: IV. Die absolute Konfiguration des Gitters, *Liebigs Ann. Chem.*, 1195-1209.

SCHLENK H & HOLMAN RT (1950a) The urea complexes of unsaturated fat acids, *Science*, **112**, 19-20.

SCHLENK H & HOLMAN RT (1950b) Separation and stabilisation of fatty acids by urea complexes, *J. Am. Chem. Soc.*, **72**, 5001-5004.

SMITH AE (1950) The crystal structure of urea-hydrocarbon and thiourea-hydrocarbon complexes, *J. Chem. Phys.*, **18**, 150-151.

SMITH AE (1952) The crystal structure of the urea-hydrocarbon complexes, *Acta Crystallogr.*, **5**, 224-235.

SYBILSKA D & SMOLKOVA-KEULEMANSOVA E (1984) Applications of inclusion compounds in chromatography. In: ATWOOD JL, DAVIES JED & MACNICOL DD, Eds., Inclusion Compounds: Vol. 3. Physical Properties and Applications, Academic Press, pp 173-243.

TAKEMOTO K & SONODA N (1984) Inclusion compounds of urea, thiourea and selenourea. In: ATWOOD JL, DAVIES JED & MACNICOL DD, Eds., Inclusion Compounds: Vol. 2. Structural Aspects of Inclusion Compounds Formed by Organic Host Lattices, Academic Press, pp 47-67.

THOMAS JM (1988) Uniform heterogeneous catalysts: the role of solid-state chemistry in their development and design, *Angew. Chem., Int. Ed. Engl.*, **27**, 1673-1691.

THOMAS JM & HARRIS KDM (1987) Organic molecules in constrained environments. In: DESIRAJU GR, Ed., Organic Solid State Chemistry, Elsevier, pp 179-206.

WHITE DM (1960) Stereospecific polymerisation in urea canal complexes, *J. Am. Chem. Soc.*, **82**, 5678-5685.

WÖHLER F (1849) Über einige Verbindungen aus der Chinonreihe, *Liebigs Ann. Chem. Pharm.*, **69**, 294-300.

YOKOYAMA F & MONOBE K (1980) Molecular association complex of urea with polyethylene: 2. The new preparation methods and morphological study, *Polymer*, **21**, 968-972.

YOKOYAMA F & MONOBE K (1983) Molecular association complex of urea with polyethylene: 3. Structural studies of the complex, *Polymer*, **24**, 149-154.

YOSHINO T, KENJO H & KUNO K (1967) Assignment of the methylene proton signals and estimation of the *meso* to racemic methylene ratios in polyacrylonitriles, *J. Polym. Sci., Part B: Polym. Lett.*, **5**, 703-709.

ZIMMERSCHIED WJ, DINERSTEIN RA, WEITKAMP AW & MARSCHNER RF (1949) Complexes of urea with linear aliphatic compounds, *J. Am. Chem. Soc.*, **71**, 2947.

ZIMMERSCHIED WJ, DINERSTEIN RA, WEITKAMP AW & MARSCHNER RF (1950) Crystalline adducts of urea with linear aliphatic compounds: a new separation process, *Ind. Eng. Chem.*, **42**, 1300-1306.

CHAPTER 2
X-RAY DIFFRACTION STUDIES

2.1 THE TECHNIQUE

2.1.1 INTRODUCTION

X-ray diffraction (XRD) is a very powerful technique which allows determination of crystal structures on a time and space average. This technique averages over the many x-ray scattering events occurring during the time taken to record the data. It thus provides information regarding average atomic positions, bond lengths and bond angles, so supplying details of molecular packing and geometry. It can be contrasted with neutron diffraction, a complementary technique in many ways [e.g. Von Dreele, 1990]. Both x-rays and neutrons of appropriate energy have wavelengths of a few angstroms, comparable to the periodic repeat distances in crystals, and so are diffracted by crystal lattices. X-rays are scattered by electrons, whereas neutrons are scattered by the atomic nuclei. However, x-ray diffraction has certain limitations. Because scattering power increases with atomic number, scattering from hydrogen atoms is weak and thus x-ray diffraction is not ideal for accurate determination of their positions. Isotopes are also indistinguishable. Furthermore, intensity falls off dramatically with increasing scattering angle, leading to problems in the structure determination of many large organic molecules, e.g. proteins. Single crystal neutron diffraction does not suffer from these limitations, but much larger crystals are required due to the low neutron flux available.

In this introduction we shall discuss some background theory to diffraction by crystals before examining the experimental aspects of x-ray diffraction. The theoretical discussion will concentrate on single crystal diffraction. However, for the most part, these concepts apply equally to powder diffraction since a powder sample is merely a random orientation of crystallites. Further background theory can be found in general references such as Atkins [1986], Bragg [1968], Dunitz [1979], Eberhart [1991], Giacovazzo *et al* [1992], Glusker & Trueblood [1972] and Stout & Jensen [1989].

2.1.2 BACKGROUND THEORY

2.1.2.1 The Crystal

A fundamental characteristic of the crystalline state is a very high degree of internal order. A crystal consists of an ordered array of atoms which is repeated in three dimensions throughout the structure. All crystals belong to one of seven crystal systems: triclinic, monoclinic, orthorhombic, rhombohedral (or trigonal), tetragonal, hexagonal and cubic. Each system has a characteristic set of internal symmetry elements, *viz* the number of axes required to generate the principle features of the crystal's shape and the angles between these axes. Taking account of additional point group symmetry elements which may be present gives us a total of 32 crystal classes. Each of these crystal classes belongs to one of 11 Laue groups.

Various terms are used to describe the internal symmetry of a crystal: these may be defined as follows [Glusker & Trueblood, 1972; Atkins, 1986].

(1) The asymmetric unit is the unique portion of the crystal structure that has no plane. axis, centre of symmetry or translational symmetry. The space group symmetry operations, when applied to the asymmetric unit, generate the contents of the unit cell.

(2) The unit cell is the smallest fundamental unit from which the entire crystal may be constructed by purely translational displacements in three dimensions. The unit cell must possess the full symmetry of the crystal.

(3) The crystal lattice is the three-dimensional, infinite network of points which defines the periodicity of the crystal. The crystal structure is constructed by convolution of the crystal lattice with a structural motif (for a primitive lattice, the structural motif is the content of the unit cell).

In three dimensions there are 14 types of unit cell, leading to 14 crystal lattices. termed the Bravais lattices, which fall into seven groups corresponding to the seven

crystal systems. A consideration of the combinations of symmetry elements that can be arranged on these 14 lattices leads to 230 distinct crystallographic space groups. Knowledge of the space group and the asymmetric unit allows generation of the entire structure.

2.1.2.2 X-Ray Diffraction

Diffraction is the elastic, coherent scattering of a beam of particles: thus, there is no energy change during the scattering event, and the scattered beam has a well-defined phase relationship with the incident beam. The diffraction of x-rays by crystals was discovered in 1912 by Friedrich, Knipping and von Laue [Friedrich *et al*, 1913; von Laue, 1913], who interpreted this phenomenon by extending the theory of optical diffraction by gratings to three dimensions. Thus each diffracted x-ray beam was viewed as a wave; for constructive interference (and hence diffraction) to occur required that the interfering wavefronts were in phase with one another. Bragg, in 1913 [Bragg & Bragg, 1913 & 1914; Bragg, 1914; see also Bragg, 1968], took an alternative although geometrically equivalent approach, considering x-ray diffraction in terms of reflection from parallel planes through points in the crystal lattice (these planes are termed 'lattice planes'). This led to Bragg's Law, which is illustrated in Fig. 2.1. Constructive interference will occur only if this law is satisfied. Diffracted rays may thus be termed 'reflections'.

$$n\lambda = 2d \sin\theta \qquad \text{Bragg's Law}$$

where n = order of diffraction†

λ = wavelength of radiation used

d = spacing between crystal lattice planes

θ = angle of incidence (or 'glancing angle')

† The parameter n is often omitted, since different orders of diffraction are embodied within the definition of Miller indices (see §2.1.2.3).

Fig. 2.1: Bragg's Law $n\lambda = 2d \sin\theta$

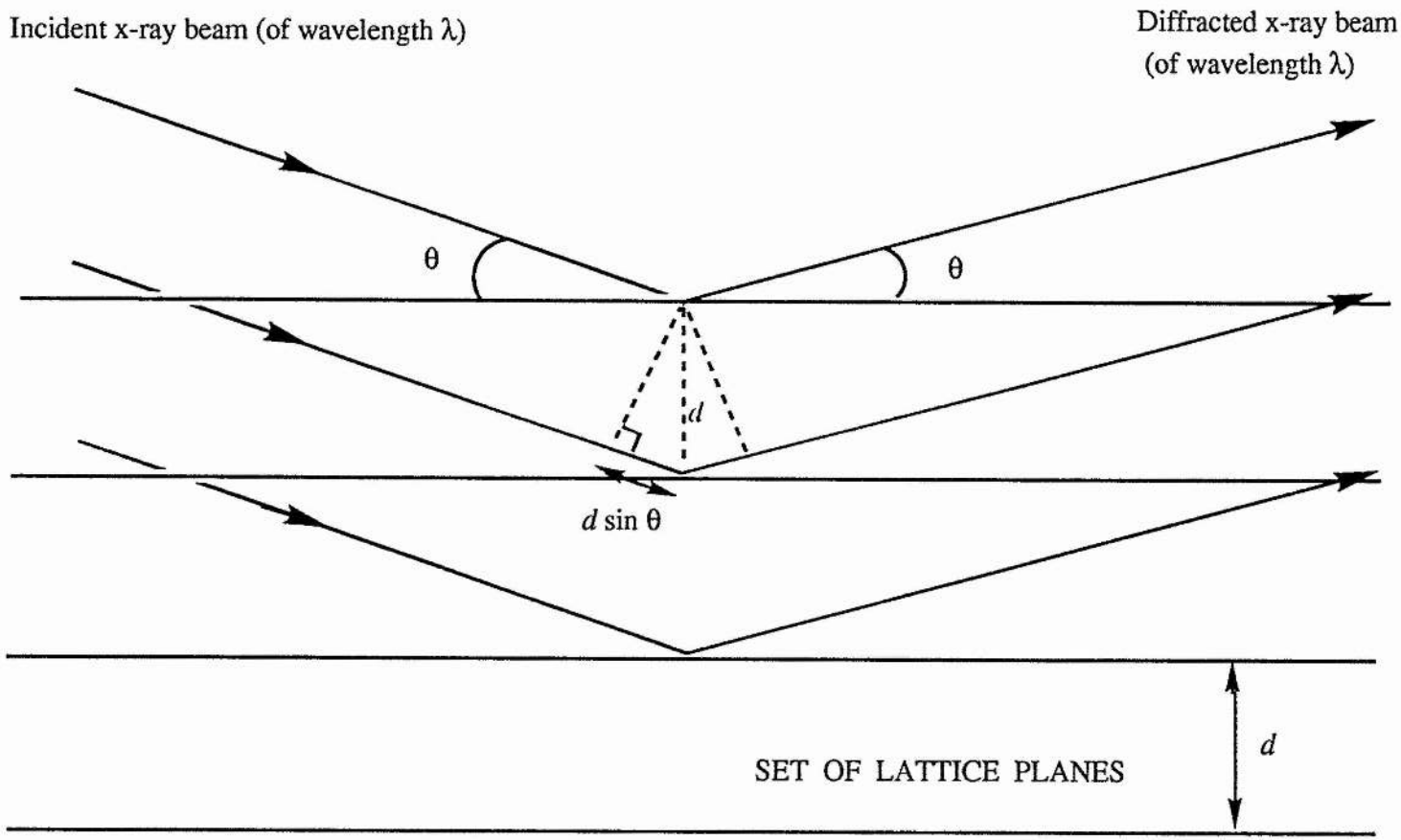

2.1.2.3 Reciprocal Space

The positions of intensity maxima in the diffraction pattern of a crystal can be understood in terms of a lattice that is reciprocal to the direct lattice of the crystal. This concept of reciprocality is a powerful tool in the analysis of x-ray diffraction data. Located in direct space are the crystal and the corresponding crystal lattice (or 'direct lattice'). The unit cell of the crystal lattice is defined by basis vectors **a**,**b**,**c** (which are, in turn, defined by lengths a,b,c and angles α,β,γ, respectively). The position of a point N of the crystal lattice may be described by a vector $\mathbf{r}_n$:

$$\mathbf{r}_n = u\mathbf{a}+v\mathbf{b}+w\mathbf{c} \qquad \text{where } (uvw) \text{ are integers: the numerical coordinates of N}$$

Located in reciprocal space are diffraction effects and the reciprocal lattice corresponding to the crystal lattice in direct space. Variables in reciprocal space are designated by asterisks: thus the reciprocal lattice is defined by basis vectors **a***,**b***,**c*** (with lengths a*,b*,c* and angles $\alpha^*,\beta^*,\gamma^*$, respectively). The position of a point G of the reciprocal lattice is described by a vector $\mathbf{r}_g^*$:

$$\mathbf{r}_g^* = h\mathbf{a}^*+k\mathbf{b}^*+l\mathbf{c}^* \qquad \text{where } (hkl) \text{ are integers: the numerical coordinates of G}$$

Concepts in reciprocal space are related to those in direct space by a Fourier transform. Thus the reciprocal lattice basis vectors **a***,**b***,**c*** are normal to the (b,c), (a,c) and (a,b) planes, respectively, of the direct crystal lattice. Consequently, the vector product $\mathbf{r}_n.\mathbf{r}_g^*$ is given by:

$$\mathbf{r}_n.\mathbf{r}_g^* = uh+vk+wl = m \qquad \text{where } m \text{ is an integer}$$

The integers (*hkl*) are used to index intensity maxima (i.e. reflections) in the diffraction pattern and are known as the Miller indices. In direct space, each (*hkl*) is associated with a set of lattice planes of spacing d_{hkl}. The Miller indices are defined such that each

lattice point is on one lattice plane for a given (*hkl*): they are thus prime with respect to each other. If the lattice parameters and the crystal system are known, d_{hkl} may be evaluated for any given (*hkl*).

The Laue condition, which is analogous to Bragg's Law, states that diffraction will occur only when the scattering vector, $\mathbf{r}_g^*$, is a vector of the reciprocal lattice. Because diffraction is an elastic scattering process, the initial and final wavevectors are equal in magnitude, i.e. $|\mathbf{k}_i| = |\mathbf{k}_f|$, where $\mathbf{r}_g^* = \mathbf{k}_f - \mathbf{k}_i$. Both wavevectors, $\mathbf{k}_i$ and $\mathbf{k}_f$, fall on the surface of a sphere of reciprocal space, of radius $1/\lambda$, drawn through the origin of the reciprocal lattice. This sphere is termed the Ewald sphere or the reflecting sphere (see Fig. 2.2). Wherever a reciprocal lattice point intersects the surface of the Ewald sphere, diffraction will occur. The Ewald sphere can thus be used to predict the direction of the reflections and hence the diffraction pattern (see §2.1.4.2).

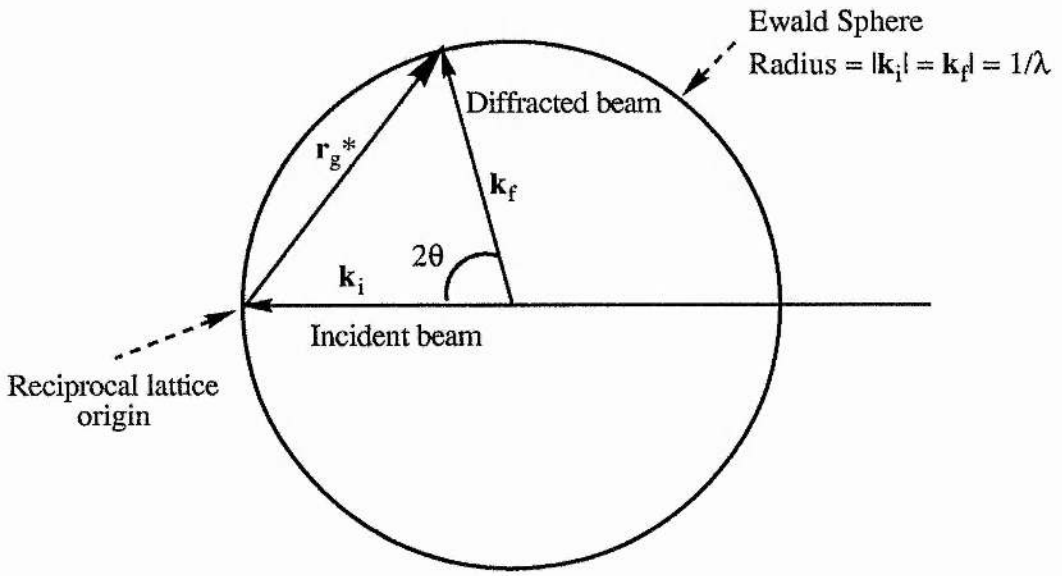

Fig. 2.2: The Ewald Sphere

2.1.3 STRUCTURE DETERMINATION

The data, which are collected using a diffractometer (see §2.1.4.2), consist of the relative intensities, *I*, of all reflections from the set of lattice planes (*hkl*) within a given range. There are three principal steps involved in determination of the crystal structure from this data:

(i) calculation of the lattice parameters and the space group

(ii) derivation of a sensible initial structural model

(iii) refinement of the structural model to minimise the difference between calculated and experimental intensities.

2.1.3.1 Scattering Characteristics

The positions, defined by three scattering angles (corresponding to 2θ in each dimension), of the intensity maxima in the diffraction pattern give the size and shape of the unit cell (i.e. the lattice parameters a,b,c,α,β,γ) via the reciprocal lattice parameters: the intensity of scattering, *I*, gives the distribution of scattering matter, hence the positions of atoms within the unit cell (i.e. the atomic positional parameters). Certain sets of reflections may have exactly zero intensity, implying that the structure contains a specific element of symmetry: this aids in the determination of the space group.

Any scattered wave has an amplitude (magnitude) and a phase. Because x-rays are scattered by electrons, the amplitude of scattering for an isolated atom depends on the number of electrons it contains and hence on its atomic number. This amplitude is termed the atomic scattering factor *f* (or atomic form factor) and is defined as:

$$f = \frac{\text{amplitude of scattering by the atom's electrons}}{\text{amplitude of scattering by a single electron}}$$

At $(\sin\theta)/\lambda=0$, *f* is equal to the atomic number; the value of *f* decreases with increase in $(\sin\theta)/\lambda$. The effective value of *f* is also affected by isotropic and anisotropic vibrations of the atom, due to either thermal motion or static disorder: variables

describing these vibrations are termed temperature factors or atomic displacement parameters.

The scattering by the crystal structure in the direction specified by the Miller indices (*hkl*) is described by the structure factor F(*hkl*), which contains information on the amplitude and phase. The structure factor at the reciprocal lattice point (*hkl*) is the Fourier transform of the electron distribution in the unit cell. F(*hkl*) is thus dependent on the nature and arrangement of the scattering material (i.e. the electron distribution, specified by $\rho(x,y,z)$) and on the direction of the scattering (specified by *h*, *k* and *l*):

$$F(hkl) = \int_x \int_y \int_z \rho(x,y,z) \exp\left[-2\pi i\,(hx + ky + lz)\right] \partial x\, \partial y\, \partial z$$

Hence, F(*hkl*) may be expressed as a complex number:

$$F(hkl) = A + iB \quad \text{where} \quad |F| = \left(A^2 + B^2\right)^{1/2}$$

$$\alpha = \tan^{-1}\left(\frac{B}{A}\right)$$

|F| represents the resultant of the scattering from the individual constituent atoms and α the resultant of the phases of the waves scattered from the individual constituent atoms.

The relative intensity *I* of any reflection (*hkl*) is proportional to $|F|^2$ in an ideally imperfect crystal. In reality, various other factors exist such that:

$$I = K\,|F|^2\,L.T.A$$

where K = scale factor

L = geometric correction (corrects for shape and position of crystal relative to x-ray beam)

T = temperature factors (corrects for thermal vibrations - isotropic and anisotropic - of atoms within crystal)

A = absorption correction (corrects for absorption of x-rays by crystal).

2.1.3.2 Derivation of the Trial Structure

A knowledge of |F| and α for each (*hkl*) would allow computation, via a three-dimensional Fourier synthesis,* of an electron density map from which the crystal structure could be solved directly. Because the intensity of the diffraction pattern is proportional to $|F|^2$, experimental data allows determination of structure factor amplitudes but not of phase angles α. This inability to extricate values of α is termed 'the phase problem'. Unfortunately, the accuracy of an electron density map is more sensitive to values of α than to those of |F|. Nevertheless, several methods can be used to circumvent this phase problem in order that a trial structure may be derived: these methods will now be outlined.

(i) Direct methods (Fourier methods). These rely on the fact that electron density is a probability distribution and, as such, can never be negative. For both centrosymmetric and non-centrosymmetric structures, the phase angles for individual reflections are constrained to certain values. From such requirements and on the grounds of probability, the phases of strong reflections can be derived; an approximate electron density map may then be generated via a Fourier synthesis, using $|E_o|$ values (obtained from the observed structure factor amplitudes $|F_o|$, where $|F_o| \propto f|E_o|$) and computed phase angles.

* A Fourier synthesis is the summation of sine and cosine waves to give a periodic function.

(ii) Patterson methods. No information on phase is required: these methods use only the indices (*hkl*) of each diffracted beam and the corresponding intensity-derived value of $|F_o|^2$. These parameters, on summation via a Fourier synthesis, lead to a Patterson map, in which the magnitude and direction of vector peaks correspond to the distance and relative orientation between atoms in the crystal. Patterson methods are most effective for structures containing a few heavy atoms which dominate the scattering sufficiently to allow their locations to be accurately determined. These locations can then be used as 'starting points' for the crystal structure refinement. Patterson methods are also successful in solving few-atom structures since the number of possible atomic connectivities is low. However, a serious problem is that of overlapping peaks (an N-atom unit cell gives rise to N^2 vector peaks on the Patterson map); for this reason, many-atom structures cannot readily be solved using Patterson methods, unless they contain a dominant scatterer.

(iii) Isomorphous replacement. This method allows direct determination of phase angles but requires a pair or a series of isomorphous crystals (i.e. crystals with identical unit cell dimensions and atomic arrangements but different atoms present). Such crystals can be identified via a preliminary Patterson map. Isomorphous replacement is the only method sufficiently powerful to allow structure determination of macromolecules such as proteins.

2.1.3.3 Refinement of the Trial Structure

We now outline two methods for improving the structural model such that the data computed from the trial structure become acceptably close to the experimental observations.

(i) Fourier methods. These methods produce an electron density difference map by comparing the electron density map generated using $|F_o|$ values with that determined from calculated structure factor amplitudes ($|F_c|$ values). (Calculated phases are used

for both electron density maps.) The coordinates of electron density maxima on the difference map are used as a basis for an improved structural model. A new difference map is then produced and the process repeated. This is continued until the difference map is as flat as possible.

(ii) Least squares method. This is applicable so long as there are many more experimental observations than parameters to be determined. Certain variables are altered, via a least squares fitting procedure, in order to minimise the disagreement between the observed and calculated structure factor amplitudes. The variables are the positional parameters and temperature factors for each atom, and the scale factor, *K*. Measurements are weighted according to their perceived accuracy.

2.1.3.4 Correctness of the Structure

One measure of the correctness of a structure is the value of its discrepancy index. R. This quantifies the agreement between $|F_o|$ and $|F_c|$, and is defined as:

$$R = \frac{\sum |\{|F_o| - |F_c|\}|}{\sum |F_o|}$$

Typically, R<8% for the final structural model, although the minimum value achievable often depends on the extent of structural disorder. Further criteria for a correct structure are that its electron density difference map has no significant peaks or troughs, and that molecular packing and geometry (and thus bond lengths and angles) seem chemically reasonable. Estimated standard deviations in bond lengths and angles should be small, and the atomic displacement parameters should have appropriate values.

All the methods of structure determination discussed may contain both random errors and systematic errors. Sources of systematic error are numerous: bonded atoms may not have spherically-symmetrical electron densities; the methods used for

modelling thermal vibrations may be oversimplified; absorption and instrumental effects may introduce errors; re-diffraction of diffracted beams may lead to erroneous intensity values. It should not be forgotten that precision, in itself, does not ensure accuracy.

2.1.4 INSTRUMENTATION

X-ray diffraction may be performed on either powder or single crystal samples. The radiation used is generally monochromatic (i.e. of single wavelength).

2.1.4.1 Powder Diffraction

Powder studies have obvious advantages regarding sample availability; however, less information is derivable since there is random orientation of the crystallites: the three-dimensional diffraction data is effectively compressed onto one dimension. Powder diffractograms (or 'powder patterns') are recorded using either a camera (such as the Debye-Scherrer) or a powder diffractometer; the diffraction pattern is generally displayed as intensity as a function of diffraction angle, 2θ. Powder patterns of well-characterised structures are often used routinely as 'finger-prints' for phase identification. Analysis of unknown structures is less successful, especially for many-atom systems, because scattering power declines markedly at high 2θ.

2.1.4.2 Single Crystal Diffraction

In contrast, single crystal studies, whilst obviously requiring a well-defined single crystal sample, can lead to routine and accurate determination of the crystal structure. The two techniques available for recording single crystal diffraction data are, in many ways, complementary: these are photographic and diffractometric techniques.

(i) Photographic techniques. These are very useful for the calculation of lattice parameters, $a,b,c,\alpha,\beta,\gamma$, knowledge of which is required before a full structure determination can be attempted. The first step is the recording of an oscillation photograph. This shows the complete reciprocal lattice, but with each plane of

reciprocal lattice points projected onto one dimension (see Fig. 2.3). The crystal is aligned along one of its crystallographic axes (if these are discernible from the external morphology) and is then oscillated about this axis through an angle of typically ±30°. This oscillation moves the crystal into the different orientations required to satisfy Bragg's Law for different diffraction maxima. The diffraction pattern is recorded on a cylindrical film surrounding the sample. This technique immediately yields the direct lattice repeat distance along the chosen crystallographic axis, as shown in Fig. 2.3.

The Weissenberg technique gives a distorted image of the distribution of lattice points on one reciprocal lattice plane, *m* (see Fig. 2.3). This technique involves placing a cylindrical screen in front of the cylindrical film, so as to expose only the selected reciprocal lattice plane, and gearing the film so that it moves parallel to the axis of rotation of the crystal. However, Weissenberg photographs are distorted and often cannot be readily indexed. Retigraph (or de Jong-Bouman) and precession techniques both give undistorted recordings of a reciprocal lattice plane, using a plane film positioned parallel to the reciprocal lattice plane to be recorded. The de Jong-Bouman technique involves rotation of both the crystal and the film about the crystal mounting axis; a given layer is selected by displacing the layer screen along the crystal axis. In the precession technique, the crystal and layer screen are subjected to precessions with different centres; translating the screen and the film results in the selection of layers.

The complementary nature of the oscillation, de Jong-Bouman and precession techniques is clearly evident on considering Fig. 2.3. The oscillation photograph shows a projection through the complete reciprocal lattice, whereas the de Jong-Bouman and precession photographs show an individual layer, *m* (perpendicular to the plane of the page in Fig. 2.3). The complete set of lattice parameters may be obtained from the appropriate combination of oscillation, de Jong-Bouman and precession photographs. Systematically-absent reflections in any of these photographs can help to identify the space group.

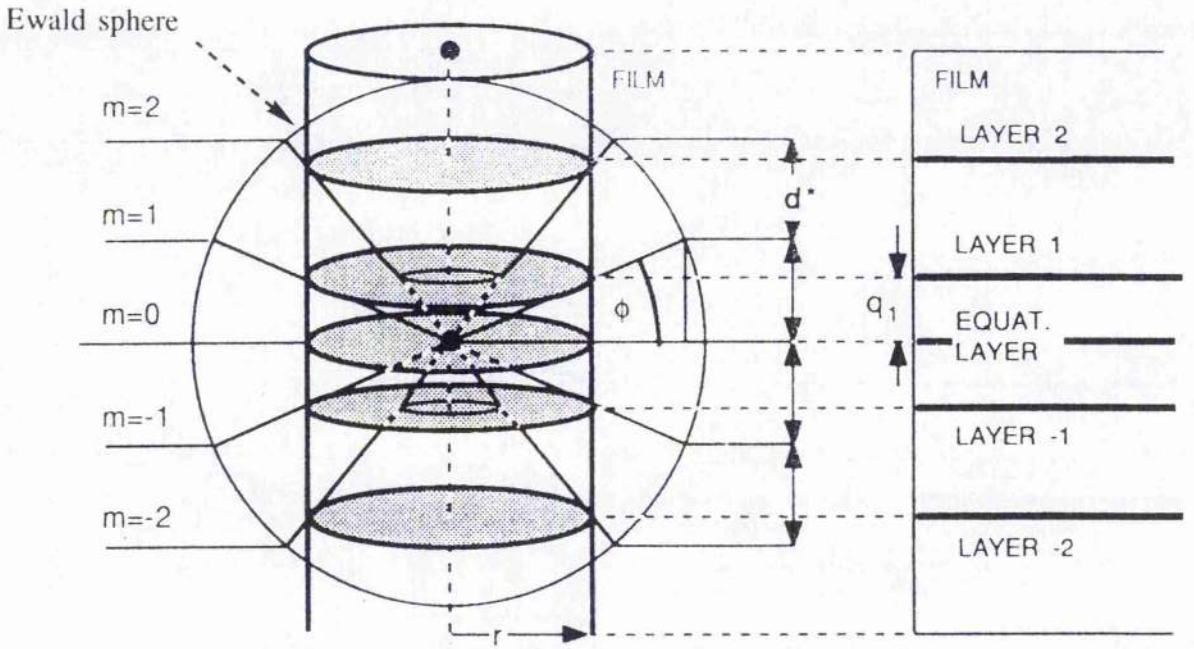

(a) Diffraction cones and layers, recorded using cylindrical film

(b) Diffraction layer lines on (unfolded) plane film

Fig. 2.3: Oscillation technique and use of Ewald sphere in calculation of direct lattice parameter, n (adapted from Eberhart [1991])

Let the radius of the Ewald sphere be L and the direct lattice parameter required be n. Other parameters are defined in the Figure.

By definition: $L = \frac{1}{\lambda}$ and $n = \frac{1}{d^*}$. From the Figure: $\tan\phi = \frac{q_1}{r}$ and $\sin\phi = \frac{d^*}{L}$. Hence: $n = \frac{\lambda}{\sin\left[\tan^{-1}\left(q_1/r\right)\right]}$

(ii) Diffractometric techniques. These are necessary for a full structure determination. A typical instrument is the four-circle diffractometer. The crystal is set in an arbitrary orientation and, the unit cell dimensions being known, the instrumental settings required to observe any particular (*hkl*) reflection are computed automatically. At each setting, the diffractometer systematically measures the intensities of all (*hkl*) within a specified range; the background intensity is also assessed. Measurement of selected reflections is repeated at regular time intervals to check for consistency during data collection. Appropriate corrections are applied to the accumulated intensity data for all (*hkl*) reflections before these data are used to solved the structure.

2.1.4.3 Techniques Used

A description of the x-ray diffraction techniques used in this work, and justification for those chosen, will be found in §2.3.2.

2.2 STRUCTURAL CHARACTERISTICS OF UREA INCLUSION COMPOUNDS

2.2.1 PRELIMINARY DISCUSSION

As described in Chapter 1, the urea inclusion compound is characterised by the packing of urea molecules in an extensively hydrogen-bonded array to form linear, parallel tunnels in which the guest molecules are located. The prerequisite features of the guest species were also discussed in Chapter 1.

We can consider the urea inclusion compound to be made up of distinguishable (although not independent) host and guest substructures. Each substructure comprises a basic structure which is subjected to an incommensurate modulation that arises from the presence of the other substructure of the urea inclusion compound. (The term 'incommensurate' will be defined below.) Each basic structure has conventional crystallographic three-dimensional periodicity. The incommensurate modulation describes structural perturbations to the basic structure arising from the interactions between host and guest. Thus, as discussed by Harris *et al* [Harris, 1988; Harris & Thomas, 1990a], the host substructure consists of a basic host structure which experiences an incommensurate modulation arising from its interaction with the guest species. This modulation self-evidently possesses the same periodicity as the basic guest structure. Similarly, the guest substructure comprises a basic guest structure which is subjected to an incommensurate modulation arising from its interaction with the host.

The periodic repeat distances of the basic host and guest structures along the channel axis, denoted c_h and c_g respectively, are generally incommensurate, i.e. no sufficiently small integers m and n can be found to satisfy the equation $mc_h = nc_g$.[†] Because of this incommensurability, the basic host and guest structures have different periodicities and often different space group symmetries.

[†] A more rigorous definition of incommensurability, considering energetics of host-guest interaction, is given by Rennie & Harris [1990]. However, for present purposes, the above definition suffices.

The nomenclature in this chapter will use 'h' to denote the host substructure, and 'g' to denote the guest substructure. Thus the basis lattice vectors for the basic host structure are $\mathbf{a}_h$, $\mathbf{b}_h$ and $\mathbf{c}_h$; those for the basic guest structure are $\mathbf{a}_g$, $\mathbf{b}_g$ and $\mathbf{c}_g$. The corresponding basis reciprocal lattice vectors are $\mathbf{a}^*_h$, $\mathbf{b}^*_h$ and $\mathbf{c}^*_h$, and $\mathbf{a}^*_g$, $\mathbf{b}^*_g$ and $\mathbf{c}^*_g$.

2.2.2 Characteristics of XRD Photographs for Urea Inclusion Compounds

Single crystal X-ray diffraction from any incommensurately modulated structure produces two sets of reflections: the 'main' reflections and the 'satellite' reflections. The positions of the main reflections are described by a reciprocal lattice which corresponds, in direct space, to the three-dimensional periodicity of the basic structure. The positions of the satellite reflections are dependent on the incommensurate modulation to this structure.

A urea inclusion compound consists of two incommensurately modulated structures: the host substructure and the guest substructure. Thus, an XRD oscillation photograph of a urea inclusion compound shows two components of x-ray scattering [Harris & Thomas, 1990a], as shown in Fig. 2.4:

(i) the 'h' diffraction pattern: a set of layer lines comprising intense, sharp, well-defined spots (diffraction maxima); the spacing between these layer lines corresponds to a periodicity, c_h, for the urea host structure of *ca.* 11.0 Å. Each point in the 'h' diffraction pattern represents both a main reflection from the host substructure and a satellite reflection from the guest substructure.

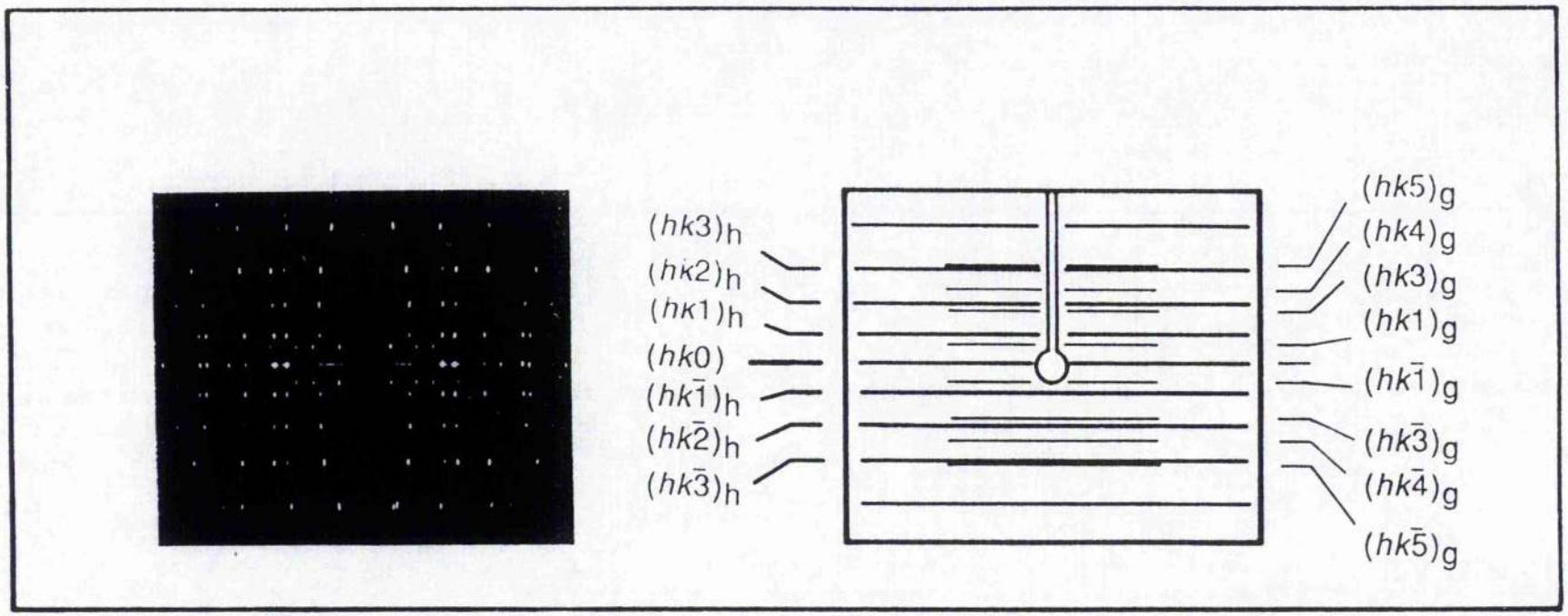

Fig. 2.4: Typical oscillation photograph for a hexagonal urea inclusion compound, showing the 'h' and the 'g' diffraction patterns

(1,10-dibromodecane/urea: from Harris *et al* [1991])

(ii) the 'g' diffraction pattern: a set of less intense, more closely spaced layer lines, which are either discrete spots or diffuse bands (or often comprise both), depending on the nature of guest ordering within the channels.[#] The periodicity, c_g, along the channel axis, as calculated from the spacing between these layer lines, is close to the predicted length of the guest molecule in its most extended (linear) conformation.[††] Each point in the 'g' diffraction pattern represents both a main reflection from the guest substructure and a satellite reflection from the host substructure.

2.2.3 Previous XRD Studies on Urea Inclusion Compounds

2.2.3.1 The Basic Host Structure

For the majority of urea inclusion compounds, the basic urea host structure remains invariant regardless of the guest species. It is this structure which fashions the external morphology of the inclusion crystals. As noted in Chapter 1, the space group and unit cell dimensions of the average basic host structure at room temperature have been determined [Schlenk, 1949; Smith, 1950 & 1952; Harris & Thomas, 1990a] by single crystal x-ray diffractometric studies: this structure belongs to the hexagonal crystal system and is chiral, with space group $P6_122$ and lattice parameters $a_h=b_h=8.218$ Å, $c_h=11.013$ Å, as determined by Harris & Thomas [1990a] for 1,10-dibromodecane/urea. Chatani *et al* [1977 & 1978] showed that the *n*-alkane/urea inclusion compounds undergo a phase transition: in the low-temperature phase, the basic host structure is orthorhombic, with probable space group $P2_12_12_1$. This was confirmed for *n*-hexadecane/urea by a detailed powder x-ray diffraction study [Harris *et al*, 1990].

Although the majority of urea inclusion compounds have this basic host structure, there are exceptions, especially where the guest molecules have short carbon

[#] Discrete spots in reciprocal space indicate three-dimensional ordering in direct space, whereas diffuse bands in reciprocal space indicate one-dimensional ordering in direct space.

[††] In fact, c_g is usually up to *ca.* 0.5 Å shorter than the predicted 'van der Waals length' of the all-*trans* guest molecule [Laves *et al*, 1965], indicating that neighbouring guest molecules are subject to longitudinal repulsive forces along the channel [Rennie & Harris, 1992].

chains. Such exceptions include 1,6-dibromohexane/urea [Schlenk, 1949; Otto, 1972], the structure of which is discussed in detail later in this chapter.

2.2.3.2 The Basic Guest Structure

Because the average basic host structure has been so fully elucidated, we have concentrated our attention in this work on the properties of the basic guest structure. The guest molecules usually exhibit substantial dynamic disorder at room temperature, undergoing translations along and reorientations about the channel axis (see subsequent chapters), but show sufficient positional ordering for an average three-dimensional lattice to be defined. The characteristics of the basic guest structure depend on the identity of the guest. However, some generalisations can be made. Single crystal photographic XRD studies [Harris & Hollingsworth, 1990; Harris & Thomas, 1990b] on diacyl peroxide/urea inclusion compounds have shown that:

(i) The periodic repeat distance, c_g, of the guest along the channel axis is dependent on the length of the guest molecule and is generally incommensurate with the periodic repeat distance, c_h, of the basic host structure along the channel axis.

(ii) The basic guest structure shows pronounced inhomogeneity. Each single crystal contains both:

a) Regions in which the guest molecules are ordered only in one dimension (along the channel axis). The 'g' diffraction pattern gives rise to diffuse bands in the oscillation photograph; in such regions there is only *intrachannel* ordering of guest molecules.

b) Regions in which the guest molecules are three-dimensionally ordered (both along the channel axis and with respect to the guests in adjacent channels). Here the 'g' diffraction pattern gives discrete spots in the oscillation photograph (see Fig. 2.4); in such regions there is *both* intrachannel and interchannel ordering. The basic guest structure in these regions is monoclinic with probable space group C2 or C2/m [Harris & Hollingsworth, 1990].

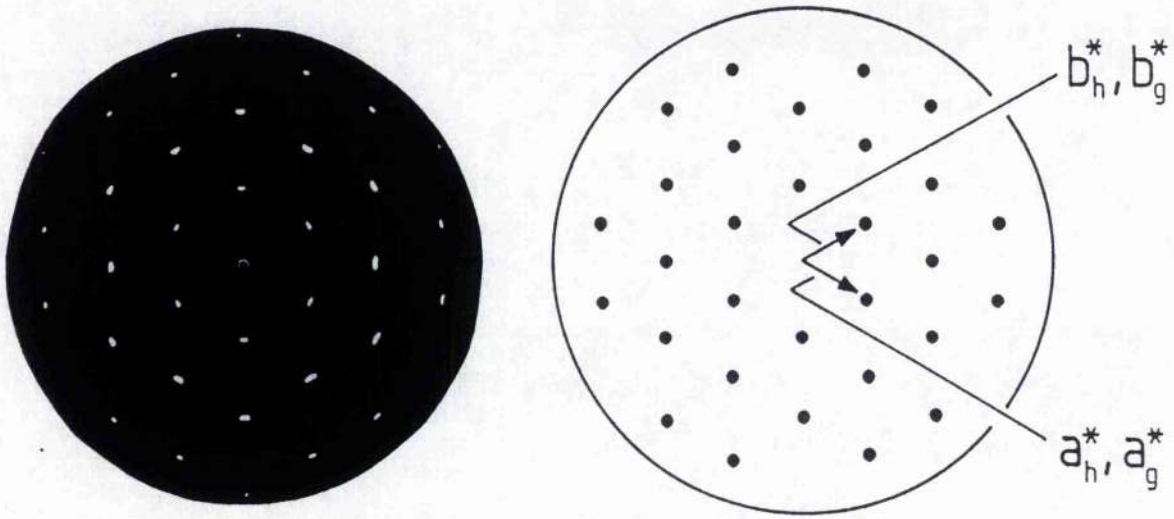

Fig. 2.5: For dioctanoyl peroxide/urea: de Jong-Bouman (*hk*0) photograph, showing the (*hk*0) reciprocal lattice net [from Harris & Hollingsworth, 1990]

Fig 2.6: De Jong-Bouman photograph for lauroyl peroxide/urea:
[from Harris & Hollingsworth, 1990]

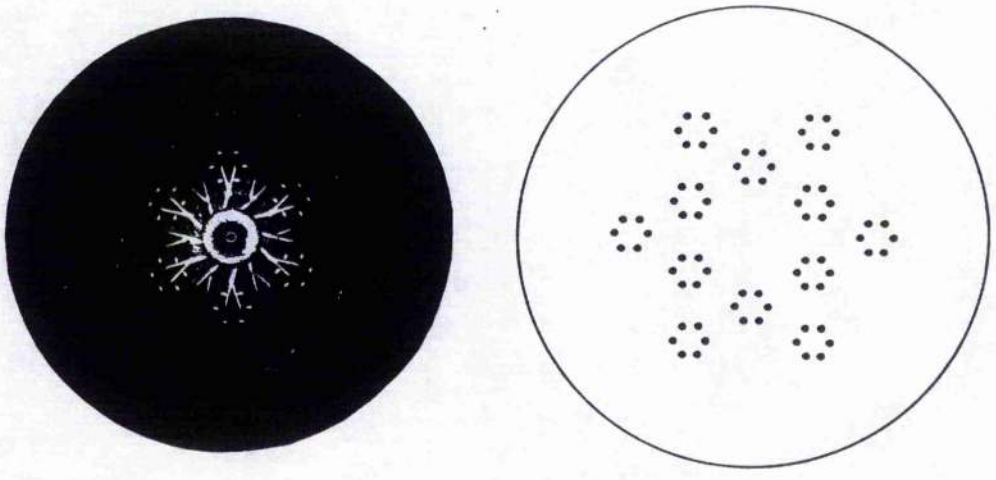

(a) De Jong-Bouman $(hk1)_g$ photograph

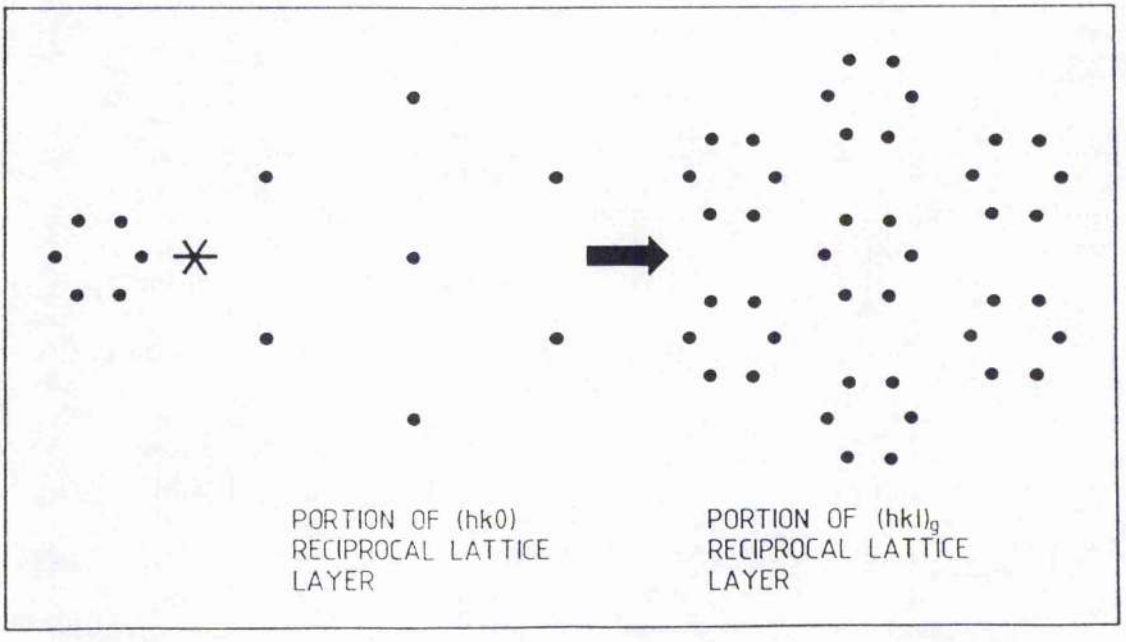

(b) Interpretation of de Jong-Bouman $(hk1)_g$ photograph as a convolution

Figs. 2.5 and 2.6a show typical de Jong-Bouman ($hk0$) and $(hk1)_g$ photographs, respectively, for diacyl peroxide/urea inclusion compounds. Each point in the ($hk0$) photograph is the superposition of an 'h' and a 'g' reflection. This diffraction pattern, which is termed the ($hk0$) reciprocal lattice net, is essentially identical for all hexagonal urea inclusion compounds. The $(hk1)_g$ diffraction pattern is a repeating array of hexagons: this may be regarded as a convolution between a set of six points at the corners of a hexagon and an array identical to the ($hk0$) reciprocal lattice net (see Fig. 2.6b). The set of six points represents six alternative positions of the $(001)_g$ reciprocal lattice point. Thus the 'g' diffraction pattern arises from six identical reciprocal lattices related by 60° rotation about c_h^*. These correspond, in direct space, to the six different domains of the basic guest structure which exist in the three-dimensionally ordered regions of the crystal. The relative packing of the guest molecules within each domain is the same, the six domains differing only in orientation by 60° rotation about the channel axis. These concepts are discussed in more detail elsewhere [Harris, 1988; Harris & Hollingsworth, 1990].

We define an offset, Δ_g, to be the distance along the channel axis between equivalent points of two guest molecules in adjacent channels as illustrated schematically in Fig. 2.7. The diacyl peroxide guest, $\{CH_3(CH_2)_{[n-2]}COO\}_2$, shows a constant offset (within experimental error) of $\Delta_g \approx 4.6$ Å, irrespective of the length of the guest molecule (i.e. irrespective of the value of c_g), as shown in Table 2.1 [Harris & Hollingsworth, 1990]. This suggests that the relative interchannel packing of the guest molecules is controlled solely by some property of the diacyl peroxide functional group.

PEROXIDE GUEST	n	c_g/Å	Δ_g/Å
dioctanoyl	8	23.9	4.63
diundecanoyl	11	31.5	4.59
lauroyl	12	34.2	4.57

Table 2.1: Values of c_g and Δ_g for diacyl peroxide guests

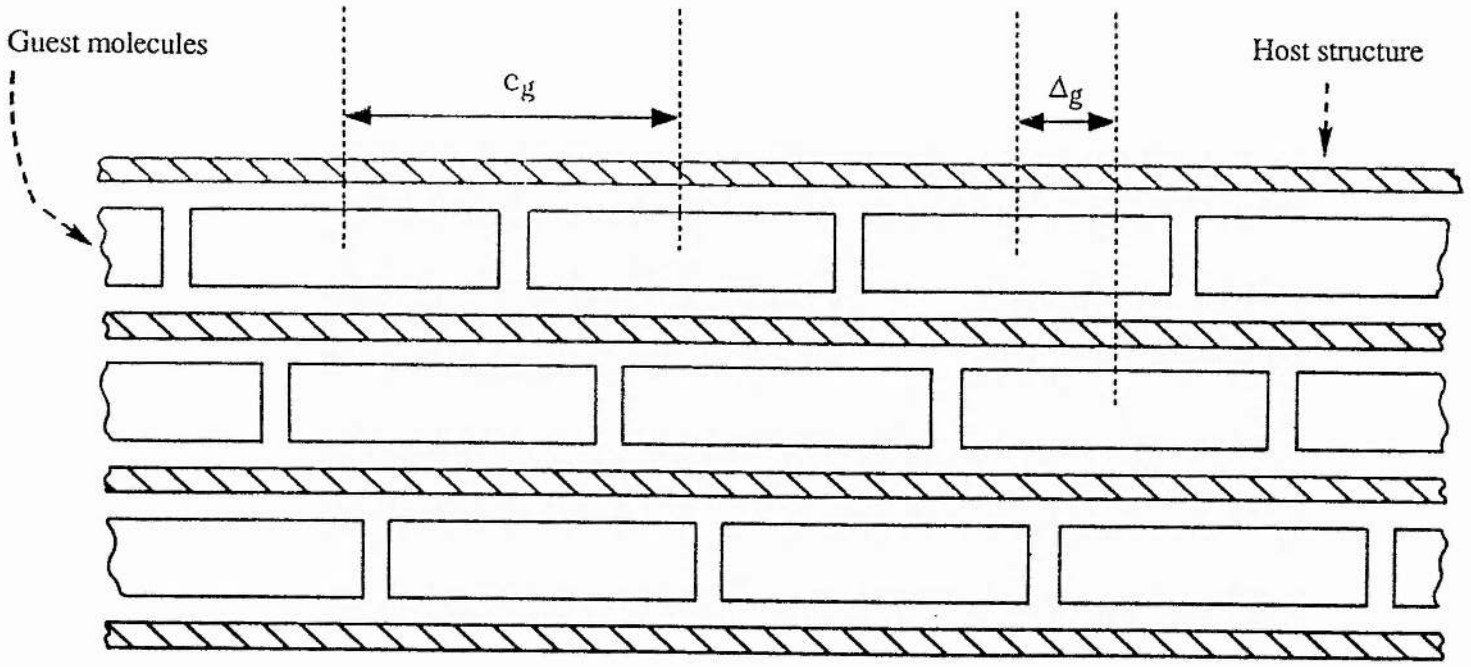

Fig. 2.7: Definitions of c_g and Δ_g within a schematic two-dimensional representation of a urea inclusion compound

Turning to other guest species in their urea inclusion compounds, we note that Δ_g values have been determined [Harris, 1988; Harris & Thomas, 1990a] for *n*-hexadecane/urea and *bis*-(6-bromohexanoyl) peroxide/urea. The *n*-hexadecane guest, $CH_3(CH_2)_{14}CH_3$, has Δ_g=0 in the three-dimensionally ordered regions, i.e. the guest molecules are at the same relative 'heights' in all channels. The reason for this is not clear (the compound is incommensurate). To further complicate the issue, Forst *et al* [1986, 1987 & 1990] have concluded that this inclusion compound has no three-dimensional guest ordering whatsoever. The Δ_g=0 mode of guest ordering has subsequently been found in other $CH_3(CH_2)_nCH_3$/urea inclusion compounds, where n=9-14 [Shannon IJ & Harris KDM, in preparation; also Harris, 1993].

The acid anhydride guest family, $CH_3(CH_2)_nCO.O.CO.(CH_2)_nCH_3$, of urea inclusion compounds shows three-dimensional guest ordering with Δ_g=0 for n=3,4 and n=6-10, but for n=5 the basic guest structure is anomalous with Δ_g=2.3 Å [Stainton NM & Harris KDM, unpublished work]. The reason for this anomaly is unclear.

The *bis*-(6-bromohexanoyl) peroxide guest. $Br(CH_2)_5(CO)OO(OC)(CH_2)_5Br$, is noteworthy in that it combines the terminal dibromo and the diacyl peroxide functional groups. However, the inclusion compound was found to exhibit predominantly one-dimensional guest ordering [Harris, 1988; Harris & Thomas, 1990a]: it is possible that the 'competition' between these two functional groups to dominate the mode of three-dimensional ordering merely achieved total loss of ordering.

2.2.4 OBJECTIVES

A preliminary investigation by Harris [1988] on 1,10-dibromodecane/urea indicated that $\Delta_g = c_g/3$. This implies that, in this case, unlike that for the diacyl peroxide/urea and *n*-alkane/urea inclusion systems, the value of Δ_g depends upon the periodic repeat distance, c_g, of the guest molecule along the channel axis, i.e. it depends upon the length of the guest molecule. The work described in this chapter focuses on the α,ω-dibromo-*n*-alkane family of guests; its aim was to investigate the generality of the above hypothesis for this family of urea inclusion compounds. Other α,ω-dihalo-*n*-alkane and 1-bromo-*n*-alkane guests have also been studied for comparison. Specific objectives included:

(1) To determine the lattice parameters, a_g, b_g, c_g, α_g, β_g, γ_g, of the basic guest structures.

(2) To determine the extent of guest ordering: one-dimensional (solely intrachannel) or three-dimensional (both intrachannel and interchannel).

(3) To determine, for the three-dimensionally ordered regions, the size of the offset, Δ_g, and the relation (if any) between Δ_g and c_g.

Some of the work discussed in this chapter has been published [Harris *et al.* 1991].

2.3 SYSTEMS STUDIED AND TECHNIQUES USED

2.3.1 UREA INCLUSION COMPOUNDS STUDIED

The urea inclusion compounds to be discussed in this chapter were prepared and characterised according to the methods detailed in Appendix A. These compounds were:

α,ω-dibromoalkane/urea:	$Br(CH_2)_nBr$	n=6-12
α,ω-diiodoalkane/urea:	$I(CH_2)_nI$	n=10
α,ω-dichloroalkane/urea:	$Cl(CH_2)_nCl$	n=10
1-bromoalkane/urea:	$Br(CH_2)_nCH_3$	n=9-12

2.3.2 XRD TECHNIQUES USED

Single crystal x-ray diffraction was used to investigate the structural properties of these UICs. The basic guest structures cannot be fully determined, due to (i) the incommensurate nature of the UICs and (ii) the guest mobility, and hence partial disorder of the guest molecules within the UICs. Therefore, photographic techniques (oscillation and de Jong-Bouman) were used in order to calculate the lattice parameters of the basic guest structures and to study aspects of the guest molecular packing. The crystals selected had dimensions *ca.* 0.2x0.2x0.8 mm^3; these were mounted along their channel axes (crystallographic **c** axes) onto glass fibres. Single crystal x-ray diffraction photographs were recorded using Ni-filtered Cu-Kα radiation (wavelength 1.5418 Å) as follows.

(i) Oscillation photographs were recorded for all samples: the angle of oscillation was ±30° about the channel axis, **c**. An Enraf-Nonius oscillation camera was used (this camera had previously been calibrated using Fisons Analar ammonium oxalate, 99.5% minimum assay.)

(ii) Where the oscillation photograph indicated that three-dimensional guest ordering was present, this was investigated further by selecting the (*hk*0) and $(hk1)_g$ layers of the guest reciprocal lattice using de Jong-Bouman photography. The instrument used for this was a Stoe Reciprocal Lattice Explorer.

Crystals of 1,6-dibromohexane/urea did not possess the long hexagonal needle-like morphology that is usual for urea inclusion compounds: this suggested that the structure was different from that of the other urea inclusion compounds studied. Preliminary photographic x-ray diffraction studies were carried out using a crystal of dimensions *ca.* 0.5x0.5x0.2 mm^3. Oscillation, de Jong-Bouman and precession techniques were used; the crystal was aligned along an arbitrarily-chosen crystallographic axis. A full structure determination was then performed, using data collected on an Enraf-Nonius CAD4 single crystal diffractometer with graphite-monochromated Mo-Kα radiation of wavelength 0.71069 Å. The data were collected, at room temperature, by Professor Mark Hollingsworth and Dr Bernard Santasiero at the University of Alberta, Edmonton. These data were then used by us to carry out the structure solution and refinement, details of which are given in §2.4.2.3, part (I).

2.4 RESULTS AND DISCUSSION

2.4.1 PHOTOGRAPHIC SINGLE CRYSTAL XRD

2.4.1.1 'h' Diffraction Pattern

For all the urea inclusion compounds studied (except 1,6-dibromohexane/urea), the 'h' diffraction pattern was found to be essentially invariant, in accordance with previous work [Harris, 1988; Harris & Thomas, 1990a]. The 'h' diffraction pattern was readily identifiable as such on the oscillation photograph: as expected, the 'h' layer lines comprised sharp, discrete reflections which were generally much more intense than those of the 'g' diffraction pattern.

2.4.1.2 'g' Diffraction Pattern

(1) α,ω-dibromoalkane guests: $Br(CH_2)_nBr$: n=7-10

Qualitatively, all the 'g' diffraction patterns were the same, varying only in the spacing between reciprocal lattice layers. Channel-axis oscillation photographs for the four compounds are shown in Fig. 2.8. In each case, the 'g' diffraction pattern contains both discrete and diffuse scattering. The diffuse scattering (sheets perpendicular to the channel axis) indicates that some regions of the crystal have solely one-dimensional ordering of the guest molecules (along the channel axis), i.e. intrachannel ordering. However, the presence of discrete reflections ('spots') indicates that other regions of the crystal have three-dimensional ordering of the guest molecules, i.e. both intrachannel and interchannel ordering. This is analogous to the situation with the diacyl peroxide guests.

Fig. 2.8: Channel-axis oscillation photographs

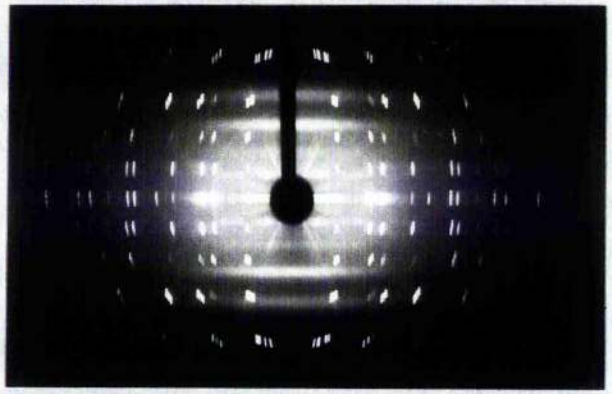

(a) 1,7-dibromoheptane/urea

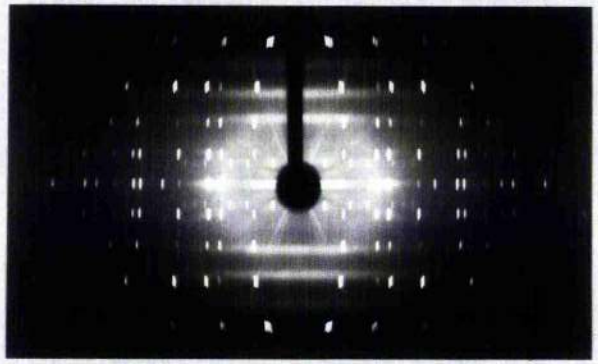

(b) 1,8-dibromooctane/urea

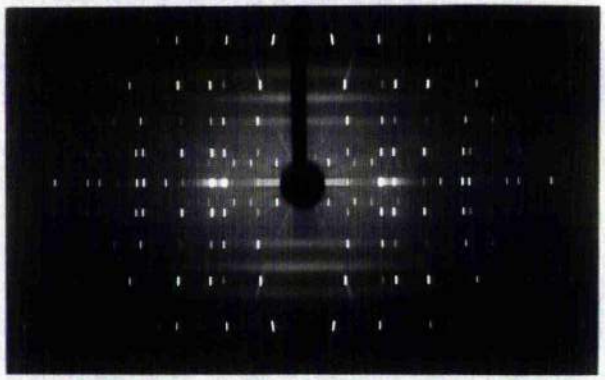

(c) 1,9-dibromononane/urea

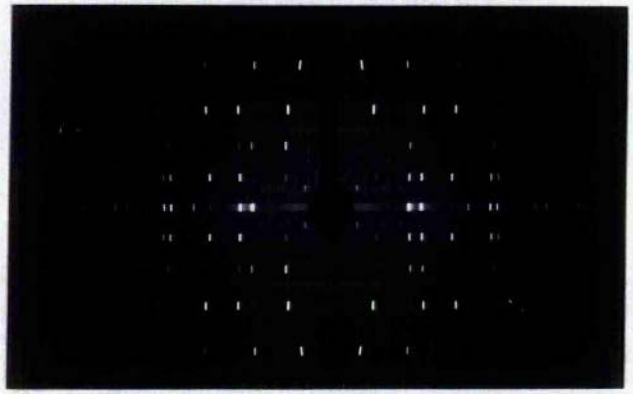

(d) 1,10-dibromodecane/urea

$Br(CH_2)_nBr$ guest:	n=7	n=8	n=9	n=10
$\|a_g\|$ / Å	9.45	9.69	10.05	10.19
$\|b_g\|$ / Å	9.45	9.69	10.05	10.19
$\|c_g\|$ / Å	14.1	15.5	17.4	18.1
α_g / °	119.5	122.0	125.2	126.3
β_g / °	119.5	122.0	125.2	126.3
γ_g / °	97.8	94.5	90.1	88.5

Table 2.2: Lattice parameters for the basic guest structure of α,ω-dibromoalkane/urea inclusion compounds. Appromixate errors, δ, in these values are:

For $|a_g|$, $|b_g|$: $\delta = \pm 0.1$ Å

For $|c_g|$: $\delta = \pm 0.4$ Å

For α_g, β_g, γ_g: $\delta = \pm 1°$

$Br(CH_2)_nBr$ guest:	n=7	n=8	n=9	n=10
$\|c_g\|$ / Å	14.1	15.5	17.4	18.1
Δ_g / Å	4.65	5.13	5.79	6.03
$3\Delta_g$ / Å	13.95	15.39	17.37	18.09

Table 2.3: Values of $|c_g|$ and Δ_g for the basic guest structure of α,ω-dibromoalkane/urea inclusion compounds.

The repeat distance, c_g, of the guest molecules along the channel axis was calculated directly from the distance between layers of the oscillation photograph (using the equation derived in Fig. 2.3). Further analysis of the 'g' diffraction pattern using de Jong-Bouman photography led to calculation of the other lattice parameters of the basic guest structure and also of the offset, Δ_g, along the channel axis between guest molecules in adjacent channels. The general methodology used for this calculation is detailed by Harris & Hollingsworth [1990: Appendix therein]. The full set of lattice parameters is listed in Table 2.2, and the values of c_g and Δ_g are given in Table 2.3. As expected, the c_g values are close to the calculated lengths of the guest molecules in the extended conformations that they are required to adopt within the channel of the urea inclusion compound. Notwithstanding experimental error, it is evident that the value of Δ_g is given by the exact relationship $\Delta_g=c_g/3$: indeed, this is required by the crystal symmetry (see below).

As expected, the de Jong-Bouman ($hk0$) photographs were essentially identical for all four inclusion compounds: the positions of the reflections were the same although their relative intensities may have differed slightly from compound to compound. A typical ($hk0$) photograph is shown in Fig. 2.9. The four $(hk1)_g$ photographs were also qualitatively identical: an example is shown in Fig. 2.10a. The $(hk1)_g$ photograph contains twice as many reflections per unit area as the ($hk0$) reciprocal lattice net. Furthermore, the positions of the $(hk1)_g$ reflections can be rationalised as a convolution between a pair of points and the ($hk0$) reciprocal lattice net: this concept is illustrated by Fig. 2.10b. (This interpretation follows the methodology used by Harris [1988] and Harris & Hollingsworth [1990] for discussion of the diacyl peroxide/urea inclusion compounds, as outlined earlier.) We deduce that:

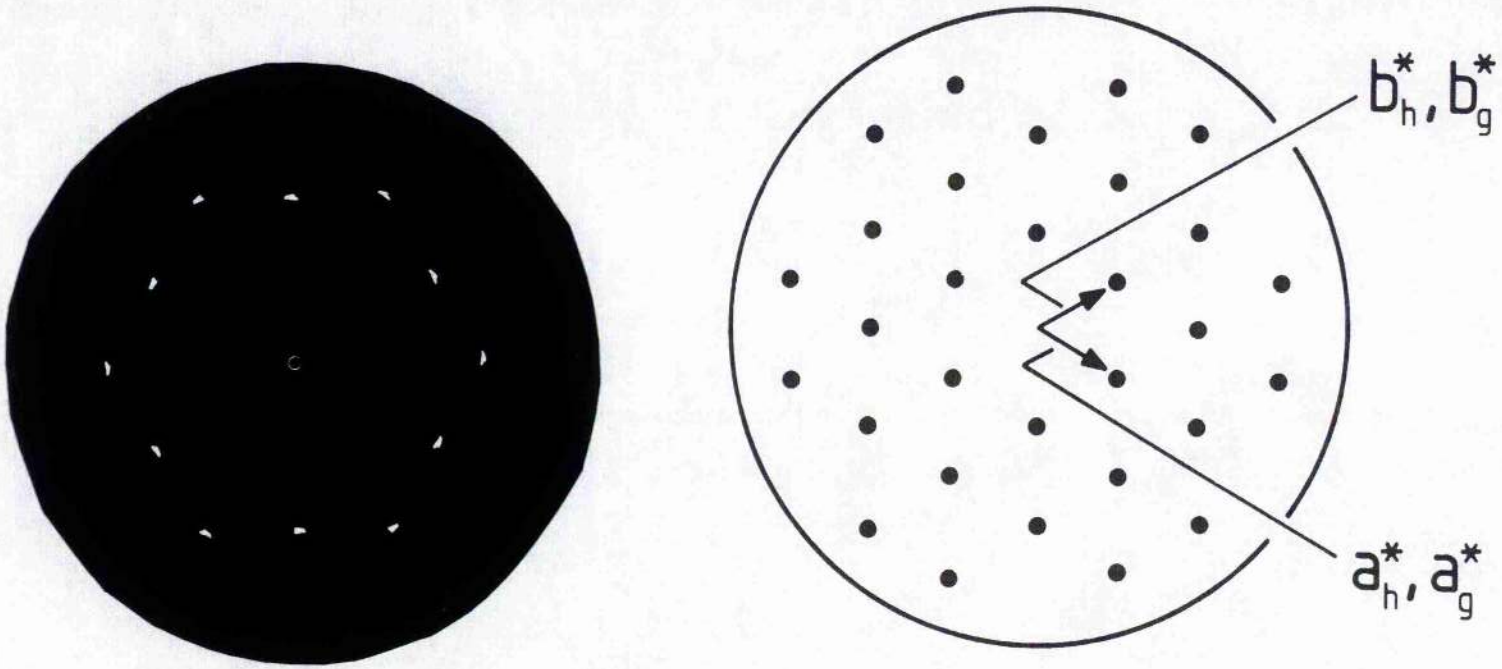

Fig. 2.9: De Jong-Bouman (*hk*0) photograph for 1,10-dibromodecane/urea

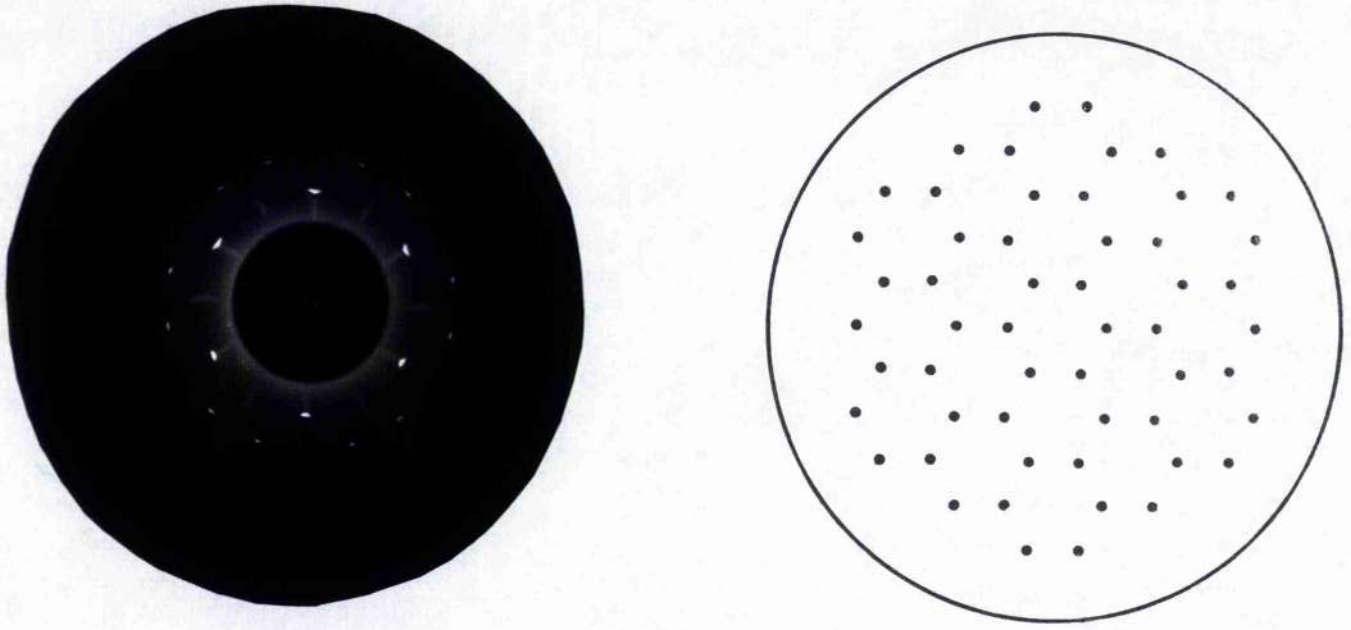

Fig. 2.10a: De Jong-Bouman $(hk1)_g$ photograph for 1,10-dibromodecane/urea

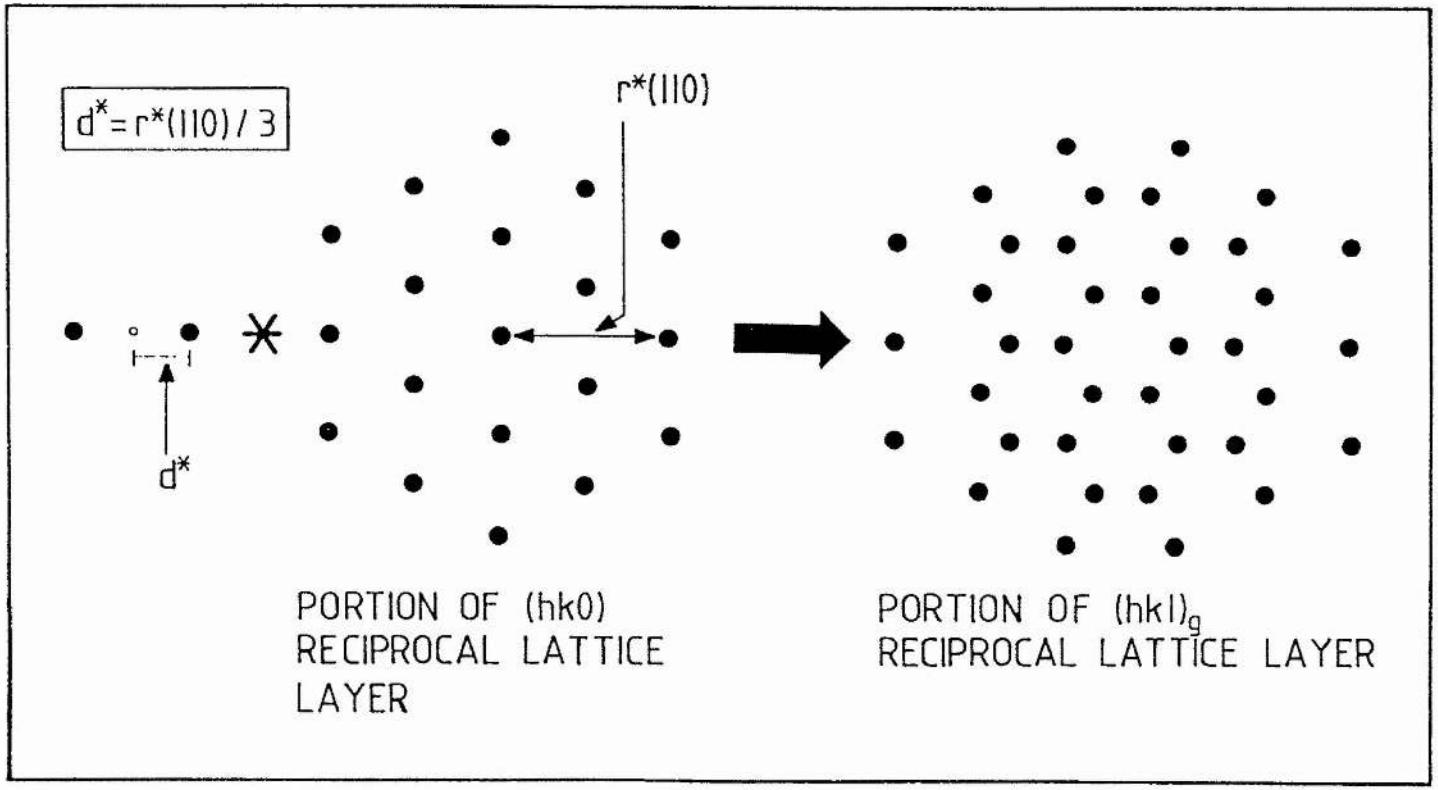

Fig. 2.10b: Interpretation of the $(hk1)_g$ photograph as a convolution between a pair of points and the $(hk0)$ reciprocal lattice net. The fact that $d^*=r^*_{(110)}/3$ is a consequence of the rhombohedral lattice symmetry of the basic guest structure.

(i) there are two domains of the basic guest structure

(ii) the lattices which define the periodicities of these domains differ in orientation by 180° rotation about the channel axis, but are otherwise identical

(iii) the metric symmetry of each of these lattices is rhombohedral (although a general triclinic system is used initially in the discussion below).

The relative packing of the guest molecules in each domain can be illustrated using a numerical labelling scheme, as shown in Fig. 2.11. This is based upon a triclinic description of the basic guest structure. Each channel is labelled with a value r according to the relative height of the guest molecules within it. Thus r signifies that the relative z-coordinates of the guest molecules in that channel are $r\Delta_g+sc_g$ (where r and s are integers, and s varies sequentially for the guest molecules along a given channel).

If indexed on the basis of a hexagonal reciprocal lattice, the 'g' reflections can be subdivided into two sets, satisfying the following conditions:

Set (1): $(hkl)_g$: $-h + k + l = 3n$ (n = integer)

Set (2): $(hkl)_g$: $h - k + l = 3n$ (n = integer)

When $l=3m$ (m=integer), each 'g' reflection satisfies both conditions, hence each $(hk0)$ 'g' reflection is the superposition of a reflection from Set (1) and a reflection from Set (2). When $l\neq3m$ (e.g. $l=1$), a reflection that satisfies one condition does not satisfy the other, hence reflections from Sets (1) and (2) occur in different positions. This accounts for the presence of twice as many observed reflections in $(hk1)_g$ as in $(hk0)$. These two sets of conditions allow the hexagonal lattice to be described alternatively as a rhombohedral lattice with two domains: the obverse setting and the reverse setting. The obverse setting corresponds to Set (1) and the reverse setting to Set (2).

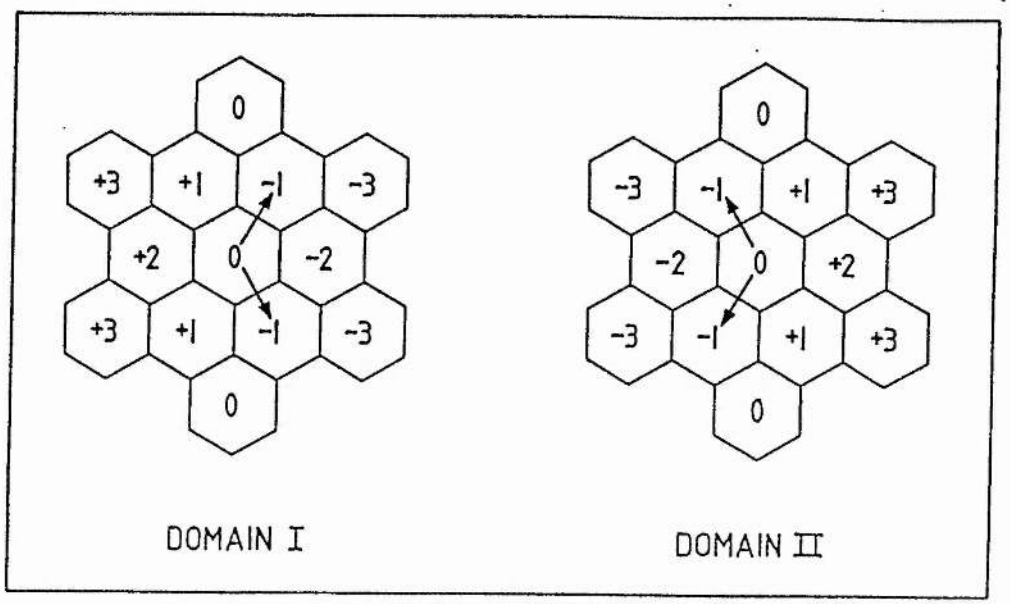

Fig. 2.11: Definition of the two domains of the basic guest structure, based on a triclinic description. The vectors shown are $\mathbf{a}_g^t$ and $\mathbf{b}_g^t$, which are directed beneath the plane of the page. The vector $\mathbf{c}_g^t$ is directed outwards perpendicular to the page.

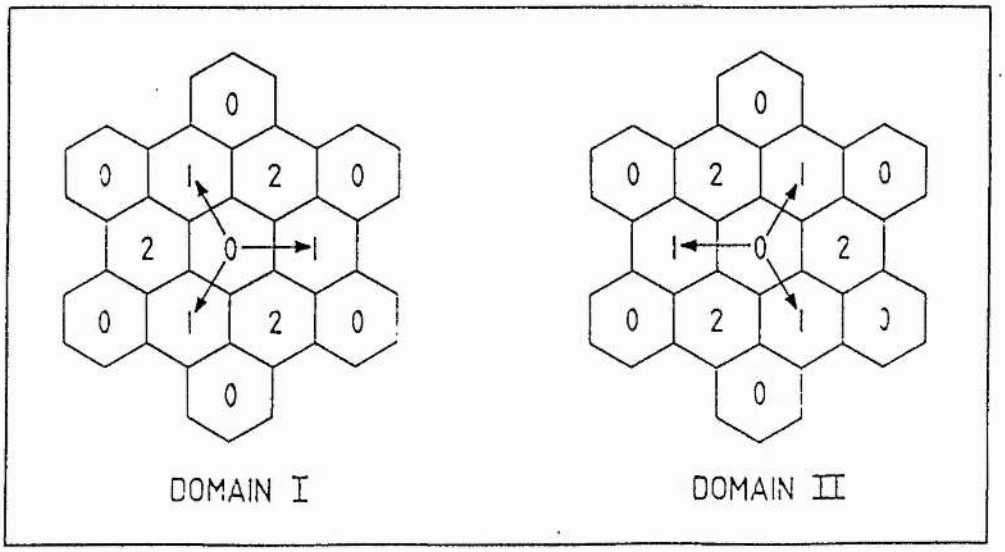

Fig. 2.12: Definition of the two domains of the basic guest structure, representing the obverse and reverse settings of the rhombohedral description. The vectors shown are $\mathbf{a}_g^r$, $\mathbf{b}_g^r$ and $\mathbf{c}_g^r$: these are directed outwards from the plane of the page.

The rhombohedral description requires that the offset, Δ_g, is given exactly by: $\Delta_g=c_g/3$. We can thus transform the triclinic representation of relative guest molecule packing within the two domains, shown in Fig. 2.11, to a rhombohedral system. Every channel labelled $(3p+q)$ in Fig. 2.11 (p=integer; q=0,1 or 2) contains guest molecules in exactly the same positions as every channel labelled q. Relabelling all such channels as q gives a packing that can be recognised as rhombohedral, as shown in Fig. 2.12.

Although we have shown here that the metric symmetry of the lattice describing the basic guest structure is rhombohedral, this does *not* prove that the structure itself is rhombohedral. Nevertheless, the Laue group of the 'g' diffraction pattern arising from each domain of the basic guest structure is probably $\bar{3}$m. This suggests that the structural symmetry *is* described, at least on a space- and time-average, by a rhombohedral space group. Since the highest possible point symmetry of an individual α,ω-dibromoalkane molecule is 2/m, the symmetry at the local level must be lower than rhombohedral. However, static positional disorder and/or dynamic disorder (see Chapters 4 & 5) could explain the fact that the average symmetry is rhombohedral.

It is instructive to contrast these results with previous work (discussed in §2.2.3.2). The diacyl peroxide/urea inclusion compounds studied contain six monoclinic domains of the basic guest structure: these domains are identical in all but orientation, each being offset from the others by 60° rotation about the channel axis. The value of Δ_g is constant (4.6 Å). For the n-alkane/urea inclusion compounds studied, the value of Δ_g is also constant (Δ_g=0). Both these urea inclusion families appear to belong to a mode of guest molecule packing for which Δ_g is independent of the repeat distance, c_g, of the basic guest structure and so effectively independent of the length of the guest molecule.

Clearly, the family of α,ω-dibromoalkane/urea inclusion compounds represents a new mode of guest molecule packing, in which Δ_g varies linearly with c_g. So, what are the factors governing the mode of interchannel ordering of the guest molecules in urea inclusion compounds? Because of the incommensurate nature of UICs, it is clear

that specific host-guest interactions cannot be responsible. However, little is known concerning the method in which information regarding the siting of a guest molecule in one channel is transmitted to the neighbouring channels. Some hypotheses include:

(i) there may be some direct electrostatic interaction between the guest molecules in neighbouring channels. These interactions would have to be effective over large distances (*ca.* ≥8Å): however, this could indeed be the case for the diacyl peroxide guests, which have a highly polar (CO)OO(OC) functional group.

(ii) there may be an indirect interaction between guest molecules in neighbouring channels transmitted via their mutual interaction with the urea molecules which form the channel wall. Included in this is the possibility that bulky substituents on the guest species could distort the channel wall, creating favoured positions for the guest molecules: in the case of the α,ω-dibromoalkanes, the terminal bromines may be viewed as bulky substituents which could play such a role.

(iii) kinetic factors relating to crystal growth may have an influence on the mode of interchannel guest ordering. However, this seems unlikely, given that two different preparation methods for 1,10-dibromodecane/urea (ours and that of Harris [1988]) led to the same mode of ordering. Their dynamic properties also suggest that, whatever the method of preparation, the guest molecules have scope for 'relaxing' into the favoured mode of packing.

If the guest ordering is controlled by factors (i) and (ii) above, the observed value of Δ_g will represent the optimum interaction between a guest molecule in one channel and the guest molecules in surrounding channels. Evidently, the identity and position of the functional group are relevant factors. If a guest molecule's functional group interacts significantly with more than one functional group in each adjacent channel, we could expect the optimum value of Δ_g to depend on the periodic repeat distance, c_g. However, if there is interaction with just one functional group, we could expect Δ_g to be constant. For guests of short molecular length, many interacting neighbours is more probable, whereas for longer guests just one interacting neighbour may be expected. This suggests that each family of urea inclusion compounds

(excluding the *n*-alkane guests, which do not possess a functional group as such) may have a 'crossover point' with respect to the mode of guest molecular ordering. The α,ω-dibromoalkanes we have studied are relatively short molecules, whereas the diacyl peroxides discussed were of much longer chain length. It is possible that within the same urea inclusion family, short guest molecules show ordering for which Δ_g is dependent on c_g, whereas longer guest molecules show a constant Δ_g. However, this theory does not appear to hold for the acid anhydride guest family, for which relatively short guest molecules have been shown to have a constant Δ_g.

(2) Other dibromoalkane guests $Br(CH_2)_nBr$

(i) n=6

It was found that the $Br(CH_2)_6Br$/urea inclusion compound has a completely different crystal structure from the higher members of the series. A full structure determination was therefore carried out, the results of which are described and discussed in §2.4.2.

(ii) n=11-12

These compounds showed diffuse bands only in the guest diffraction pattern of the oscillation photographs, indicating solely intrachannel (one-dimensional) ordering. A typical oscillation photograph is shown in Fig. 2.13a.

(3) Other dihaloalkane guests

(i) 1,10-diiododecane: $I(CH_2)_{10}I$

This guest showed the same structural behaviour as that of the n=7-10 family of dibromoalkane guests: three-dimensional ordering with $\Delta_g=c_g/3$:

$$c_g=19.1\ (\pm0.4)\ \text{Å}$$

$$\Delta_g=6.3\ (\pm0.2)\ \text{Å}$$

The oscillation photograph is shown in Fig. 2.13b and the full set of lattice parameters for the basic guest structure is listed in Table 2.4.

Fig. 2.13: Channel-axis oscillation photographs for various urea inclusion compounds

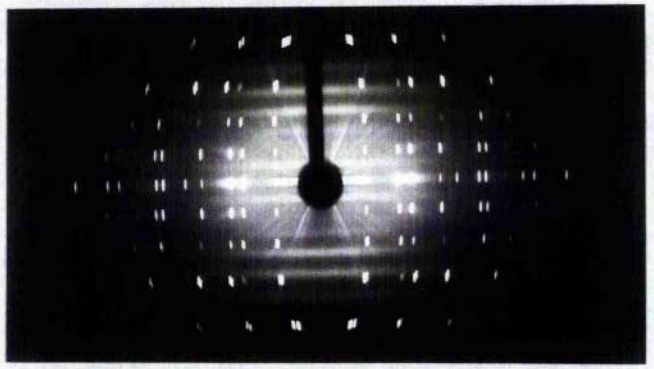

(a) 1,11-dibromoundecane/urea

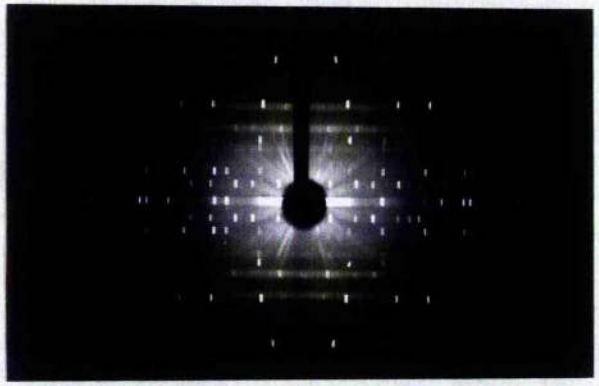

(b) 1,10-diiododecane/urea

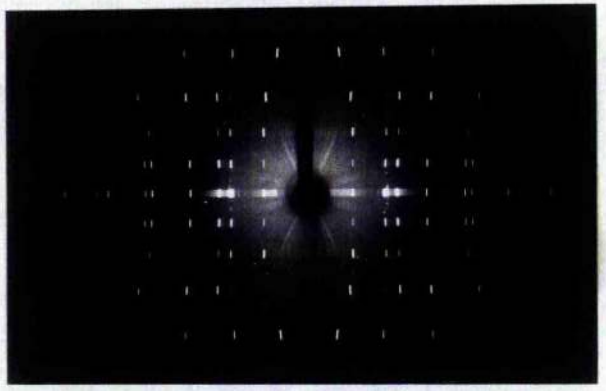

(c) 1,10-dichlorodecane/urea

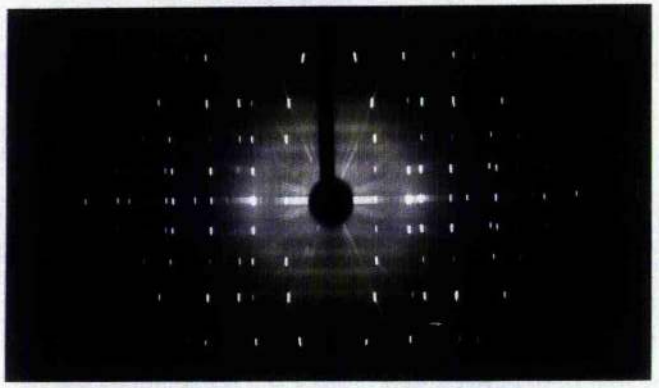

(d) 1-bromododecane/urea

Parameter	Value	Error, δ
$\|a_g\|$ / Å	10.37	±0.1
$\|b_g\|$ / Å	10.37	±0.1
$\|c_g\|$ / Å	19.1	±1.4
α_g / °	127.6	±1
β_g / °	127.6	±1
γ_g / °	86.7	±1

Table 2.4: Lattice parameters for the basic guest structure of 1,10–diiododecane/urea

(ii) 1,10-dichlorodecane: $Cl(CH_2)_{10}Cl$

The oscillation photograph for this urea inclusion compound (see Fig. 2.13c) showed only diffuse bands in the 'g' diffraction pattern, indicating no interchannel ordering (i.e. the basic guest structure is ordered only in one-dimension, along the channel axis).

(4) 1-bromoalkane guests: $Br(CH_2)_nCH_3$: n=9-12

These guests showed only diffuse bands in the guest diffraction pattern, indicating solely intrachannel ordering of guest molecules. A typical oscillation photograph is shown in Fig. 2.13d.

In the light of these results, certain questions present themselves.

(i) Why do the n=11-12 α,ω-dibromoalkane guests lack three-dimensional ordering? No explanation is apparent, unless the crystals were contaminated by solvent co-inclusion. Due to the low solubilities of 1,11-dibromoundecane and 1,12-dibromododecane in methanol, ethanol had been used as the preparation solvent: this may have a higher propensity to be co-included in the urea channels.

thus disrupting the guest molecular ordering. Nevertheless, solution state NMR of these UICs dissolved in d_6-dimethylsulphoxide showed that solvent inclusion was negligible.

(ii) Why does the 1,10-diiododecane guest show the same $\Delta_g=c_g/3$ mode of ordering as for the dibromoalkane guests? It is plausible that the bulky iodine substituents, of van der Waals radius 2.15 Å (c.f. bromine: 1.95 Å; chlorine: 1.80 Å [Atkins, 1986]), distort the urea channel wall, leading to a 'locking-in' of guest molecules. Therefore, as the guest molecules are relatively short, an ordering mode dependent on the guest repeat distance, c_g, may be expected.

(iii) Why should the 1,10-dichlorodecane guest not show any three-dimensional ordering? It may be that there are no dominant features of the guest functional groups which can dictate any 'locking-in' mechanism compatible with either of the modes of ordering cited above. However, the *n*-alkane guests do not have well-defined functional groups, as such, and yet they *do* show three-dimensional ordering, with $\Delta_g=0$.

(iv) The lack of three-dimensional ordering for the 1-bromoalkane guests is a more complex issue as the guest molecules are unsymmetric. The relative orientation of adjacent molecules along the same channel (i.e. head-to-head or head-to-tail) becomes relevant and may be responsible for lack of three-dimensional ordering.

Harris [1988] puts forward the argument that the precise structural characteristics of the guest substructure often depend critically upon the history of the UIC crystal being examined, the important aspects of this history being the process of crystal growth and the extent of x-radiation undergone. However, for the majority of inclusion compounds investigated in the present work, more than one crystal of each was studied. Some crystals of those compounds containing shorter chain guests (e.g. 1,7-dibromoheptane/urea) visibly decomposed over the course of an experiment: the results from such crystals were disregarded. However, with these exceptions, the results obtained were reproducible.

2.4.2 CRYSTAL STRUCTURE DETERMINATION OF 1,6-DIBROMOHEXANE/UREA

2.4.2.1 Morphology

As already stated, the external crystal morphology suggested that 1,6-dibromohexane/urea is not a conventional urea inclusion compound: instead of being hexagonal needles, the crystals were truncated pyramids. Plan and side views of a typical crystal are shown in Fig. 2.14.

Fig: 2.14: Morphology of the 1,6-dibromohexane/urea crystal

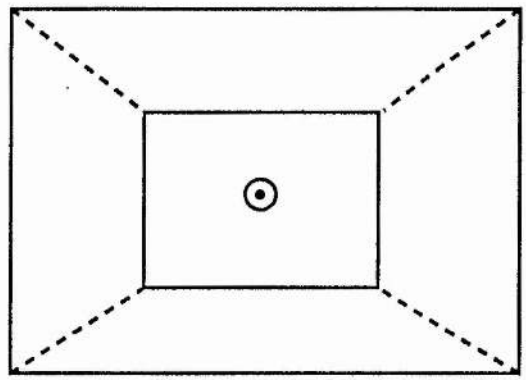

Plan view

⊙ Crystal aligned along this axis (≡ **a** axis), which is perpendicular to plane of page in plan view

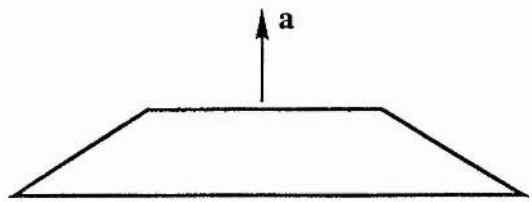

Side view

2.4.2.2 Photographic XRD Studies

The oscillation photograph for 1,6-dibromohexane/urea is shown in Fig 2.15a. As is common with urea inclusion compounds containing short-chain guest molecules, the thermal stability of 1,6-dibromohexane/urea appears low: when left in daylight at room temperature for a few days, it showed evidence of partial decomposition to polycrystalline urea. Fig. 2.15b shows the oscillation photograph of such a partially-decomposed compound.

Unusually for a urea inclusion compound, the diffraction pattern on the oscillation photograph comprises only one set of layer lines and can be rationalised in terms of a *unique* three-dimensionally periodic reciprocal lattice: this implies that the host and guest substructures are commensurate. Because of this commensurability, a full structure solution was possible. The de Jong-Bouman (0*kl*) and (1*kl*) photographs are shown in Fig. 2.16. The (1*kl*) photograph shows a diffraction pattern identical, in terms of positions of maxima, to the (0*kl*) diffraction pattern, although the (0*kl*) has two mirror planes whereas the (1*kl*) has only one, as is shown by the intensity of the reflections. These photographs, and the information given by the (*h*0*l*) precession photograph also recorded, show that the structure is monoclinic ($\alpha=\gamma=90°$) and belongs to space group $P2_1/n$. The lattice parameters calculated from these photographs were as follows:

a = 8.45 (±0.1) Å

b = 10.95 (±0.1) Å

c = 13.62 (±0.4) Å

β = 92.5° (±1°)

Fig. 2.15: Oscillation photographs (about **a** axis) for 1,6-dibromohexane/urea

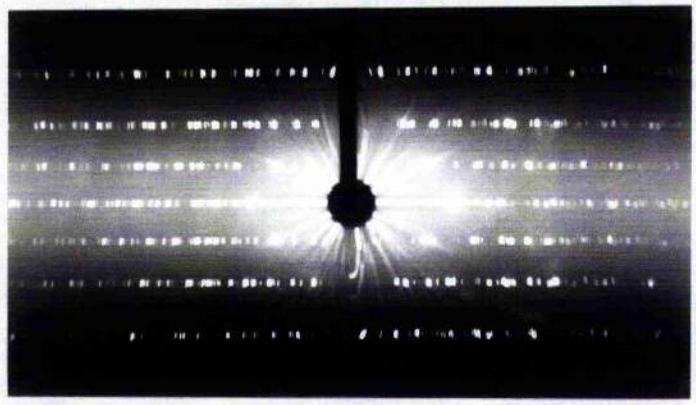

(a) For a compound of high structural integrity

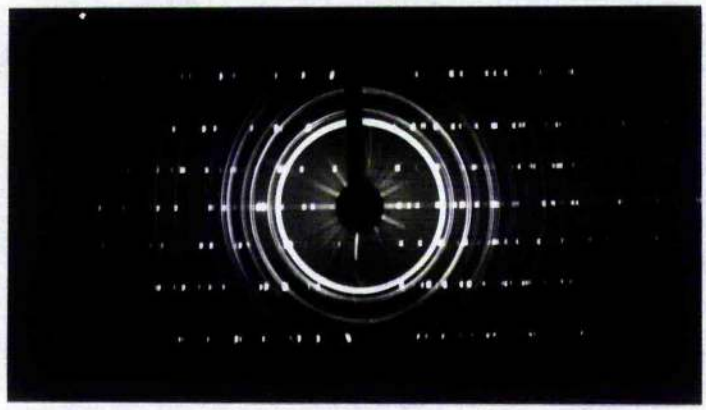

(b) For a partially-decomposed compound

Fig. 2.16: De Jong-Bouman photographs for 1,6-dibromohexane/urea

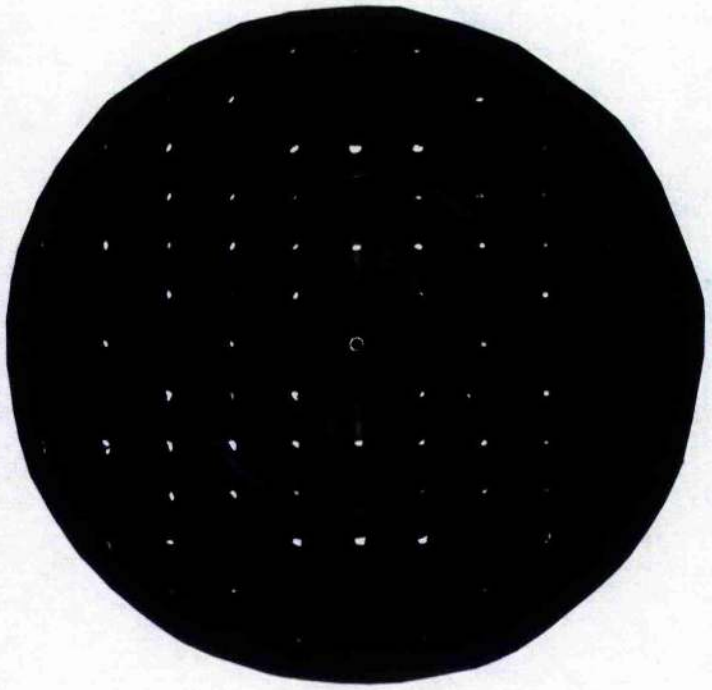

(a) (0*kl*) photograph

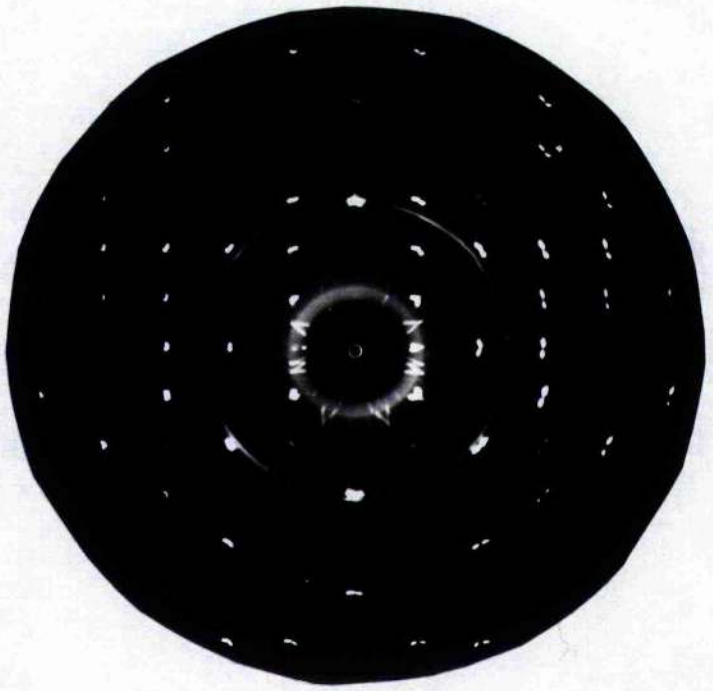

(b) (1*kl*) photograph

2.4.2.3 Crystal Structure Determination

(I) Details of structure solution and refinement

The crystallographic data were as follows. Content of unit cell: $2(C_6H_{12}Br_2).12(NH_2.CO.NH_2)$. Crystal system: monoclinic. Space group: $P2_1/n$. Content of asymmetric unit: $1/2(C_6H_{12}Br_2).3(NH_2.CO.NH_2)$. Lattice parameters:* a=8.587 Å, b=10.899 Å, c=13.468 Å, β=92.80°, $\alpha=\gamma$=90°. V=1258.96 Å. λ(Mo-Kα)=0.71069 Å, μ(Mo-Kα)=31.81 cm^{-1}, F(000)=620.00. 2814 diffractometric data were measured in the ranges $0\leq h\leq 11$; $0\leq k\leq 14$; $-17\leq l\leq 17$.

The data were corrected for absorption using the measured crystal dimensions.† The structure was solved using direct methods (the SHELXS86 program) and refined using full-matrix least squares methods (SHELX76). Hydrogen atoms were located from electron density difference maps. Due to the poor behaviour of free refinement of the hydrogen atom positions, the carbon-hydrogen bond lengths were fixed at 1.080 Å and soft restraints were applied to the positions of hydrogens bonded to nitrogen. 183 parameters were refined; 2248 reflections (for which $F > 3\sigma(F)$) were included in the refinement. Unit weights were given to all reflections.

(II) Results

The atomic coordinates of the non-hydrogen atoms in the asymmetric unit are given in Table 2.5. Values of the anisotropic thermal parameters, U_{ij}, for the non-hydrogen atoms are shown in Table 2.6. The atomic coordinates and the isotropic thermal parameters, U, of the hydrogen atoms are given in Table 2.7. Interatomic distances and angles are listed in Tables 2.8 & 2.9, respectively. Also listed in each of these Tables are the estimated standard deviations (ESD) in the values quoted.

---

* The lattice parameters used in the structure determination were those determined diffractometrically by Professor Mark Hollingsworth; these values are in close agreement with those determined from our XRD photographs (see §2.4.2.2).

† These were as follows: face $(0\bar{1}4)$: 0.197 mm; (012): 0.277; $(02\bar{1})$: 0.309; $(\bar{0}\bar{1}4)$: 0.238; $(\bar{0}10)$: 0.332; $(0\bar{2}1)$: 0.312; $(\bar{1}00)$: 0.348; $(10\bar{1})$: 0.318; (201): 0.340. (It was necessary to supply nine faces as the crystal morphology was not precisely that of a truncated pyramid.)

Table 2.5: Atomic coordinates for the non-hydrogen atoms
(with corresponding ESD shown below each value)

ATOM	X/A	Y/B	Z/C
Br1	0.1357	0.1438	0.9626
	0.0001	0.0001	0.0001
C2	-0.0407	0.2099	1.0306
	0.0010	0.0008	0.0008
C5	-0.0896	0.3354	0.9931
	0.0010	0.0008	0.0008
C8	0.0323	0.4346	1.0157
	0.0009	0.0008	0.0007
N11	0.5435	0.1486	0.9575
	0.0007	0.0005	0.0005
C12	0.5112	0.2517	0.9048
	0.0007	0.0006	0.0005
N13	0.4821	0.3551	0.9551
	0.0007	0.0005	0.0004
O14	0.5098	0.2518	0.8105
	0.0005	0.0004	0.0003
N15	0.8320	-0.0174	0.7483
	0.0007	0.0005	0.0005
C16	0.8899	0.0871	0.7120
	0.0007	0.0006	0.0005
N17	0.8101	0.1914	0.7226
	0.0007	0.0005	0.0005
O18	1.0169	0.0865	0.6687
	0.0005	0.0004	0.0004
N19	1.1930	0.3176	0.7201
	0.0007	0.0005	0.0005
C20	1.1073	0.4220	0.7107
	0.0007	0.0006	0.0005
N21	1.1699	0.5259	0.7484
	0.0007	0.0005	0.0005
O22	0.9751	0.4201	0.6676
	0.0005	0.0004	0.0004

Table 2.6: Anisotropic thermal parameters, Uij, for the non-hydrogen atoms
(with corresponding ESD shown below each value)

ATOM	U11	U22	U33	U23	U13	U12
Br1	0.0423	0.0327	0.0741	0.0030	0.0275	0.0021
	0.0005	0.0005	0.0007	0.0005	0.0004	0.0004
C2	0.0326	0.0312	0.0740	0.0116	0.0202	0.0056
	0.0040	0.0044	0.0067	0.0044	0.0042	0.0034
C5	0.0362	0.0295	0.0721	0.0017	0.0066	0.0016
	0.0044	0.0044	0.0068	0.0043	0.0044	0.0035
C8	0.0263	0.0342	0.0522	0.0015	0.0035	0.0036
	0.0037	0.0043	0.0055	0.0040	0.0035	0.0031
N11	0.0341	0.0137	0.0275	0.0022	-0.0004	0.0010
	0.0031	0.0025	0.0031	0.0025	0.0025	0.0024
C12	0.0111	0.0152	0.0272	-0.0007	0.0016	-0.0035
	0.0025	0.0029	0.0034	0.0026	0.0023	0.0022
N13	0.0350	0.0145	0.0279	-0.0021	0.0069	-0.0012
	0.0031	0.0026	0.0032	0.0024	0.0025	0.0024
O14	0.0274	0.0139	0.0175	0.0012	0.0051	-0.0012
	0.0023	0.0021	0.0023	0.0018	0.0019	0.0018
N15	0.0326	0.0123	0.0375	0.0043	0.0141	-0.0048
	0.0032	0.0026	0.0036	0.0025	0.0027	0.0023
C16	0.0179	0.0173	0.0226	-0.0038	0.0040	0.0004
	0.0028	0.0030	0.0033	0.0026	0.0024	0.0024
N17	0.0266	0.0131	0.0391	-0.0001	0.0107	0.0015
	0.0028	0.0026	0.0036	0.0025	0.0026	0.0022
O18	0.0235	0.0153	0.0260	0.0006	0.0082	0.0013
	0.0023	0.0022	0.0026	0.0019	0.0019	0.0018
N19	0.0250	0.0182	0.0358	0.0013	-0.0008	0.0035
	0.0028	0.0027	0.0037	0.0026	0.0026	0.0023
C20	0.0210	0.0157	0.0180	0.0015	0.0071	0.0014
	0.0029	0.0030	0.0031	0.0025	0.0024	0.0023
N21	0.0298	0.0138	0.0318	-0.0034	-0.0027	-0.0021
	0.0030	0.0026	0.0034	0.0024	0.0025	0.0022
O22	0.0208	0.0138	0.0279	0.0016	0.0002	-0.0008
	0.0022	0.0021	0.0026	0.0019	0.0019	0.0018

Table 2.7: Atomic coordinates and isotropic thermal parameter, U, for the hydrogen atoms (with corresponding ESD shown below each value)

ATOM	X/A	Y/B	Z/C	U
H3	-0.0089	0.2165	1.1089	0.2117
	0.0010	0.0008	0.0008	0.0314
H4	-0.1382	0.1479	1.0196	0.2117
	0.0010	0.0008	0.0008	0.0314
H6	-0.1104	0.3299	0.9135	0.2117
	0.0010	0.0008	0.0008	0.0314
H7	-0.1962	0.3611	1.0271	0.2117
	0.0010	0.0008	0.0008	0.0314
H9	0.1104	0.4690	0.9617	0.2117
	0.0009	0.0008	0.0007	0.0314
H10	0.0245	0.5002	1.0753	0.2117
	0.0009	0.0008	0.0007	0.0314
H23	0.6971	0.1586	1.0046	0.9606
	0.0203	0.0299	0.0256	0.0850
H24	0.3967	0.0454	0.9809	0.9606
	0.0346	0.0257	0.0125	0.0850
H25	0.4701	0.2881	1.0405	0.9606
	0.0529	0.0260	0.0085	0.0850
H26	0.4804	0.4350	0.9595	0.9606
	0.0530	0.0112	0.0138	0.0850
H27	0.7546	-0.0500	0.8339	0.9606
	0.0241	0.0276	0.0300	0.0850
H28	0.9901	-0.0299	0.8749	0.9606
	0.0297	0.0235	0.0122	0.0850
H29	0.5864	0.1177	0.7247	0.9606
	0.0288	0.0242	0.0184	0.0850
H30	0.7021	0.2449	0.6056	0.9606
	0.0391	0.0185	0.0244	0.0850
H31	1.1333	0.1866	0.7467	0.9606
	0.0350	0.0215	0.0115	0.0850
H32	1.0337	0.3058	0.5824	0.9606
	0.0357	0.0218	0.0269	0.0850
H33	1.3050	0.5297	0.7318	0.9606
	0.0135	0.0310	0.0291	0.0850
H34	1.1606	0.5707	0.8134	0.9606
	0.0298	0.0240	0.0067	0.0850

Table 2.8: Interatomic distances

Atoms	Distance / Å	ESD / Å
Br1---C2	1.946	0.008
C2---C5	1.511	0.011
C5---C8	1.525	0.011
C2---H3	1.080	*
C2---H4	1.080	*
C5---H6	1.080	*
C5---H7	1.080	*
C8---H9	1.080	*
C8---H10	1.080	*
N11---C12	1.352	0.008
N13---C12	1.344	0.008
O14---C12	1.268	0.008
N11---H23	1.440	0.277
N11---H24	(1.730)	n/a
N13---H25	1.370	0.167
N13---N26	0.873	0.111
N15---C16	1.344	0.008
N17---C16	1.338	0.008
O18---C16	1.262	0.007
N15---H27	1.404	0.236
N15---H28	(2.131)	n/a
N17---H29	(2.083)	n/a
N17---H30	(1.882)	n/a
N19---C20	1.358	0.008
N21---C20	1.342	0.008
O22---C20	1.250	0.007
N19---H31	(1.564)	n/a
N19---H32	(2.254)	n/a
N21---H33	1.193	0.072
N21---H34	1.010	0.114

* $\Rightarrow$ Lengths of these C---H bonds fixed at 1.080 Å

n/a $\Rightarrow$ ESD not given by program as refinement of these hydrogen positions was poor

Table 2.9: Interatomic angles

Atoms	Angle / °	ESD / °
H3-C2-Br1	108.6	0.3
H4-C2-Br1	108.7	0.3
H4-C2-H3	109.5	*
C5-C2-Br1	112.8	0.6
C5-C2-H3	108.5	0.6
C5-C2-H4	108.6	0.5
H6-C5-C2	108.1	0.6
H7-C5-C2	108.7	0.5
H7-C5-H6	109.5	*
C8-C5-C2	113.5	0.7
C8-C5-H6	108.4	0.5
C8-C5-H7	108.6	0.5
H9-C8-C5	123.7	0.5
H10-C8-C5	123.4	0.5
H10-C8-H9	109.5	*
H23-N11-C12	109.2	10.3
N13-C12-N11	118.1	0.6
O14-C12-N11	121.2	0.6
O14-C12-N13	120.8	0.6
H25-N13-C12	90.0	9.2
H26-N13-C12	150.9	13.5
H26-N13-H25	118.2	9.1
H27-N15-C16	135.3	13.2
N17-C16-N15	118.7	0.5
O18-C16-N15	120.5	0.6
O18-C16-N17	120.8	0.6
N21-C20-N19	117.8	0.6
O22-C20-N19	120.3	0.6
O22-C20-N21	121.9	0.6
H33-N21-C20	109.5	13.3
H34-N21-C20	133.6	11.2
H34-N21-H33	105.3	9.4

* $\Rightarrow$ H-C-H angles constrained to 109.5° due to fixing of C---H bond lengths

The final value of the R-factor was 7.3%. Whereas the refinement of the non-hydrogen atom positions was well-behaved, yielding intuitively reasonable parameters, many of the refined parameters for the hydrogen atoms are not reasonable. This is reflected in some excessively long bond lengths, some large ESDs in the bond angles and some high isotropic thermal parameters. It is possible that the absorption correction may not have been entirely realistic: this may be a reason for the poor behaviour of the hydrogen atom refinement.

Fig. 2.17 shows two views along the channel axis, **b**, of a single channel of 1,6-dibromohexane/urea and Fig. 2.18 shows a view perpendicular to the (ab) plane. Although the central portion of the $Br(CH_2)_6Br$ molecules is predominantly in the linear, *trans*, extended conformation, it can be seen that the Br end-groups are exclusively in the *gauche* conformation: this is unusual for a $Br(CH_2)_nBr$ molecule in its urea inclusion compound and is discussed further in Chapter 3. Note that the angle of tilt of the molecule relative to the channel axis is more pronounced than in 'conventional' urea inclusion compounds.

2.4.2.4 Discussion

Previous work on 1,6-dibromohexane/urea has been carried out by Schlenk [1949] and Otto [1972], although neither of these workers actually solved the structure. Schlenk [1949] notes that its structure is not of the conventional hexagonal type and Otto [1972] found that the structure is monoclinic and quotes the following lattice parameters, which agree closely with our values:

$a = 8.69$ Å

$b = 11.03$ Å

$c = 13.80$ Å

$\beta = 92.6°$

Fig. 2.17: CHEMX plots of the structure of 1,6-dibromohexane/urea: views of a single channel down the **b** axis

(H atoms have been omitted from both plots)

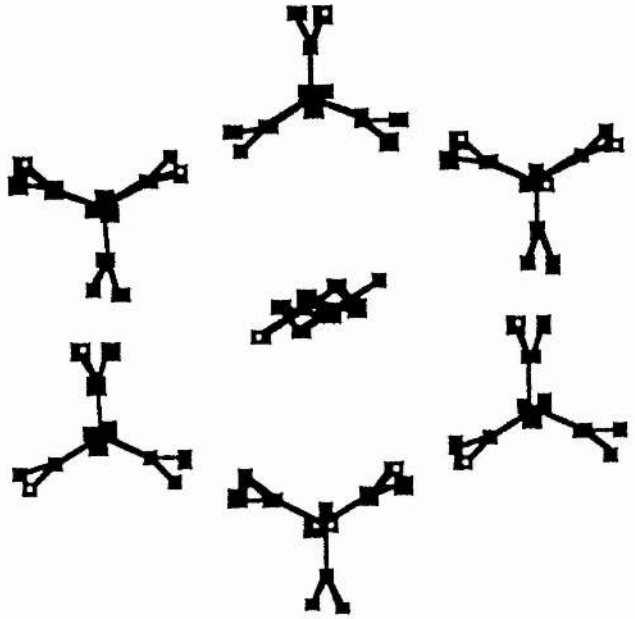

(a) With atomic radii zero

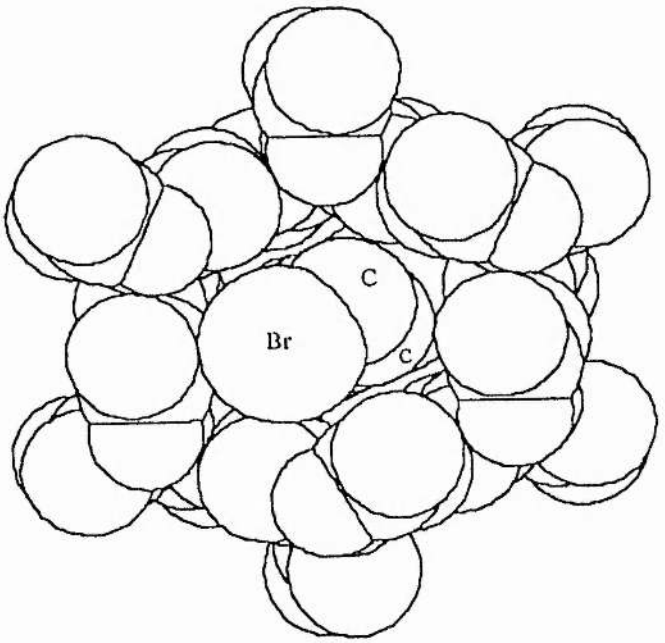

(b) With van der Waals radii shown

Fig. 2.18: CHEMX plot of the structure of 1,6-dibromohexane/urea: a view perpendicular to the (ab) plane

(H atoms have been omitted and, for clarity, the ureas in front of and behind the $C_6H_{12}Br_2$ molecules have been removed)

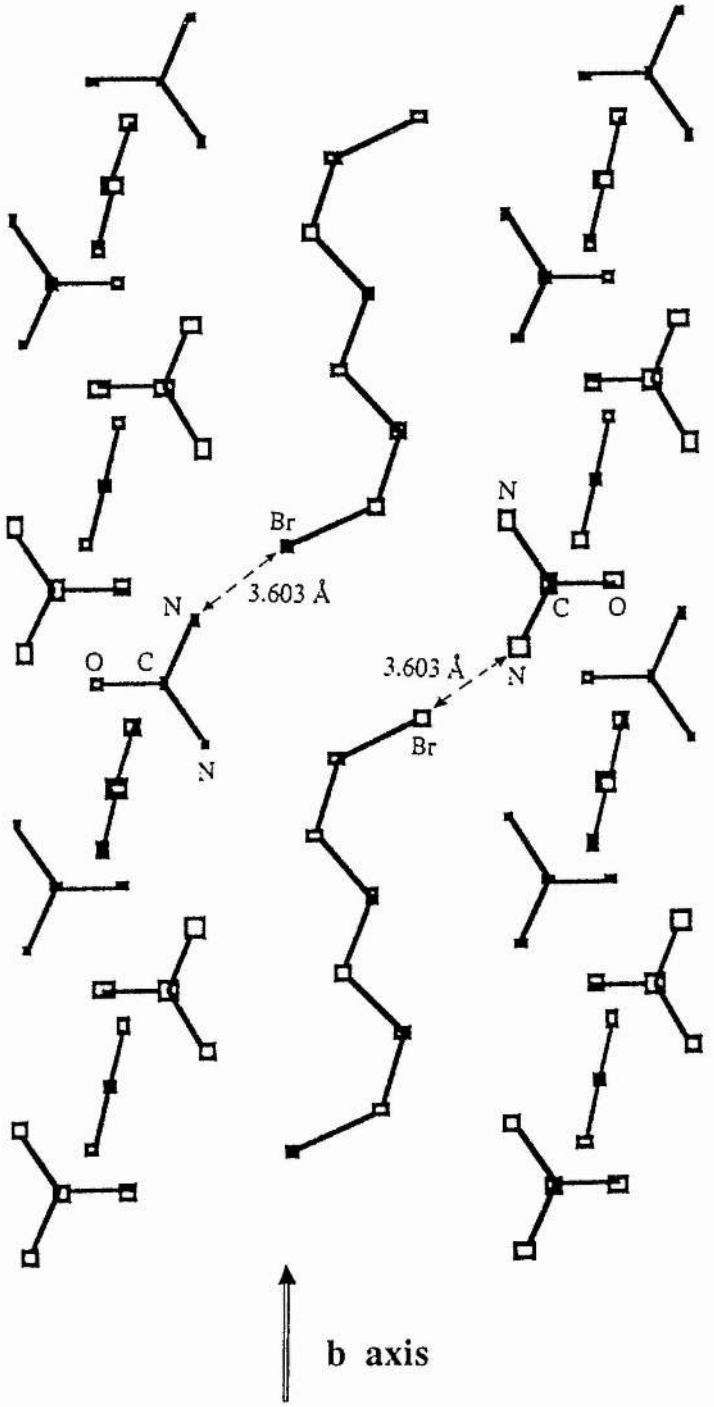

Interestingly, Schlenk [1949] found that 1,5-dibromopentane/urea *was* of the conventional hexagonal type, implying that 1,6-dibromohexane/urea is a structurally anomalous member of the α,ω-dibromoalkane/urea inclusion family. The reason for this anomaly is unclear. If 1,5-dibromopentane/urea is indeed hexagonal, it cannot be that the 1,6-dibromohexane guest is too short to be stabilised within the usual hexagonal host framework. However, the driving force behind its forming this novel structure (in preference to simple non-inclusion) could be the opportunity to lock in commensurably to the host, presumably via some coordination of the Br end-groups to the urea molecules. It has recently been found [Hollingsworth MD, unpublished work] that 1-bromo-6-chlorohexane/urea has the same structure as 1,6-dibromohexane/urea. This implies that *one* Br end-group is sufficient to achieve this commensurability.

Finally, as the commensurate nature of the 1,6-dibromohexane/urea structure is detectable by x-ray diffraction, it seems unlikely that the guest molecules exhibit significant motion: this contrasts with the considerable dynamics shown by guest molecules in 'conventional' urea inclusion compounds (see Chapter 4).

2.5 CONCLUSIONS

2.5.1 SUMMARY OF RESULTS

Photographic single crystal XRD studies of the urea inclusion compounds of $Br(CH_2)_nBr$, where n=7-10, have shown that each single crystal contains *both* regions in which the guest molecules are ordered only in one dimension (along the channel axis) and regions in which the guest molecules are three-dimensionally ordered. For the regions of three-dimensional ordering, there are two domains of the basic guest structure: the lattices which define the periodicities of these domains differ only by 180° rotation about the channel axis and have rhombohedral metric symmetry. In these regions, the value along the channel axis of the offset, Δ_g, between neighbouring guest molecules in adjacent channels is given by the exact relationship:

$$\Delta_g = \frac{c_g}{3}$$

This represents a new mode of guest molecular ordering which contrasts with those guest families for which Δ_g is known to be constant, e.g. *n*-alkanes: Δ_g=0; acid anhydrides: Δ_g=0 (in general); diacyl peroxides: Δ_g=4.6 Å. Factors controlling the mode of intermolecular guest packing are thought to involve either direct electrostatic interaction between the guest molecules in neighbouring channels or indirect interaction transmitted via the urea molecules which form the channel walls.

$I(CH_2)_{10}I$/urea was also found to belong to this $\Delta_g=c_g/3$ mode of guest molecular ordering. However, there was no evidence, from the oscillation photographs, for three-dimensional guest molecular ordering either in $Cl(CH_2)_{10}Cl$/urea or in $Br(CH_2)_nBr$/urea with n=11-12.

It was found that $Br(CH_2)_6Br$/urea has a totally different structure from that of 'conventional' urea inclusion compounds. Single crystal x-ray diffraction photographs showed that the structure of $Br(CH_2)_6Br$/urea is monoclinic and that the host and guest structures are commensurate with one another. Consequently, it was possible to solve the complete structure using x-ray diffractometric methods.

2.5.2 FUTURE WORK

Further studies could be done to establish the reasons for one and/or three-dimensional ordering of the guest molecules in these urea inclusion compounds, for the mode of interchannel guest packing in the three-dimensionally ordered regions, and for the existence of structurally anomalous members within certain families of urea inclusion compounds. These include the following.

2.5.2.1 Low-Temperature Studies

The studies described here were carried out at ambient temperature, where the guest molecules have considerable mobility (as discussed in Chapter 4). Variable temperature x-ray diffraction studies could give us a clearer understanding of the factors affecting guest molecule ordering. The α,ω-dibromoalkane/urea inclusion family undergoes a phase transition, similar to that of the *n*-alkane/urea inclusion family, to a low-temperature orthorhombic phase. Investigation of the inclusion compound structure below the phase transition temperature (in the range *ca.* 135-166 K for the compounds studied here: see Appendix B) could give insight into the changes occurring at the phase transition.†

2.5.2.2 Extended Range of Guest Molecules

Investigation of longer and shorter guest molecules within the families already studied could indicate the generality or otherwise of the conclusions drawn, and the prevalence of anomalous structures. Studies on new guest families could also be instructive, e.g. diketones, and other symmetric guest species. Once such urea inclusion compounds are understood, mixed functionality species as guests and even mixed guest systems could be studied. Such studies would be possible provided the stability of the inclusion compounds was such as to allow facile preparation.

---

† To date, there has been no satisfactory study of guest molecular ordering in any urea inclusion compound below the phase transition. Preliminary photographic studies [Harris, 1988] on the diacyl peroxide/urea inclusion system at low temperature (down to 183 K) showed no significant structural changes, other than the expected slight contraction of the host structure on cooling. However, this family of urea inclusion compounds is not thought to undergo a phase transition.

2.5.2.3 Different Hosts

The study of the same guest species within different host frameworks could afford interesting structural comparisons. Some alternative hosts are thiourea, perhydrotriphenylene, tri-*ortho*-thymotide and deoxycholic acid.

2.5.2.4 Decomposition Studies

As mentioned earlier, some of the inclusion compounds studied here, especially those containing the shorter chain guest molecules, became increasingly polycrystalline with heat, time and/or x-ray exposure. A study of the cause, rate and mechanism of decomposition of such compounds could reveal the factors which determine their structural stability. It is possible that diffuse guest scattering (leading to an assignment of one-dimensional ordering) may, in fact, be a consequence of thermal or x-ray induced composition. This was proposed by Harris [1990] during studies of x-ray scattering from monohalocyclohexane/thiourea.

2.5.2.5 Complementary Techniques

The use of techniques such as computer simulation could be instructive by providing the theoretically optimum structure of these compounds. This could also yield significant insight regarding the factors determining the Δ_g offset, and enable us to understand and predict into which category of interchannel guest ordering a particular family of urea inclusion compounds will fall. Such techniques could also elucidate factors governing the formation of anomalous guest structures.

Techniques such as Raman spectroscopy, neutron scattering and ^2H solid state nuclear magnetic resonance spectroscopy (discussed in Chapters 3, 4 & 5, respectively) provide dynamic and conformational information regarding the guest species. This information will be complementary to the structural information derived from these x-ray diffraction studies in building up a coherent picture of the physical properties of these inclusion compounds.

2.6 REFERENCES

ATKINS PW (1986) Physical Chemistry, 3rd Edition, Oxford University Press, pp 549-574.

BRAGG WL (1914) The structure of some crystals as indicated by their diffraction of x-rays, *Proc. R. Soc. London, Ser. A*, **89**, 248-277.

BRAGG WL (1968) X-ray crystallography, *Scientific American*, **219** (1), 58-70.

BRAGG WH & BRAGG WL (1913) The reflection of x-rays by crystals, *Proc. R. Soc. London, Ser. A*, **88**, 428-438.

BRAGG WH & BRAGG WL (1914) The structure of the diamond, *Proc. R. Soc. London, Ser. A*, **89**, 277-291.

CHATANI Y, TAKI Y & TADOKORO H (1977) Low temperature form of urea adducts with *n*-paraffins, *Acta Crystallogr., Sect. B*, 33. 309-311.

CHATANI Y, ANRAKU H & TAKI Y (1978) Phase transition and structure change of urea adducts with *n*-paraffin and paraffin-type compounds, *Mol. Cryst. Liq. Cryst.*, **48**, 219-231.

DUNITZ JD (1979) X-Ray Analysis and the Structure of Organic Molecules, Cornell University Press.

EBERHART JP (1991) Structure and Chemical Analysis of Materials, John Wiley & Sons.

FORST R, BOYSEN H, FREY F, JAGODZINSKI H & ZEYEN C (1986) Phase transitions and ordering in urea inclusion compounds with *n*-paraffins, *J. Phys. Chem. Solids*, **47**, 1089-1097.

FORST R, JAGODZINSKI H, BOYSEN H & FREY F (1987) Diffuse scattering and disorder in urea inclusion compounds: $OC(NH_2)_2+C_nH_{[2n+2]}$, *Acta Crystallogr., Sect. B*, **43**, 187-197.

FORST R, JAGODZINSKI H, BOYSEN H & FREY F (1990) The disordered crystal structure of urea inclusion compounds: $OC(NH_2)_2+C_nH_{[2n+2]}$, *Acta Crystallogr., Sect. B*, **46**, 70-78.

FRIEDRICH W, KNIPPING P & VON LAUE M (1913) Interferenzerscheinungen bei Röntgenstrahlen, *Ann. Physik*, **41**, 971-988.

GIACOVAZZO C, MONACO HL, VITERBO D, SCORDARI F, GILLI G, ZANOTTI G & CATTI M (1992) Fundamentals of Crystallography, Oxford University Press.

GLUSKER JP & TRUEBLOOD KN (1972) Crystal Structure Analysis: A Primer, Oxford University Press.

HARRIS KDM (1988) Studies of urea inclusion compounds and other solids, PhD Thesis, University of Cambridge.

HARRIS KDM (1990) Investigation of a time-dependent 'non-discrete' component of x-ray scattering from monohalocyclohexane/thiourea inclusion compounds, *J. Solid State Chem.*, **84**, 280-288.

HARRIS KDM (1993) Investigating the structure and dynamics of a family of organic solids: the alkane/urea inclusion compounds, *J. Solid State Chem.*, special issue, in press.

HARRIS KDM & HOLLINGSWORTH MD (1990) Structural properties of the guest species in diacyl peroxide/urea inclusion compounds: an x-ray diffraction investigation, *Proc. R. Soc. London, Ser. A*, **431**, 245-269.

HARRIS KDM & THOMAS JM (1990a) Structural aspects of urea inclusion compounds and their investigation by x-ray diffraction: a general discussion, *J. Chem. Soc., Faraday Trans.*, **86**, 2985-2996.

HARRIS KDM & THOMAS JM (1990b) Probing the properties of urea inclusion compounds, *Mol. Cryst. Liq. Cryst.*, **186**, 177-184.

HARRIS KDM, GAMESON I & THOMAS JM (1990) Powder x-ray diffraction studies of a low-temperature phase transition in the *n*-hexadecane/urea inclusion compound, *J. Chem. Soc., Faraday Trans.*, **86**, 3135-3143.

HARRIS KDM, SMART SP & HOLLINGSWORTH MD (1991) Structural properties of α,ω-dibromoalkane/urea inclusion compounds: a new type of interchannel guest molecule ordering, *J. Chem. Soc., Faraday Trans.*, **87**, 3423-3429.

LAVES F, NICOLAIDES N & PENG KC (1965) Comparison of the lengths of molecules in urea and in thoiurea adducts, *Z. Kristallogr.*, **121**, 258-282.

OTTO J (1972) Bestimmung der Wirtsstruktur von 1,4-Dichlorbutan-Harnstoff, ein Beitrag zur Bestätigung eines allgemeinen Bauprinzips für die Einschluss-verbindungen des Harnstoffs und des Thioharnstoffs, *Acta Crystallogr., Sect. B*, **28**, 543-551.

RENNIE AJO & HARRIS KDM (1990) A mathematical model of one-dimensional inclusion compounds: a new approach towards understanding commensurate and incommensurate behaviour, *Proc. R. Soc. London, Ser. A*, **430**, 615-640.

RENNIE AJO & HARRIS KDM (1992) A quantitative analysis of guest periodicity in one-dimensional inclusion compounds, *J. Chem. Phys.*, **96**, 7117-7124.

SCHLENK W (1949) Die Harnstoff-Addition der aliphatischen Verbindungen, *Liebigs Ann. Chem.*, **565**, 204-240.

SMITH AE (1950) The crystal structure of urea-hydrocarbon and thiourea-hydrocarbon complexes, *J. Chem. Phys.*, **18**, 150-151.

SMITH AE (1952) The crystal structure of the urea-hydrocarbon complexes, *Acta Crystallogr.*, **5**, 224-235.

STOUT GH & JENSEN LH (1989) X-Ray Structure Determination: A Practical Guide, John Wiley & Sons.

VON DREELE RB (Summer 1990) X-ray and neutron crystallography: a powerful combination, *Los Alamos Science*, 133-157.

VON LAUE M (1913) Eine quantitative Prüfung der Theorie für die Interferenzerscheinungen bei Röntgenstrahlen, *Ann. Physik*, **41**, 989-1002.

CHAPTER 3
RAMAN SPECTROSCOPIC STUDIES

3.1 THE TECHNIQUE

3.1.1 INTRODUCTION

The Raman effect was discovered in 1928 by C.V. Raman, and the development of laser sources in the mid-1960's has allowed Raman spectroscopy to become a routine laboratory technique. It can, in principle, be used for the study of molecular translations, rotations and vibrations. As discussed by Sloane [1971] and Davies [1984], Raman spectroscopy is complementary to the absorption process of infrared spectroscopy, many vibrations being active in either Raman or infrared, or both. Activity is governed by molecular symmetry and polarity: in general, symmetric vibrations and non-polar groups are most easily studied by Raman, antisymmetric vibrations and polar groups by infrared.

Raman has an advantage over infrared in the generality of its experimental set-up: study of the whole range of molecular rotational and vibrational levels need involve only one dispersive system, one detector and one sample cell (glass or quartz). In contrast, infrared spectroscopy requires different set-ups for different frequency ranges. Raman also has advantages in ease of sample preparation. However, infrared spectroscopy is the better technique for quantitative analysis. For the present study of α,ω-dibromoalkane/urea inclusion compounds, Raman spectroscopy was chosen in preference to infrared, because the infrared spectra of urea inclusion compounds are dominated by absorption of the urea.

The following section outlines the theory underlying Raman spectroscopy; further details on theory and chemical applications may be found in general references [e.g. LSMC, 1991; Grasselli *et al*, 1981; Long, 1977].

3.1.2 General Principles of Raman Spectroscopy

When a molecule is subjected to an electromagnetic field, the resulting perturbation of the molecule's electron cloud gives rise to an induced dipole moment, $\vec{P}$, which is not necessarily parallel to the electric field vector, $\vec{E}$. This induced dipole moment is related to the electric field vector by the power series:

$$\vec{P} = \vec{\vec{\alpha}}.\vec{E} + \frac{1}{2}\vec{\vec{\beta}}:\vec{E}.\vec{E} + \ldots$$

where $\vec{\vec{\alpha}}$ is the molecular polarisability tensor (of rank 2)

$\vec{\vec{\beta}}$ is the molecular hyperpolarisability tensor (of rank 3)

For relatively weak incident radiation, such as that produced by a continuous laser, the hyperpolarisability contribution to the induced dipole is negligible, so only the first term of this series is significant. Thus:

$$\vec{P} = \vec{\vec{\alpha}}\,\vec{E} \qquad \text{- eqn (1)}$$

This can be written:

$$\begin{pmatrix} P_x \\ P_y \\ P_z \end{pmatrix} = \begin{pmatrix} \alpha_{xx} & \alpha_{xy} & \alpha_{xz} \\ \alpha_{yx} & \alpha_{yy} & \alpha_{yz} \\ \alpha_{zx} & \alpha_{zy} & \alpha_{zz} \end{pmatrix} \begin{pmatrix} E_x \\ E_y \\ E_z \end{pmatrix}$$

$\vec{\vec{\alpha}}$ may be decomposed into three tensors such that:

$$\vec{\vec{\alpha}} = \vec{\vec{\alpha}}_{\text{isotropic}} + \vec{\vec{\alpha}}_{\text{anisotropic}} + \vec{\vec{\alpha}}_{\text{antisymmetric}}$$

These three tensors are defined respectively by the invariants $\bar{\alpha}$, γ^2 and δ^2, where:

$$\bar{\alpha} = 1/3\ (\alpha_{xx} + \alpha_{yy} + \alpha_{zz})$$

$$\gamma^2 = 1/2\ [\{(\alpha_{xx} - \alpha_{yy})^2 + (\alpha_{yy} - \alpha_{zz})^2 + (\alpha_{zz} - \alpha_{xx})^2\} + 1/2\ \{(\alpha_{xy} + \alpha_{yx})^2 + (\alpha_{yz} + \alpha_{zy})^2 + (\alpha_{zx} + \alpha_{xz})^2\}]$$

$$\delta^2 = 3/4\ [(\alpha_{xy} - \alpha_{yx})^2 + (\alpha_{yz} - \alpha_{zy})^2 + (\alpha_{zx} - \alpha_{xz})^2)]$$

$\bar{\alpha}$ is termed the average polarisability or trace, γ the symmetric anisotropy and δ the antisymmetric anisotropy. However, $\vec{\vec{\alpha}}$ is generally real and symmetric, hence $\alpha_{xy} = \alpha_{yx}$ and $\alpha_{xz} = \alpha_{zx}$ and $\alpha_{yz} = \alpha_{zy}$. There are thus only 6 independent terms and $\delta^2 = 0$. $\bar{\alpha}$ is isotropic, so is independent of the orientation of the molecule, unlike γ which depends on the orientation of the molecule.

The vibrations of the molecule are now considered. The nuclei oscillate about their equilibrium positions: a non-linear molecule of N nuclei has (3N-6) normal coordinates Q_i, each describing a specific mode of vibration. For a given mode of vibration of frequency υ the normal coordinate may be expressed $Q = Q_0 \cos(2\pi\upsilon t)$, Q_0 being the normal coordinate amplitude at equilibrium. Because $\vec{\vec{\alpha}}$ is dependent on the geometry of the molecule, it varies with Q. Thus, for a given normal coordinate Q, $\vec{\vec{\alpha}}$ can be developed in a Taylor series as follows:

$$\vec{\vec{\alpha}} = \vec{\vec{\alpha}}_0 + \left[\frac{\partial \vec{\vec{\alpha}}}{\partial Q}\right]_{Q=0} . Q + \frac{1}{2!}\left[\frac{\partial^2 \vec{\vec{\alpha}}}{\partial Q^2}\right]_{Q=0} . Q^2 + \ldots \qquad \text{- eqn (2)}$$

Under the harmonic hypothesis, in which the amplitude of vibrations is small, only the first two terms of this series are considered.

Substituting eqn (2) into eqn (1) gives:

$$\vec{P} = \vec{\vec{\alpha}}_0.\vec{E} + Q.\vec{\vec{\alpha}}'.\vec{E} \qquad \text{where } \vec{\vec{\alpha}}' = \left[\frac{\partial \vec{\vec{\alpha}}}{\partial Q}\right]_{Q=0} \qquad \text{- eqn (3)}$$

A mode of vibration with normal coordinate Q will be Raman active only if at least one of the 9 components of $\vec{\vec{\alpha}}'$ is different from zero.

Let the applied radiation be a monochromatic electromagnetic wave with electric field vector $\vec{E}$ such that :

$$\vec{E} = \vec{E}_0 \cos(2\pi\upsilon_0 t)$$

Substituting into eqn (3) gives:

$$\vec{P} = \vec{\vec{\alpha}}_0.\vec{E}_0 \cos(2\pi\upsilon_0 t) + Q_0.\vec{\vec{\alpha}}'.\vec{E}_0[\cos(2\pi\upsilon_0 t)\cos(2\pi\upsilon t)]$$

Hence:

$$\vec{P} = \vec{\vec{\alpha}}_0.\vec{E}_0 \cos(2\pi\upsilon_0 t) + \frac{Q_0}{2}.\vec{\vec{\alpha}}'.\vec{E}_0[\cos 2\pi(\upsilon_0+\upsilon)t + \cos 2\pi(\upsilon_0-\upsilon)t]$$

Thus, for a normal mode of vibration of frequency υ, the induced dipole gives rise to three emissions with frequencies of υ_0, $(\upsilon_0+\upsilon)$ and $(\upsilon_0-\upsilon)$ respectively (Fig. 3.1). These correspond to the three relaxational scattering processes that can occur when the molecule is excited (to the virtual energy levels shown) by a photon $h\upsilon_0$.

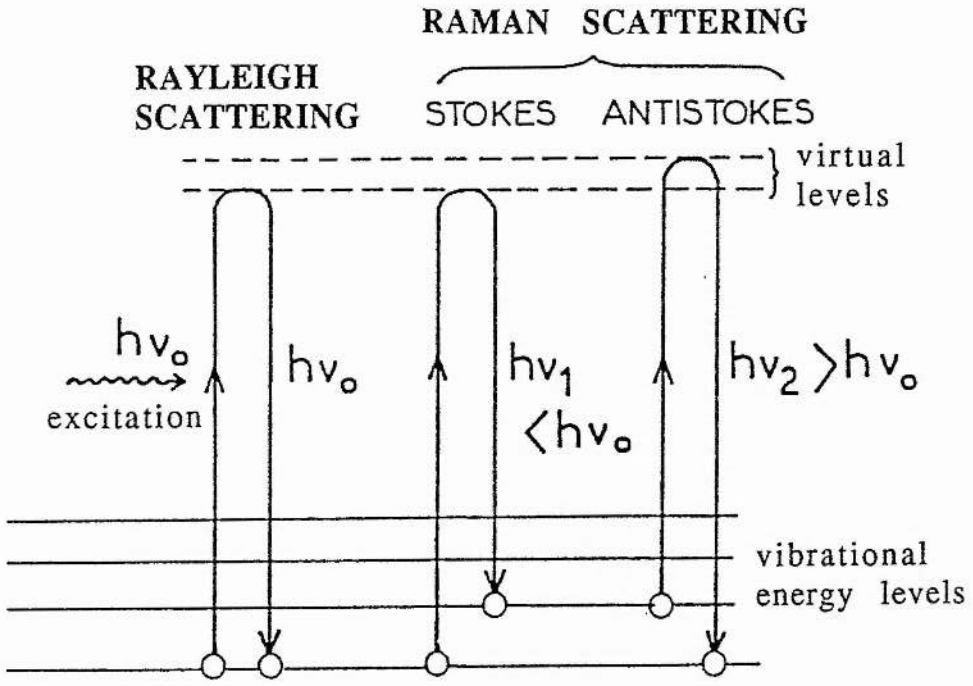

Fig. 3.1: Origin of Raman scattering ($h\upsilon_1 < h\upsilon_0 < h\upsilon_2$)

[adapted from LSMC, 1991]

The resultant scattering may be Rayleigh or Raman:

(1) Rayleigh scattering: return to the initial energy level by emission of a photon $h\upsilon_0$, giving rise to elastic scattering (i.e. without change in frequency with respect to the exciting radiation)

(2) Raman scattering: inelastic scattering, of which there are two forms:

- Raman Stokes: return to a higher energy level by emission of a photon $h\upsilon_1$ such that:

$$\text{energy change} = h\upsilon_0 - h\upsilon_1 \qquad \text{where } \upsilon_1 < \upsilon_0$$

- Raman anti-Stokes: return to an lower energy level by emission of a photon $h\upsilon_2$ such that:

$$\text{energy change} = h\upsilon_0 - h\upsilon_2 \qquad \text{where } \upsilon_2 > \upsilon_0$$

The frequency of Raman scattering is symmetrical since:

$$\Delta\upsilon = |\upsilon_0 - \upsilon_1| = |\upsilon_0 - \upsilon_2|$$

However, the Stokes and anti-Stokes intensities differ, the intensity of any transition being dependent on the population of the initial energy level. By the Boltzmann distribution, a higher energy level is always less populated (at least for vibrations), hence the intensity of anti-Stokes scattering is always weaker than that of the corresponding Stokes scattering. In practice, therefore, we usually study the Raman Stokes scattering: it is the value $\Delta\bar{\upsilon}$ (in cm^{-1}) that is actually measured ($\bar{\upsilon} = \upsilon/c$, where c is the speed of light in a vacuum).

3.1.3 DEPOLARISATON RATIO

The electric field vector of electromagnetic radiation may be decomposed into three mutually orthogonal components (polarisations). In Raman spectroscopy, the intensity of this polarised radiation may be denoted I_{RS}, where R and S refer to the polarisations of the incoming laser beam and the scattered rays, respectively (i.e. horizontal or vertical with respect to the plane of scattering). For a non-oriented sample (i.e. liquid or gas) in the direct geometry set-up normally used (see §3.1.4), it can be shown that:

$$I_{VV} = \frac{45\left(\bar{\alpha}'\right)^2 + 4\left(\gamma'\right)^2}{45} \qquad \text{and} \qquad I_{VH} = I_{HV} = I_{HH} = \frac{\left(\gamma'\right)^2}{15}$$

where $\bar{\alpha}'$ and γ' are the derivatives, with respect to Q, of $\bar{\alpha}$ and γ respectively (as defined in §3.1.2).

The depolarisation ratio, ρ, of the scattered light is defined [e.g. Strommen, 1992] as:

$$\rho = \frac{I_{VH}}{I_{VV}}$$

Therefore, in the general case:

$$\rho = \frac{I_{VH}}{I_{VV}} = \frac{3\left(\gamma'\right)^2}{45\left(\bar{\alpha}'\right)^2 + 4\left(\gamma'\right)^2}$$

Let us consider two specific cases.

1. If $\alpha_{xy}' = \alpha_{yx}' = \alpha_{xz}' = \alpha_{zx}' = \alpha_{yz}' = \alpha_{zy}' = 0$

and $\alpha_{xx}' = \alpha_{yy}' = \alpha_{zz}'$

then $\bar{\alpha}' = \alpha_{zz}'$ and $\left(\gamma'\right)^2 = 0$

hence $I_{VV} = \left(\alpha_{zz}'\right)^2$ and $I_{VH} = 0$

thus $\rho = 0$

The mode of vibration is totally polarised.

2. If $\alpha_{xy}' = \alpha_{yx}'$; $\alpha_{xz}' = \alpha_{zx}'$; $\alpha_{yz}' = \alpha_{zy}'$, with at least one of these terms $\neq 0$

and $\alpha_{xx}' = \alpha_{yy}' = \alpha_{zz}' = 0$

then $\overline{\alpha}' = 0$

hence $I_{VV} = \frac{4(\gamma')^2}{45}$ and $I_{VH} = \frac{(\gamma')^2}{15}$

thus $\rho = 0.75$

The mode of vibration is totally 'anisotropic', i.e. it is depolarised.

In summary, for a given vibrational mode:

$0 \leq \rho \leq 0.75$ i.e. $0 \leq I_{VH} \leq 0.75\, I_{VV}$

If $\rho = 0$ $\Rightarrow$ mode totally polarised

If $\rho = 0.75$ $\Rightarrow$ mode depolarised

3.1.4 THE EXPERIMENTAL SET-UP

The apparatus comprises four essential elements: the laser, the optical transfer device (incorporating the sample holder and cryostatic attachment), the monochromator (double or triple) and the detector (photomultiplier or bank of diodes). The general set-up in direct geometry (defined below) is shown in Fig. 3.2. Laser light is used as the incident radiation because a high-energy monochromatic source is required in order to produce an easily observable Raman effect. The gas may be either neutral atoms (e.g. He-Ne) or ions (e.g. Ar^+, Kr^+). The plasma emits several parasitic rays of intensity similar to that of the Raman scattering; these are eliminated using an interferential filter.

The radiation emitted by the laser is polarised vertically by construction (due to the Brewster angles). To turn this polarisation by 90°, a half-wave crystal is used (with $\lambda/2$ corresponding to the frequency of emission). The Raman effect is usually observed at 90° to the direction of the excitation: this is termed direct geometry. (A

back-scattering (or retro) geometry may also be used, in which the scattering is observed at 180° to the direction of excitation.) As the scattered light can have any direction, a polariser is used to select either the horizontal or vertical component. In order to balance the response of the system to scattered radiations polarised horizontally and vertically, a quarter-wave crystal (or quartz scrambler) is placed between the polariser and the monochromator. This circularises all polarisations equally (ie. I_{VV}, I_{VH}, I_{HV} and I_{HH}), hence allowing a direct comparison between the light intensities obtained in the Raman spectra.

The instrumental resolution is determined by the size of the entrance and exit slits of the monochromators. The detector is usually coupled to a computer, thus allowing the summation of several acquisitions of the spectrum.

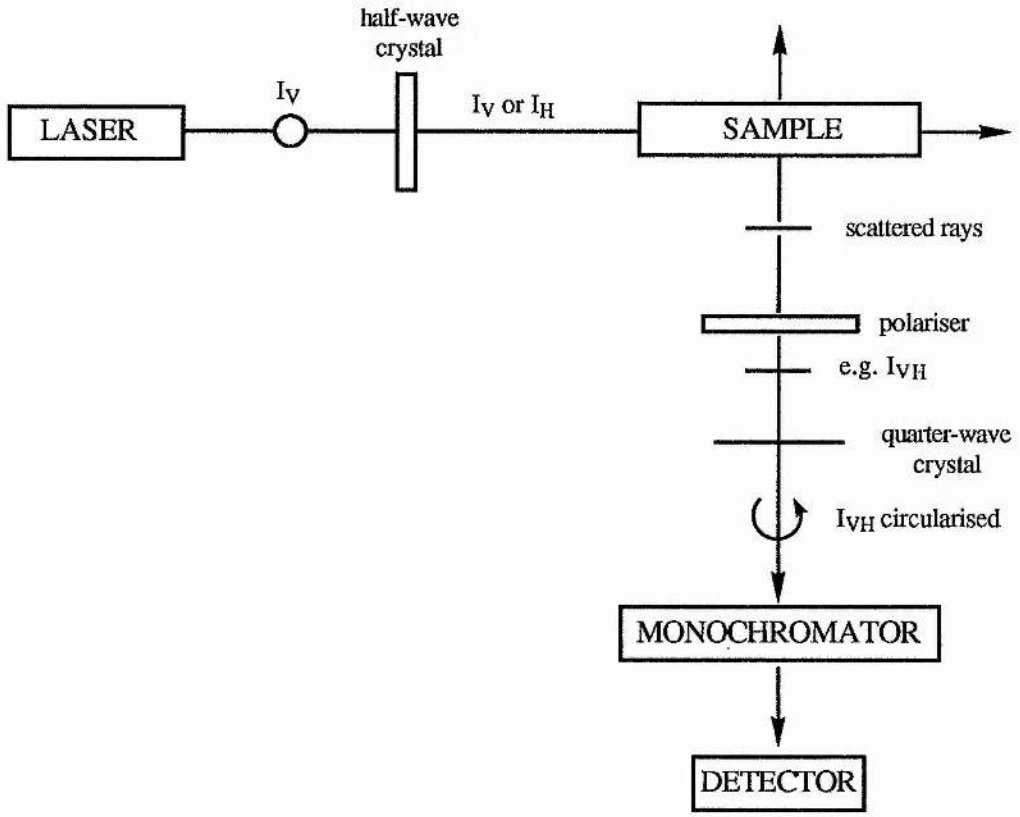

Fig. 3.2: Experimental set-up in direct geometry

3.1.5 REFERENCE FRAMES

Consider the relationship between the molecular reference frame, g, and the space-fixed (or laboratory) reference frame, F. In our experiments, the long axis (**z**) of the crystal was aligned along the **Z** axis of the laboratory reference frame and the xy plane was randomly oriented with respect to the XY plane, as shown in Fig. 3.3. This is termed the semi-oriented set-up. The study of a semi-oriented single crystal using polarised radiation allows us to distinguish, *a priori*, the Raman bands of vibrations which have different symmetries.

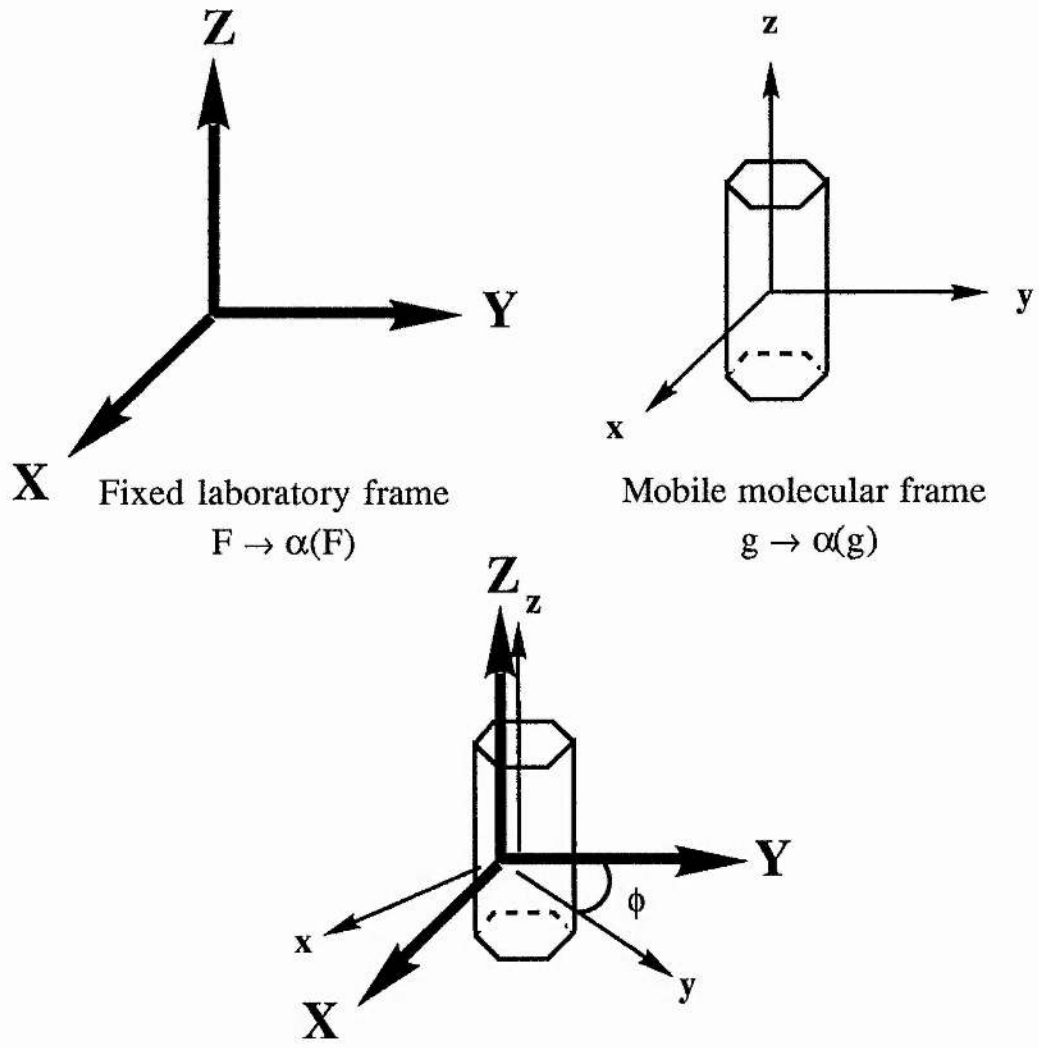

Fig. 3.3: Relationship between space-fixed and molecular reference frames

Although the **z** and **Z** axes are equivalent in space, there is an offset between the xy and XY planes equal to the angle ϕ. In order to convert the molecular components (α_{ij}') of the derivative of the polarisability tensor to those measured experimentally (α_{IJ}') in the fixed reference frame, a rotation matrix R is introduced [e.g. Snyder, 1971] such that:

$$\alpha'(F) = R\,\alpha'(g)\,R'$$

i.e. $$\alpha_{IJ}' = \sum_{ij} \left(R_{Ii}\,\alpha_{ij}'\,R_{jJ}' \right)$$

where $$R = \begin{bmatrix} \cos\phi & \sin\phi & 0 \\ -\sin\phi & \cos\phi & 0 \\ 0 & 0 & 1 \end{bmatrix}$$

and R' is the transpose matrix of R.

The fixed frame polarisation being studied is denoted using the Porto nomenclature, generally written:

A(IJ)B

where
- A = direction of propagation of laser
- I = orientation of laser polariser
- J = orientation of observation polariser
- B = direction of propagation of scattered light

Our experimental set-up in direct geometry allows study of Y(IJ)X, giving four possible polarisations: Y(ZZ)X, Y(ZY)X, Y(XZ)X and Y(XY)X, as shown in Fig. 3.4. In theory Y(ZY)X ≡ Y(XZ)X: however, comparison of these polarisations is useful for checking the calibration of the spectrometer. In retro geometry, the possible polarisations are X(ZZ)$\overline{X}$, X(ZY)$\overline{X}$, X(YZ)$\overline{X}$ and X(YY)$\overline{X}$. (For brevity, polarisations may be denoted ZZ, XZ, XY, etc, and refer to direct geometry unless otherwise stated.) Because the retro geometry was used primarily for purposes of verification, the theory discussed here refers to the direct geometry set-up.

For the semi-oriented set-up described previously, the intensity of the Raman spectrum in a given polarisation is proportional to the square of the corresponding component of the derivative of the polarisability tensor in the fixed reference frame, averaged over all values of ϕ [Snyder, 1971]:

i.e. $$I_{IJ} \propto \overline{(\alpha_{IJ}')^2}$$

where $$\overline{(\alpha_{IJ}')^2} = \sum_{ij} \overline{(R_{Ii}\,\alpha_{ij}'\,R_{jJ}')^2} \qquad \text{and} \qquad \bar{x} \equiv \frac{1}{2\pi}\int_{\phi=0}^{\phi=2\pi} x\, d\phi$$

By matrix calculation, we find that:

For Y(ZZ)X:

$$I_{ZZ} \propto \overline{(\alpha_{ZZ}')^2} \quad \text{where} \quad \overline{(\alpha_{ZZ}')^2} = (\alpha_{zz}')^2$$

For Y(XZ)X:

$$I_{XZ} \propto \overline{(\alpha_{XZ}')^2} \quad \text{where} \quad \overline{(\alpha_{XZ}')^2} = \frac{1}{2}\left[(\alpha_{xz}')^2 + (\alpha_{yz}')^2\right]$$

For Y(XY)X:

$$I_{XY} \propto \overline{(\alpha_{XY}')^2} \quad \text{where} \quad \overline{(\alpha_{XY}')^2} = \frac{1}{8}\left[(\alpha_{xx}' - \alpha_{yy}')^2 + 4(\alpha_{xy}')^2\right]$$

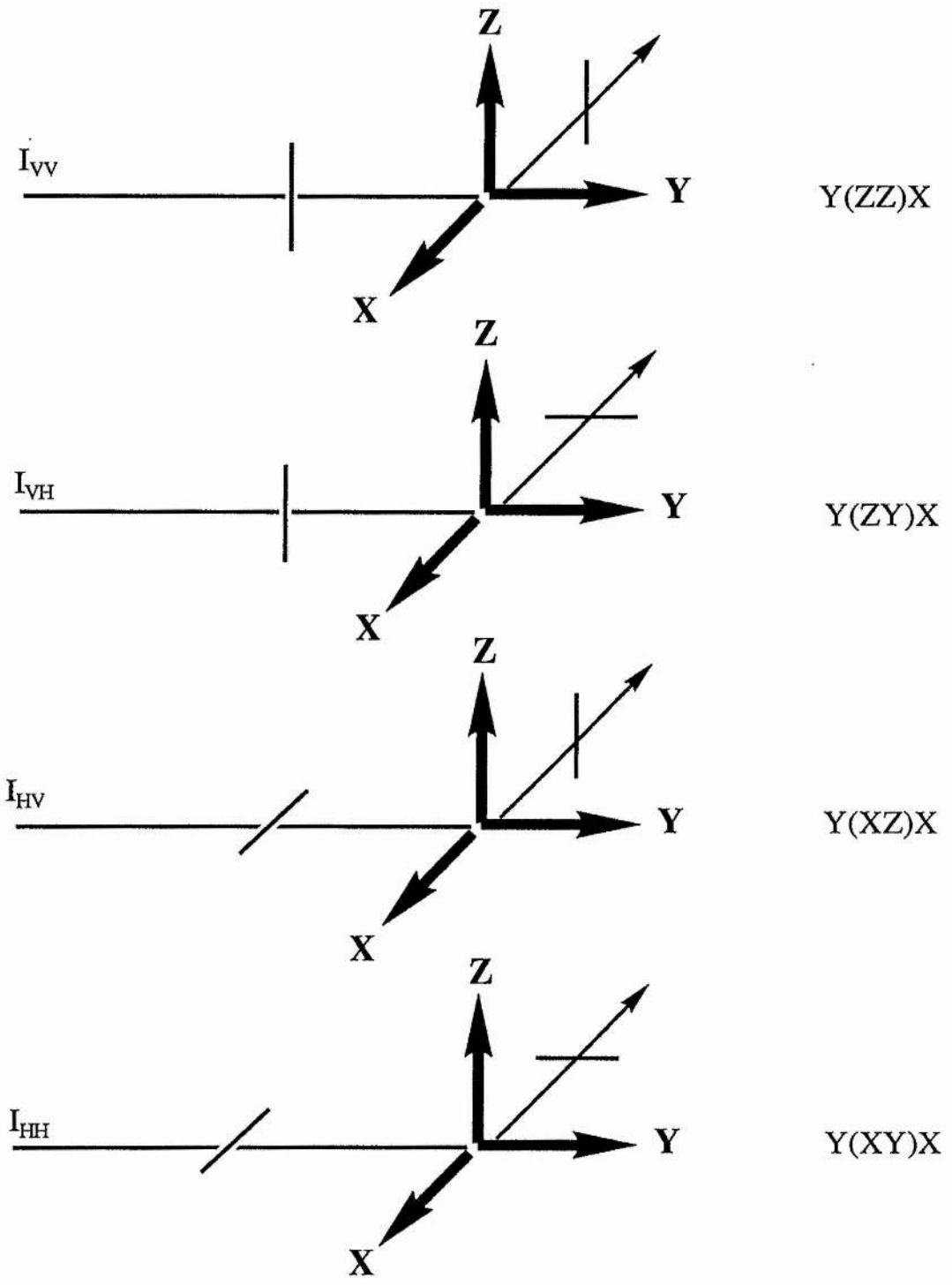

Fig. 3.4: Possible configurations of the experimental set-up in direct geometry

3.2 VIBRATIONAL ANALYSIS

The Raman spectrum of a urea inclusion compound is expected to show bands corresponding to two sets of vibrational modes:

(i) those due to the urea host structure; the frequency of these modes may be expected to remain more or less constant, regardless of the guest molecule.

(ii) those due to the guest molecule; in this study, α,ω-dibromo-*n*-alkane guests $Br(CH_2)_nBr$ (where n = 7-10, in general) were investigated. The number and frequencies of the modes is a function of n.

3.2.1 MODES DUE TO UREA

For the urea host, there are two types of vibrational modes: internal modes and external modes. Internal modes are due to the individual urea molecules, whereas external modes arise from the unit cell, due to the fact that the urea molecules constitute a lattice. Hence the external modes are often termed 'lattice modes'. Because the frequency $\bar{\upsilon}$ of any vibration is inversely related to the vibrating mass M:

$$\bar{\upsilon} = \frac{1}{2\pi}\sqrt{\frac{k}{M}}$$

where k is the force constant, the lattice modes occur at low frequency (< *ca.* 300 cm^{-1}) and the internal modes occur at higher frequencies.

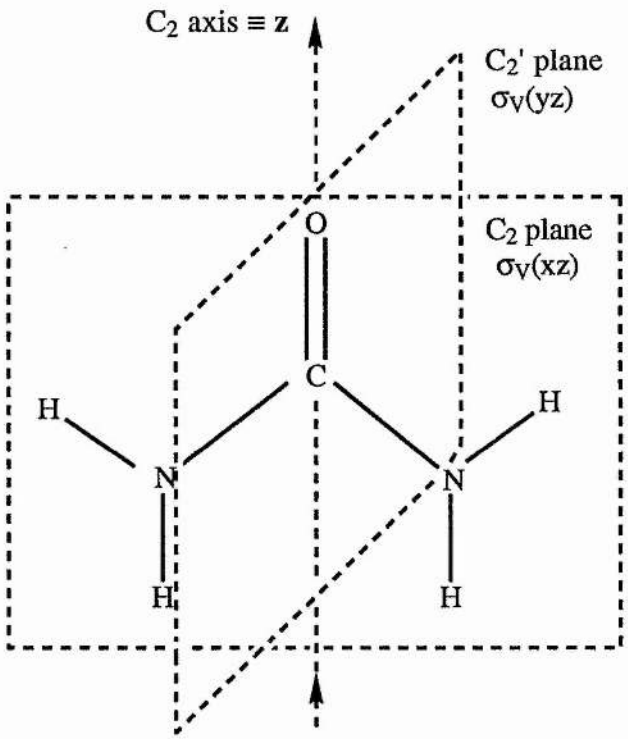

Fig. 3.5: An isolated urea molecule and its symmetry elements

Fig. 3.5 shows an isolated urea molecule. This is planar and belongs to the point group C_{2v}. It has 18 internal vibrations as follows:

$$\Gamma_{urea} = 7A_1 + 2A_2 + 3B_1 + 6B_2$$

At room temperature, the urea host structure is hexagonal with space group $P6_122$ and 6 molecules per unit cell [Schlenk, 1949; Smith, 1950 & 1952]. The site symmetry of the urea molecule is C_2 and the factor group D_6. The correlation given in Scheme 3.1 shows 45 internal and 13 external vibrations to be Raman active:

$$\Gamma_{Raman}^{int} = 9A_1 + 18E_1 + 18E_2$$

$$\Gamma_{Raman}^{ext} = 2A_1 + 5E_1 + 6E_2$$

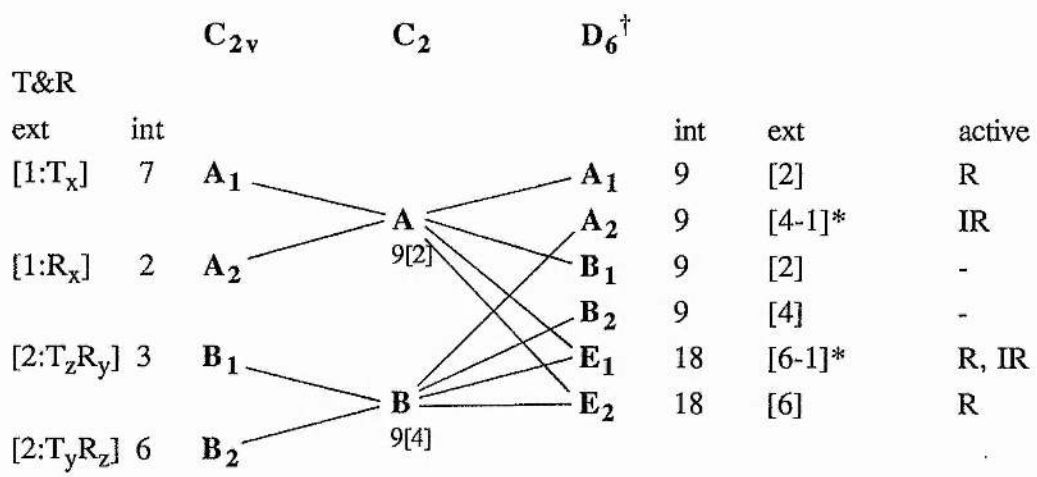

Scheme 3.1: Correlation for the high temperature (hexagonal) phase

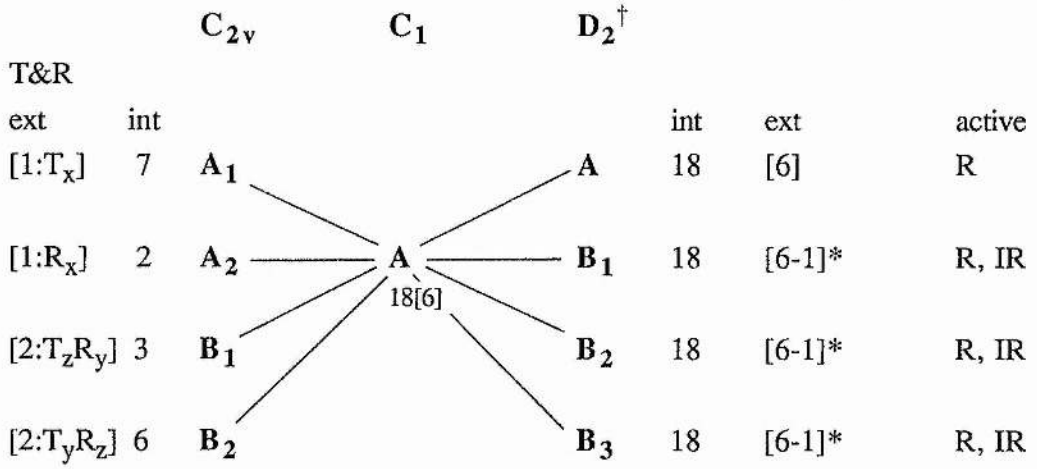

Scheme 3.2: Correlation for the low temperature (orthorhombic) phase

† C_2 axis of point group C_{2v} is parallel to C_2' axis of factor groups D_6 and D_2
* Subtraction of the 3 translations in phase (E_1 and E_2 are doubly degenerate)

Abbreviations:
T&R ⇒ translations and rotations
ext ⇒ no. of external modes [denoted in square brackets]
int ⇒ no. of internal modes
R, IR ⇒ Raman, infrared

At low temperature, the urea host structure in *n*-alkane/urea inclusion compounds is orthorhombic, having undergone a phase transition [Chatani *et al*, 1977 & 1978]. Our studies by differential scanning calorimetry (see Appendix B) suggest that this is also the case for α,ω-dibromoalkane/urea inclusion compounds. The orthorhombic phase has space group $P2_12_12_1$, site symmetry C_1, factor group D_2 and four molecules per unit cell. This gives the correlation shown in Scheme 3.2 with 72 internal and 21 external Raman active vibrations:

$$\Gamma_{\text{Raman}}^{\text{int}} = 18A + 18B_1 + 18B_2 + 18B_3$$

$$\Gamma_{\text{Raman}}^{\text{ext}} = 6A + 5B_1 + 5B_2 + 5B_3$$

In practice, the difference between the spectra above and below the phase transition is minimal, and we thus interpret both sets of vibrations on the assumption that the urea is in the hexagonal phase (i.e. as at high temperature). This is justifiable in view of the fact that the urea structure undergoes only a weak deformation at the transition point [Chatani *et al*, 1978; Harris *et al*, 1990].

The character table for D_6 indicates that the Raman-active components of the polarisability tensor for the high temperature symmetry elements are:

A_1: xx, yy, zz

E_1: xz, yz

E_2: xx, yy, xy

Recalling that:

For Y(ZZ)X: $\overline{(\alpha_{ZZ}')^2} = (\alpha_{zz}')^2$

For Y(XZ)X: $\overline{(\alpha_{XZ}')^2} = \frac{1}{2}\left[(\alpha_{xz}')^2 + (\alpha_{yz}')^2\right]$

For Y(XY)X: $\overline{(\alpha_{XY}')^2} = \frac{1}{8}\left[(\alpha_{xx}' - \alpha_{yy}')^2 + 4(\alpha_{xy}')^2\right]$

we can devise a correlation table of activity for the symmetry elements:

	POLARISATION		
	ZZ	XZ	XY
A_1	√	×	poss
E_1	×	√	×
E_2	×	×	√

3.2.2 MODES DUE TO THE GUEST MOLECULES

3.2.2.1 General Considerations

The vibrational modes of the guest molecules necessarily reflect the constraints imposed by their one-dimensional environment of urea channels. In this analysis, all the α,ω-dibromoalkane molecules are assumed to be in the all-*trans* conformation. In theory, the number and frequency of vibrational modes are dependent on chain length, n. In particular, we expect 'odd/even relationships' for the α,ω-dibromoalkane guests ($Br(CH_2)_nBr$), i.e. one behavioural relationship along the n = 7, 9, ... series and a second behavioural relationship along the n = 8, 10, ... series. This distinction between the n-odd and n-even series arises from the different relative positions of the two Br end-groups on a given molecule, which is evident if we consider the *trans* conformations of the included chains, as shown in Fig. 3.6. For n-odd the Br atoms of any given molecule are mutually eclipsed, whereas for n-even the Br atoms are staggered by 180° relative to one another.

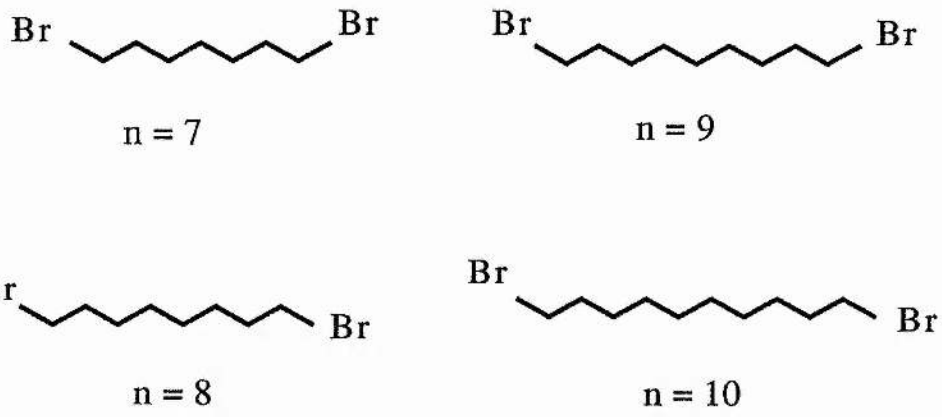

Fig. 3.6: Extended *trans* linear conformation of guest molecules

In the all-*trans* conformation, the odd chains belong to the point group C_{2v} and the even chains to the point group C_{2h}. The total number of vibrational modes expected for each dibromoalkane molecule is detailed in Table 3.1 and may be summarised as follows:

C7: $\Gamma_{vib} = 19A_1 + 13A_2 + 17B_1 + 14B_2 = 63$ modes

C9: $\Gamma_{vib} = 24A_1 + 17A_2 + 22B_1 + 18B_2 = 81$ modes

C8: $\Gamma_{vib} = 21A_g + 15B_g + 16A_u + 20B_u = 72$ modes

C10: $\Gamma_{vib} = 26A_g + 19B_g + 20A_u + 25B_u = 90$ modes

The character tables for C_{2v} and C_{2h} show that the Raman active components of the derived polarisability tensor for each symmetry element are:

C_{2v} A_1: xx, yy, zz

A_2: xy

B_1: xz

B_2: yz

C_{2h}	A_g:	xx, yy, zz, xy
	B_g:	xz, yz
	A_u:	Raman inactive
	B_u:	Raman inactive

Again, recalling that:

For Y(ZZ)X: $\overline{(\alpha_{ZZ}')^2} = (\alpha_{zz}')^2$

For Y(XZ)X: $\overline{(\alpha_{XZ}')^2} = \frac{1}{2}\left[(\alpha_{xz}')^2 + (\alpha_{yz}')^2\right]$

For Y(XY)X: $\overline{(\alpha_{XY}')^2} = \frac{1}{8}\left[(\alpha_{xx}' - \alpha_{yy}')^2 + 4(\alpha_{xy}')^2\right]$

we can predict the activities of each symmetry element:

		POLARISATION		
		ZZ	XZ	XY
C_{2v}				
	A_1	√	×	poss
	A_2	×	×	√
	B_1	×	√	×
	B_2	×	√	×
C_{2h}				
	A_g	√	×	√
	B_g	×	√	×
	A_u		Raman inactive	
	B_u		Raman inactive	

TABLE 3.1: PREDICTED VIBRATIONAL MODES OF THE DIBROMOALKANE

	n odd: point group C_{2v}								n even: point group C_{2h}							
Dibromoalkane	$C_7H_{14}Br_2$				$C_9H_{18}Br_2$				$C_8H_{16}Br_2$				$C_{10}H_{20}Br_2$			
Symmetry element	A_1	A_2	B_1	B_2	A_1	A_2	B_1	B_2	A_g	B_g	A_u	B_u	A_g	B_g	A_u	B_u
$\Gamma\nu$(C-Br)	1	0	1	0	1	0	1	0	1	0	0	1	1	0	0	1
$\Gamma\delta$(C-C-Br)	1	0	1	0	1	0	1	0	1	0	0	1	1	0	0	1
$\Gamma\nu$(C-C)	3	0	3	0	4	0	4	0	4	0	0	3	5	0	0	4
$\Gamma\delta$(C-C-C)	3	0	2	0	4	0	3	0	3	0	0	3	4	0	0	4
$\Gamma\nu(CH_2)$	4	3	3	4	5	4	4	5	4	4	4	4	5	5	5	5
$\Gamma\omega(CH_2)$	3	0	4	0	4	0	5	0	4	0	0	4	5	0	0	5
$\Gamma t(CH_2)$	0	4	0	3	0	5	0	4	0	4	4	0	0	5	5	0
$\Gamma r(CH_2)$	0	3	0	4	0	4	0	5	0	4	4	0	0	5	5	0
$\Gamma\delta(CH_2)$	4	0	3	0	5	0	4	0	4	0	0	4	5	0	0	5
$\Gamma tor(BrCH_2\text{-}CH_2)$	0	1	0	1	0	1	0	1	0	1	1	0	0	1	1	0
$\Gamma tor(CH_2\text{-}CH_2)$	0	2	0	2	0	3	0	3	0	2	3	0	0	3	4	0
Γtotal	19	13	17	14	24	17	22	18	21	15	16	20	26	19	20	25

3.2.2.2 The Longitudinal Acoustic Mode

(I) Definition

Longitudinal acoustic modes, or LAMs, correspond to stationary vibrational waves with one or more nodes in the longitudinal displacements of the skeletal carbon atoms [Minoni & Zerbi, 1982]. Only modes with an odd number of nodes are Raman active, and Raman intensity strongly decreases with increasing number of nodes. LAM-1, which has one node and is often called 'the accordion mode' (Fig. 3.7), gives rise to the strongest LAM line in the Raman spectrum.

(II) Previous Studies

The LAM-1 mode has been modelled (primarily for polymers) using various different approaches:

(i) The elastic rod model

Mizushima & Shimanouchi [1949] have approximated the *trans* planar 'polymethylene' molecule to an elastic rod of length L, density ρ and Young's modulus E, for which the LAM-1 frequency, $\bar{\upsilon}$, at a specific temperature, is given by:

$$\bar{\upsilon} = \frac{1}{2Lc}\frac{E^{1/2}}{\rho}$$

where c is the speed of light in a vacuum. The frequency of the LAM-1 mode is thus inversely proportional to the length of the molecule. This model is a good approximation for solid phase polyethylene; however, α,ω-dibromoalkanes have heavy Br end-groups, which perturb the LAM-1 vibration (due to their large inertial masses), thus affecting its frequency. These end-groups are not taken into account in the simple elastic rod model.

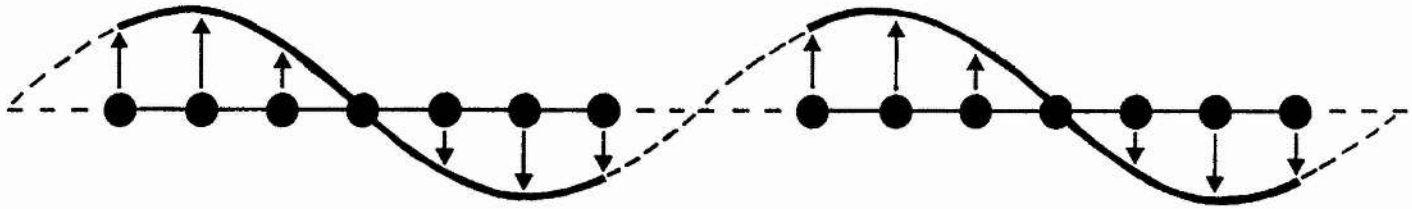

Fig. 3.7: Profile of the LAM-1 mode, showing the vibrational displacements of the atoms (The longitudinal motion is represented as transverse, for clarity)

(ii) The Minoni-Zerbi model

The chain model of Minoni & Zerbi [1982] is more realistic. Here the α,ω-dibromoalkane molecule is treated as a one-dimensional, infinite system, the repeat unit of which is a single, symmetric chain (Fig. 3.8). Groups of atoms are taken as point masses, M representing the terminal substituents (in this case CH_2Br) and m representing the CH_2 units. F is the intrachain force constant and f the force constant between chains. The *trans* planar geometry of the real system is again approximated to a linear one. Interactions are taken to the immediate neighbours and only longitudinal displacements are considered.

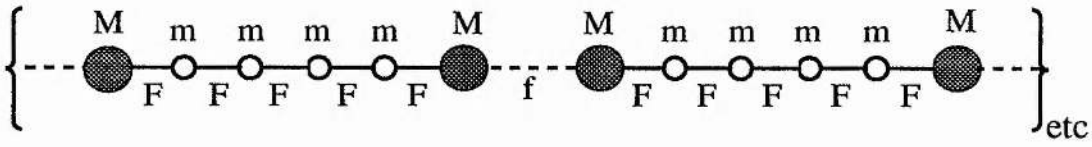

Fig. 3.8: The Minoni-Zerbi model for an infinite system

From an examination of the equations of the atomic motion (which is simple harmonic), the following dispersion relation is derived:

$$\omega^2 = \frac{2F}{m}(1-\cos\vartheta)$$

where $\omega = 2\pi c\,\bar{\upsilon}$ = angular frequency ($\bar{\upsilon}$ being the LAM frequency)

ϑ = the molecular phase

A value for F can be extracted by approximating ω for a particular value of f to the dispersion curve derived by Schaufele & Shimanouchi [1967] for polyethylene.

The molecular phase relation turns out to be:

$$\sin(N-1)\vartheta\,(\cos\vartheta-1)\,[(2K-1-2K^2)\cos\vartheta + 2K^2 - 2K + R - 2RK]$$
$$+\ \cos(N-1)\vartheta\,\sin\vartheta\,[(1-2K)(\cos\vartheta-1)-R]\ +\ R\sin\vartheta\cos kL\ =\ 0$$

where $R = f/F$

$K = M/m$

N = number of point masses in repeat unit

$k = 2\pi\bar{\upsilon}$ =wavevector

L = distance between point masses (i.e. intermolecular bond length)

This equation has N solutions in ϑ for each wavevector k; for Raman scattering, $k \approx 0$ (since $\bar{\upsilon}$ is relatively small). As F, f, m and M are known, the molecular phase relation can be solved (taking k=0) to give values for ϑ. LAM frequencies can then be calculated using the dispersion relation.

The simplest case is a system of isolated chains, i.e. f = 0. For isolated chains:

$\vartheta = 0$ for $\omega = 0$ (pure translation)

$\vartheta = \frac{\pi}{n}$ for LAM-1 (where n = number of C atoms)

The $\omega = 0$ and LAM-1 modes may be represented as shown in Fig. 3.9a; the LAM-1 occurs in the low-frequency region of the Raman spectrum (0-300 cm^{-1}). As end-group mass and/or chain length increases, the LAM-1 frequency decreases.

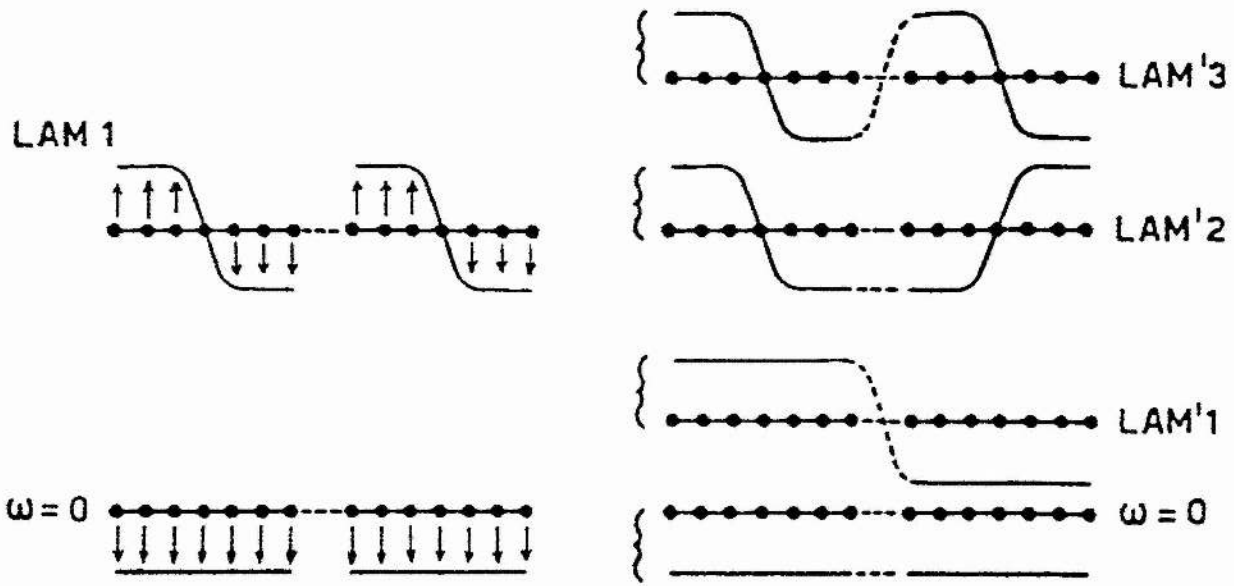

(a) Isolated chains (b) Coupled chains

ω = 0	→	ω = 0 and LAM′-1
LAM-1	→	LAM′-2 (coupling in opposite sense)
		LAM′-3 (coupling in same sense)

Fig. 3.9: Profiles of the vibrational displacements for LAM modes

(In this representation, from Minoni & Zerbi [1982], the sinusoidal envelope is approximated to a square wave)

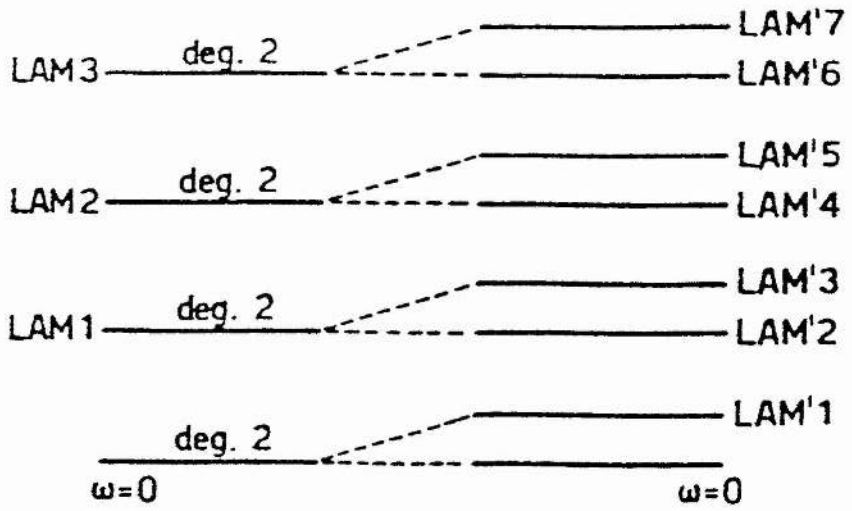

Two isolated chains (levels doubly degenerate)

Two coupled chains

Fig. 3.10 Evolution of LAM′ modes when coupling is introduced [from Minoni & Zerbi, 1982]

This model can be extended to consider the case of coupled chains (i.e. f > 0). Chains may be coupled either in the same sense or after a rotation of 180° (Fig. 3.9b). This coupling leads to an asymmetric splitting of each vibrational level into two components corresponding to the *g* and *u* modes (*gerade* and *ungerade*, respectively) of the coupled chains. New LAM′ modes are thus generated as shown (Figs. 3.9b & 3.10). The extent of splitting is a function of the strength of the force constant, f, which couples the two chains. As f increases, both the frequency and the intensity of the LAM′-3 (pseudo LAM-1) increase. In the general case:

$\bar{\upsilon}$(LAM-1) = $\bar{\upsilon}$(LAM′-3) if f = 0 ⇒ isolated chains

$\bar{\upsilon}$(LAM-1) < $\bar{\upsilon}$(LAM′-3) if f » 0 ⇒ coupled chains

However, $\bar{\upsilon}$(LAM-1) and $\bar{\upsilon}$(LAM′-3) always occur in the same frequency region, even for strongly coupled chains.

In a real system a strong f may correspond to a hydrogen bond (*ca.* 0.5 mdyn/Å), and a weak f to a van der Waals interaction (*ca.* 0.05 mdyn/Å). For comparison, 5 mdyn/Å is of the order of the force constant F for the C-C bond in the *trans* conformation.

Viras *et al* [1989 & 1991] have applied the Minoni-Zerbi model to the 'pure' crystalline α,ω-dibromoalkanes, the success of this approach depending on whether n was even or odd. They used the following parameters (taking k=0):

F = 4.2 mdyn/Å

f = 0.05 mdyn/Å

m = 2.33 x 10^{-26} kg (for the CH_2 groups)

M = 1.56 x 10^{-25} kg (for the CH_2Br groups)

These values were determined from the work of Krimm & Hsu [1978] on *n*-alkane force constants, in accordance with experimental studies by Olf & Fanconi

[1973]. As Viras *et al* [1989 &1991] do not quote numerical values for their calculated frequencies, we have repeated their calculations, using the above parameters. The theoretical LAM-1 frequencies obtained for some α,ω-dibromoalkanes ($Br(CH_2)_nBr$, where n=7-10) are shown in Table 3.2. These are compared with the experimental values, at 173 K, of Viras and co-workers. For the n-even molecules, the theoretical and experimental frequencies are in reasonable agreement. However, Viras *et al* [1991] note that for the n-odd molecules, even reducing the value of f to zero did not lower the theoretical frequencies sufficiently to give agreement with experiment.

n	calc. $\bar{\upsilon}$ / cm^{-1}	obs. $\bar{\upsilon}$ / cm^{-1}
7	158	140
8	145	150
9	135	121
10	127	126

Table 3.2: LAM-1 frequencies for crystalline $Br(CH_2)_nBr$: calculated values (using Minoni-Zerbi model) versus observed values [Viras *et al*, 1989 & 1991]

(iii) Calculations of Edwards and coworkers

Edwards *et al* [1991] have carried out calculations of force constants for various n-even *n*-alkanes and terminally-substituted *n*-alkanes, their aim being to investigate the effect on LAM-1 frequency of substituting end-groups with heavy atoms. They showed that the LAM-1 frequency decreases with increase in chain length and with increase in terminal mass. They used a modified version of the Snyder-Schachtschneider [1963] program with a simple valence force field and interaction constants. Input data consisted of molecular parameters, symmetry elements, the

number of atoms in the molecule, the molecular stereochemistry and the molecular vibrations. They find that, for the even α,ω-dibromoalkanes, the LAM-1 occurs at the frequencies, $\bar{\upsilon}$, shown in Table 3.3. The stretching force constant used was 2.90 mdyn/Å. Their observed values are also shown for comparison; the temperature was not specified.

n	calc. $\bar{\upsilon}$ / cm^{-1}	obs. $\bar{\upsilon}$ / cm^{-1}	diff. = $\Delta\bar{\upsilon}$ / cm^{-1}
8	148.6	149.0	- 0.4
10	124.5	123.8	+ 0.7
12	106.8	108.0	- 1.2
14	90.5	96.0	- 0.5

Table 3.3: Calculated and observed LAM-1 frequencies for crystalline $Br(CH_2)_nBr$ [Edwards *et al*, 1991]

(iv) LAM-TAM coupling theory of Mazur & Fanconi

Mazur & Fanconi [1979] have performed a normal mode analysis for the acoustic modes of *n*-alkanes, $CH_3(CH_2)_nCH_3$, with n=6-18. The aim of this work was to compare the calculated intensities and frequencies of the LAM-1 modes with experimental values. They have shown that, for the n-odd molecules, there is a coupling between an 'unperturbed' LAM-1 and an 'unperturbed' transverse acoustic mode, TAM-4, which leads to a shift in frequency of both vibrations. They propose that such vibrational modes can interact provided they belong to the same symmetry species and their unperturbed frequencies are close to each other. Therefore, this coupling cannot occur for the n-even molecules since LAM-1 has symmetry A_g and TAM-4 has symmetry B_u (although LAM-1 and TAM-3 have the same symmetry and may interact if their frequencies are sufficiently similar). However, for the n-odd

molecules, LAM-1 and TAM-4 both belong to symmetry species A_1 and to point group C_{2v}. The coupling occurs through Fermi-type resonance, which is created by the difference in masses between the terminal methyl groups and the methylene repeat units. The maximum coupling for the *n*-alkanes occurs when n=11.

3.2.2.3 Existence of *Gauche* Defects

(I) Definition

Although the bulk conformation of the α,ω-dibromoalkane molecules in the urea channel is *trans*, there may be a small percentage of end-group Br's which are in the *gauche* conformation, as illustrated by the Newman projections shown in Fig. 3.11. We term such end-groups '*gauche* defects'. For molecules containing *gauche* defects, the molecular point symmetry is C_1, as discussed by Snyder [1967]: all vibrations are thus Raman active.

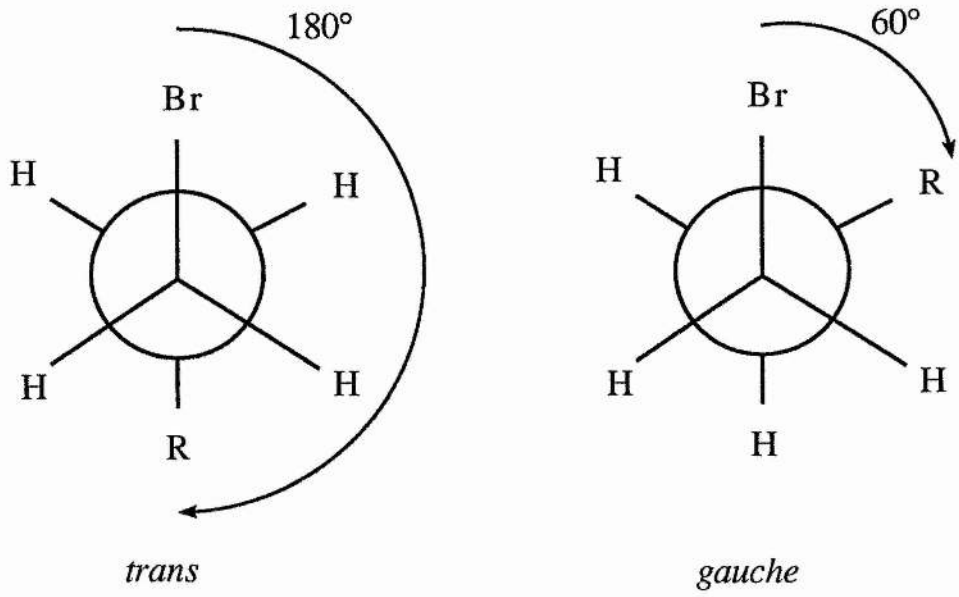

Fig. 3.11: Newman projections showing the *trans* and *gauche* conformers at the terminal carbon (R represents the rest of the chain)

The ν(C-Br) stretching modes for the *trans* and *gauche* conformations have different characteristic frequencies in the 300-1000 cm^{-1} region of the Raman spectrum. Despite their different symmetries, these modes can be used to probe the existence of *gauche* defects.

(II) Previous Studies

The *n*-alkane/urea inclusion compounds have already been studied from the point of view of CH_3 *gauche* defects. Unlike the *trans* and *gauche* bands due to the stretching ν(C-Br), the rocking r(CH_3) *trans* and *gauche* bands occur at similar frequencies in the Raman spectrum, so it is more difficult to distinguish between them. Nevertheless, Kobayashi *et al* [1990] have studied the n-even *n*-alkane guests, $CH_3(CH_2)_nCH_3$ where n=14-22, by Raman spectroscopy: they quote an average of *ca.* 5% of *gauche* end-groups at room temperature, irrespective of chain length.

The proportion of *gauche* to *trans* end-groups, P(gt)/P(tt), was calculated from the relative intensities, I(gt)/I(tt), of the *trans* and *gauche* r(CH_3) bands measured in the ZZ polarisation. To allow for the different polarisations of the *trans* and *gauche* modes, a factor of 0.45 was introduced, calculated according to the bond polarisability model of Kim *et al* [1989]:

$$\frac{P(gt)}{P(tt)} = 0.45\,\frac{I(gt)}{I(tt)}$$

Studies of the *n*-alkane/urea inclusion compounds, using other techniques, have yielded wildly inconsistent values for the proportion of CH_3 *gauche* defects. A summary of these studies is given in Table 3.4. From the values given for G, we conclude that there *may* be a chain-length dependence, the proportion of *gauche* defects generally being higher in the shorter molecules. However, this conclusion is not clear-cut and, notwithstanding the diversity of chain lengths studied, there is evidently much controversy. An alternative conclusion is that studies by vibrational spectroscopy

suggest that the percentage of *gauche* defects is low (≤~7%), whereas studies by ^2H NMR give a much higher value (≥~15%), and computational methods yield variable results.

Reference	n	$\mathcal{G}$ /%	Method
Wood *et al* [1989]	16	'small'	Raman / infrared
Casal [1990]	13-19	< 3	Infrared
Lee *et al* [1992]	13,23,33	< 3	MDS
Kobayashi *et al* [1990]	14-22	~ 5	Raman
Newton [1990]	19	< 7	Raman
Cannarozzi *et al* [1991]	8,10,12,16,19,36	7-15	^2H NMR
Imashiro *et al* [1989]	7-10	16-25	^{13}C NMR / MMC
Vold *et al* [1989]	19	40	^2H NMR / MDS

Table 3.4: Percentage ($\mathcal{G}$) of CH_3 *gauche* defects in $CH_3(CH_2)_nCH_3$/urea inclusion compounds

Abbreviations: NMR = nuclear magnetic resonance spectroscopy
MDS = molecular dynamics simulations
MMC = molecular mechanics calculations

Although the *gauche* defects in $Br(CH_2)_nBr$/urea inclusion compounds have not been studied as such, Meakins [1955] has carried out dielectric loss spectroscopy on $Br(CH_2)_{10}Br$/urea. He concluded that the Br end-groups undergo motions independent from the rest of the guest molecule: we suggest that these motions may be the source of *trans*↔*gauche* interconversion.

3.3 OBJECTIVES

The purpose of this Raman spectroscopic study was to characterise the α,ω-dibromoalkane/urea inclusion compounds through the identification and interpretation of their vibrational modes occurring in the spectral range 20-2000 cm^{-1}. Spectra were recorded both above and below the phase transition temperature.† Specific objectives were as follows:

(I) For the urea host:

i) verification of the hexagonal (or orthorhombic) phase, in order to assess the integrity of the inclusion compounds (pure crystalline urea being tetragonal)

ii) study of the urea 'lattice modes'

(II) For the dibromoalkane guests:

i) study of the frequency of the longitudinal acoustic mode, and whether this frequency is affected by the constraining environment of the guest molecules

ii) analysis of *gauche* defects at the chain ends by study of the ν(C-Br) *gauche* and *trans* bands, and investigation of the evolution of the relative intensities of these bands as a function of:

(a) end-substituent (by comparison with other α,ω-dihaloalkane guests)

(b) temperature

(c) pressure

The ratio of the intensity of the *gauche* band relative to that of the *trans* is denoted $I_{g/t}$: this is defined in different ways depending on the spectra being considered (see later).

† Differential scanning calorimetry (Appendix B) showed the phase transition temperature to be *ca.* 156 K for 1,8-dibromooctane/urea, for example.

3.4 EXPERIMENTAL CONDITIONS*

3.4.1 SAMPLES STUDIED

The inclusion compounds were prepared as detailed in Appendix A. The samples were single crystals of α,ω-dihaloalkane/urea-h_4 inclusion compounds. Typical crystal dimensions were *ca.* 3.0 x 0.5 x 0.5 mm^3. Each crystal was sealed in a thin glass tube with its long axis (which corresponds to the channel axis **c**) parallel to the **Z** axis of the laboratory reference frame, i.e. in the semi-oriented set-up described previously. The sample tube was placed in a cryostat, allowing investigations in the 80 K to 300 K temperature range; the temperature measurement was accurate to ±3 K.

3.4.2 SPECTRAL CONDITIONS

The incident radiation was the 5145 Å (514.5 nm) line of an Ar^+ ion Spectra Physics laser, of power in the region 150-300 mW at the sample. Spectra were generally recorded in three frequency ranges: 20-300 cm^{-1}, 300-1000 cm^{-1} and 1040-2000 cm^{-1}. Spectrometers used were a triple-monochromator Dilor Z24 and a double-monochromator Jobin-Yvon Ramanor (the latter principally for the 20-300 cm^{-1} region). The spectral slit widths were 1.45 cm^{-1} in the low-frequency (20-300 cm^{-1}) region and 2.74 cm^{-1} above.

3.4.2.1 General Study of $Br(CH_2)_nBr$/Urea

The samples studied were $Br(CH_2)_nBr$/urea, generally with n=7, 8, 9, 10. Spectra were recorded in the low temperature phase (denoted LT) at 93 K or 108 K and in the high temperature phase (denoted HT) at 298 K. Polarisations used were Y(ZZ)X, Y(XZ)X, Y(ZY)X and Y(XY)X in direct geometry, and X(ZZ)$\overline{X}$, X(ZY)$\overline{X}$, X(YZ)$\overline{X}$ and X(YY)$\overline{X}$ in retro geometry. The spectral range investigated was *ca.* 20-2000 cm^{-1}.

---

* Details of the sample and experimental conditions for the study of 1,6-dibromohexane/urea are given later (§3.6.2).

3.4.2.2 Detailed Study of ν(C-Br) *Gauche* Bands

Additional spectra were recorded in order to follow the evolution of $I_{g/t}$ as a function of :

(a) end-substituent

Spectra were recorded at 298 K in the direct ZZ, XZ and XY polarisations for $Cl(CH_2)_8Cl$/urea, $Br(CH_2)_8Br$/urea and $I(CH_2)_8I$/urea in the frequency ranges 450-650 cm^{-1}, 500-700 cm^{-1} and 500-800 cm^{-1}, respectively (these being appropriate frequency ranges for the respective ν(C-X) stretching modes [Dollish *et al*, 1974]).

(b) temperature

$Br(CH_2)_8Br$/urea was studied in the direct {ZZ+XZ} polarisation in the frequency range 500-700 cm^{-1} over the temperature range 93 K to 203 K. Spectra were recorded at intervals of 20 K; smaller temperature intervals (of 5 K) were used near the phase transition (i.e. *ca.* 156 K).

*(c) hydrostatic pressure**

These experiments were carried out at 298 K using a home-built device described in detail by Martin *et al* [1986]. The nature of these experiments allowed only polycrystalline samples to be studied; those used were $Br(CH_2)_nBr$/urea with n = 7, 9 and 11 (to probe chain length effects for the n-odd series). The pressure range was 1 bar to 6 kbar; He was used as the compressing fluid. Unpolarised spectra were recorded (in direct geometry) on the double-monochromator Jobin-Yvon Ramanor spectrometer in the frequency range 500-700 cm^{-1}.

* The experimental work in §3.4.2.2 part (c) was carried out by Dr François Guillaume and Abdelkarim El Baghdadi.

3.4.3 METHODS OF SPECTRAL ANALYSIS

The general spectra (described in §3.4.2.1 above) were used for study of both urea and guest modes across the entire spectral region (20-2000 cm^{-1}). In addition, the low-frequency spectra (20-300 cm^{-1}) were used to study the LAM-1 mode. It was expected that the LAM-1 bands would be partially hidden under bands due to urea: therefore, frequencies and bandwidths of the LAM-1 were determined by fitting several Lorentzian functions, convoluted to a triangular instrumental resolution, to the experimental profiles. The following equation was used for each Lorentzian function; the scaling factor accounts for the difference between the calculated and experimental intensities (the former being equal to unity), and the fitted parameters were Δ, η and $\bar{\upsilon}_{max}$:

$$\hat{I}(\bar{\upsilon}) = 2c \int_0^{\infty} [\exp(-\sigma t) \cdot \exp(-2\pi i c \bar{\upsilon} t)]\, dt$$

where $I(\bar{\upsilon}) = \eta \hat{I}(\bar{\upsilon})$ and $\hat{I}(\Delta) = \frac{\hat{I}(0)}{2}$

where $I(\bar{\upsilon})$ = experimental intensity of band

$\hat{I}(\bar{\upsilon})$ = calculated intensity of band

$\eta = \int_{-\infty}^{\infty} I(\bar{\upsilon})\, d\bar{\upsilon}$ = scaling factor ≡ amplitude of fitted band

$\bar{\upsilon} = \bar{\upsilon}' - \bar{\upsilon}_{max}$ where: $\bar{\upsilon}'$ is frequency of band (cm^{-1})

$\bar{\upsilon}_{max}$ is maximum frequency of band (cm^{-1})

$\Delta = \frac{\sigma}{2\pi c}$ = half-width of band at half-height (cm^{-1})

t = time (s)

c = speed of light in a vacuum ($cm.s^{-1}$)

For the mid-frequency spectra (300-1000 cm^{-1}), an integration program was used to determine relative intensities of the ν(C-X) bands: this involved calculation by the trapezium method of the surface area under the bands between specified frequency limits. The *gauche:trans* band intensity ratio $I_{g/t}$ was then evaluated, from the general spectra (described in §3.4.2.1 above), for all the compounds in the different polarisations at the two temperatures studied. Using the spectra described in §3.4.2.2, the evolution of $I_{g/t}$ was followed as a function of end-substituent, temperature and pressure.

This work was carried out at the Université de Bordeaux 1; some of it has been published [Smart *et al*, 1992; see also Smart *et al*, submitted for publication & Smart *et al*, in preparation].

TABLE 3.5: OBSERVED RAMAN FREQUENCIES (CM^{-1}) FOR UREA MODES

n=7		n=8		n=9		n=10				
LT	HT	LT	HT	LT	HT	LT	HT	ASSIGN.[T]	POL.[N]	SYM.[Y]
1714	1705	**1715**	**1706**	1719	1707	**1714**	**1707**	$\delta(NH_2)$	ZZ	A_1
1687	1678	**1688**	**1680**	1688	1677	**1685**	**1667**	$\delta(NH_2)$	XZ	E_1
1669	1660	**1668**	**1662**	1669	1664	**1668**	**1661**	$\delta(NH_2)$	XZ	E_1
1602	1595	**1599**	**1598**	1601	1598	**1594**	**1594**	$\delta(NH_2)$*	XZ	E_1
1551	1557	**1553**	**1559**	1556	1563	**1551**	**1565**	ν(CO)	ZZ	A_1
1525	1511	**1525**	**1514**	1528	1513	**1524**	**1509**	ν_a(CN)	XZ	E_1
1130	1140	**1133**	**1142**	1141	1143	**1132**	**1141**	$r(NH_2)$	ZZ	A_1
1071	1070	**1061**	**1064**	1064	1064	**1066**	**1066**	$r(NH_2)$	XZ	E_1
1030	1025	**1030**	**1025**	1030	1025	**1030**	**1025**	ν_s(CN)†	ZZ	A_1
612	608	**614**	**609**	616	608	**612**	**607**	δ(NCO)	XZ	E_1
534	530	**535**	**530**	536	531	**535**	**529**	δ(NCO)	ZZ	A_1
184	163	**185**	**164**	186	163	**185**	**166**		XY	E_2
132	132	**136**	**129**	136	128	**137**	**129**	lattice	ZZ	A_1
101	97	**104**	**96**	99	96	**102**	**98**	modes	XZ	E_1
60	55	**60**	**55**	60	58	-	**60**		?	?

* very weak
† very intense

3.5 RESULTS AND DISCUSSION

In general, the total number of bands observed both at high and low temperature is consistently lower than the number predicted theoretically. The missing bands are presumably of very low intensity: either they lie under stronger bands or they cannot be distinguished from the noise in the spectrum.

Lowering the temperature generally results in an increase in band frequency by several cm^{-1} and a sharpening of the bands. Other differences in the spectra on going to low temperature are minimal. In particular, the total number of bands observed is the same as at high temperature, indicating that any structural changes occurring are small; a hexagonal-phase analysis thus seems justified both for the high-temperature and the low-temperature spectra.†

3.5.1 UREA HOST

The frequencies of the vibrational modes due to the host remain more or less constant for all chain lengths of the guest. The band frequencies have been listed, with their assignments, in Table 3.5. The external vibrations (lattice modes) of urea all occur at low frequencies (i.e. < 300 cm^{-1}). The δ(NCO) modes occur at *ca.* 530 cm^{-1} and *ca.* 608 cm^{-1} in the HT phase; the other internal urea modes occur in the high frequency region (1000-2000 cm^{-1}).

Note the very intense ν_s(CN) mode, which occurs at 1025 cm^{-1} (HT) and 1030 cm^{-1} (LT): this peak is of A_1 symmetry, is strongly ZZ polarised and is characteristic of hexagonal (and orthorhombic) urea, as noted, *inter alia*, by Fawcett & Long [1975], Le Brumant *et al* [1984] and Casal [1984]. Due to its extreme intensity, we did not actually record it in our spectra. Instead, this mode was used, prior to recording the spectra, to:

† Although the orthorhombic phase is the more general (hexagonal being a special case of orthorhombic), the hexagonal-phase analysis is simpler and is conventionally the one chosen.

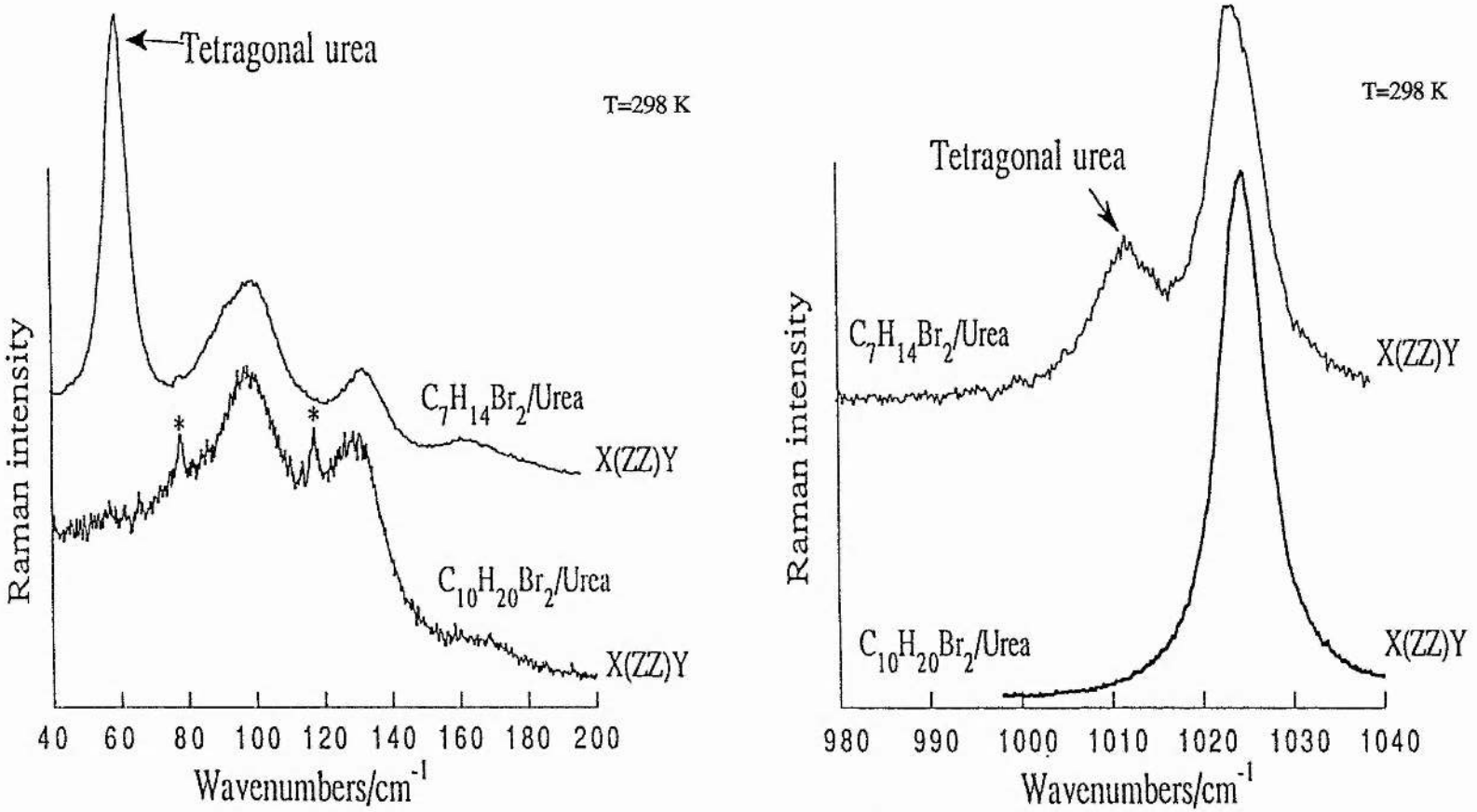

(a) The urea lattice mode spectral region

(b) The ν(C-N) stretching mode spectral region

Fig. 3.12: X(ZZ)Y-polarised Raman spectra for a partly decomposed urea inclusion compound ($C_7H_{14}Br_2$/urea) and for one of high structural integrity ($C_{10}H_{20}Br_2$/urea). The asterisks indicate Ar^+ emission lines (occurring at 77 cm^{-1} and 117 cm^{-1} for λ_0=514.5 nm).

- verify the structural integrity of our inclusion compounds (the corresponding peak for pure crystalline urea occurs at 1010 cm^{-1} at HT)
- ensure the spectrometer was well calibrated
- optimise the experimental conditions such that this peak was indeed strongly ZZ polarised (by comparison with the XZ and XY polarisations).

Raman spectra of a partly decomposed urea inclusion compound are shown in Fig. 3.12, illustrating the presence of bands at 60 cm^{-1} and 1010 cm^{-1} due to tetragonal urea. These spectra are contrasted with those of a urea inclusion compound of high structural integrity.

3.5.1.1 Lattice Modes

These occur at frequencies of < 300 cm^{-1}. As discussed previously, a maximum of 13 Raman active modes are expected for the HT phase:

$$\Gamma_{ext} = 2A_1 + 5E_1 + 6E_2$$

of which A_1 is ZZ active (possibly also active in XY)

E_1 is XZ active

E_2 is XY active

Fig. 3.13 shows low-frequency Raman spectra for one sample (1,8-dibromo–octane/urea) in ZZ, XZ and XY polarisations at LT and HT. Of the four observed lattice modes, three have been assigned as having the following symmetries:

$$A_1 + E_1 + E_2$$

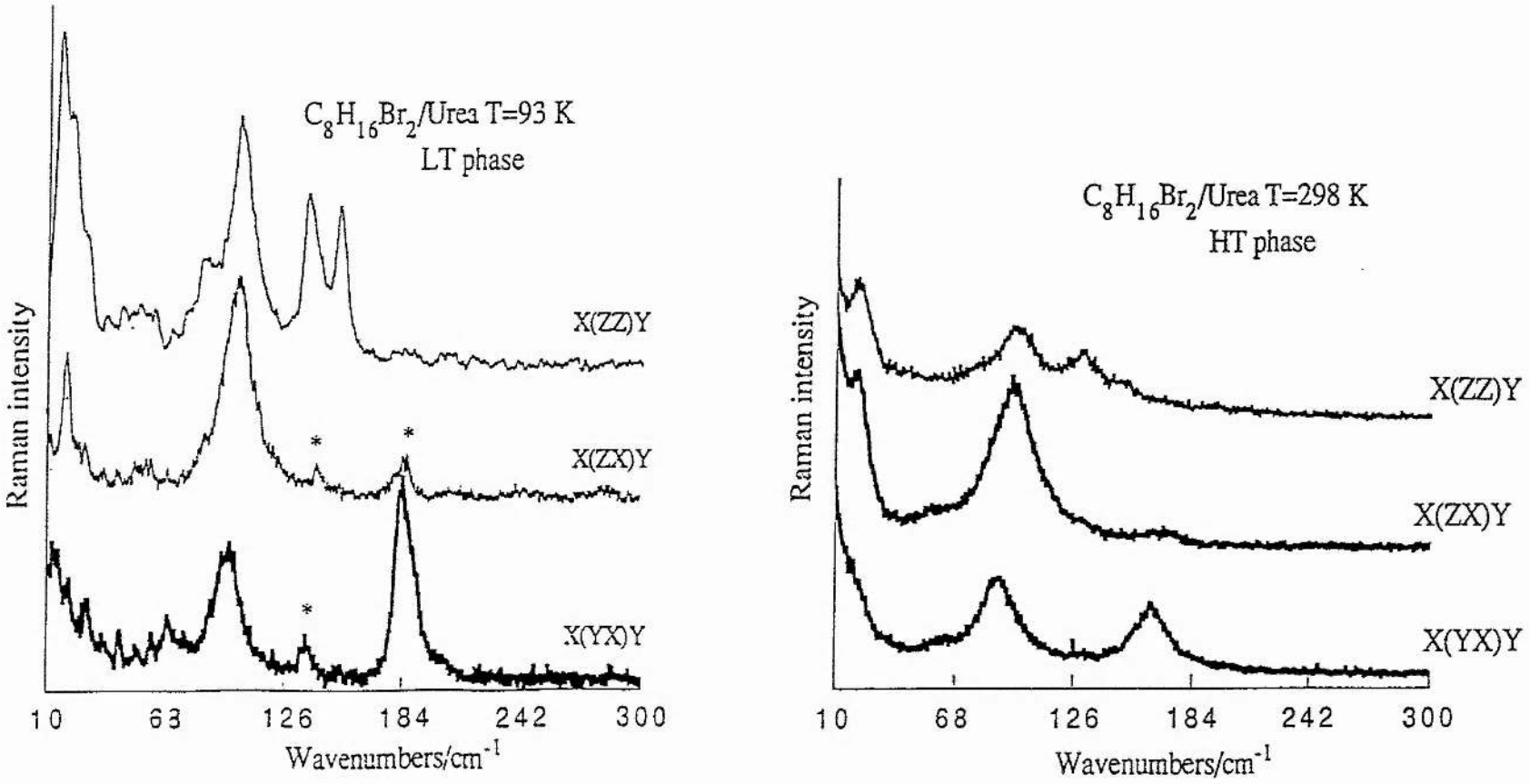

Fig. 3.13: Low-frequency Raman spectra, illustrating bands due to the urea lattice modes of 1,8-dibromooctane/urea for different polarisations in the LT and HT phases

Some of the lattice modes reflect the changes in channel structure which occur at the phase transition. Note that:

(i) The band at 185 cm^{-1} at LT, which is polarised XY (i.e. E_2 symmetry) moves considerably (to 164 cm^{-1}) on going to high temperature. Scheme 3.1 (see §3.2.1) shows that E_2 modes arise from T_zR_y and T_yR_z coupled translations and rotations. Although this band cannot be definitively assigned to a well-defined lattice vibration, it is not incompatible with an oscillation (or 'breathing') of the urea channel in the plane perpendicular to the **c** axis. At the phase transition there is a drastic change in frequency of this vibration as the channel radius dilates (LT $\rightarrow$ HT) or contracts (HT $\rightarrow$ LT), as described by Chatani *et al* [1978]. This assignment is in accord with Le Brumant *et al* [1984].

(ii) The ZZ polarised band at *ca.* 135 cm^{-1} at LT and *ca.* 130 cm^{-1} at HT is of A_1 symmetry. Scheme 3.1 shows that A_1 modes result from translations T_x along and rotations R_x. Therefore, this band may be assigned tentatively to the 'stretching' of the urea channel in the **c** direction. This assignment is in disagreement with that of Kobayashi *et al* [1990], who attribute this band to the 'totally symmetric breathing mode of the lattice' (i.e. perpendicular to the **c** axis). However, our spectra show that the frequency variation with temperature for the band at 135 cm^{-1} is much smaller than for the band at 185 cm^{-1}. This suggests that ours is more likely to be the correct assignment. Nevertheless, because the host lattice constitutes a spiral, these two 'respiration' modes are related, and they may both have both XY- and ZZ-polarised components.

(iii) The broad XZ-polarised band at 101 cm^{-1} (symmetry E_1) does not shift significantly with change of temperature. This band is observed by both Le Brumant *et al* [1984] and Fawcett & Long [1975].

(iv) The other band arising from lattice vibrations occurs at *ca.* 60 cm^{-1} and is of comparatively weak intensity at both LT and HT. It is not obviously polarised, hence a definitive assignment to a vibrational mode is difficult; indeed, there may be several different modes contributing to this band. Fawcett & Long [1975] and Le Brumant *et al* [1984] assign this band to a ZZ polarised vibration (i.e. symmetry A_1) of hexagonal urea. However, a sharp, intense peak at 60 cm^{-1} is characteristic of tetragonal urea. Since the band at 60 cm^{-1} in our spectra was broad and not very intense, it is probably akin to that seen by Fawcett & Long [1975] and Le Brumant *et al* [1984].

3.5.1.2 Internal Modes

All the internal modes of urea occur at frequencies above 300 cm^{-1}. As discussed previously, there are a maximum of 45 Raman active modes at HT, as follows:

$$\Gamma_{int} = 9A_1 + 18E_1 + 18E_2$$

In total, we have identified 11 internal modes of urea in the frequency range 300-2000 cm^{-1} at HT with symmetries:

$$5A_1 + 6E_1$$

However, spectra were not recorded above 2000 cm^{-1}, in which region Fawcett & Long [1975] predict 4 $\nu(NH_2)$ stretching modes. The 11 modes that we did observe are assigned as follows:

$\delta(NH_2)$:	$1A_1 + 3E_1$
$r(NH_2)$:	$1A_1 + 1E_1$
$\delta(NCO)$:	$1A_1 + 1E_1$
$\nu(CN)$:	$1A_1 + 1E_1$
$\nu(CO)$:	$1A_1$

The A_1 modes are polarised ZZ, the E_1 modes XZ. These assignments agree with the observations of Le Brumant *et al* [1984].

The presence of the hexagonal phase of urea is confirmed by the very intense ν_s(CN) band at 1025 cm^{-1} (as noted previously), and also by the characteristic frequencies of the two δ(NCO) bending modes, which occur at 608 cm^{-1} (E_1) and 530 cm^{-1} (A_1) in the HT phase. By comparison, tetragonal urea is characterised by a sharp band at 60 cm^{-1}, and two δ(NCO) bands and a ν_s(CN) band at 556, 570 and 1010 cm^{-1}, respectively, at HT [e.g. Fawcett & Long, 1975; Le Brumant *et al*, 1984; Casal, 1984, 1985 & 1990].

3.5.2 DIBROMOALKANE GUEST

The frequencies of the Raman bands due to the guest molecules, with their proposed assignments, are presented in Table 3.6.

3.5.2.1 The LAM-1 Mode

ZZ-polarised Raman spectra illustrating the LAM-1 bands at LT and HT are shown in Fig. 3.14 a&b. The existence of bands due to the LAM-1 mode confirms that the dibromoalkane molecules are indeed in the all-*trans* conformation within the urea channels and that they do not contain mid-chain kinks. This mode is strongly ZZ polarised. Lorentzians fitted to the spectra recorded in the ZZ polarisation at LT and HT yield the LAM-1 frequencies, $\bar{\upsilon}$, and bandwidths, σ, given in Table 3.7.

TABLE 3.6: OBSERVED RAMAN FREQUENCIES (CM^{-1}) FOR MODES OF THE DIBROMOALKANE

n=7		n=8		n=9		n=10				
LT	HT	LT	HT	LT	HT	LT	HT	ASSIGN.[T]	POL.[N]	SYM.[Y]
										n_{odd} / n_{even}
1460	1456	**1462**	**1458**	1460	1459	**1458**	**1452**	$\delta(CH_2)$	ZZ	A_1 / A_g
1435	1436	**1432**	**1435**	1434	1437	**1434**	**1436**	$\delta(CH_2)$	ZZ	A_1 / A_g
1362		**1345**							ZZ	
1337	-	**1323**	**1341**	1328	1340	**1319**	**1338**	$\delta(CH_2)$	ZZ	A_1 / A_g
1288	1290	**1297**	**1297**	1300	-	**1296**	**1289**	$t(CH_2)$	XZ	B_2 / B_g
1244	1246	**1239**	**1239**	1269	1260	**1261**	**1258**	$\omega(CH_2)$?	ZZ	A_1 / A_g
1210	1211								ZZ	
1197	1199	**1206**	**1207**	1206	1205	**1202**	**1200**	$\omega(CH_2)$?	ZZ	A_1 / A_g
1086	1085	**1095**	**1092**	1098	1096	**1103**	**1100**	ν(C-C)	ZZ	A_1 / A_g
993	996	**998**	**990**	996	-	**984**	**979**	$\nu(CH_2)$*	XY	A_2 / A_g
803	814	**798**	**803**	800	-	**796**	**794**	$r(CH_2)$	XZ	B_2 / B_g
736	726	**739**	**730**	740	726	**737**	**732**	$r(CH_2)$	XZ	B_2 / B_g
656	653	**662**	**660**	663	659	**662**	**654**	$\nu(CBr)_t$	ZZ	A_1 / A_g
570	571	**569**	**570**	571	570	**570**	**569**	$\nu(CBr)_g$	XY	-
443	442	**441**	**443**	468	468	**468**	**466**	δ(CCBr)	ZZ	A_1 / A_g
				453	454			δ(CCBr)	XZ	B_1 / -
338	-	**336**	**339**	362	363	**369**	**367**	?	ZZ	A_1 / A_g
249	hidden	**-**	**-**	227	hidden	**-**	**-**	TAM?	ZZ	A_1 / -
212	204	**-**	**-**	205	hidden	**-**	**-**	TAM-4?	ZZ	A_1 / -
132	133	**151**	**151**	115	116	**122**	**126**	LAM-1	ZZ	A_1 / A_g
81	89	**87**	**89**	96	91	**100**	**92**	?	XY?	?
21	21	**20**	**20**	24	22	**18**	**-**	tor(CH_2CH_2)?	XZ	B_2 / B_g

t ⇒ trans

g ⇒ gauche

* ⇒ weak

⇒ overlapping bands

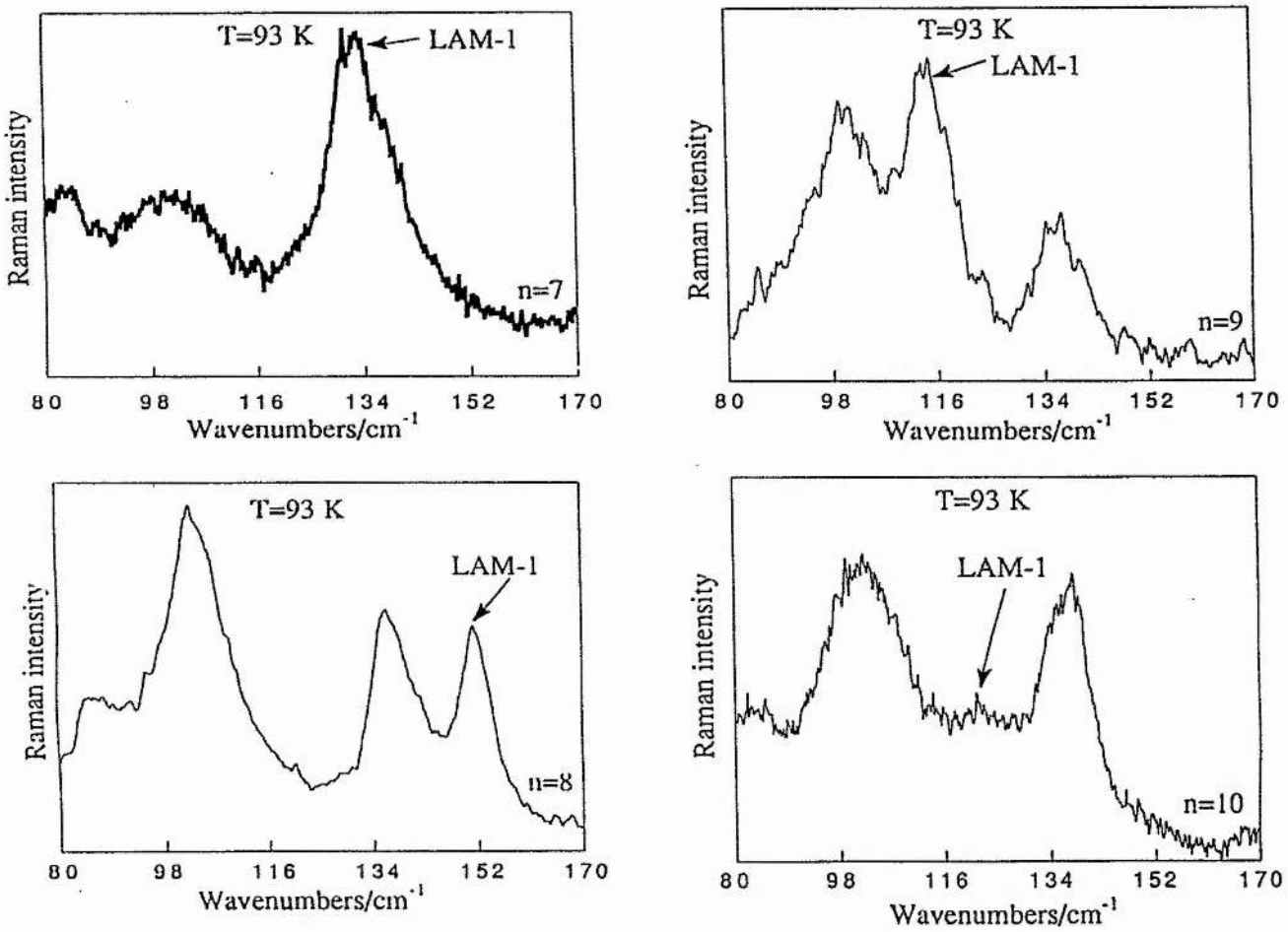

Fig. 3.14a: Low-frequency X(ZZ)Y-polarised Raman spectra, illustrating the LAM-1 bands for $C_nH_{2n}Br_2$/urea inclusion compounds in the LT phase

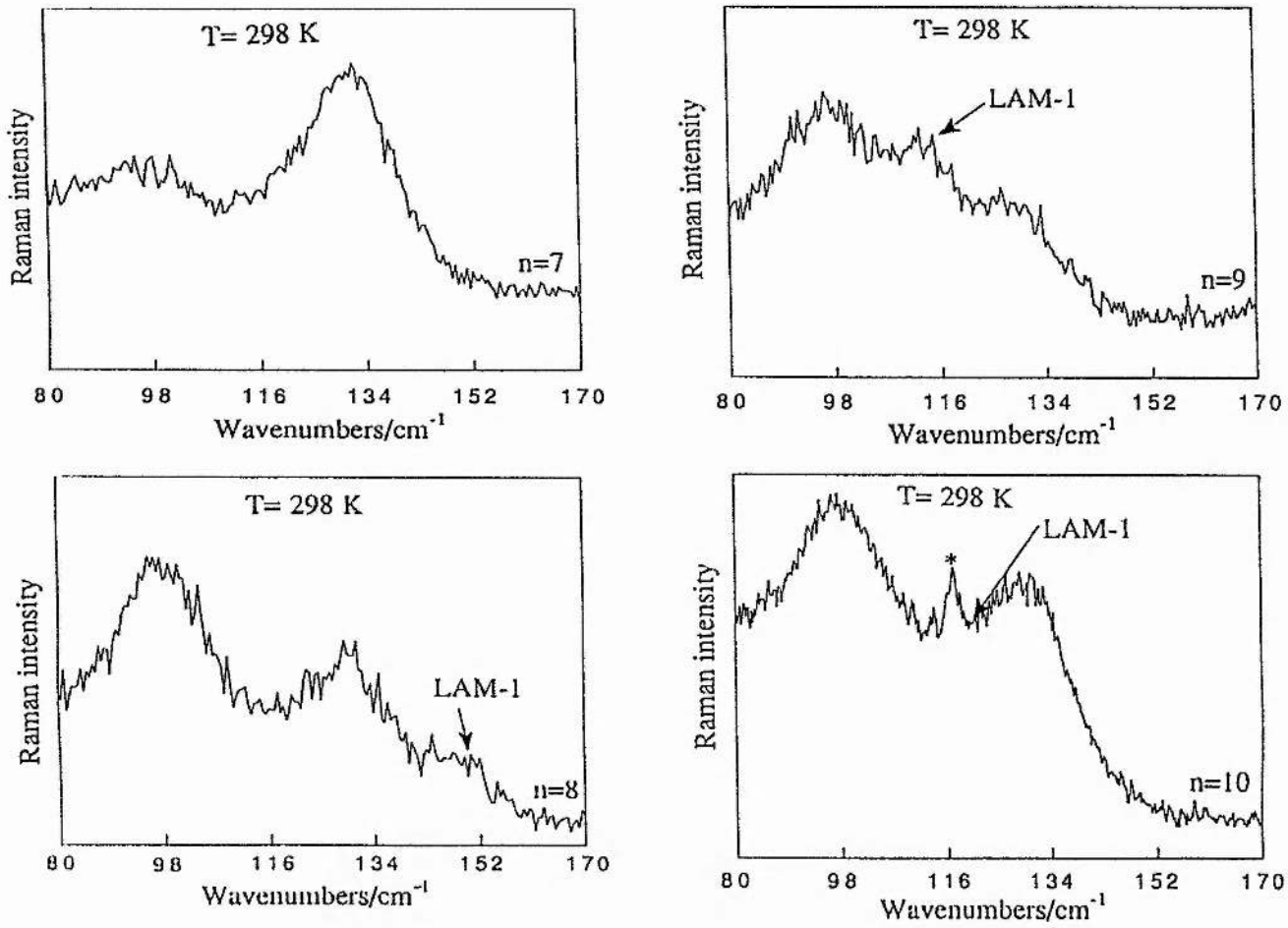

Fig. 3.14b: Low-frequency X(ZZ)Y-polarised Raman spectra, illustrating the LAM-1 bands for $C_nH_{2n}Br_2$/urea inclusion compounds in the HT phase

n	LT		HT	
	$\bar{\upsilon}$ /cm^{-1}	σ/cm^{-1}	$\bar{\upsilon}$/cm^{-1}	σ/cm^{-1}
7	132	5.0	133	7.1
8	151	4.9	151	7.1
9	115	4.3	116	7.0
10	122	3.4	126	7.9

Table 3.7: LAM-1 frequencies and bandwidths

The uncertainty in these values at LT is generally ($\bar{\upsilon} \pm 0.5$) cm^{-1} and ($\sigma \pm 0.2$) cm^{-1}. For 1,10-dibromodecane/urea, there is a larger uncertainty in the frequency and bandwidth since the LAM-1 mode is hidden under urea lattice modes. The uncertainties in $\bar{\upsilon}$ and σ are slightly greater in the HT phase since the band is broadened: it is probable that the LAM-1 vibration is perturbed by other molecular motions which are increased at high temperature (e.g. molecular reorientation).

As expected, the LAM-1 frequencies of the α,ω-dibromoalkanes in their urea inclusion compounds decrease with increasing chain length within the n-odd and n-even series. There does not appear to be any significant temperature dependence. Perhaps surprisingly, our experimental LAM-1 frequencies are in close agreement (see Table 3.8) with those quoted for the pure α,ω-dibromoalkanes by Viras *et al* [1989 & 1991] and Edwards *et al* [1991]. Hence it seems that the constraining environment of the urea channel structure has little influence on the frequency of the LAM-1 mode.

Table 3.8: Observed and calculated frequencies for LAM-1 mode of $C_nH_{2n}Br_2$ in urea inclusion compounds and as 'pure' crystalline solids

	OBSERVED FREQUENCIES / CM^{-1}				CALCULATED FREQUENCIES / CM^{-1}	
	UREA INCLUSION COMPOUND (our results)		'PURE' DIBROMOALKANE (from literature)			
DIBROMOALKANE	LT Phase	HT Phase	Viras *et al* [1989&1991]	Edwards *et al* [1991]	M-Z Model*	Edwards *et al* [1991]
$C_7H_{14}Br_2$	132	133	140	-	158	-
$C_8H_{16}Br_2$	151	151	150	149	145	149
$C_9H_{18}Br_2$	115	116	121	-	135	-
$C_{10}H_{20}Br_2$	122	126	126	124	127	125

* Calculated using the Minoni-Zerbi model, with force constants f=0.05 mdyn/Å and F=4.2 mdyn/Å

Table 3.8 also lists the LAM-1 frequencies calculated using the Minoni-Zerbi model described above (with force constants f= 0.05 mdyn/Å and F = 4.2 mdyn/Å) and those quoted by Edwards *et al* [1991] for the n-even dibromoalkanes. For the Minoni-Zerbi model, we find that the agreement between calculated and experimental values for the LAM-1 frequency is good only in the case of the n-even dibromoalkanes. This supports the LAM-TAM coupling theory of Mazur & Fanconi [1979] (discussed in §3.2.2.2, part (II)(iv)). Thus, the discrepancy between the calculated and the experimental LAM-1 frequencies for the n-odd dibromoalkanes can be explained by the existence of a coupling between the 'unperturbed' LAM-1 and TAM-4 modes. This coupling is only possible in the case of the n-odd molecules, for which LAM-1 and TAM-4 belong to the same symmetry species. Indeed, bands which we tentatively assign to TAM modes can be seen in the low-frequency ZZ-polarised Raman spectra of the n-odd (but not the n-even) dibromoalkane/urea inclusion compounds (e.g. Fig. 4.14 c; see also Table 3.6).

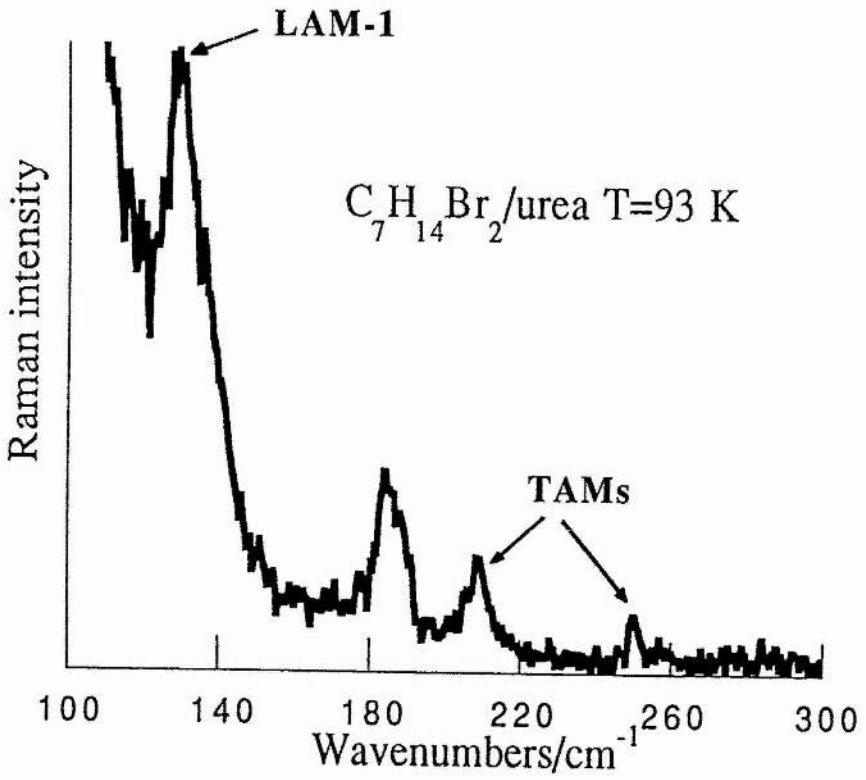

Fig. 3.14c: Low-frequency X(ZZ)Y-polarised Raman spectrum, illustrating the LAM-1 and TAM modes for $C_7H_{14}Br_2$/urea in the LT phase

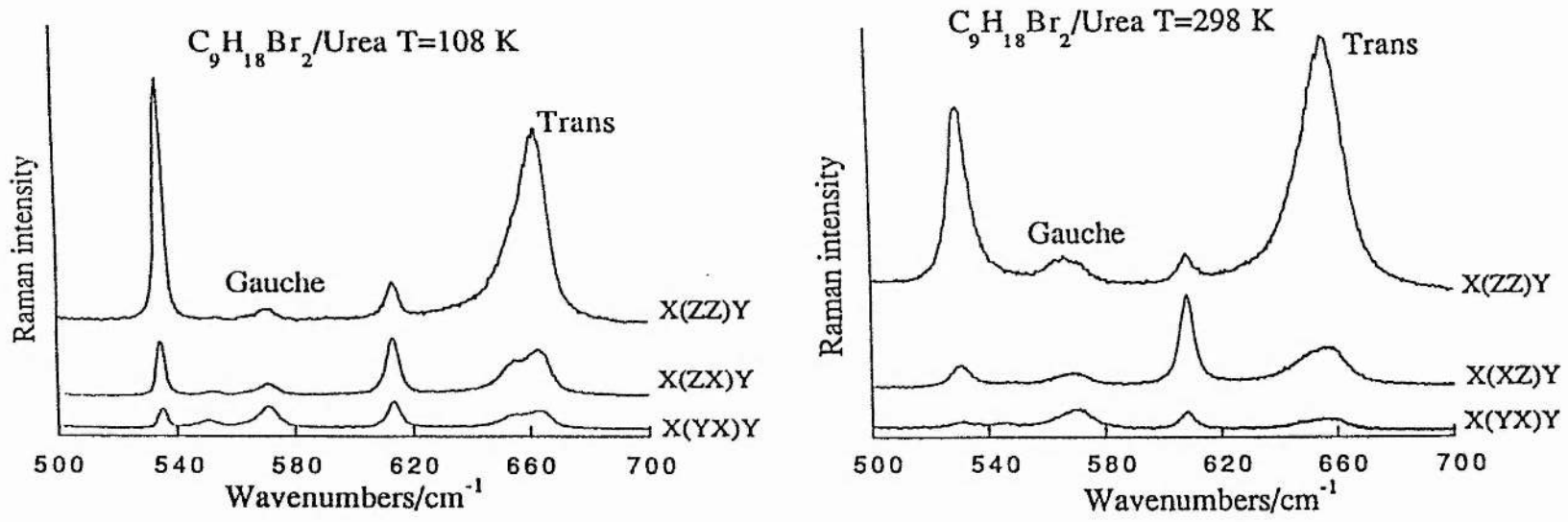

Fig. 3.15: Raman spectra illustrating the ν(C-Br) *trans* and *gauche* bands of $C_9H_{18}Br_2$/urea for different polarisations in the LT and HT phases

3.5.2.2 Analysis of *Gauche* Defects

(i) Identification of the ν(C-Br) gauche band

We recall that Table 3.1 (§3.2.2.1) shows that the ν(C-Br) stretching mode for α,ω-dibromoalkanes in the end-*trans* conformation comprises the following symmetries:

$\Gamma\nu(\text{C-Br}) = A_1 + B_1$ for C7 and C9 (point group: C_{2v})

$\Gamma\nu(\text{C-Br}) = A_g + B_u$ for C8 and C10 (point group: C_{2h})

for which:

C_{2v} - A_1 is ZZ active (possibly also active in XY)

- B_1 is XZ active

C_{2h} - A_g is ZZ and XY active

- B_u is Raman inactive

Fig. 3.15 shows Raman spectra illustrating the ν(C-Br) stretching modes in the ZZ, XZ and XY polarisations for one sample (1,9-dibromononane/urea) at both LT and HT. It can be seen that the ν(C-Br) *trans* band is polarised ZZ and occurs at a frequency of *ca.* 656 cm^{-1} in the HT phase. The ν(C-Br) *gauche* band is also apparent: it occurs at *ca.* 570 cm^{-1} in the HT phase, is much less intense than the ν(C-Br) *trans* and is less strongly ZZ polarised. In fact, it appears to be polarised preferably XY.

The ratio of intensities, $I_{g/t}$, of the *gauche* and *trans* bands can be calculated in various ways. We have evaluated (see Table 3.9) three ratios for $I_{g/t}$ for the α,ω-dibromoalkane/urea inclusion compounds:

I^g_{VV}/I^t_{VV} I^g_{HH}/I^t_{VV} $\sum I^g/\sum I^t$

Ratio (1) Ratio (2) Ratio (3)

As discussed in §3.2.2.3 part (II), Kobayashi *et al* [1990] after Kim *et al* [1989] used intensities in the ZZ polarisation in their study of *gauche* CH_3 groups in the *n*-alkane/ urea inclusion compounds.† We thus report Ratio (1) for comparison. However, the ν(C-Br) *trans* mode is strongly polarised ZZ, but the ν(C-Br) *gauche* mode is polarised preferably XY. The relative intensity of a given band in a given polarisation is dependent on the depolarisation ratio, ρ, for the mode, and it is clear that the value of ρ for the ν(C-Br) *trans* mode differs from that for the ν(C-Br) *gauche*. However, the ratio of *gauche* intensity in the XY polarisation to *trans* intensity in the ZZ polarisation (Ratio (2)) introduces errors due to the comparison of different components of the derivative of the molecular polarisability tensor. The ratio of all the intensities summed over all polarisations appears intuitively the most valid ratio: this is Ratio (3) and is given by:

$$\frac{\sum I^g}{\sum I^t} = \frac{I^g_{VV} + 2I^g_{VH} + I^g_{HH}}{I^t_{VV} + 2I^t_{VH} + I^t_{HH}}$$

We have verified experimentally that this is equivalent to the band intensity ratio of spectra recorded using circularised incident radiation and circularised scattered radiation. Ratio (3) is henceforth denoted $\Im_{g/t}$.

Table 3.9 thus shows these three intensity ratios for each sample at LT and HT. Despite our limited knowledge regarding the relationship between intensity ratio and proportion of *gauche* defects, we propose that the extent of *gauche* defects at the chain ends is in the range 4-15 % (corresponding to $\Im_{g/t}$ values). There is no discernible relationship for any of the compounds between relative *gauche* intensity and chain length, nor is there any *significant* change in relative *gauche* intensity on crossing the phase transition (although there *may* genuinely be a slight increase in proportion of *gauche* defects in the HT phase).

† To apply the bond polarisability model of Kim *et al* [1989] to the α,ω-dibromoalkane/urea inclusion compounds would require theoretical calculations involving normal modes and their Raman activities: such calculations are complex and time-consuming, but are a prospect for future work.

Table 3.9: Values for various $I_{g/t}$ ratios for $C_nH_{2n}Br_2$/urea, where n=7-10, at LT and HT

	LOW TEMPERATURE			HIGH TEMPERATURE			
SAMPLE	I^g_{VV}/I^t_{VV}	I^g_{HH}/I^t_{VV}	$\sum I^g/\sum I^t$	I^g_{VV}/I^t_{VV}	I^g_{HH}/I^t_{VV}	$\sum I^g/\sum I^t$	AVERAGE
$C_7H_{14}Br_2$/urea	0.08	0.09	0.17	0.09	0.07	0.15	0.11
$C_8H_{16}Br_2$/urea	0.01	0.03	0.05	0.04	0.04	0.08	0.04
$C_9H_{18}Br_2$/urea	0.03	0.06	0.09	0.06	0.05	0.13	0.07
$C_{10}H_{20}Br_2$/urea	0.02	0.08	0.10	0.05	0.07	0.13	0.07
AVERAGE	0.04	0.06	0.10	0.06	0.06	0.12	0.07

Notes:
(i) Intensities were calculated from the spectra using an integration program (trapezium method)
(ii) Direct and retro values of $I_{g/t}$ were averaged
(iii) Experimental error is in the region of *ca.* ±0.03

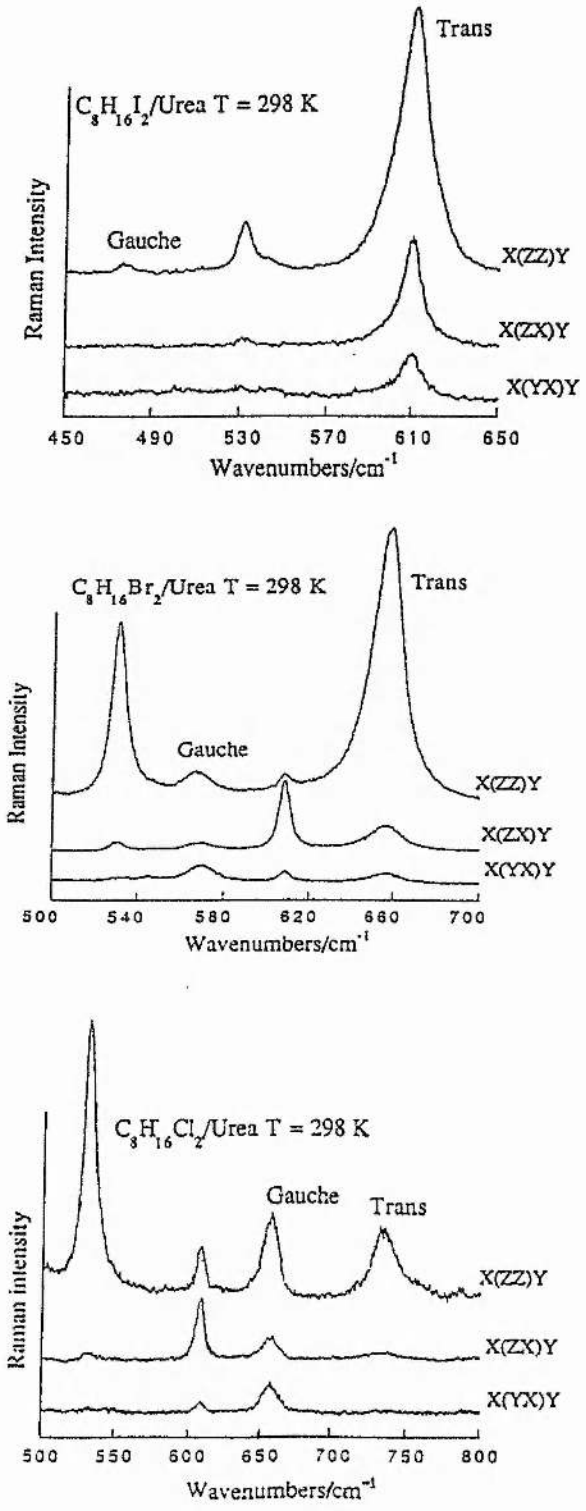

Fig. 3.16: Polarised Raman spectra illustrating the ν(C-X) stretching regions of $C_8H_{16}X_2$/urea (where X=Cl, Br and I) in the HT phase

(ii) Evolution of gauche/trans intensity ratio

(a) Study as a function of terminal substituent

Typical spectra, recorded in the ZZ, XZ and XY polarisations at 298 K for $X(CH_2)_8X$/urea, where X= Cl, Br and I, are shown in Fig. 3.16. The frequencies of the *gauche* and *trans* bands and the intensity ratios $\Im_{g/t}$ are shown in Table 3.10.

X	FREQUENCY / cm^{-1}		$\Im_{g/t}$
	$\nu(C\text{-}X)_{gauche}$	$\nu(C\text{-}X)_{trans}$	
Cl	656	734	1.03 ≡ 51%
Br	570	660	0.08 ≡ 7%
I	476	610	0.01 ≡ 1%

Table 3.10: ν(C-X) band frequencies and $\Im_{g/t}$ values for $X(CH_2)_8X$/urea

Thus it appears that the proportion of *gauche* defects decreases as the size of the terminal substituent increases. Presumably the *gauche* conformation becomes relatively more difficult to accommodate within the urea channel on going from Cl to Br to I end-group. We assume here that the $\Im_{g/t}$ ratios may be compared for the three compounds: this approach is justified by the fact that, for the liquid-phase dihaloalkanes, the measured depolarisation ratios for the three ν(C-X) *trans* bands are comparable, as are those for the three ν(C-X) *gauche* bands.

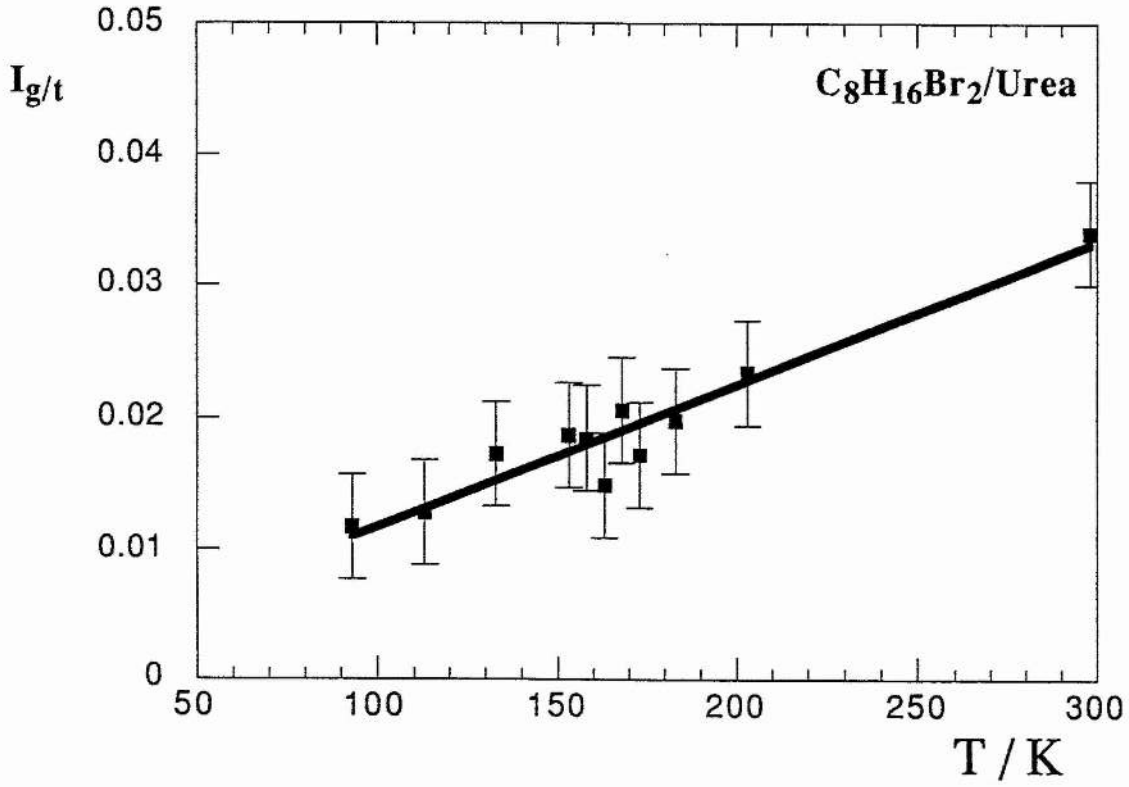

Fig. 3.17: Temperature dependence of the proportion of *gauche*, relative to *trans*, Br end-groups in $C_8H_{16}Br_2$/urea

(b) Study as a function of temperature

The spectra recorded for 1,8-dibromooctane/urea in polarisation {ZZ+XZ} show that $I_{g/t}$ increases slightly with temperature but exhibits no dramatic jump at the phase transition, where $I_{g/t}$ is defined for these spectra as:

$$I_{g/t} = \frac{I^{g}_{ZZ+XZ}}{I^{t}_{ZZ+XZ}}$$

From this we conclude that the proportion of *gauche* defects has a weak direct dependence on temperature. The evolution of $I_{g/t}$ with temperature is shown in Fig. 3.17. As discussed by Chatani *et al* [1978], the lattice parameters **a** and **b** of the urea host structure increase slightly with temperature (**c** remaining constant): this may allow a greater proportion of end-groups to adopt the *gauche* conformation.

(c) Study as a function of pressure

The spectra were qualitatively similar for all three samples ($Br(CH_2)_nBr$/urea with n=7, 9, 11), and were reproducible and reversible, being identical for the high-to-low pressure and low-to-high pressure cycles. Constant band frequencies for the ν_s(C-N) and the two δ(NCO) modes, characteristic of hexagonal urea (at *ca.* 1025, 610 and 530 cm^{-1}, respectively), implied that the inclusion compound does not decompose under pressure. The ratio $I_{g/t}$ is defined for these spectra as:

$$I_{g/t} = \frac{I^{g}_{unpolarised}}{I^{t}_{unpolarised}}$$

$I_{g/t}$ increases markedly with pressure for all three samples; typical spectra illustrating this increase for 1,11-dibromoundecane/urea are shown in Fig. 3.18. The change in molecular volume of the guest molecules, ΔV, on increasing the applied pressure, P, can be calculated from the relationship:

$$\ln (I_{g/t}) \propto -P\left[\frac{\Delta V}{RT}\right]$$

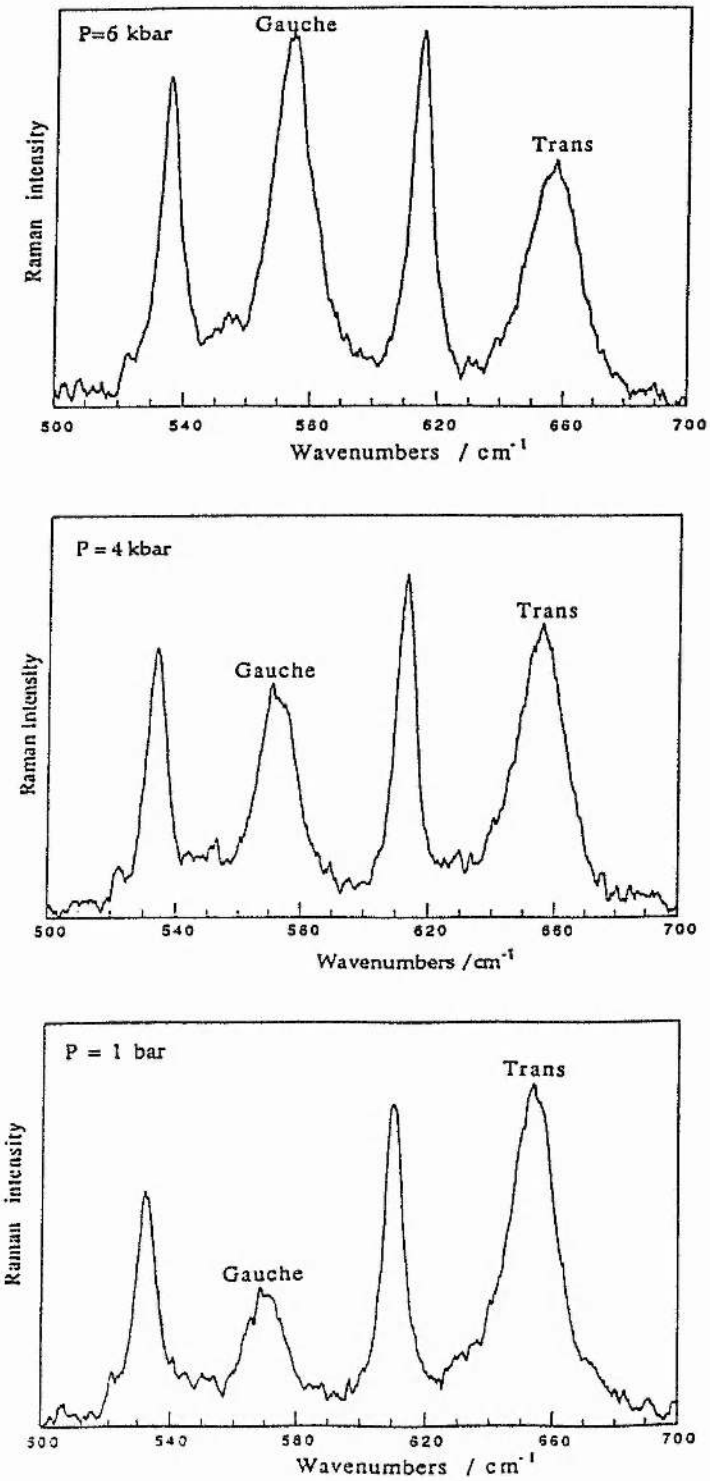

Fig. 3.18: Evolution of the Raman spectrum in the ν(C-X) stretching region as a function of pressure for $C_{11}H_{22}Br_2$/urea at 298 K

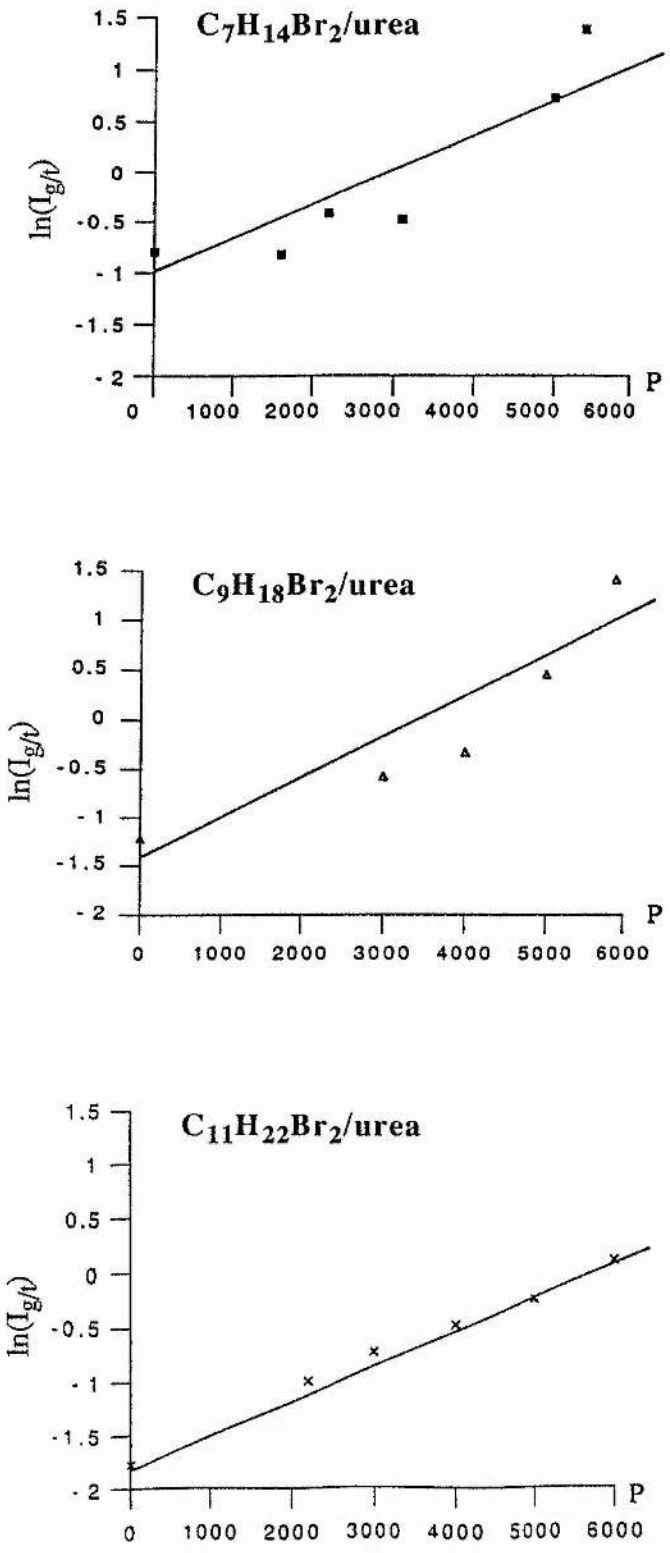

Fig. 3.19: Pressure dependence of $\ln(I_{g/t})$ for $C_nH_{2n}Br_2$/urea (where n=7,9 and 11) at 298 K

where R is the universal gas constant and T is the temperature (298 K). Fig. 3.19 shows this relationship graphically for the three samples. However, it can be seen that the relationship holds well only for 1,11-dibromoundecane/urea. The gradient of the best-fit line for this compound gives ΔV=7.4 cm^3mol^{-1}.

Because the samples used were polycrystalline, no absolute estimate of the proportion of *gauche* defects can be inferred (due to problems of multiple scattering); however, there is a clear trend to increasing proportion with increasing pressure. Fukao *et al* [1990] show that the cross-sectional area of the (ab) plane of the unit cell decreases with increasing pressure, hence compression could 'trap' the end-groups of the guest molecules into the *gauche* conformation. This is, however, the converse argument to that given above for the temperature-dependence of *gauche* defects. The pressure-dependence of the proportion of *gauche* defects clearly requires further investigation.

Finally, it should be stressed that this behaviour is observed for the urea inclusion compound under the hydrostatic pressure generated by He as the compressing fluid. Other compressing fluids, such as N_2, CO_2, Ar, Xe, etc, may give different results, since the possibility that the compressing fluid enters the channels cannot be excluded.

3.5.2.3 Other Vibrations of the Guest Molecule

The other bands attributable to vibrations of the guest molecule are predominantly polarised ZZ (i.e. A_1 or A_g symmetry) with the exception of the rocking and twisting CH_2 modes, which are polarised XZ (B_2 or B_g symmetry). The assignments are generally in line with those given by Le Brumant *et al* [1984] and by Fawcett & Long [1975] for *n*-alkanes included in urea. Points to note:

(i) Several bands arising from vibrations of the guest molecules occur in the low-frequency (< 300 cm^{-1}) region of the spectrum, as also noted by Cho *et al* [1986]. Definitive assignment of these bands has not been possible.

(ii) In the HT phase there is a noticeable broadening of the $\delta(CH_2)$ and $t(CH_2)$ bands: Wood *et al* [1989] have proposed that such band-broadening is due to the fast reorientations of the guest molecules in the channels.

(iii) At LT, the frequencies of the bands assigned to δ(C-C-Br) bending and ν(C-C) stretching modes increase by an average of *ca.* 10 cm^{-1}, within the n-odd or the n-even series, as chain length increases. However, with these exceptions (and the exception of the LAM-1), band frequencies do not shift markedly with chain length, and differences between the spectra of n-odd and n-even guest molecules are not generally evident.

(iv) Theoretically, we predict that the longer the guest molecule, the greater will be the number of vibrational modes observed. In practice, this is not the case. There are probably two reasons for this: firstly, some modes occur at the same frequency and, secondly, modes at similar frequencies tend to couple with each other. A single band in the Raman spectrum may thus be due to several different modes.

3.6 STUDY OF 1,6-DIBROMOHEXANE / UREA

3.6.1 INTRODUCTION

In Chapter 2 it was found that, unlike 'conventional' urea inclusion compounds, 1,6-dibromohexane/urea is commensurate and has an monoclinic structure at room temperature, and that the bromine end-groups on the guest molecules exist only in the *gauche* conformation. However, it is not known whether 1,6-dibromohexane/urea undergoes a low-temperature phase transition similar to that shown by the 'conventional' α,ω-dibromoalkane/urea inclusion compounds.

Studies of 'pure' crystalline 1,6-dibromohexane [Viras *et al*, 1989] have shown that its low-frequency Raman spectrum contains bands assigned to whole-chain single-node bending modes (27 cm^{-1} and 34 cm^{-1} at 263 K; 30 cm^{-1} and 35 cm^{-1} at 173 K) and the longitudinal acoustic mode LAM-1 (199 cm^{-1} at 263 K; 201 cm^{-1} at 173 K). Other low-frequency bands were observed at 45 cm^{-1} and 118 cm^{-1} at 263 K, and 50 cm^{-1}, 115 cm^{-1}, 125 cm^{-1} and 166 cm^{-1} at 173 K.

The present study has two aims. Firstly, since the 1,6-dibromohexane molecule in its urea inclusion compound exists exclusively in an unusual conformation with both end-groups *gauche*, we can use its urea inclusion compound to characterise the vibrational properties of *gauche* end-groups in terminally brominated *n*-alkanes. Secondly, Raman spectroscopy allows us to study the contrast between the urea channel structure of 1,6-dibromohexane/urea and that of 'conventional' α,ω-dibromoalkane/urea inclusion compounds.

3.6.2 EXPERIMENTAL

A single crystal of 1,6-dibromohexane/urea was used, of approximate dimensions 2.0 x 1.0 x 0.5 mm. This was sealed in a thin glass tube; however, its orientation with respect to the laboratory reference frame could not be readily ascertained. The sample tube was then placed in the cryostat. Spectral conditions were as detailed in §3.4.2: the spectrometer used was a triple-monochromator Dilor Z24. Spectra were recorded for the spectral regions 50-300 cm^{-1} and 300-1000 cm^{-1} at

298 K (denoted HT) and at 90 K (denoted LT). A spectrum was also recorded for the 1000-1040 cm^{-1} spectral region at 298 K. The direct geometry set-up was used and the polarisation was 'mixed', i.e. {ZZ+XZ}. The absence, in both the HT and LT spectra, of a sharp peak at 60 cm^{-1}, characteristic of 'pure' crystalline urea, was taken as confirmation of the structural integrity of the inclusion compound.

3.6.3 RESULTS AND DISCUSSION

We consider first the Raman spectra of 1,6-dibromohexane/urea recorded at 298 K. The ν(C-N) mode for urea in 1,6-dibromohexane/urea occurs at 1024 cm^{-1}, which is in close agreement with the corresponding mode for the 'conventional' α,ω-dibromoalkane/urea inclusion compounds (1025 cm^{-1}), perhaps suggesting similarity in the hydrogen-bonding involving the NH_2 groups in these structures.

Fig. 3.20a shows the low-frequency Raman spectrum at 298 K. The band at 225 cm^{-1} is assigned as the LAM-1 mode for the 1,6-dibromoalkane molecule containing *gauche* end-groups at each end of the molecule. This band was not observed for the 'conventional' α,ω-dibromoalkane/urea inclusion compounds: the probability of a guest molecule containing *gauche* end-groups at *both* ends in a 'conventional' UIC is low.

Fig. 3.20b shows the Raman spectrum for the 300-1000 cm^{-1} spectral region at 298 K. The ν(C-Br) mode for 1,6-dibromohexane/ urea is at 567 cm^{-1} and is close to our previous assignment for the *gauche* Br end-group in the 'conventional' α,ω-dibromoalkane/urea inclusion compounds (570 cm^{-1}). This result confirms our previous conclusion that there is a proportion of *gauche* end-groups in the 'conventional' α,ω-dibromoalkane/urea inclusion compounds.

Fig. 3.20: Raman spectra for $C_6H_{12}Br_2$/urea in the HT phase

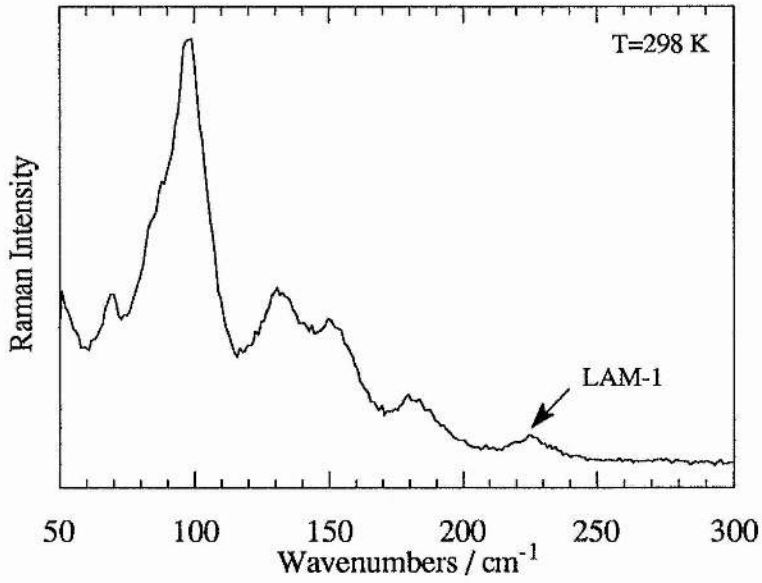

(a) For the 50-300 cm^{-1} spectral region

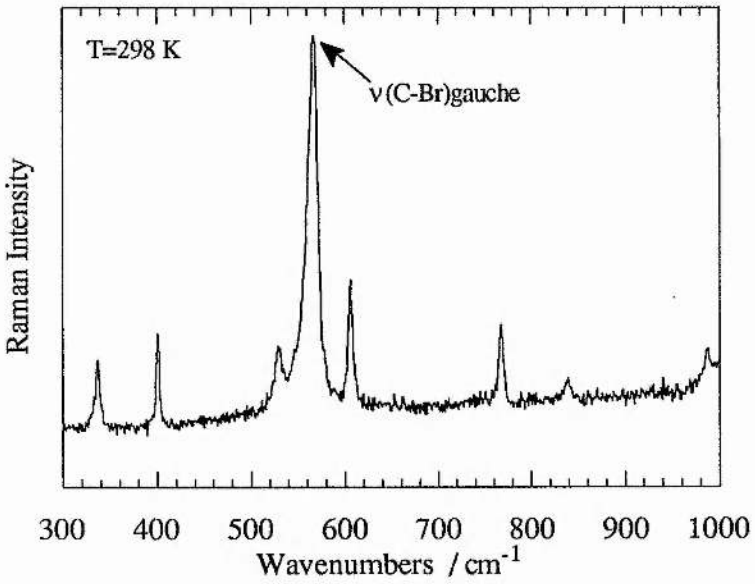

(b) For the 300-1000 cm^{-1} spectral region

Table 3.11: Observed bands in the Raman spectra of $C_6H_{12}Br_2$/urea in the spectral region 50-1000 cm^{-1} at 298 K

RAMAN BAND	TENTATIVE ASSIGNMENT		Comparison with conventional UICs*
Frequency / cm^{-1}	Urea or Guest	Mode	Frequency / cm^{-1}
51	guest	?	-
69	urea?	lattice mode?	57
87	guest?	?	90
97	urea	lattice mode	97
131	urea	lattice mode	130
151	?	?	-
181	urea?	lattice mode?	164 (185 at LT)
225	guest	LAM-1	dept on chain length
335	guest?	?	356 (339 for n=8)
402	?	?	-
530	urea	δ(NCO)	530
567	guest	ν(C-Br)*gauche*	570
606	urea	δ(NCO)	608
767	?	?	-
840	?	?	-
988	guest	$\nu(CH_2)$	988

*The values quoted here are the average frequencies, at 298 K, of the corresponding bands for $C_nH_{2n}Br_2$/urea, where n=7-10

Listed in Table 3.11 are the observed band frequencies at HT with their tentative assignments for the 50-1000 cm^{-1} spectral region. For comparison, frequencies of the corresponding bands (where they occur) for 'conventional' $C_nH_{2n}Br_2$/urea (n=7-10) are also given. Whereas some of the bands assigned to urea 'lattice modes' are of comparable frequencies for the two structures, others differ substantially, reflecting the

different structural properties of the host in these materials. In particular, the band at 181 cm^{-1} for 1,6-dibromohexane/urea is noteworthy: the corresponding mode for the conventional α,ω-dibromoalkane/urea inclusion compounds is at 164 cm^{-1} at HT, and in view of our assignment of this mode as a 'breathing' of the urea channel in the plane perpendicular to the long axis **c**, this result may suggest a narrower tunnel diameter for 1,6-dibromohexane/urea. In contrast, the band at 131 cm^{-1} corresponds closely in frequency to the band we assigned as a 'stretching' of the urea channel in the **c** direction. The band at 151 cm^{-1} has no equivalent in the spectra of the 'conventional' α,ω-dibromoalkane/urea inclusion compounds.

In the higher frequency region, the bands attributed to δ(NCO) bending modes of urea are of very similar frequency for $C_6H_{12}Br_2$/urea and 'conventional' $C_nH_{2n}Br_2$/ urea inclusion compounds. The other bands are harder to assign: the existence of many bands at frequencies substantially different from those for 'conventional' $C_nH_{2n}Br_2$/ urea (where n=7-10) presumably reflects the fact that the 1,6-dibromohexane guest molecule is relatively short and thus has effectively heavier end-groups (relative to the rest of the molecule), which would affect band frequency. Because the spectra were effectively unpolarised, it was not possible to assign these bands via symmetry considerations.

The Raman spectra of 1,6-dibromohexane/urea recorded at 90 K (Fig. 3.21) contrast markedly with the spectra recorded at 298 K. As shown in Fig. 3.21a, there is a dramatic change in the urea lattice modes in the LT phase compared with the HT phase, there being a considerably greater number of bands (with significantly smaller linewidths) in the LT phase. In contrast, the 'conventional' α,ω-dibromoalkane/urea inclusion compounds show few differences in the urea lattice modes between the HT and LT phases. This evidence suggests that 1,6-dibromohexane/urea *does* undergo a phase transition at a temperature between 298 K and 90 K, and that the difference in the urea structure between the HT and LT phases is considerable.

Fig. 3.21: Raman spectra for $C_6H_{12}Br_2$/urea in the LT phase

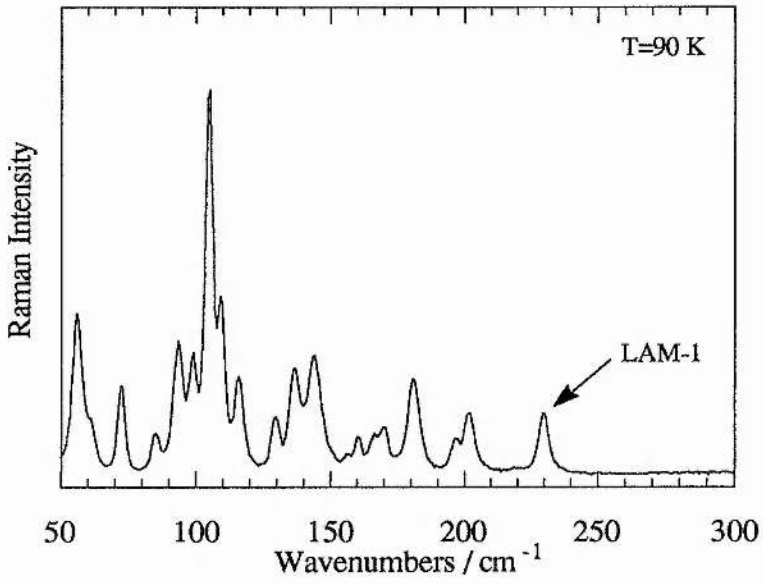

(a) For the 50-300 cm^{-1} spectral region

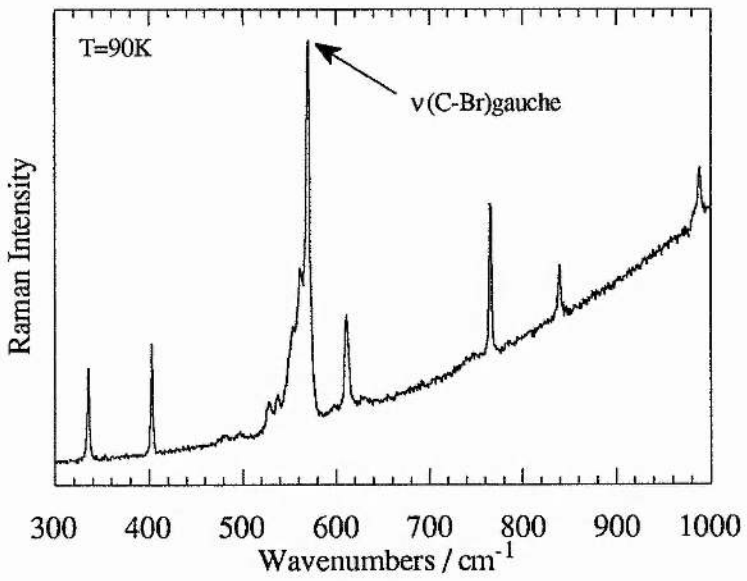

(b) For the 300-1000 cm^{-1} spectral region

From the spectrum of the higher frequency region at 90 K (Fig. 3.21b), it is clear that the 1,6-dibromohexane molecule still exists exclusively with *gauche* end-groups in the low-temperature phase, since there is no evidence for the ν(C-Br) band characteristic of the *trans* end-group. However, the ν(C-Br) band for the *gauche* end-group has developed some structure in the 90 K spectrum, with two subsidiary peaks on the low-frequency side of the main peak at 570 cm^{-1}. The origin of these subsidiary peaks has not yet been ascertained.

3.7 CONCLUSIONS

3.7.1 STUDY OF $X(CH_2)_nX$ / UREA FOR $n > 6$

In general, the number of vibrational bands observed in the Raman spectra of the α,ω-dibromoalkane/urea inclusion compounds was considerably less than expected; the observed bands were predominantly of symmetries A_1 and E_1 for the urea, and A_1 or A_g for the dibromoalkane molecule.

3.7.1.1 Urea Host Structure

The structural integrity of the inclusion compounds was verified by the presence of vibrational frequencies characteristic of hexagonal urea, especially the ν_s(CN) and δ(NCO) modes. The minimal change in spectral characteristics on passing through the phase transition suggests that the low temperature orthorhombic phase is, in fact, very similar in structure to the high temperature hexagonal phase (as has been proposed previously [Chatani, 1978; Harris *et al*, 1990]).

3.7.1.2 Dibromoalkane Guest Molecule

(I) The LAM-1 Mode

The LAM-1 modes were identified at LT and less readily at HT. As expected, the frequency was found to diminish, within each n-odd or n-even series, with increase in the length of the guest molecule. On applying the Minoni-Zerbi coupled chain model to the α,ω-dibromoalkanes, we found that the calculated LAM-1 frequencies were in reasonable agreement with the experimental values for the n-even dibromoalkane guest molecules. For the n-odd dibromoalkane guest molecules, the calculated LAM-1 frequencies did not agree with the experimental values: it is believed that the LAM-1 and the TAM-4 couple, by virtue of their identical symmetry and similar frequencies, and that this coupling perturbs the LAM-1 frequency.

(II) Gauche Defects

Both *trans* and *gauche* ν(C-Br) stretching modes were identified for all the samples studied. The *gauche/trans* band intensity ratios suggest that the percentage of end-groups in the *gauche* conformation is in the range *ca.* 4-15%. Studies of the evolution of the intensity ratio $I_{g/t}$ as a function of terminal substituent, temperature and pressure show that:

(a) $I_{g/t}$ decreases markedly with increase in size of terminal substituent
(b) $I_{g/t}$ increases (but only very slightly) with increasing temperature
(c) $I_{g/t}$ increases markedly with increase in applied pressure (at least for n-odd series)

In the current study, changes in the *gauche/trans* intensity ratios were used to indicate approximate changes in the proportion of *gauche* defects. These changes (i.e. the trends) have much greater validity than the absolute values, given the differences in polarisation of the ν(C-Br) *trans* and *gauche* modes.

3.7.2 Study of 1,6-Dibromohexane/Urea

The Raman spectra show that the 1,6-dibromohexane molecule in its urea inclusion compound has *gauche* groups at both ends, yet exhibits a LAM-1 mode. To our knowledge, this is the first example of such a molecule. This study confirms our assignment of the $\nu(\text{C-Br})_{gauche}$ stretching frequency. It also confirms that the urea host structure of 1,6-dibromohexane/urea is measurably different at room temperature from that of 'conventional' α,ω-dibromoalkane/urea inclusion compounds (as shown in Chapter 2), and that it undergoes a significant structural change to a low-temperature phase at a temperature between 298 K and 90 K.

3.8 REFERENCES

CANNAROZZI GM, MERESI GH, VOLD RL & VOLD RR (1991) Conformation and stability of alkane/urea inclusion compounds: evidence from deuterium NMR spectroscopy, *J. Phys. Chem.*, **95**, 1525-1527.

CASAL HL (1984) Raman spectroscopic determination of the integrity of urea inclusion compounds, *Appl. Spectrosc.*, **38**, 306-309.

CASAL HL (1985) Order-disorder transitions of urea inclusion adducts: a study by vibrational spectroscopy, *J. Phys. Chem.*, **89**, 4799-4803.

CASAL HL (1990) Conformations of *n*-alkanes in urea inclusion adducts, *J. Phys. Chem.*, **94**, 2232-2234.

CHATANI Y, TAKI Y & TADOKORO H (1977) Low temperature form of urea adducts with *n*-paraffins, *Acta Crystallogr., Sect. B*, **33**, 309-311.

CHATANI Y, ANRAKU H & TAKI Y (1978) Phase transition and structure change of urea adducts with *n*-paraffin and paraffin-type compounds, *Mol. Cryst. Liq. Cryst.*, **48**, 219-231.

CHO Y, KOBAYASHI M & TADOKORO H (1986) Raman band profiles and mobility of polymethylene chains, *J. Chem. Phys.*, **84**, 4636-4642.

DAVIES JED (1984) Spectroscopic studies of inclusion compounds. In: ATWOOD JL, DAVIES JED & MACNICOL DD, Eds., Inclusion Compounds: Vol. 3. Physical Properties and Applications, Academic Press, pp 37-68.

DOLLISH FR, FATELEY WG & BENTLEY FF (1974) Characteristic Raman Frequencies of Organic Compounds, John Wiley & Sons.

EDWARDS HGM, FAWCETT V & LUNG MT (1991) Force constant calculations of the LAM-1 modes of *n*-alkanes and their substituted α-monohalo- and α,ω-dihalo-species in their extended zig-zag planar configurations as found in urea inclusion compounds, *J. Inclusion Phenom. Mol. Recogn. Chem.*, **11**, 267-279.

FAWCETT V & LONG DA (1975) Raman spectroscopic studies of urea/*n*-paraffin clathrates, *J. Raman Spectrosc.*, **3**, 263-275.

FUKAO K, HORIUCHI T, TAKI S & MATSUSHIGE K (1990) Phase transitions of urea adducts with *n*-paraffins under high pressure, *Mol. Cryst. Liq. Cryst.*, **180B**, 405-416.

GRASSELLI JG, SNAVELY MK & BULKIN BJ (1981) Chemical Applications of Raman Spectroscopy, John Wiley & Sons.

HARRIS KDM, GAMESON I & THOMAS JM (1990) Powder x-ray diffraction studies of a low-temperature phase transition in the *n*-hexadecane/urea inclusion compound, *J. Chem. Soc., Faraday Trans.*, **86**, 3135-3143.

IMASHIRO F, KUWAHARA D, NAKAI T & TERAO T (1989) Study on conformations of *n*-alkanes in urea inclusion compounds using C-H dipolar switching-angle sample spinning nuclear magnetic resonance and MM2 molecular mechanics calculations, *J. Chem. Phys.*, **90**, 3356-3362.

KIM Y, STRAUSS HL & SNYDER RG (1989) Conformational disorder in the binary mixture n-$C_{50}H_{102}$/n-$C_{46}H_{94}$: a vibrational spectroscopic study, *J. Phys. Chem.*, **93**, 485-490.

KOBAYASHI M, KOIZUMI H & CHO Y (1990) Molecular motion of *n*-alkane chains in urea inclusion adducts studied by analysis of Raman band profiles, *J. Chem. Phys.*, **93**, 4659-4672.

KRIMM S & HSU SL (1978) Longitudinal acoustic mode in polymers: IV. LAM-3 of the general perturbed rod and applications to paraffins and polymers, *J. Polym. Sci., Polym. Phys. Ed.*, **16**, 2105-2114.

LE BRUMANT J, JAFFRAIN M & LACRAMPE G (1984) Raman spectroscopic study of low-temperature phase transitions and molecular motion in urea clathrates, *J. Phys. Chem.*, **88**, 1548-1554.

LEE K-J, MATTICE WL & SNYDER RG (1992) Molecular dynamics of paraffins in the *n*-alkane/urea clathrate, *J. Chem. Phys.*, **96**, 9138-9143.

LONG DA (1977) Raman Spectroscopy, McGraw-Hill.

LSMC: Members of the LABORATOIRE DE SPECTROSCOPIE MOLÉCULAIRE ET CRISTALLINE (1991) Spectrométries infrarouge à transformée de Fourier et Raman, Manual for the 'Session d'Initiation', Université de Bordeaux 1.

MARTIN JJ, CAVAGNAT R, CORNUT JC, COUZI M, DALEAU G, DEVAURE J, MAISSARA M & MOKHLISSE R (1986) A variable-temperature hydrostatic pressure cell for Raman scattering experiments, *Appl. Spectrosc.*, **40**, 217-223.

MAZUR J & FANCONI B (1979) Raman spectra of *n*-alkanes: I. Raman intensities of longitudinal acoustic modes, *J. Chem. Phys.*, **71**, 5069-5080.

MEAKINS RJ (1955) The dielectric properties of urea occlusion compounds, *Trans. Faraday Soc.*, **51**, 953-961.

MINONI G & ZERBI G (1982) End effects on longitudinal accordion modes: fatty acids and layered systems, *J. Phys. Chem.*, **86**, 4791-4798.

MIZUSHIMA S & SHIMANOUCHI T (1949) Raman frequencies of *n*-paraffin molecules, *J. Am. Chem. Soc.*, **71**, 1320-1324.

NEWTON A (1990) Etude par spectroscopie de diffusion Raman de la dynamique du *n*-nonadecane inclus dans de l'urée, Rapport de Stage, Université de Bordeaux 1.

OLF HG & FANCONI B (1973) Low-frequency Raman-active lattice vibrations of *n*-paraffins, *J. Chem. Phys.*, **59**, 534-544.

SCHAUFELE RF & SHIMANOUCHI T (1967) Longitudinal acoustic vibrations of finite polymethylene chains, *J. Chem. Phys.*, **47**, 3605-3610.

SCHLENK W (1949) Die Harnstoff-Addition der aliphatischen Verbindungen, *Liebigs Ann. Chem.*, **565**, 204-240.

SLOANE H (1971) The technique of Raman spectroscopy: a state-of-the-art comparison to infrared, *Appl. Spectrosc.*, **25**, 430-439.

SMART SP, HARRIS KDM, GUILLAUME F & EL BAGHDADI A (1992) Raman spectroscopic studies of urea inclusion compounds containing α,ω-dibromoalkane guests, *Mol. Cryst. Liq. Cryst.*, **211**, 157-166.

SMART SP, EL BAGHDADI A, GUILLAUME F & HARRIS KDM (submitted for publication) Conformational and vibrational properties of α,ω-dihalogenoalkane/ urea inclusion compounds: a Raman scattering investigation.

SMART SP, EL BAGHDADI A, GUILLAUME F & HARRIS KDM (in preparation) Characterisation of *gauche* end-groups in α,ω-dibromoalkanes: Raman spectroscopic studies of the 1,6-dibromohexane/urea inclusion compound.

SMITH AE (1950) The crystal structure of urea-hydrocarbon and thiourea-hydrocarbon complexes, *J. Chem. Phys.*, **18**, 150-151.

SMITH AE (1952) The crystal structure of the urea-hydrocarbon complexes, *Acta Crystallogr.*, **5**, 224-235.

SNYDER RG (1967) Vibrational study of the chain conformation of the liquid *n*-paraffins and molten polyethylene, *J. Chem. Phys.*, **47**, 1316-1360.

SNYDER RG (1971) Raman scattering activities for partially oriented molecules, *J. Mol. Spectrosc.*, **37**, 353-365.

SNYDER RG & SCHACHTSCHNEIDER JH (1963) Vibrational analysis of the *n*-paraffins: I. Assignments of infrared bands in the spectra of C_3H_8 through *n*-$C_{19}H_{40}$, *Spectrochim. Acta*, **19**, 85-116.

STROMMEN DP (1992) Specific values of the depolarisation ratio in Raman spectroscopy: their origins and significance, *J. Chem. Ed.*, **69**, 803-807.

VIRAS K, VIRAS F, CAMPBELL C, KING TA & BOOTH C (1989) Low-frequency Raman spectra of even α,ω-disubstituted *n*-alkanes, *J. Phys. Chem.*, **93**, 3479-3483.

VIRAS F, VIRAS K, CAMPBELL C, KING TA & BOOTH C (1991) Low-frequency Raman spectra of odd α,ω-disubstituted *n*-alkanes, *J. Polym. Sci., Part B, Polym. Phys.*, **29**, 1467-1471.

VOLD RL, VOLD RR & HEATON NJ (1989) Deuterium nuclear magnetic resonance and molecular dynamics in alkane/urea inclusion compounds, *Adv. Magn. Reson.*, **13**, 17-41.

WOOD KA, SNYDER RG & STRAUSS HL (1989) Analysis of the vibrational bandwidths of alkane-urea clathrates, *J. Chem. Phys.*, **91**, 5255-5267.

CHAPTER 4
NEUTRON SCATTERING STUDIES

4.1 THE TECHNIQUE

4.1.1 INTRODUCTION

The neutron was discovered in 1932 by Chadwick. It has zero electrical charge, diameter of the order of 10^{-15} m, mass comparable to that of a proton (1.67×10^{-27} kg) and magnetic spin of $\frac{1}{2}$. Neutrons are produced either at a continous source by the fission of heavy atoms in a nuclear reactor (e.g. Institut Laue-Langevin, Grenoble) or at a pulsed spallation source, by bombarding a uranium target with accelerated protons (e.g. ISIS, Didcot). Discussion of methods of neutron production may be found elsewhere [e.g. Bée, 1988; Carlile, 1988a & b; Willis *et al*, 1991].

The neutrons produced may be either accelerated further using, for example, graphite at high temperature, or slowed down using a moderator, such as liquid hydrogen or deuterium. When suitably moderated, the thermal neutron has an energy similar to that of atomic vibrations and rotations (i.e. a few meV), and a wavelength of the order of interatomic distances (i.e. a few Å). These properties make it an ideal probe for the study of atomic and molecular structure and dynamics. For comparison, photons of appropriate energy allow the study of structural properties of materials (x-ray diffraction), but their high energy is incompatible with the study of dynamic properties. Conversely, photons of long wavelength may be used to probe dynamic properties (Raman, infrared and microwave spectroscopies), but they have wavelengths too long to allow the study of structural properties.

When a neutron beam interacts with a sample, the neutrons may be either absorbed (leading to γ emission) or scattered. The relative extents of absorption and scattering depend on the relative cross-sections for these two processes: these are denoted σ_a and σ_s respectively. For organic molecules, σ_a is small and σ_s is large. Neutrons are scattered isotropically by nuclei (the nuclei acting as point scatterers) and,

by virtue of their spin, also give rise to magnetic scattering via dipole-dipole interactions. This latter fact enables neutron scattering to be used for the study of magnetic properties. The dominant scattering process, however, is the neutron-nucleus interaction (magnetic scattering being negligible unless the sample is paramagnetic) and the neutron scattering theory outlined in this chapter will assume that this is the sole interaction. Scattering power varies non-systematically with atomic number, such that isotopes and neighbouring elements of the Periodic Table are easily distinguishable. An exchange of energy may occur which is of the order of transitions between vibrational and rotational levels.

The main limiting factor in neutron scattering experiments is that available neutron beams have inherently low flux. A further difficulty arises because, by virtue of its relatively small diameter and lack of charge, a neutron can travel large distances without being scattered or absorbed. This means that neutrons are only weakly scattered by the very particles they probe and that detection of the scattered neutrons is difficult. In practice, detectors use one of the few atoms that absorb neutrons strongly enough to produce ionising radiation: examples are ^{10}B, ^{3}He and ^{6}Li [Bailey *et al*, 1981]. These two problems mean that neutron scattering is a signal-limited technique. However, it is complementary to techniques based on scattering of x-rays, electrons and light, and, notwithstanding the above limitations, is very informative in its own right. It allows study of many aspects of the solid, liquid and amorphous states, our interest being chiefly in its use in molecular spectroscopy.

4.1.2 BACKGROUND THEORY

This section gives a brief outline of the essential theory underlying the scattering of neutrons; further details may be found in references by Bée [1988], Carlile [1988a], Pynn [1990], Gunn [1988] and Willis *et al* [1991].

According to the de Broglie relation, a neutron of mass m travelling with velocity **v** can be described in terms of its kinetic energy E, its de Broglie wavelength

λ, and its wavevector **k**, which points along the trajectory of its motion (where h is Planck's constant):

Kinetic Energy	$E = \frac{1}{2} mv^2 = \left(\frac{h}{2\pi}\right)^2 \frac{\mathbf{k}^2}{2m}$
De Broglie Wavelength	$\lambda = \frac{h}{mv}$
Wavevector	$\mathbf{k} = \frac{2\pi}{\lambda} = \left(\frac{2\pi}{h}\right) mv$

A scattering event is characterised by its scattering law, $S(\mathbf{Q},\omega)$, which expresses the scattered intensity, S, as a function of the variables **Q** and ω, where **Q** is the scattering vector and its magnitude is proportional to the momentum transfer, and ω is proportional to the energy transfer. $S(\mathbf{Q},\omega)$ may be defined [e.g. Willis *et al*, 1991] as the probability that the scattering system will undergo an energy change dE ($=\hbar\omega$) accompanied by a momentum transfer $\hbar\mathbf{Q}$. The following equations define **Q** and ω:

Momentum transfer	$= \left(\frac{h}{2\pi}\right)\mathbf{Q} = \left(\frac{h}{2\pi}\right)(\mathbf{k}_f - \mathbf{k}_i)$
	$= \hbar\mathbf{Q} = \hbar(\mathbf{k}_f - \mathbf{k}_i)$
Energy transfer	$= E_f - E_i = \hbar\omega = \left(\frac{\hbar^2}{2m}\right)(\mathbf{k}_f^2 - \mathbf{k}_i^2)$

where $\mathbf{k}_i$ and $\mathbf{k}_f$ are, respectively, the initial and final wavevectors

and E_i and E_f are, respectively, the initial and final energies

The scattering event may be represented by a scattering triangle defining **Q**, as shown in Fig. 4.1. By convention, the energy transfer is defined as positive when the neutron gains energy and the sample loses energy.

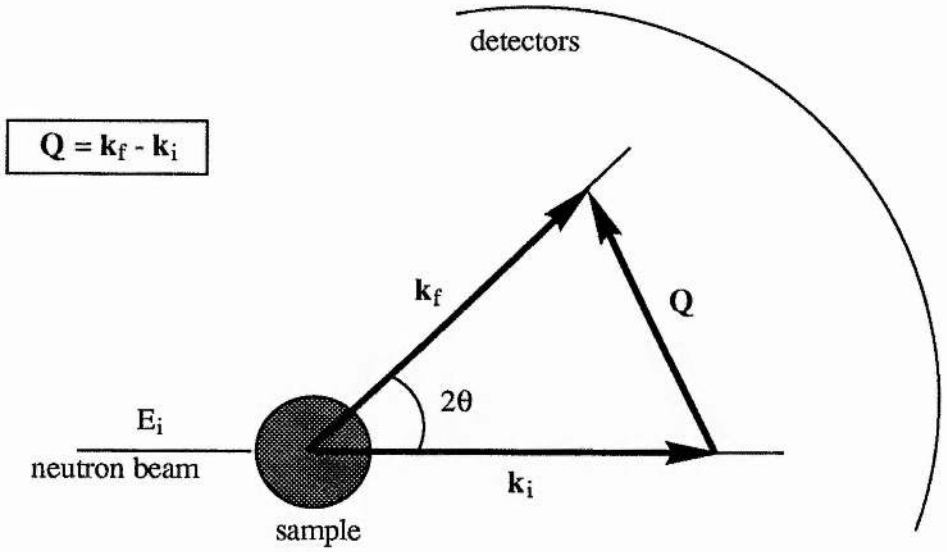

Fig. 4.1: Scattering triangle, defining **Q**

A scattering experiment measures the partial double differential scattering cross-section: this gives the fraction of neutrons which are scattered, by an array of N atoms with cross-section σ, at an angle 2θ into a solid angle $d\Omega$ with energy change dE:

$$\frac{\partial^2\sigma}{\partial\Omega\partial E} = \frac{1}{\hbar}\frac{\partial^2\sigma}{\partial\Omega\partial\omega} \equiv \frac{1}{\hbar} N \frac{\mathbf{k}_f}{\mathbf{k}_i} S(\mathbf{Q},\omega)$$

The scattering law $S(\mathbf{Q},\omega)$ is the time Fourier transform of the intermediate scattering function $I(\mathbf{Q},t)$:

$$S(\mathbf{Q},\omega)=\frac{1}{2\pi}\int_{-\infty}^{\infty} \exp\{-i\omega t\}\, I(\mathbf{Q},t)dt$$

Following the Van Hove formalism [1954]:

$$I(\mathbf{Q},t) = \frac{1}{N}\sum_{i=1}^{N}\sum_{j=1}^{N} \langle\, b_i \exp\{-i\mathbf{Q}\mathbf{r}_i(0)\}\, b_j \exp\{i\mathbf{Q}\mathbf{r}_j(t)\}\,\rangle$$

where b_i and b_j are the scattering lengths of the nuclei at $\mathbf{r}_i$ and $\mathbf{r}_j$, respectively. The angular brackets < > denote the average over all possible starting times for observations of the system: this is equivalent to the average over all possible thermodynamic states of the sample. This equation can be separated into two components, which correspond to the incoherent scattering law $S_{inc}(\mathbf{Q},\omega)$ and the coherent scattering law $S_{coh}(\mathbf{Q},\omega)$:

$$I_{inc}(\mathbf{Q},t) = \frac{1}{N}\left[\left(\langle b^2 \rangle - \langle b \rangle^2 \right) \sum_{i=1}^{N} \exp\{-i\mathbf{Q}(\mathbf{r}_i(0) - \mathbf{r}_i(t))\} \right]$$

$$I_{coh}(\mathbf{Q},t) = \frac{1}{N}\left[\langle b^2 \rangle \sum_{i=1}^{N} \sum_{j=1}^{N} \exp\{-i\mathbf{Q}(\mathbf{r}_i(0) - \mathbf{r}_j(t))\} \right] \quad \text{where } i \neq j$$

$I(\mathbf{Q},t)$ may be derived for various motional models; it is, in turn, the space Fourier transform of the time-dependent pair-correlation function $G(\mathbf{r},t)$:

$$I(\mathbf{Q},t) = \int_{-\infty}^{\infty} \exp\{i\mathbf{Q}\mathbf{r}\}\, G(\mathbf{r},t)\, d\mathbf{r}$$

where:

$$G_{inc}(\mathbf{r},t) = \frac{1}{N}\left\langle \sum_{i=1}^{N} \delta\{\mathbf{r} + \mathbf{r}_i(0) - \mathbf{r}_i(t)\} \right\rangle$$

$$G_{coh}(\mathbf{r},t) = \frac{1}{N}\left\langle \sum_{i=1}^{N} \sum_{j=1}^{N} \delta\{\mathbf{r} + \mathbf{r}_i(0) - \mathbf{r}_j(t)\} \right\rangle \quad \text{where } i \neq j$$

$G(\mathbf{r},t)$ may be defined [Willis *et al*, 1991] as the probability that, given a particle at the origin at time zero, there will be some particle (including the original one) at position $\mathbf{r}$ at time t.

These equations constitute the Van Hove formalism [1954] in defining the relationship between neutron scattering and the relative positions and motions of atoms.

It is the simplicity of this relationship which underpins the success of this technique as a probe of atomic structure and dynamics. **Q** and ω are thus related, via Fourier transforms, to space and time respectively, and as **Q** is a vector quantity, the technique allows the study of properties of the sample in specific orientations.

These equations show that a neutron scattering experiment involves two types of scattering, coherent and incoherent, depending on the manner of nuclear interaction. Coherent scattering occurs when the incident neutron wave interacts with all the nuclei in the sample in a coordinated fashion, such that all the scattered waves have definite relative phases, and so can interfere with each other. Coherent scattering reflects collective properties of the sample; it depends on the relative distances between the sample's constituent atoms and thus provides structural information.

Conversely, incoherent scattering occurs when the incident neutron wave interacts independently with each nucleus in the sample. The scattered waves from the different nuclei have random relative phases and so cannot interfere with each other in a coordinated manner. Incoherent scattering may, for example, arise from the interaction of a neutron wave with the same atom but at different positions and times. Incoherent scattering provides information about atomic and molecular motions, so is used in the study of dynamic properties.

4.1.3 Scattering Cross-Sections

The scattering of a neutron by a single nucleus is described by its scattering cross-section, σ_s, which is quoted in barns (1 barn $\equiv 10^{-28}$ m^2). This may be visualised as the effective area presented by the nucleus to the passing neutron. The scattering length, b, which is related to the scattering cross-section by the equation $\sigma_s=4\pi\langle b^2\rangle$, indicates the strength of the interaction between the neutron and the scattering nucleus; b is characteristic of a particular nucleus, depending solely on its identity and spin state, and being independent of the incident energy of the neutron. The total scattering length for a given isotope is averaged over all its spin states, and for a given element is averaged over all its isotopes.

According to the previous equations, the total scattering can be written as:

$$S(\mathbf{Q},\omega) = \left[\langle b^2 \rangle - \langle b \rangle^2 \right] S_{inc}(\mathbf{Q},\omega) + \langle b \rangle^2 S_{coh}(\mathbf{Q},\omega)$$

Thus, the scattering cross-section may be split into its coherent and incoherent components:

$$\sigma_s = \sigma_{coh} + \sigma_{inc}$$

where $\sigma_{coh} = 4\pi \langle b \rangle^2$ = coherent scattering cross-section
$\sigma_{inc} = 4\pi \left[\langle b^2 \rangle - \langle b \rangle^2 \right]$ = incoherent scattering cross-section

and $\langle b \rangle$ denotes the ensemble average of b over all isotopes and spin states
$\langle b^2 \rangle$ denotes the ensemble average of b^2 over all isotopes and spin states

Values of scattering cross-sections for common nuclei may be found elsewhere [e.g. Bée, 1988]; those relevant to the current discussion are shown in Table 4.1. The incoherent scattering cross-section of hydrogen is very much greater than the total scattering cross-section of carbon or any other commonly encountered nucleus. Therefore, neutron scattering of most organic compounds is dominated by incoherent scattering from hydrogen. Consequently, incoherent neutron scattering is often used for study of the dynamics of organic molecules. The contrast between the incoherent scattering cross-sections for hydrogen and deuterium enables selective study of parts of the molecule, scattering from the rest of the molecule being minimised by deuteration. Vanadium, being a purely incoherent scatterer, is often used as a standard in incoherent scattering experiments.

NUCLEUS	σ_{coh}/barn	σ_{inc}/barn
^1H	1.8	79.9
^2H	5.6	2.0
C	5.6	0.0
V	0.0	5.2

Table 4.1: Values of scattering cross-sections

4.1.4 ELASTIC, INELASTIC AND QUASIELASTIC SCATTERING

Neutron scattering can be either elastic, inelastic or quasielastic, depending on the energy change involved. Elastic scattering results in no energy change, i.e. $\hbar\omega=0$; thus the direction of the neutron wavevector **k** changes, but its magnitude remains constant (i.e. $|\mathbf{k}_i|=|\mathbf{k}_f|$). Elastic scattering occurs for atoms localised in space; it always satisfies the following equation, where $\mathbf{Q}_0$ is the elastic momentum transfer vector:

$$|\mathbf{Q}_0| = \left(\frac{4\pi}{\lambda}\right)\sin\theta$$

Elastic coherent scattering constitutes neutron diffraction (occurring in accordance with Bragg's Law) and gives details about equilibrium structure.

In contrast, inelastic scattering results in an exchange of *both* energy and momentum between the incident neutron and the scattering nucleus; thus both the direction and the magnitude of the neutron wavevector change. Inelastic scattering results from the interaction of atomic and molecular vibrations with the neutron beam. The energy difference between the incident neutron and the scattered neutron is equal to a quantum, $h\upsilon$ ($=\hbar\omega$), of energy, υ being the frequency of the atomic or molecular motion. Inelastic incoherent scattering is used for study of the motions of individual atoms or molecules, whereas inelastic coherent scattering is used for study of the dynamics of collective periodic motions, such as phonon dispersion curves.

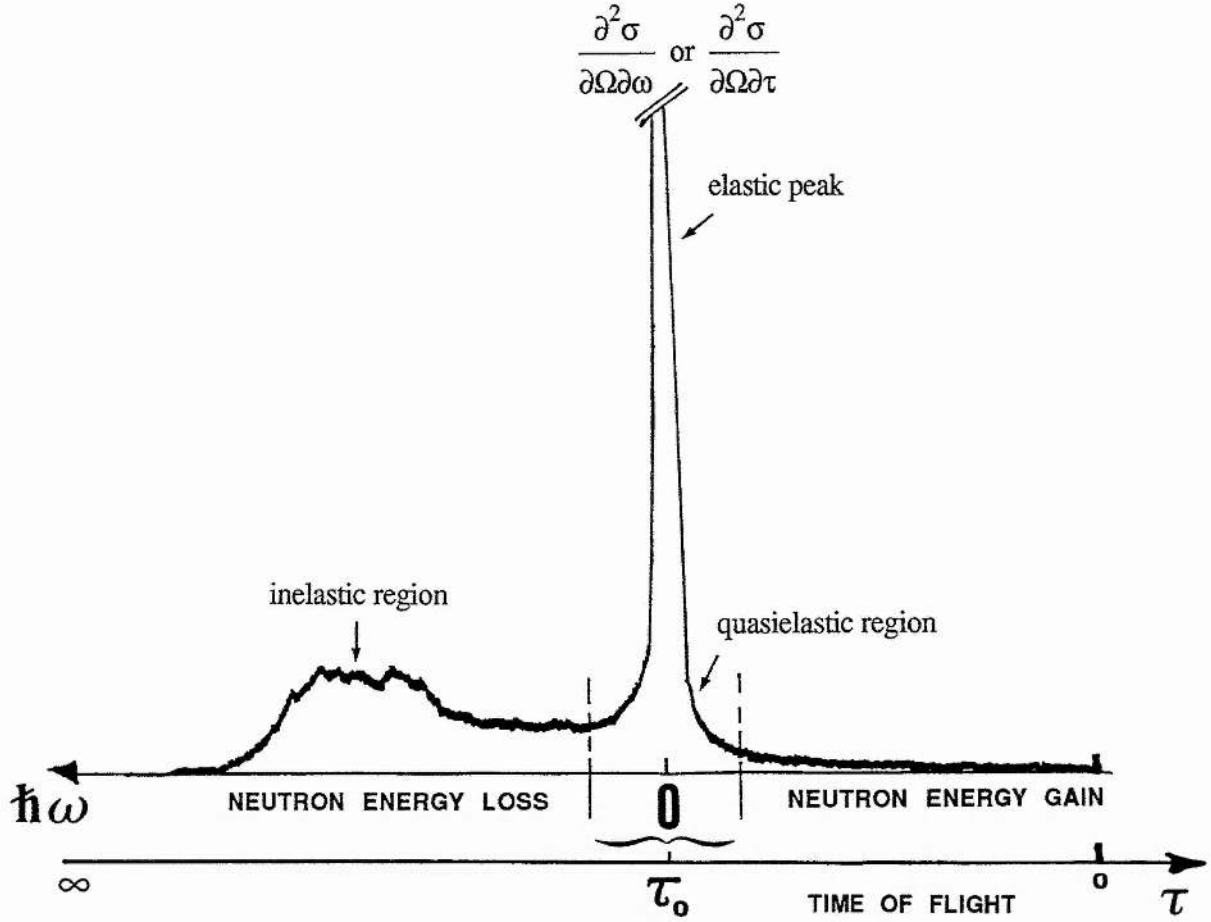

Fig. 4.2: Example of an incoherent neutron scattering spectrum, illustrating the three regions of neutron scattering: this spectrum was recorded using a time-of-flight spectrometer (see §4.1.6) [adapted from Guillaume, 1988]

Scattering is termed quasielastic in that region where the energy change on scattering tends to zero. Quasielastic scattering results from low energy (<1meV) inelastic processes, such as translational and rotational diffusion: such scattering broadens the elastic line of the spectrum. This class of scattering is discussed further in §4.1.5.

The intensity of incoherent neutron scattering spectra is a function of both the momentum transfer, $\hbar\mathbf{Q}$, and the energy transfer, $\hbar\omega$. For a given value of 2θ (and hence a given value of $\mathbf{Q}$), the spectrum may be divided into the three regions of scattering discussed above, as shown in Fig. 4.2.

4.1.5 Incoherent Quasielastic Neutron Scattering

4.1.5.1 Use of IQNS

Each class of neutron scattering can be used to probe specific aspects of a system. In this work we use incoherent quasielastic neutron scattering (IQNS) to study the motion of both the guest and the host molecules within urea inclusion compounds, specifically:

(i) The α,ω-dibromoalkane guest molecules in their urea-d_4 inclusion compounds
(ii) The urea host molecules in the *n*-hexadecane-d_{34}/urea inclusion compound

As the scattering is incoherent, it provides details about the dynamics of these molecules; it is also quasielastic, and thus results from atomic and molecular diffusion. Diffusional motion may be divided into two classes: translational diffusion, in which the centre of mass of the diffusing atom or molecule moves, and rotational diffusion, in which the centre of mass remains stationary but rotation of the molecule or groups within the molecule occurs.

Both translational and rotational diffusion occur randomly with respect to time; they often take place simultaneously on different time-scales. The instrumental resolution is necessarily non-zero, and is approximated by a triangular, Lorentzian or

Gaussian function (depending on the spectrometer). The instrumental resolution defines the time-scale over which motions are observable: for quasielastic scattering the instrumental resolution is typically between several neV and 100 μeV. Observable time-scales are thus 10^{-7} to 10^{-12} s: these correspond closely with the typical jump frequencies for translational and rotational diffusion (i.e. 10^{9} to 10^{12} jumps per second).

4.1.5.2 IQNS Theory

An atom diffusing within a fixed volume has an incoherent scattering law $S(\mathbf{Q},\omega)$ in the quasielastic region which may be separated into two components: a purely elastic component and a quasielastic component centred on $\omega=0$. This can be written generally [e.g. Leadbetter & Lechner, 1979; Carlile, 1988a] as:

$$S(\mathbf{Q},\omega)=A_0(\mathbf{Q})\delta(\omega)+\sum A_n(\mathbf{Q})L_n(\omega)$$

where $\delta(\omega)$ is the Dirac delta function:

$$\delta(\omega)=\infty \text{ at } \omega=0;\ \delta(\omega)=0 \text{ at } \omega\neq 0 \text{ and } \int_{-\infty}^{+\infty}\delta(\omega)d\omega = 1$$

and $L_n(\omega)$ are Lorentzian functions:

$$L_n(\omega) = \frac{1}{\pi}\frac{\tau_n}{1+\omega^2\tau_n^2} \equiv \frac{1}{\pi}\frac{\Delta_n^{-1}}{1+\omega^2\Delta_n^{-2}}$$

(where Δ = HWHH, t = correlation time)

and n is the number of Lorentzian functions and depends on the model used:

$$\sum_{n=0}^{n} A_n(\mathbf{Q}) = 1$$

The intermediate scattering law is then:

$$I(\mathbf{Q},t) = A_0(\mathbf{Q})+\sum_n A_n(\mathbf{Q})\exp(-\Delta\omega_n t)$$

The elastic $A_0(\mathbf{Q})\delta(\omega)$ and quasielastic $\Sigma A_n(\mathbf{Q})L_n(\omega)$ terms contain information on the geometry and time-scales of the diffusion. The Lorentzians arise from the different types of motion occurring in the sample. The proportion of the scattered intensity which is purely elastic is termed the elastic incoherent structure factor (EISF):

$$\text{EISF} = A_0(\mathbf{Q}) = \frac{I_0}{I_0 + \sum I_n} = \frac{\text{ELASTIC INTENSITY}}{\text{TOTAL INTENSITY}}$$

The theoretical EISF may thus be compared with that found experimentally (i.e. measured from the spectrum) in order to assess the validity of the fitted motional models. The EISF describes the static limit of the diffusing atoms (i.e. their average positions over time).

The precise shape of the EISF as a function of **Q** is characteristic of the geometry of the diffusional process. For unbounded translational diffusion, the EISF is always zero since there is no perfectly elastic component. For rotational diffusion, the EISF is unity at **Q**=0 and falls to a minimum at a **Q** value which is an inverse function of the radius of gyration of the rotation; past this minimum the EISF versus **Q** function is oscillatory in nature. The EISF is thus indicative of the geometry of the diffusional process. In order to analyse small-amplitude motions in detail (e.g. determination of number of sites for a jump process), it is often necessary to record spectra at high **Q** values. For a dynamic process, analysis of the temperature-dependence of the quasielastic scattering allows determination of the activation energy.

4.1.6 INSTRUMENTATION

The objective of a neutron scattering experiment is to determine the scattered intensity, $S(\mathbf{Q},\omega)$, at a given momentum transfer, $\hbar\mathbf{Q}$, as a function of energy transfer, $\hbar\omega$. There are three ways to determine the energy of a neutron: by measurement of its velocity, its wavelength or its rate of precession in a magnetic field. Each of these three parameters is determined using a different type of spectrometer: the direct geometry

time-of-flight (t-o-f) spectrometer, the inverted geometry spectrometer and the neutron spin-echo spectrometer, respectively. As shown in Table 4.2, each spectrometer has a characteristic energy resolution and corresponding motional time-scales that may be observed [Bée, 1988; Carlile, 1988a]:

spectrometer	resolution /μeV	time-scales /s
direct geometry t-o-f	10-100	10^{-10}-10^{-13}
inverted geometry	1-20	10^{-10}-10^{-11}
neutron spin-echo	0.005-1	10^{-7}-10^{-10}

Table 4.2: Resolution and observable time-scales for the different types of spectrometer

4.1.6.1 Direct Geometry Time-of-Flight Spectrometer

This type of spectrometer uses rotating mechanical choppers, which open at specified time intervals, to select out the incident neutron energy. The scattered neutrons are timed over the known distance from the sample to a bank of detectors (typically ^{10}B) which are set at a range of scattering angles. The distribution of velocities of the scattered neutrons can thus be measured and the energy spectrum derived. Since the incident neutron energy is known (by prior calibration), an energy transfer spectrum may be constructed. The t-o-f geometry spectrometer has relatively low resolution but a large available energy transfer range. The spectrometer used in this work was the direct geometry t-o-f spectrometer IN5 at the Institut Laue-Langevin (ILL) in Grenoble.

4.1.6.2 Inverted Geometry Spectrometer

This type of spectrometer uses a white incident neutron beam and selects out from the scattered radiation a single neutron energy using an energy analyser. In

practice, the wavelength of the scattered radiation is analysed by Bragg diffraction from a single crystal. The resolution is dependent on the scattering angle 2θ, and is optimised (at *ca.* 0.5-10 μeV) as 2θ tends to 180°: consequently, this type of spectrometer is also called the backscattering spectrometer. Examples are IN10 and IN13 at the ILL. The backscattering spectrometer gives the advantage of high resolution but with a small energy transfer range.

4.1.6.3 Neutron Spin-Echo Spectrometer

This type of spectrometer uses the neutron's magnetic moment to detect its energy change, the underlying principle being that a polarised neutron travelling a known distance in a magnetic field precesses about the direction of the field. The number of precessions undergone is proportional to the neutron velocity, the magnitude of the magnetic field and the direction of the field with respect to the neutron spin. Monitoring change in precession rate during the scattering event will thus give change in neutron velocity and hence energy. The final spin state of the neutron, relative to its initial spin state, determines whether or not an 'echo' is produced. An example of a neutron spin-echo spectrometer is IN11 at the ILL.

4.1.7 Data Treatment

Various corrections need to be applied to the raw data before models can be fitted. Details of general corrections that may be required can be found in Lindley & Mayers [1988] and Springer [1972]. Those pertinent to IN5 data are outlined below: they constitute the data reduction program INX [Rieutord, 1990].

Firstly, the experimental set-up itself gives rise to a non-negligible scattering (or 'background'): to take account of this, a spectra is recorded of the empty sample-holder. Secondly, the spectra are measured at variable scattering angle, so in order to render them comparable with each other, it is necessary to normalise the detectors. This is done using the spectrum of vanadium, which is a completely incoherent and isotropic scatterer. Thus, a typical neutron scattering experiment requires:

(i) measurement of the sample spectrum

(ii) measurement of the spectrum of the empty sample-holder

(iii) measurement of the spectrum of vanadium

Data reduction consists of:

- normalisation of each spectrum with respect to total number of neutrons used

- subtraction of the background (i.e. the spectrum of the empty sample-holder)

- normalisation of each sample spectrum against that of the vanadium standard

- conversion of the data from time-of-flight to energy

- regrouping of the spectra so as to improve the quality of the signal, and elimination of data from the detectors which were situated at scattering angles corresponding to coherent scattering ('Bragg peaks').

- correction of the spectra for absorption of the sample (the extent of absorption depends on the thickness of the sample)

- correction for the efficiency of the detectors, which varies with the wavelength of the scattered neutrons

These corrections allow spectra measured at different scattering angles during one experiment to be compared, either with each other, or with spectra recorded during another experiment. The spectral data may then be analysed using various models of atomic and molecular motion, details of which are described fully in Bée [1988] and Guillaume [1988].

4.2 INVESTIGATION OF GUEST MOLECULAR MOTION

4.2.1 BACKGROUND AND AIMS

4.2.1.1 Previous Studies

The guest molecules which lie within urea inclusion compounds undergo considerable motion in the high temperature phase. Alkane/urea inclusion compounds are known [Pemberton & Parsonage, 1965] to display a phase transition from a low-temperature orthorhombic phase to a high-temperature hexagonal phase. In the high-temperature phase, the *n*-alkane molecules undergo rapid rotations about the channel axis [Gilson & McDowell, 1959 & 1961; Connor & Blears, 1969] and translations along the channel axis [Fukao *et al*, 1986]. These motions occur at a much slower rate in the low-temperature phase. We believe that the phase transition which occurs in the α,ω-dibromoalkane/urea inclusion compounds has similar consequences for the motion of the α,ω-dibromoalkane molecules.

A wide range of *n*-alkane/urea incluson compounds has been studied from the viewpoint of guest molecular motion. Inelastic incoherent neutron scattering investigations [Guillaume, 1988; Guillaume *et al*, 1990 & 1991] of $C_{19}H_{40}$/urea-d_4 indicate the existence, along the channel axis at very low temperature (1.5 K), of a longitudinal acoustic mode of frequency 12 cm^{-1}. At higher temperatures, this mode becomes strongly overdamped; in addition, quasielastic broadening indicates that restricted translational motions are occurring. There is also evidence, in the high temperature phase, for a diffusive rotational motion about the channel axis. However, these conclusions are in conflict with those of Boysen *et al* [1988], who performed incoherent neutron scattering studies on *n*-hexadecane/urea-d_4. These workers propose a model of $2\pi/6$ jump motion (with correlation time *ca.* 7 ps) of the guest molecules about the channel axis, in conjunction with overdamped librations.

Other studies, using different techniques, of various guest species (mainly *n*-alkanes) have invoked numerous models for guest molecular motion. Wood *et al* [1989] have developed an approach to investigate Raman band-widths, in which the reorientational motion of the *n*-alkane CH_2 groups is modelled as a damped Brownian

harmonic oscillator. Also from a Raman study, Cho *et al* [1986a &b] propose a $2\pi/6$ jump model for the docosane ($C_{20}H_{42}$) guest. Models derived from nuclear magnetic resonance (NMR) spectroscopic studies propose large amplitude oscillations [Bell & Richards, 1969], uniform uniaxial rotations [Casal *et al*, 1984a & b] and $2\pi/3$ jumps [Meirovitch & Belsky, 1984]. Greenfield *et al* [1985 & 1989] have studied $C_{19}D_{40}$/ urea-h_4 by ^{2}H NMR and have modelled the reorientations of the guest molecules about the channel axis both by jump motions and by rotational diffusion. Lee *et al* [1992] model the motion of *n*-alkane guests, using molecular dynamics simulations, as rotation of the CH_2 groups about the channel axis.

Previous work on the dynamics of α,ω-dibromoalkane guests is not extensive. Dielectric loss spectroscopy has been used [Meakins, 1955] to study the dynamic properties of $Br(CH_2)_{10}Br$ in its urea inclusion compound. The fact that a signal is detected suggests, *per se*, that the Br end-groups undergo motions independently from one another.† Bell & Richards [1969] have studied $Br(CH_2)_{10}Br$/urea by ^{1}H NMR spectroscopy: they conclude, on the basis of T_1 measurements, that rapid rotation of the guest molecules about the channel axis occurs, even at low temperatures. They find evidence for additional guest motion at higher temperatures, and suggest that this may be either segmental motions of the guest molecules or reorientational motions of the urea molecules (the latter hypothesis is investigated in Chapter 5). Guest motion of $Br(CD_2)_{10}Br$/urea is also investigated by ^{2}H NMR spectroscopy in Chapter 5.

4.2.1.2 Outline of Current Study

We aim to compare and contrast the motions of the α,ω-dibromoalkane guest molecules with those of the *n*-alkane guest molecules. The presence of the heavier Br end-group, *vis-à-vis* the CH_3 end-group, may affect guest dynamics. The average guest structural properties in these two families of inclusion compounds differ: $\Delta_g=c_g/3$

† Dielectric absorption is shown to be due to the orientation of long-chain dipoles within the urea inclusion compound. The $Br(CH_2)_{10}Br$ molecule in its fully extended *trans* conformation has a resultant zero dipole moment, hence should give no dielectric absorption. This implies that the two C-Br dipoles of a given molecule are capable of orientation independently of one another.

for $Br(CH_2)_nBr$/urea (as seen in Chapter 2), whereas for $CH_3(CH_2)_nCH_3$/urea, Δ_g=0. It is plausible that this difference in structure may have an effect on the guest dynamics. The previous studies, cited above, on $Br(CH_2)_nBr$/urea inclusion compounds investigated only one chain length, *viz* n=10. The current work focuses on the motion of the guest molecules in $Br(CH_2)_nBr$/urea-d_4 inclusion compounds, where n=8-10: we thus study chain-length dependence. These compounds were investigated over the temperature range 120-280 K in order to establish the translational and reorientational dynamics of the guest molecules on the picosecond time-scale. The use of semi-oriented polycrystalline samples allows molecular motions about and along the channel axis **c** to be studied independently, as described below. Appropriate models were fitted to the experimental data, and the results then compared with previous studies of the dynamics of *n*-alkane/urea inclusion compounds. This work has recently been published [Smart *et al*, 1992; Guillaume *et al*, 1992; see also Guillaume *et al*, submitted for publication].

4.2.1.3 Experimental Considerations

As outlined previously, IQNS investigations allow us to assess the exact geometry of the molecular motions, via the evolution of the EISF with **Q**. More specifically, the scattering law can be written:

$$S(\mathbf{Q},\omega) = \text{Fourier transform of } \langle \exp\{i\mathbf{Q}\mathbf{d}(t)\}\rangle$$

$$\text{where } \mathbf{d}(t) = \mathbf{r}(t)-\mathbf{r}(0) = \text{displacement of the proton}$$

This equation can be written in terms of the perpendicular sine and cosine components of **Q**.**d**. Two experimental geometries can thus be adopted, in which **Q** is either parallel or perpendicular to **d**, in order to analyse precisely the motions occurring along and about the urea channel axis. These experimental geometries are shown in Fig 4.3:

(i) the momentum transfer vector **Q** is parallel to the urea channel axis **c**. This geometry allows study of the motion of the guest molecules *along* the **c** axis and is denoted $\mathbf{Q}_{//}$.

(ii) **Q** is perpendicular to the urea channel axis **c**. This geometry allows study of the reorientation of the guest molecules *about* the **c** axis and is denoted $\mathbf{Q}_{\perp}$.

In the $\mathbf{Q}_{//}$ geometry (Fig. 4.3a), the channel axes lie in the scattering plane and form an angle of 135° with the incoming neutron beam; this condition for $\mathbf{Q}_{//}$ geometry is satisfied only when the scattering angle 2θ is 90°. In the $\mathbf{Q}_{\perp}$ geometry (Fig. 4.3b), the channel axes are perpendicular to the scattering plane: this condition is satisfied for any value of 2θ.

Our studies had the following requirements: temperature $5 \leq T \leq 300$ K, resolution of the order of 10-100 μeV, momentum transfer $|\mathbf{Q}_0|$ in the range $0<|\mathbf{Q}_0|<3$ Å^{-1}. Of the suitable spectrometers, the direct geometry time-of-flight spectrometer IN5 was chosen; as $T \geq 5$ K, the vibrational spectrum can be measured in neutron energy gain (i.e. sample energy loss). This instrument is described in The Yellow Book [Blank & Maier, 1988] and is shown schematically in Fig. 4.4. Its resolution is in the range 20-160 μeV, corresponding to $5<\lambda_0<16$ Å and $0.6<|\mathbf{Q}_0|<5.5$ Å. This allows study of time-scales in the range *ca.* 0.3-100 ps. The resolution function is almost precisely triangular in shape, so allowing easy assessment of quasielastic broadening.

4.2.2 Experimental Details

The α,ω-dibromoalkane/urea-d_4 inclusion compounds were prepared as detailed in Appendix A, except for the sample of 1,8-dibromooctane/urea-d_4, which was kindly provided by Mr Ali Mahdyarfar. The deuteration of the host urea ensured that the incoherent scattering contribution from the urea molecules was minimised, such that the dynamic properties of the guest molecules could be studied selectively. The degree of deuteration of the host molecules was estimated by infrared spectroscopy to be ≥98%.

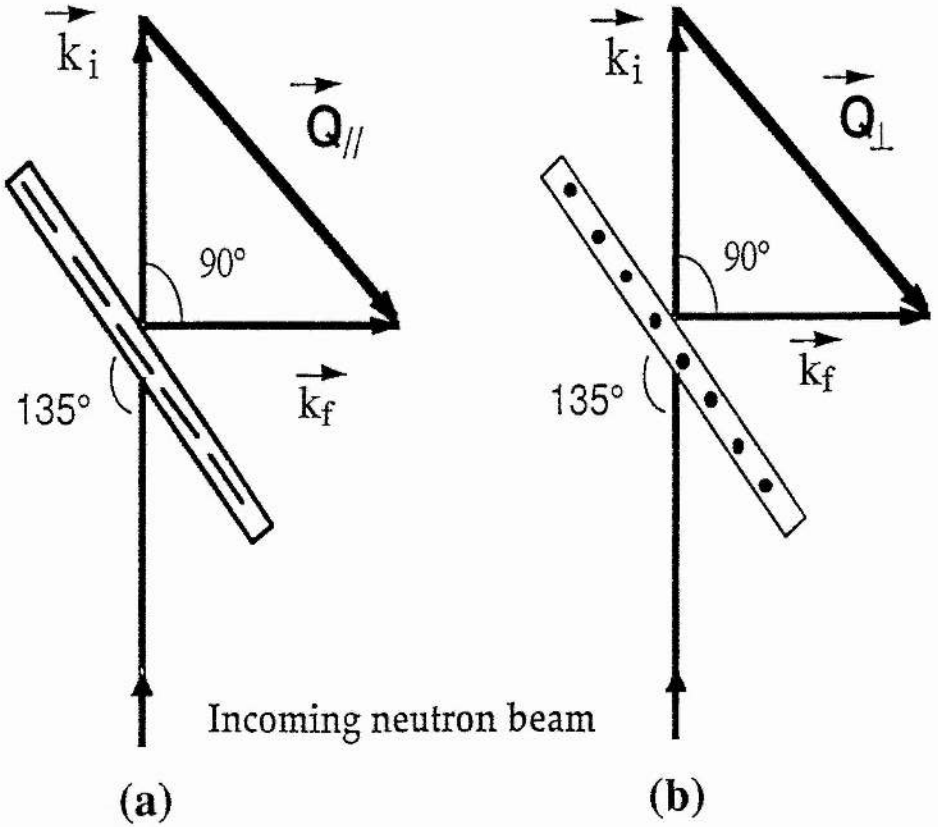

Fig. 4.3: The two experimental geometries:
(a) **Q** is parallel to the urea channel axis for 2θ=90° (b) **Q** is perpendicular to the urea channel axis

The incident and scattered wavevectors lie in the plane of the page.

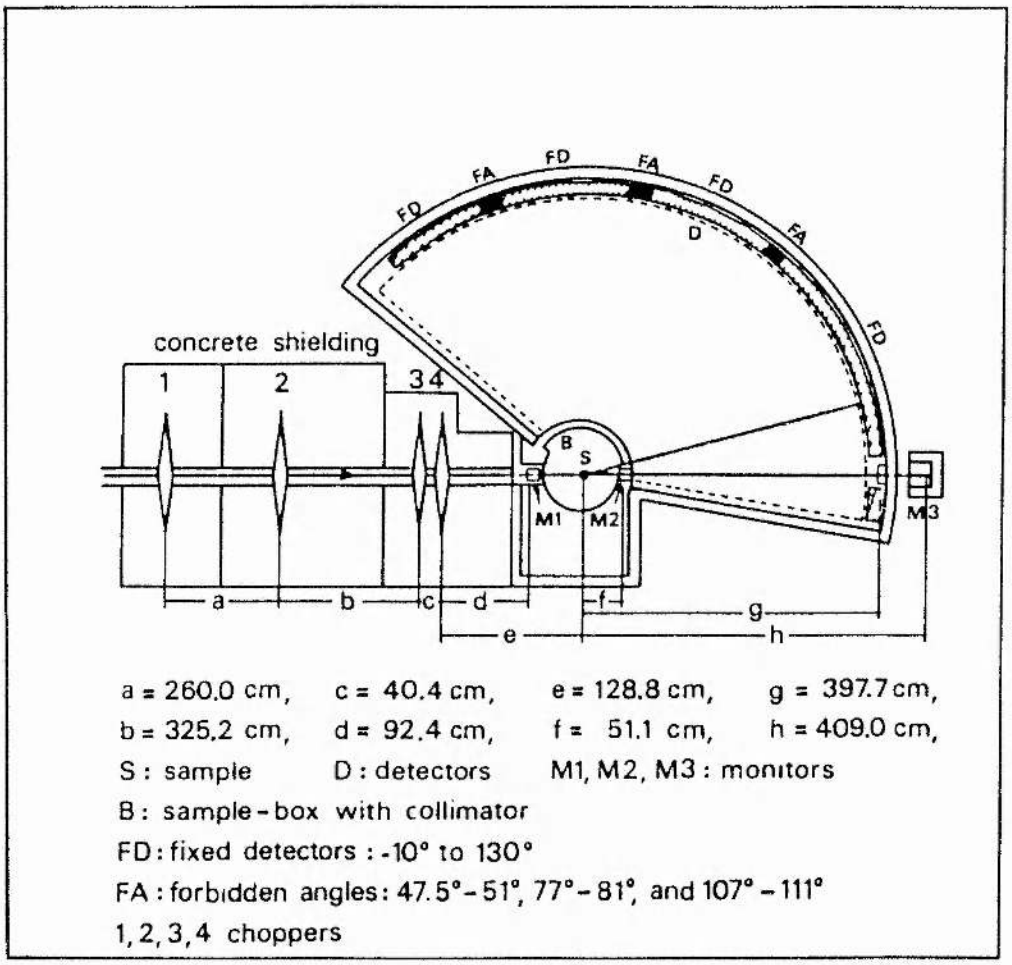

Fig. 4.4: Schematic view of the t-o-f spectrometer IN5 [from Blank & Maier, 1988]

Semi-oriented polycrystalline samples were used, comprising single crystals (of typical dimensions 0.5 x 0.5 x 5 mm^3) placed in a grooved aluminium sample holder such that the channel axes (crystallographic **c** axes) of all crystals were parallel to each other. The crystallographic **a** and **b** axes (perpendicular to the channel axis) were randomly oriented with respect to rotation about the channel axis. IQNS experiments were carried out using the time-of-flight spectrometer IN5 at the Institut Laue-Langevin in Grenoble. Experimental conditions were as follows:

incident $\lambda = 6$ Å

spectral resolution (at full-width half-maximum) = 67 μeV

standard sample = vanadium

The sample thickness was chosen such that transmission was approximately 90%: this ensured that the effects of multiple scattering could be neglected in the data analysis. Temperature control was achieved (to ±2 K) using a helium-cooled cryostat.

The urea inclusion compounds studied were $Br(CH_2)_nBr$/urea-d_4, with n=8-10. The phase transition temperatures for these compounds are in the range 135-157 K (as shown by differential scanning calorimetry: see Appendix B). Temperatures below and above the phase transition are denoted LT and HT, respectively. The neutron scattering was measured as a function of:

(i) Length of guest molecule: Spectra were recorded for $Br(CH_2)_nBr$/urea-d_4, with n=8,9,10, at 120 K and 240 K in the $\mathbf{Q}_{//}$ geometry, and at 240 K in the $\mathbf{Q}_{\perp}$ geometry.
(ii) Temperature: Spectra were recorded for $Br(CH_2)_9Br$/urea-d_4, in both the $\mathbf{Q}_{//}$ and the $\mathbf{Q}_{\perp}$ geometries, over the temperature range 120-280 K, at intervals of 40 K.

The detectors were normalised using the spectrum of a vanadium standard, recorded at 5 K, for both the $\mathbf{Q}_{//}$ and $\mathbf{Q}_{\perp}$ geometries. The vanadium standard had the same dimensions as the sample and was measured under identical experimental conditions. The measured scattering at a given angle 2θ was normalised for all sample counts, the data obtained for the empty Al sample holder was subtracted and the

resultant data normalised against the same data obtained for the vanadium standard. Thus:

$$\text{Normalised sample counts} = \frac{\left[\frac{\text{sample counts at } 2\theta}{\text{total sample counts}}\right] - \left[\frac{\text{Al can counts at } 2\theta}{\text{total can counts}}\right]}{\left[\frac{\text{V counts at } 2\theta}{\text{total V counts}}\right] - \left[\frac{\text{Al can counts at } 2\theta}{\text{total can counts}}\right]}$$

These, and the other corrections outlined in §4.1.7, were carried out using the INX data reduction program [Rieutord, 1990]. The spectrum of vanadium recorded at 5 K was also used as the instrumental resolution function.

4.2.3 Results and Discussion

4.2.3.1 Qualititative Analysis of Results

(i) Experiments in $Q_{//}$ geometry

The IQNS spectra of $Br(CH_2)_9Br$/urea-d_4, recorded in the $\mathbf{Q}_{//}$ geometry for the LT and HT phases, are shown in Figs. 4.5a and 4.6a, respectively; spectra of the other two compounds studied are qualitatively similar. At LT, quasielastic broadening is negligible but inelastic peaks (termed 'side-peaks') are observed at *ca.* 0.7 meV: these correspond to a very low-frequency vibration (oscillatory motion). In view of the very low energy of these side-peaks, this oscillatory motion is probably a collective excitation of the guest molecules, i.e. a longitudinal acoustic-type mode (rather than intramolecular oscillations). At HT, the observed profiles consist of two components: (i) the side-peaks, which are considerably broadened and (ii) a quasielastic broadening of the elastic line. Component (i) corresponds to the oscillatory motions seen in the LT phase: these become heavily damped above the phase transition temperature. Component (ii) corresponds to a translatory motion of the whole guest molecule in the **c** direction.

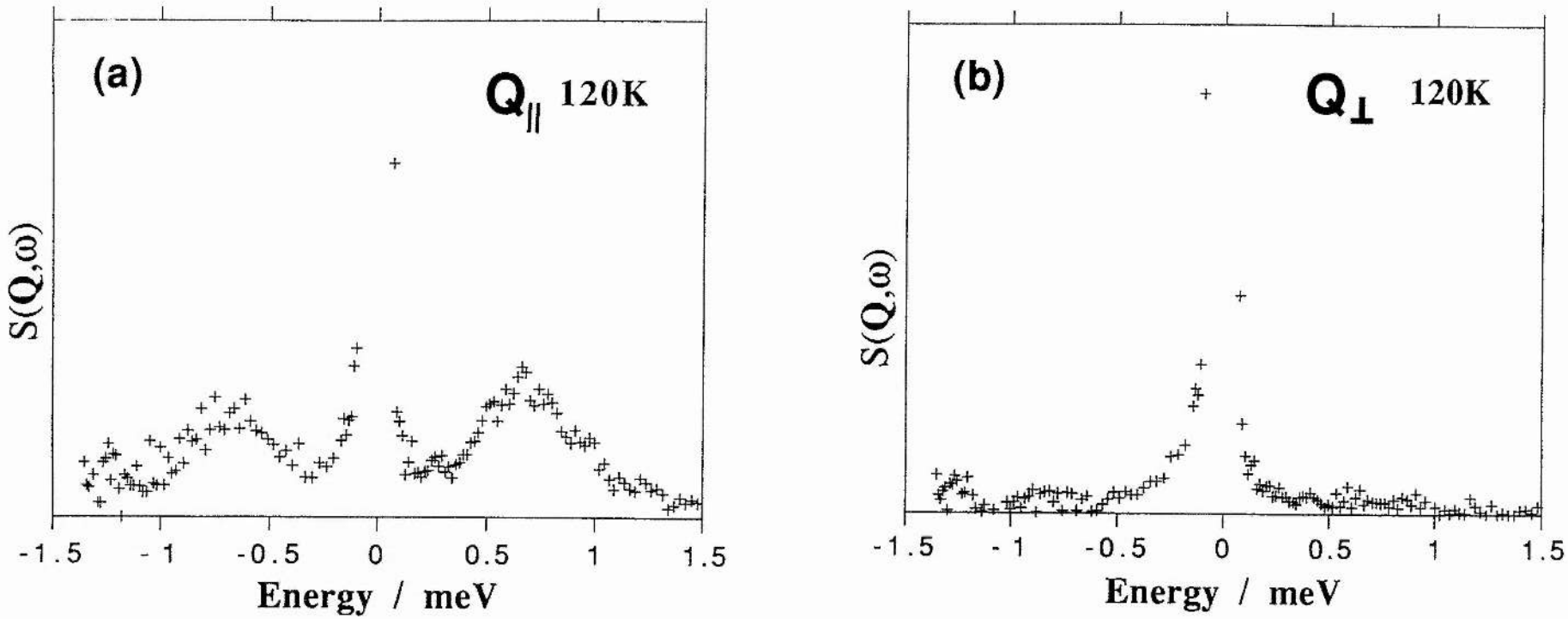

Fig. 4.5: Experimental spectra for $Br(CH_2)_9Br$/urea-d_4 in the LT phase (at 120 K) recorded in (a) $\mathbf{Q}_{//}$ and (b) $\mathbf{Q}_{\perp}$ geometries. The scale expansion factor is x100.

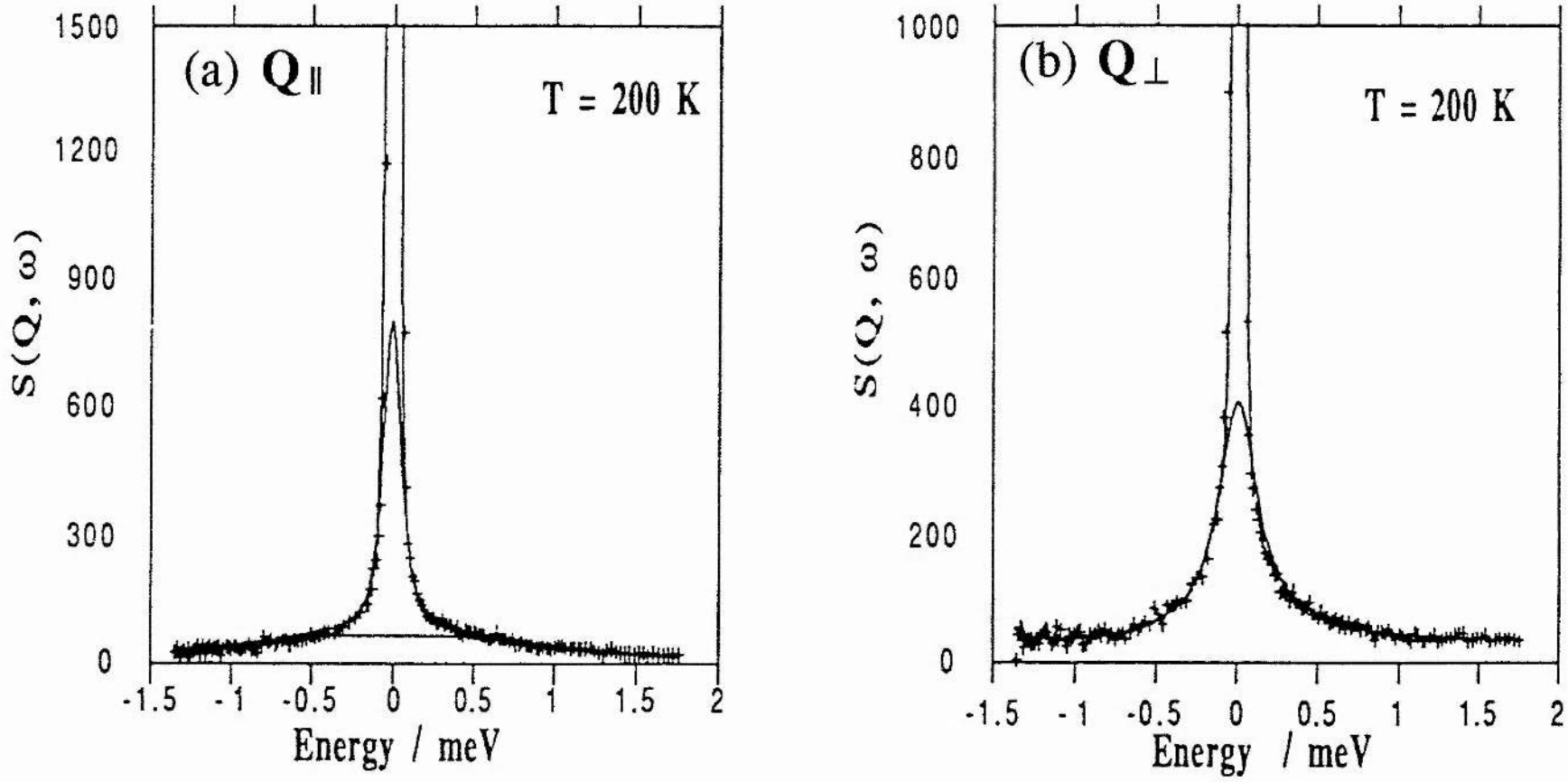

Fig. 4.6: Experimental and fitted spectra for $Br(CH_2)_9Br$/urea-d_4 in the HT phase (at 200 K) recorded in (a) $\mathbf{Q}_{//}$ and (b) $\mathbf{Q}_{\perp}$ geometries.

The experimental points are shown as crosses and the fitted scattering law as solid lines (the fitting of the spectra is discussed in §4.2.3.2). The scale expansion factor is x4.

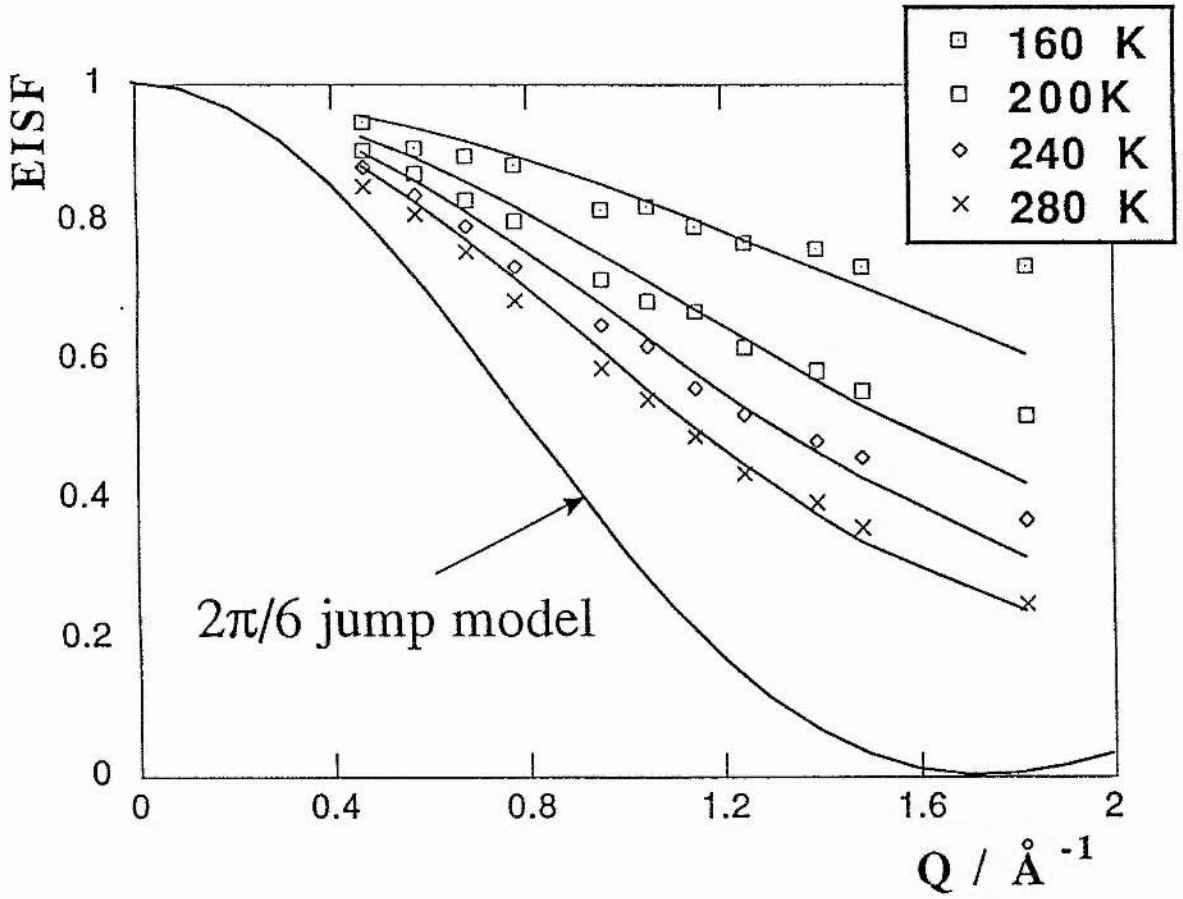

Fig. 4.7: Comparison between experimental EISF plots (symbols) for $Br(CH_2)_9Br$/urea-d_4 in the $Q_\perp$ geometry at various temperatures and theoretical EISF curves (calculated using eqn (D)) for uniaxial rotational diffusion in a one-fold cosine potential. For comparison, the theoretical curve for the $2\pi/6$ jump model (eqn (C)) is also shown.

(ii) Experiments in the $\mathbf{Q}_\perp$ geometry

The IQNS spectra of $Br(CH_2)_9Br$/urea-d_4, recorded in the $\mathbf{Q}_\perp$ geometry for the LT and HT phases, are illustrated in Figs. 4.5b and 4.6b, respectively. Spectra recorded at 240 K of the other two compounds studied were qualitatively similar to Fig. 4.6b (spectra at LT were not recorded for these two compounds in this geometry). In the LT phase, only the elastic peak is seen (quasielastic broadening being negligible); there is no evidence for side-peaks. The spectrum in the HT phase shows considerable quasielastic broadening; this corresponds to a reorienting motion of the guest molecules about the **c** axis.

4.2.3.2 Quantitative Analysis of Results

(I) Models Used

(i) $\mathbf{Q}_{//}$ geometry: translations along the channel axis

The translations of the guest molecules along the channel axis may be separated into two components: the motion of the centre of mass of the molecule (translatory motion) and the motion of the constituent atoms relative to the centre of mass (oscillatory motion). These motions are assumed to be uncorrelated with respect to time, so giving an intermediate scattering function:

$$I^t(\mathbf{Q},t) = I^{osc}(\mathbf{Q},t).I^{trans}(\mathbf{Q},t)$$

where $I^{osc}(\mathbf{Q},t)$ refers to oscillatory motions and $I^{trans}(\mathbf{Q},t)$ refers to translatory motions. This corresponds to a scattering law of the general form:

$$S^t(\mathbf{Q}, \omega) = S^{osc}(\mathbf{Q},\omega) \otimes S^{trans}(\mathbf{Q},\omega)$$

where $\otimes$ denotes the convolution. The following scattering law has thus been derived:

$$S^t(\mathbf{Q}, \omega) = \exp\left\{-Q^2\langle r^2\rangle\right\} . \left[S^{trans}(\mathbf{Q},\omega) + F_1^{osc}(\mathbf{Q}, \omega) + F_2^{osc}(\mathbf{Q}, \omega)\right] \qquad \text{- eqn (A)}$$

where F_1 and F_2 define the shape of the side-peaks, in accordance with the model of a damped harmonic oscillator:

$$F_1^{osc}(\mathbf{Q}, \omega) = \frac{Q^2 \langle r^2 \rangle K_0 \Omega_0^2}{\pi (\Omega_0^2 - \omega^2)^2 + \pi K_0^2 \omega^2}$$

$$F_2^{osc}(\mathbf{Q}, \omega) = \frac{[Q^2\langle r^2\rangle]^2}{2\pi}\left[\left(\frac{K_0}{1-q^2}\right)\left(\frac{1}{\omega^2 + K_0^2} + \frac{16\,\Omega_0{}^2\,(1-q^2) - (4\Omega_0{}^2 - \omega^2)}{(4\Omega_0{}^2 - \omega^2)^2 + 4K_0{}^2\omega^2}\right)\right] \quad \text{- eqns (B)}$$

where the fitted parameters are as follows:

$\langle r^2 \rangle$ = mean square amplitude of the oscillations (along the channel axis)

K_0 = damping factor

Ω_0 = mean frequency of the oscillator

and $q = \frac{K_0}{2\Omega_0}$

The translatory component, $S^{trans}(\mathbf{Q},\omega)$, is modelled as a continuous linear diffusion between two rigid impermeable boundaries. This has an intermediate scattering function as derived by Hall & Ross [1981]:

$$I^{trans}(\mathbf{Q}, t) = A_0^{trans}(\mathbf{Q}) + \sum_{n=1}^{\infty} A_n^{trans}(\mathbf{Q}) \,.\, \exp(-\Delta\omega_n t)$$

This corresponds, on Fourier transformation, to the following scattering law:

$$S^{trans}(\mathbf{Q}, \omega) = A_0^{trans}(\mathbf{Q})\, \delta(\omega) + \sum_{n=1}^{\infty} A_n^{trans}(\mathbf{Q}) \,.\, L_n(\omega)$$

with:

$$A_0^{trans}(\mathbf{Q}) = j_0^2\left[\frac{QL}{2}\right], \qquad A_n^{trans}(\mathbf{Q}) = \frac{4(QL)^2\left[1 - (-1)^n \cos(QL)\right]}{\left[(QL)^2 - (n\pi)^2\right]^2}$$

and $$\sum_{n=0}^{\infty} A_n^{trans}(\mathbf{Q}) = 1$$

where:

j_0 = spherical Bessel function of zero order

$L_n(\omega)$ = Lorentzians of half-width half-height given by: $\Delta\omega_n = D_t\left[\frac{n\pi}{L}\right]^2$

The fitted parameters are:

L = translational length

D_t = translational diffusion coefficient

For the experimental Q range used in our experiments, it is sufficient to consider just two $L_n(\omega)$ functions in the scattering law, thus giving:

$$S^{trans}(\mathbf{Q}, \omega) = A_0^{trans}(\mathbf{Q})\,\delta(\omega) + \sum_{n=1}^{2} A_n^{trans}(\mathbf{Q}) \,.\, L_n(\omega)$$

(ii) $\mathbf{Q}_\perp$ geometry: rotations about the channel axis

The model for rotations of the guest molecules about the channel axis was chosen as follows. From the experimental data, an experimental EISF, $A_0(\mathbf{Q})$, can be calculated as a function of $\mathbf{Q}$, as outlined in §4.1.5: this is illustrated in Fig. 4.7. It can be seen that $A_0(\mathbf{Q})$ decreases with increasing temperature: a jump model cannot account for this behaviour. Such an EISF indicates that the motional amplitude increases with temperature. For comparison, we have also plotted in Fig. 4.7 the calculated EISF for $2\pi/6$ jump rotations, as given by Bée [1988]:

$$A_0(\mathbf{Q}) = \frac{1}{6}\sum_{p=1}^{6} J_0\left[2Q.r\,\sin\left(\frac{\pi p}{6}\right)\right] \qquad \text{- eqn (C)}$$

where J_0 = zero order Bessel function of the first kind

r = radius of gyration = 1.39 Å for straight-chain CH_2 groups

p = number of jump sites

We immediately conclude that a $2\pi/6$ jump model is not valid. A rotational model which is to hold good for the temperatures we have studied should correspond to smaller amplitude reorientations than the $2\pi/6$ jump model. In addition, the absence of low-frequency side-peaks in both the LT and the HT phase suggests that the motion is diffusive rather than oscillatory.

We thus propose a model which we found is applicable at all the temperatures studied: this is uniaxial rotatonal diffusion in a one-fold cosine potential, a model first developed by Dianoux & Volino [1977]. Shown in Fig. 4.7 are the experimental EISF plots at various temperatures versus the theoretical curves calculated using this model (eqn (D): see later). This model has the following scattering law:

$$S^r(\mathbf{Q}, \omega) = A_0^{rot}(\mathbf{Q})\, \delta(\omega) + \sum_{m=1}^{\infty} A_m^{rot}(\mathbf{Q})\, .\, L_m(\omega)$$

where $L_m(\omega)$ = Lorentzians of half-width half-height given by: $\Delta\omega_m = D_r\, m^2$

Because our crystals were randomly oriented with respect to rotation about the channel axis (specified by rotation angle φ), it is necessary to average over φ, so giving the following expression for the EISF:

$$A_0^{rot}(\mathbf{Q}) = \frac{1}{\pi\,[I_0(\gamma)]^2} \int_0^{\pi} J_0(2Q.r.\sin\varphi)\, I_0(2\gamma\cos\varphi)\, d\varphi \qquad \text{- eqn (D)}$$

The fitted parameters are D_r and γ, where D_r is the rotational diffusion coefficient, and γ is related both to the effective potential barrier, V_0, for the rotations and to the mean angle, $\bar{\phi}$, of fluctuations about the channel axis:

$$V_0 = 2k_B T\gamma \qquad \text{and} \qquad \bar{\phi} = \cos^{-1}\left[\frac{I_1(\gamma)}{I_0(\gamma)}\right]$$

In these equations, k_B is the Boltzmann constant, T is temperature in Kelvin, r is the radius of gyration (=1.39 Å), J_0 is the Bessel function of the first kind and zero order, and I_0 and I_1 are the modified Bessel functions of zero and first order, respectively.

For the Q range investigated in these experiments (0-2 $Å^{-1}$), it is sufficient to consider the scattering law up to six $L_m(\omega)$, giving:

$$S^r(\mathbf{Q}, \omega) = A_0^{rot}(\mathbf{Q})\,\delta(\omega) + \sum_{m=1}^{6} A_m^{rot}(\mathbf{Q}) \,.\, L_m(\omega) \qquad \text{- eqn (E)}$$

(II) Fitting Procedure

Theoretical scattering laws for fitting to the experimental $\mathbf{Q}_{//}$ and $\mathbf{Q}_{\perp}$ spectra were obtained by convoluting eqns (A) and (E), respectively, with the instrumental resolution function, as follows:

$$S^{theory}(\mathbf{Q}, \omega) = A_0(\mathbf{Q}).V(\mathbf{Q}, \omega) + \sum_{i=1}^{N} A_i(\mathbf{Q}) \,.\, \left[L_i(\omega) \otimes T(\mathbf{Q}, \omega)\right]$$

where $V(\mathbf{Q},\omega)$ denotes the spectrum of the vanadium standard at 5 K (representing the instrumental lineshape function for the elastic peak), and $T(\mathbf{Q},\omega)$ denotes a triangular instrumental resolution function determined by fitting the experimental spectrum for the vanadium standard at 5 K.

For the $\mathbf{Q}_{//}$ geometry, only the data from the detector at scattering angle $2\theta=90°$ were fitted, since it is only at this angle that **Q** is exactly parallel to **c**. For the $\mathbf{Q}_{\perp}$ geometry, the scattering law was fitted simultaneously (using a common set of parameters) to each individual spectrum recorded in the range $30°<2\theta<120°$ (excluding those containing significant coherent scatttering): this approach implicitly takes into account the Q-dependence of the scattering law.

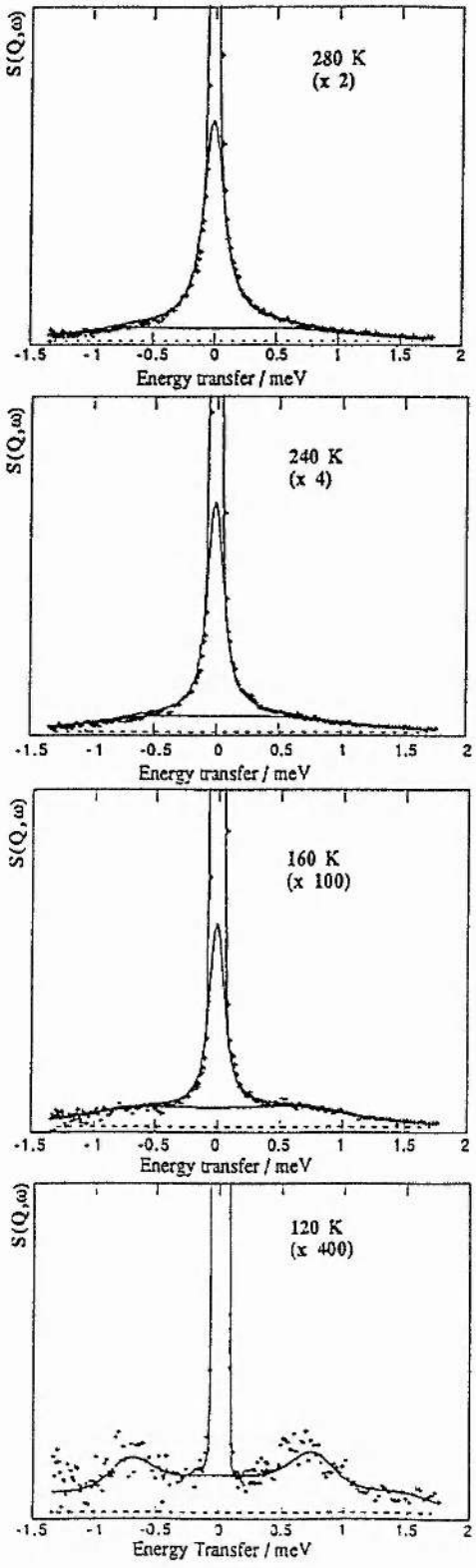

Fig. 4.8: Experimental and fitted spectra for $Br(CH_2)_9Br$/urea-d_4, recorded in the $\mathbf{Q}_{//}$ geometry as a function of temperature in the LT (120 K) and HT phases. The $\mathbf{Q}_{//}$ geometry corresponds to Q_0=1.5 Å^{-1}.

Table 4.3: Best-fit parameters for spectra of $Br(CH_2)_9Br$/urea-d_4 recorded in the $\mathbf{Q}_{//}$ geometry, as a function of temperature, T.

n	T /K	$Q^2\langle r^2\rangle$	Ω_0 /meV	K_0 /meV	$D_t/10^{-6}cm^2s^{-1}$	L /Å	$\sqrt{\langle r^2\rangle}$ /Å
9	120	0.8	0.8	0.5	-	-	0.6
9	160	1.2	0.9	0.9	0.7	0.9	0.7
9	200	1.2	0.8	1.0	1.3	1.3	0.7
9	240	1.4	0.8	1.0	2.4	1.6	0.8
9	280	1.5	0.8	0.8	7.0	2.3	0.8

Notes: The experimental data were collected on the detector at $2\theta = 90°$.

Table 4.4: Best-fit parameters for spectra of $Br(CH_2)_nBr$/urea-d_4 recorded in the $\mathbf{Q}_{//}$ geometry, as a function of chain length, n.

(a) At T=120 K:

n	T /K	$Q^2\langle r^2\rangle$	Ω_0 /meV	K_0 /meV	D_t /$10^{-6}cm^2s^{-1}$	L /Å	$\sqrt{\langle r^2\rangle}$ /Å
8	120	0.7	0.9	0.5	-	-	0.6
9	120	0.8	0.8	0.5	-	-	0.6
10	120	0.7	1.0	0.7	-	-	0.6

(b) At T=240 K:

n	T /K	$Q^2\langle r^2\rangle$	Ω_0 /meV	K_0 /meV	D_t /$10^{-6}cm^2s^{-1}$	L /Å	$\sqrt{\langle r^2\rangle}$ /Å
8	240	2.1	0.9	0.7	5.8	2.1	1.0
9	240	1.4	0.8	1.0	2.4	1.6	0.8
10	240	1.4	0.8	1.2	2.7	1.8	0.8

Notes: The experimental data were collected on the detector at $2\theta = 90°$.

(III) Results Obtained

(i) $Q_{//}$ geometry

Shown in Fig. 4.8, as a function of temperature in the LT and HT phases, are the fitted spectra for $Br(CH_2)_9Br$/urea-d_4. The best-fit parameters obtained are listed in Table 4.3 for $Br(CH_2)_9Br$/urea-d_4 at temperatures in the range 120-280 K, in Table 4.4a for $Br(CH_2)_nBr$/urea-d_4 (n=8-10) at 120 K and in Table 4.4b for $Br(CH_2)_nBr$/urea-d_4 (n=8-10) at 240 K.

Some observations can be made regarding the values of these parameters:

1. There is some uncertainty in the parameters pertaining to the oscillatory motion. This is due in part to the very low intensity of the side-peaks, but also to the fact that, at 280 K, the Ω_0 and K_0 parameters are correlated.† Thus Ω_0 was fixed at the value obtained for 240 K (i.e. 0.8 meV) in order to derive K_0; greater uncertainty therefore exists in the values of Ω_0 and K_0 at 280 K.

2. For the $Br(CH_2)_9Br$ guest in the temperature range 120-280 K, Table 4.3 shows that Ω_0 decreases slightly and K_0 increases with increase in temperature: this explains the overdamping of the motion at HT. $\langle r^2 \rangle$ increases with temperature, hence the amplitude of the oscillations is increased at HT. L and D_t both increase with increase in temperature. They have values in the range: $0.9<L<2.3$ Å; $0.7<D_t<7.0$ Å. On the assumption of Arrhenius behaviour for D_t, the variation of D_t with temperature in the HT phase corresponds to an activation energy for guest translations of (6 ± 1) kJmol^{-1}.

3. For $Br(CH_2)_nBr$ guests with n=8-10 at 120 K, Table 4.4a shows that neither Ω_0 nor K_0 appears to have an n-dependence. For $Br(CH_2)_nBr$ guests with n=8-10 at 240 K, Table 4.4b shows that Ω_0 remains approximately constant and K_0 increases with increase in n. For L and D_t it is difficult to assign a definitive trend with n; this

---

† When K_0 is large relative to Ω_0, as occurs at T≥280 K, eqns (B) become functions of Ω_0^2/K_0.

may depend on the parity of n: both L and D_t decrease when n is increased from 8 to 10 in the n-even series.

4. Despite the uncertainty in the parameters for the oscillatory motion, the values vindicate the assumed time-decoupling of the oscillatory and translatory motions, the quasielastic broadening being of the order of a few tens of μeV, whereas the oscillation frequency, Ω_0, is in the range 0.8-0.9 meV.

(ii) $Q_\perp$ geometry

The fitted spectra (at Q_0=1.5 $Å^{-1}$) for $Br(CH_2)_9Br$/urea-d_4 are displayed, as a function of temperature in the HT phase, in Fig. 4.9. The best-fit parameters obtained are listed in Table 4.5 for $Br(CH_2)_9Br$/urea-d_4 at temperatures in the range 120-280 K, and in Table 4.6 for $Br(CH_2)_nBr$/urea-d_4 at 240 K for n=8-10. Because the value of V_0 varies with temperature, the Arrhenius equation does not apply, so it is not possible to evaluate an activation energy. Fig. 4.10 displays the Q-dependence of the spectra at 280 K.

The trends displayed by the data listed in Tables Y & Z are as follows:

1. Table 4.5 shows that D_r increases with increase in temperature. $\bar{\phi}$ increases and hence V_0 decreases with increase in temperature.

2. Table 4.6 shows that, at 240 K, D_r decreases and $\bar{\phi}$ increases with increase in n. These parameters have values ranging as follows: $0.16<D_r<0.23$ ps^{-1}; $21<\bar{\phi}<54°$.

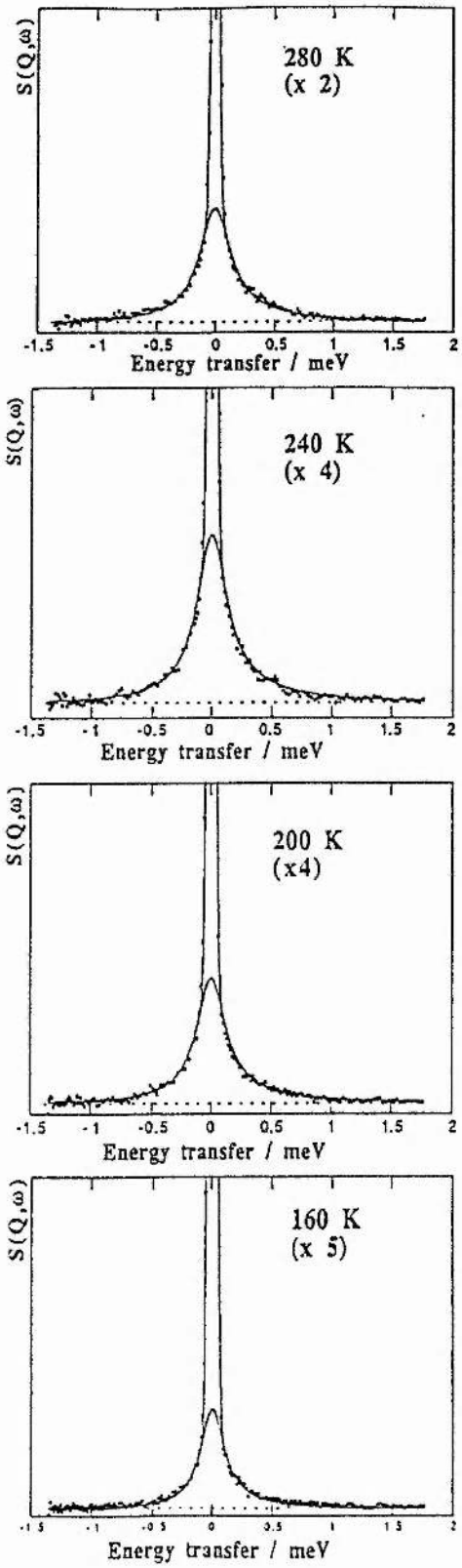

Fig. 4.9: Experimental and fitted spectra for $Br(CH_2)_9Br$/urea-d_4, recorded in the $\mathbf{Q}_\perp$ geometry at Q_0=1.5 Å^{-1}, as a function of temperature in the HT phase.

Table 4.5: Best-fit parameters for spectra of $Br(CH_2)_9Br$/urea-d_4 recorded in the $\mathbf{Q}_\perp$ geometry, as a function of temperature, T.

n	T /K	γ	D_r /ps^{-1}	$\bar{\phi}$ /°	V_0 /kJmol^{-1}
9	160	6.0	0.16	21	15.9
9	200	3.2	0.19	33	10.6
9	240	2.4	0.20	41	9.5
9	280	1.9	0.21	54	8.8

Table 4.6: Best-fit parameters for spectra of $Br(CH_2)_nBr$/urea-d_4 recorded in the $\mathbf{Q}_\perp$ geometry at 240 K, as a function of chain length, n.

n	T /K	γ	D_r /ps^{-1}	$\bar{\phi}$ /°	V_0 /kJmol^{-1}
8	240	1.9	0.23	47	7.6
9	240	2.4	0.20	41	9.5
10	240	2.4	0.19	41	9.6

Notes: All experimental spectra from detectors in the range $30° < 2\theta < 120°$ were fitted simultaneously.

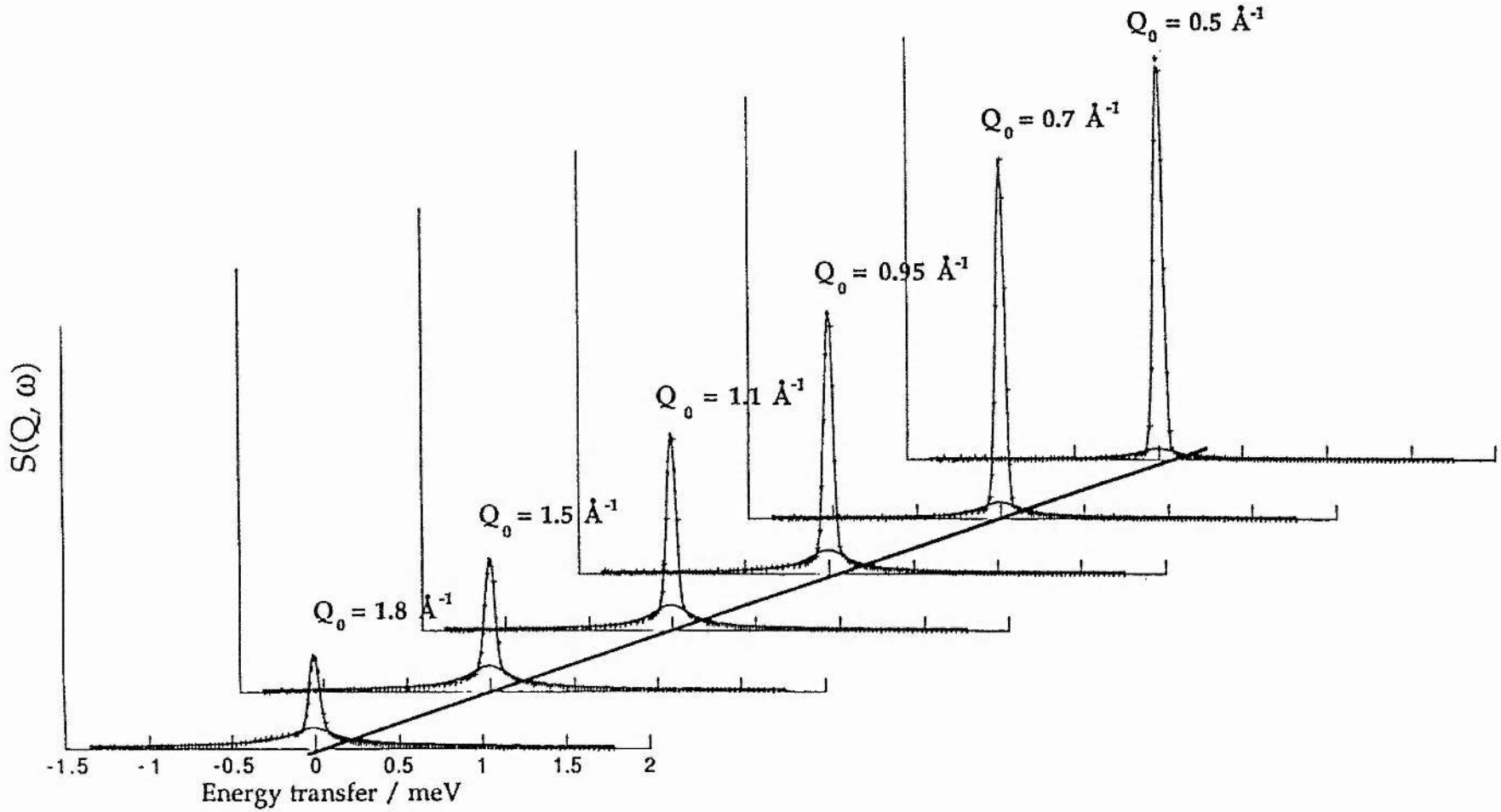

Fig. 4.10: Q-dependence of the experimental and fitted spectra for $Br(CH_2)_9Br$/urea-d_4 recorded in the $\mathbf{Q}_\perp$ geometry at 280 K

4.2.3.3 Comparison with Previous Studies

Our spectra are qualitatively similar to those previously cited for *n*-nonadecane/urea-d_4 [Guillaume *et al*, 1990 & 1991] in the $\mathbf{Q}_{//}$ and $\mathbf{Q}_{\perp}$ geometry. The parameters of our fits can be compared with those obtained previously by Guillame *et al* [1990 & 1991], using the same motional models. However, exact quantitative agreement is not expected as both the guest species and the chain length were different in the two studies.

(i) $\mathbf{Q}_{//}$ geometry

The best-fit parameters for the translatory component in the HT phase are of the same order of magnitude, as shown in Table 4.7a. The values for the low-frequency side-peaks in the LT phase are also comparable, as shown in Table 4.7b.

Fukao *et al* [1986], following measurement of x-ray integrated intensities of meridional Bragg reflections of *n*-hexadecane/urea, have also modelled the motion of the guest molecules along the **c** axis: their parameters analogous to our translational lengths, L, are of the same order of magnitude at equivalent temperatures.

Source	Guillaume *et al* [1990&1991]	Our results
Sample	$C_{19}H_{40}$/urea-d_4	$Br(CH_2)_nBr$/urea-d_4 (n=8-10)
Temperature range	$160 \leq T \leq 306$ K	$160 \leq T \leq 280$ K
Transational length	$1.1 < L < 2.7$ Å	$0.9 < L < 2.3$ Å
Diffusion coeff.	$(1.1 < D_t < 15).10^{-6} cm^2 s^{-1}$	$(0.7 < D_t < 7.0).10^{-6} cm^2 s^{-1}$

Table 4.7a: Comparison of parameters for translatory component of motion along the channel at HT

Source	Guillaume *et al* [1990&1991]	Our results
Sample	$C_{19}H_{40}$/urea-d_4	$Br(CH_2)_nBr$/urea-d_4 (n=8-10)
Temperature	T=140 K	T=120 K
Oscillator freq.	Ω_0=1.2 meV	Ω_0=0.8 meV

Table 4.7b: Comparison of parameters for low-frequency side-peaks in the LT phase

(ii) $\boldsymbol{Q}_\perp$ *geometry*

Again, our best-fit parameters for the HT phase are comparable with those for *n*-nonadecane/urea-d_4, as shown in Table 4.8.

Source	Guillaume *et al* [1990&1991]	Our results
Sample	$C_{19}H_{40}$/urea-d_4	$Br(CH_2)_nBr$/urea-d_4 (n=8-10)
Temperature range	$160 \leq T \leq 306$ K	$160 \leq T \leq 280$ K
Potential barrier	$5 < V_0 < 11$ kJmol^{-1}	$8 < V_0 < 16$ kJmol^{-1}
Diffusional coeff.	$0.10 < D_r < 0.30$ ps^{-1}	$0.16 < D_r < 0.21$ ps^{-1}
Fluctuation angle	$28 < \bar{\phi} < 66°$	$21 < \bar{\phi} < 54°$

Table 4.8: Comparison of parameters for uniaxial rotational diffusion about the channel axis at HT

Our values for V_0, the potential barrier for rotations, are in reasonable agreement with the activation energies, E_a, given by Bell & Richards [1969] for the reorientational motion of $Br(CH_2)_{10}Br$ in its urea inclusion compound: for free rotational diffusion, they quote E_a=9.2 kJmol^{-1}; for molecular reorientation between two potential minima of very unequal depth, they quote E_a=10.9 kJmol^{-1}.

Our parameters for the reorientational motion of the guest molecules may also be compared with those obtained for *n*-alkane guests using techniques other than IQNS. From ^2H NMR experiments, Greenfield *et al* [1985] quote a value of $D_r=2.0x10^{11}$ s^{-1} for the guest motion in $C_{19}D_{40}$/urea-h_4, as modelled by unrestricted diffusive rotation: this is two orders of magnitude different from our D_r values. Although Cho *et al* [1986a & b] used a $2\pi/6$ jump model for the motion of the docosane ($C_{20}H_{42}$) guest, their correlation times (*ca.* 0.7 ps), deduced from Raman bandwidths, are the same order of magnitude as our D_r values. Applying the model of a damped Brownian harmonic oscillator, Wood *et al* [1989] quote $\bar{\phi}=44°$ and $\bar{\phi}=41°$ for the $C_{14}H_{30}$ and $C_{20}H_{42}$ guests respectively at 300 K, in reasonable agreement with our range for $\bar{\phi}$. However, their value for effective harmonic frequency (*ca.* 6 ps^{-1}) is considerably larger than our D_r values for uniaxial rotational diffusion; their model also takes into account overdamped librations of the guest molecules on a slightly shorter time-scale (*ca.* 1 ps). (Such librations, corresponding to low-frequency side-peaks in spectra recorded in the $\mathbf{Q}_\perp$ geometry, were not observed in our studies.) Lee *et al* [1992] quote $\bar{\phi}\leq 40°$ for *n*-alkane guests using molecular dynamics simulations, but their approach considers just a single guest molecule in one urea channel, so the validity of their results is questionable.

An IQNS study subsequent to ours [Harris *et al*, 1992a] has shown qualitatively similar results for $I(CH_2)_8I$/urea-d_4: this is perhaps surprising, given the very much greater atomic mass and van der Waals radius of I compared with Br. In contrast, recent IQNS experiments on $(CH_3(CH_2)_6CO.O)_2$/urea-d_4 [Harris *et al*, 1992a] show that both the translational and the reorientational motions (if any) of the dioctanoyl peroxide molecules occur on much longer time-scales than for the *n*-alkane or α,ω-dihaloalkane guests. Further, the reorientations are of much smaller amplitude, and there is no evidence for a low-temperature longitudinal acoustic mode.

4.3 INVESTIGATION OF HOST MOLECULAR MOTION

4.3.1 BACKGROUND AND AIMS

^{2}H NMR studies of *n*-nonadecane/urea [Heaton *et al*, 1989] have indicated that the host urea molecules undergo 180° jumps about their C=O axes. From spectral simulations, these workers propose a jump frequency for this motion of *ca.* 2.0 x 10^6 s^{-1} at 303 K. These studies, which are discussed further in Chapter 5, showed no evidence for rotation of the NH_2 groups about the C-N bond. The theoretical scattering law for a uniaxial rotational motion is given below: this law averages over all orientations of the momentum transfer vector **Q** for a polycrystalline sample, and is thus denoted simply $S(Q,\omega)$. Similarly, the EISF is denoted $A_0(Q,\omega)$. Each proton in the urea molecule is assumed to jump between two equivalent sites.

$$S(Q,\omega) = A_0(Q)\delta(\omega) + A_1(Q).\frac{1}{\pi}.\frac{\tau}{1+\omega^2\tau^2} \qquad \text{- eqn (F)}$$

where:

$$A_0(Q) = \frac{1}{2}\left[1 + \frac{j_0(Qd_1) + j_0(Qd_2)}{2}\right] \qquad \text{- eqn (G)}$$

$A_1(Q) = 1 - A_0(Q)$

d_1 and d_2 are the jump distances as defined in Fig. 4.11

(equal to 2.26 Å and 4.10 Å, respectively)

j_0 denotes the spherical Bessel function of order zero

2τ defines the mean residence time of each urea proton at each jump site.

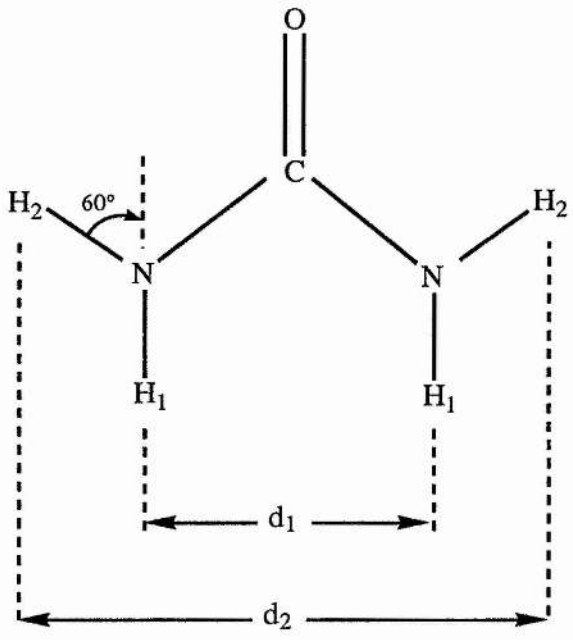

Fig. 4.11: Urea molecule, defining the jump distances d_1 and d_2

The current IQNS investigation of *n*-hexadecane-d_{34}/urea-h_4 set out to confirm limits for the motional time-scale of these 180° jumps of the host molecules for an *n*-alkane/urea inclusion compound. The use of a technique distinct from ^{2}H NMR allows comparisons to be drawn regarding the consistency of quantitative results. The neutron time-scale is of the order of picoseconds, considerably shorter than that (*ca.* 10^{-8} to 10^{-3} seconds) of ^{2}H NMR studies. We also aimed to assess the degree of time correlation, if any, between the motions of the host and the guest. This work has been published [Harris *et al*, 1992b].

4.3.2 Experimental Details

The compound studied was *n*-hexadecane-d_{34}/urea-h_4, which was kindly prepared by Mr Ian Shannon. The *n*-hexadecane-d_{34} used for this preparation was obtained commercially from MSD isotopes and was ≥99% isotopically pure. The deuteration of the guest minimised its contribution to the incoherent scattering to less than *ca.* 1.7% of the total incoherent scattering.

The sample used was polycrystalline. IQNS spectra were recorded at 300 K using the t-o-f spectrometer IN5 at the Institut Laue-Langevin.† The spectra were recorded for elastic momentum transfer in the range 0-2 $Å^{-1}$, with an incident wavelength of 6 Å and an instrumental resolution of 60 μeV. The spectrum of a vanadium standard was also recorded at 5 K. Data reduction was as outlined previously (see §4.1.7 & §4.2.2) using the INX program [Rieutord, 1990].

4.3.3 Results and Discussion

The experimental spectrum recorded at 300 K is shown in Fig. 4.12 and is compared with the instrumental resolution (approximated by the spectrum of the vanadium standard at 5 K) for the detector corresponding to the largest scattering angle measured ($2\theta=120°$). (At this scattering angle the quasielastic broadening can be assumed to be maximum). In fact, the quasielastic part of the spectrum has low intensity and a width (0.15 meV) consistent with that observed previously in the IQNS studies of *n*-nonadecane-h_{40}/urea-d_4 at 300 K [Guillaume *et al*, 1990]. The very low intensity of this quasielastic broadening may be explained by the fact that, given the ≥99% isotopic purity of the deuterated guest used, the intensity of the incoherent scattering from the host relative to that from the guest will be *ca.* 60:1. Therefore, this quasielastic broadening may be attributable to incoherent scattering arising from the guest molecules (i.e. from the deuterium and from the residual (≤1%) ^1H impurities).

† This temperature is well above the phase transition temperature of 151.8 K reported by Pemberton & Parsonage [1965].

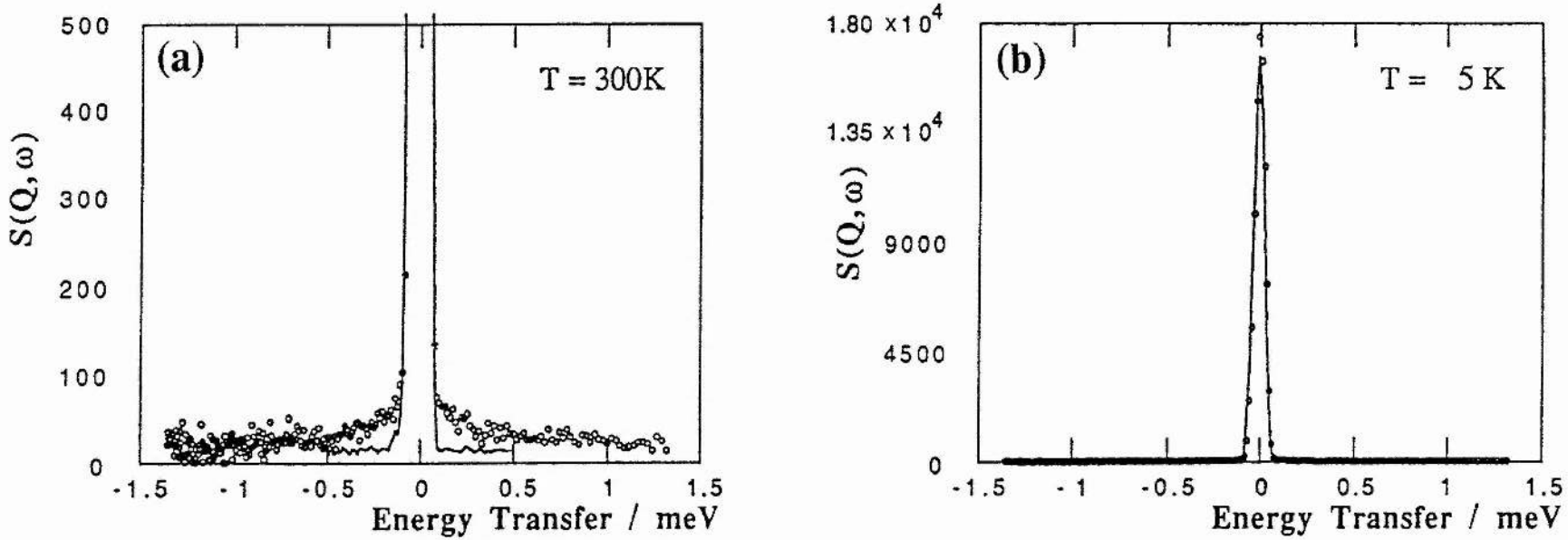

Fig. 4.12: IQNS spectra, recorded at the 2θ=120° scattering angle, for:

(a) *n*-hexadecane-d_{34}/urea-h_4 at 300 K (the scale expansion factor is x40)

(b) vanadium standard at 5 K (this spectrum defines the instrumental resolution)

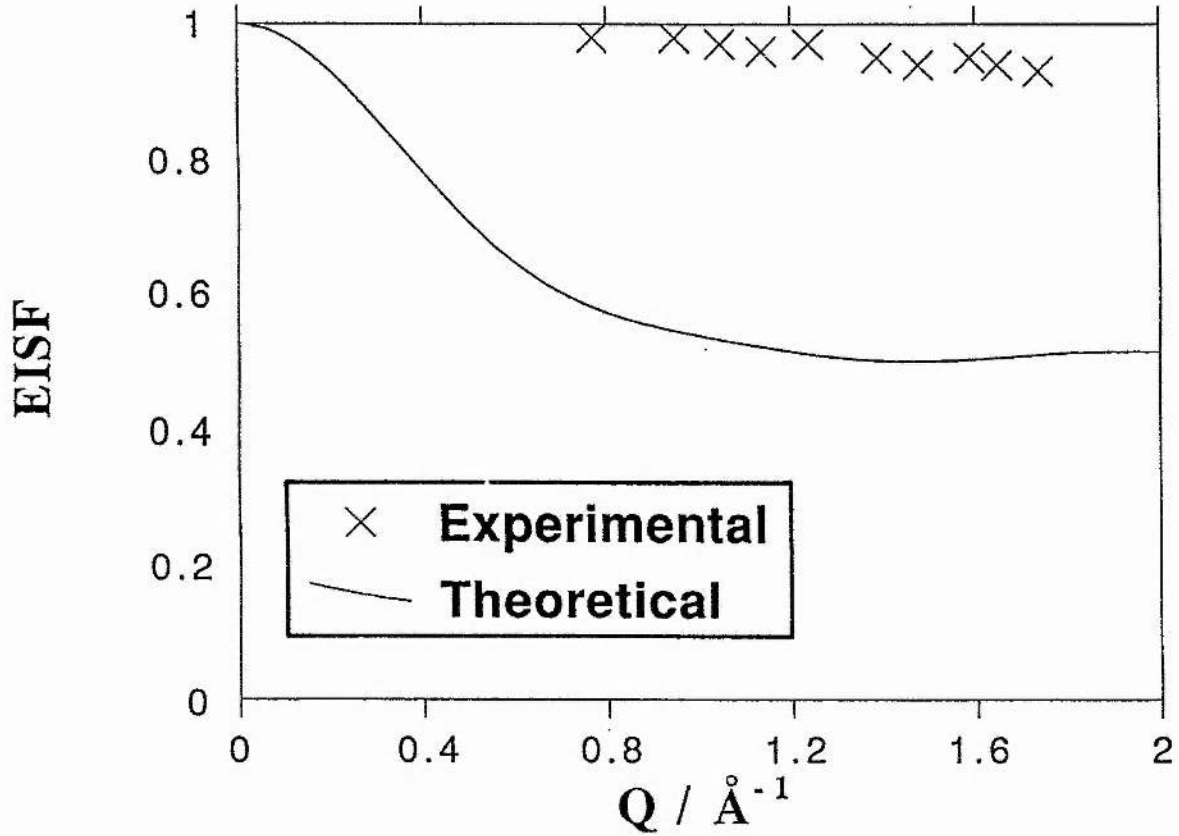

Fig. 4.13: Comparison of experimental (x) and theoretical (——) plots of EISF versus Q:
the theoretical graph has been calculated using eqn (F) for 180° jumps of the urea molecule about its C=O axis

The experimental data were fitted using a single Lorentzian function convoluted with the instrumental resolution. This allowed determination of the experimental EISF as a function of momentum transfer Q. Fig. 4.13 shows the variation of the experimental EISF with Q as compared to the theoretical EISF versus Q curve (which was calculated using eqn (G)). The lack of agreement between these curves implies that no 180° jump motion of the type modelled occurs on the instrumental time-scale. This suggests that any such motion of the host urea molecules, if it does indeed occur, must have a significantly longer time-scale: this is in agreement with the previous ^2H NMR studies of *n*-nonadecane/urea [Heaton *et al*, 1989]. Our results also confirm that no rapid rotation of the NH_2 groups about the C-N bond occurs on the picosecond time-scale. As already mentioned, Heaton *et al* [1989] have found no evidence for such rotations on the 10^{-3}-10^{-8} s ^2H NMR time-scale.

This work thus indicates that no rapid motions occur (on the picosecond time-scale) of the urea molecules in *n*-hexadecane-h_{34}/urea-d_4; we conclude that the motions proposed by Heaton *et al* [1989] at 300 K for *n*-nonadecane-h_{40}/urea-d_4 must occur on a time-scale longer than *ca.* 50 x 10^{-12} s. This lower limit for the motional time-scale, which we denote τ_L, was derived from an empirical relationship which assumes that quasielastic broadenings (defined at half-width half-maximum) can be evaluated reliably only if they are larger than *ca.* one-fifth of the instrumental resolution, Δ (defined at full-width half-maximum and here equal to *ca.* 60 μeV). Thus, the value of τ_L given above was deduced using the equation:

$$\tau_L \geq \frac{\bar{h}}{(\Delta/5)} \qquad \text{i.e.} \qquad \tau_L \geq \frac{5\bar{h}}{\Delta} \qquad \text{- eqn (H)}$$

Since we know (see §4.2) that the translational and rotational motion of the guest molecules in urea inclusion compounds, in general, occurs on the picosecond time-scale at 300 K, we conclude that the dynamics of the host and guest molecules are uncorrelated (i.e. time-independent), at least at this temperature. It is possible that this

finding may be a consequence of the incommensurate nature of urea inclusion compounds. This topic is discussed again in Chapter 5, which reports the use of ^2H NMR spectroscopy to study both host and guest molecular motion.

A subsequent study of *n*-decane-d_{22}/urea-h_4 by IQNS [Harris *et al*, 1992a] is in agreement with our results, concluding that the motion of the urea molecules occurs on a time-scale longer than 200 ps. Further studies are necessary to define more precisely the rate of urea motion for comparison with Heaton *et al* [1989]: to probe longer time-scales by IQNS would require much higher instrumental resolution (i.e. a smaller value of Δ in eqn (H)). This may be possible using a neutron spin-echo spectrometer.

4.4 CONCLUSIONS

4.4.1 GUEST MOTION

4.4.1.1 General Conclusions

The technique of IQNS, using semi-oriented polycrystalline samples, allowed study of the motion of the guest molecules in $Br(CH_2)_nBr$/urea inclusion compounds with n=8-10. The two experimental geometries revealed the existence, in the HT phase, of two motions of the guest molecules: a translational motion along the channel axis and a uniaxial rotational diffusion about the channel axis. The translational motion comprises a purely translatory component and an oscillatory component (probably corresponding to a longitudinal acoustic-type mode): these two components are time-decoupled.

The experimental spectra were fitted using uncorrelated models: restricted translational diffusion and uniaxial rotational diffusion in a one-fold cosine potential. These fits were satisfactory, and it was not necessary to consider more sophisticated models (such as correlated translation and rotation in a screw-like motion) in order to obtain meaningful parameters. In general, our parameters are in good agreement with previous studies using similar motional models: the behaviour of the α,ω-dibromo-alkane guests appears to be similar to that of the *n*-alkane guests, the replacement of the CH_3 end-group by Br having no significant effect on the mechanism of guest dynamics.

4.4.1.2 Improvements to the Models

Further developments in the methodology for interpretation of the experimental spectra could lead to more accurate modelling of the guest motions. The scattering laws used here for the $\mathbf{Q}_{//}$ and $\mathbf{Q}_{\perp}$ spectra did not consider the possibility of coupling between the translational and reorientational motions. Since these motions occur on the same time-scale, and in view of the fact that the urea molecules are arranged in a helical manner in the channel walls, correlation of the translations and reorientations in a screw-type motion of the guest molecules seems plausible.

The $\mathbf{Q}_{//}$ spectra were fitted for only one value of Q_0 (corresponding to the scattering angle $2\theta=90°$). If the scattering geometry could be modified so that $\mathbf{Q}$ is parallel to $\mathbf{c}$ at several values of 2θ, this would allow measurement of $\mathbf{Q}_{//}$ spectra for different values of Q_0, and the Q-dependence of the scattering law could then be taken into account in the fitting procedure.

4.4.2 HOST MOTION

The motion of the urea molecules in *n*-hexadecane-d_{34}/urea-h_4 was studied by IQNS using a polycrystalline sample. The spectra, recorded at 300 K, show no evidence for any motion of the urea molecules on the instrumental time-scale (10^{-10}-10^{-13} s). We conclude that the 180° flips of the urea molecules, proposed by Heaton *et al* [1989] for *n*-nonadecane/urea at 300 K, must occur on a time-scale longer than *ca.* 50×10^{-12} s. We thus infer that the motions of the host and guest molecules are uncorrelated, at least at 300 K.

4.5 REFERENCES

BAILEY RT, NORTH AM & PETHRICK RA (1981) Molecular Motion in High Polymers, Oxford University Press, pp 359-373.

BÉE M (1988) Quasielastic Neutron Scattering: Principles and Applications in Solid State Chemistry, Biology and Materials Science, Adam Hilger.

BELL JD & RICHARDS RE (1969) Nuclear spin relaxation studies on urea+hydrocarbon clathrates, *Trans. Faraday Soc.*, **65**, 2529-2536.

BLANK H & MAIER B, Eds. (1988) The Yellow Book: Guide to Neutron Research Facilities at the ILL, Institut Laue-Langevin (Grenoble), pp 52-53.

BOYSEN H, FREY F & BLANK H (1988) IQNS study of hexadecane motions in urea inclusion compounds, *Mater. Sci. Forum*, **27/28**, 123-128.

CASAL HL, CAMERON DG & KELUSKY EC (1984a) A ^{2}H NMR study of molecular motions of nonadecane-d_{40} in a urea inclusion adduct, *J. Chem. Phys.*, **80**, 1407-1410.

CASAL HL, CAMERON DG, KELUSKY EC & TULLOCH AP (1984b) A spectroscopic study of the structure and dynamics of the urea inclusion adduct of stearic acid, *J. Chem. Phys.*, **81**, 4322-4327.

CARLILE CJ (1988a) Quasielastic neutron scattering. In: NEWPORT RJ, RAINFORD BD & CYWINSKI R, Eds., Neutron Scattering at a Pulsed Source, Adam Hilger, pp 305-323.

CARLILE CJ (1988b) Lectures on neutron scattering techniques: 1. The production of neutrons, Report No. RAL-88-070, Rutherford Appleton Laboratory (Didcot).

CHATANI Y, ANRAKU H & TAKI Y (1978) Phase transition and structure change of urea adducts with *n*-paraffins and paraffin-type compounds, *Mol. Cryst. Liq. Cryst.*, **48**, 219-231.

CHO Y, KOBAYASHI M, TADOKORO H (1986a) Raman band profiles and mobility of polymethylene chains, *J. Chem. Phys.*, **84**, 4636-4642.

CHO Y, KOBAYASHI M, TADOKORO H (1986b) Theory of reorientational motional broadening of vibrational spectral bands in the solid state, *J. Chem. Phys.*, **84**, 4643-4650.

CONNOR TM & BLEARS DJ (1969) Laboratory and rotating frame proton magnetic relaxation measurements of urea-d_4-fatty acid adducts, *Mol. Phys.*, **17**, 435-438.

DIANOUX AJ & VOLINO F (1977) Random motion of a uniaxial rotator in an N-fold cosine potential: correlation functions and neutron incoherent scattering law, *Mol. Phys.*, **34**, 1263-1277.

FUKAO K, MIYAJI H & ASAI K (1986) Anharmonic vibration of *n*-paraffin molecules in urea adducts, *J. Chem. Phys.*, **84**, 6360-6368.

GILSON DFR & MCDOWELL CA (1959) Molecular motion of enclathrated compounds as studied by nuclear magnetic resonance, *Nature*, **183**, 1183-1184.

GILSON DFR & MCDOWELL CA (1961) Nuclear magnetic resonance studies of urea and thiourea adducts, *Mol. Phys.*, **4**, 125-134.

GREENFIELD MS, VOLD RL & VOLD RR (1985) Deuterium relaxation and vibrationally averaged quadrupole coupling in an alkane/urea clathrate, *J. Chem. Phys.*, **83**, 1440-1443.

GREENFIELD MS, VOLD RL & VOLD RR (1989) Deuterium spin relaxation and guest motion in the *n*-nonadecane/urea clathrate, *Mol. Phys.*, **66**, 269-298.

GUILLAUME F (1988) Etude de la dynamique de chaines hydrocarbonées (alkylene-diammonium, alkylammonium et *n*-alcane) en phases solides desordonées par diffusion incohérente inelastique des neutrons, Thèse, Université de Bordeaux 1.

GUILLAUME F, SOURISSEAU C & DIANOUX AJ (1990) Inelastic incoherent neutron scattering study of molecular motions of *n*-nonadecane in urea clathrate, *J. Chem. Phys.*, **93**, 3536-3541.

GUILLAUME F, SOURISSEAU C & DIANOUX AJ (1991) Rotational and translational motions of *n*-nonadecane in the urea inclusion compound as evidenced by incoherent quasielastic neutron scattering, *J. Chim. Phys. (Paris)*, **88**, 1721-1739.

GUILLAUME F, HARRIS KDM & DIANOUX AJ (1992) Molecular motions in urea inclusion compounds, ILL Annual Report 1991, Institut Laue-Langevin (Grenoble), pp 74-77.

GUILLAUME F, SMART SP, HARRIS KDM & DIANOUX AJ (submitted for publication) Neutron scattering investigations of guest molecular dynamics in α,ω-dibromo-alkane/urea inclusion compounds.

GUNN JMF (1988) Mainly diffraction; Incoherent inelastic scattering; Connection with the Schrödinger equation. In: NEWPORT RJ, RAINFORD BD & CYWINSKI R, Eds., Neutron Scattering at a Pulsed Source, Adam Hilger, pp 5-35, 36-55 & 56-67 resp.

HALL PL & ROSS DK (1981) Incoherent neutron scattering functions for random jump diffusion in bounded and infinite media, *Mol. Phys.*, **42**, 673-682.

HARRIS KDM, GUILLAUME F, DIANOUX AJ & ADAMS M (1992a) Incoherent quasi-elastic neutron scattering studies of host and guest molecular dynamics in urea inclusion compounds, ISIS Experimental Report No. RB/3412, Rutherford Appleton Laboratory (Didcot).

HARRIS KDM, GUILLAUME F, SMART SP, SOURISSEAU C & DIANOUX AJ (1992b) Neutron scattering investigation of host molecular motion in the hexadecane/urea inclusion compound, *J. Chem. Res. (S)*, 276-277.

HEATON NJ, VOLD RL & VOLD RR (1989) Deuterium quadrupole echo study of urea motion in urea/*n*-alkane inclusion compounds, *J. Am. Chem. Soc.*, **111**, 3211-3217.

LEE K-J, MATTICE WL & SNYDER RG (1992) Molecular dynamics of paraffins in the *n*-alkane/urea clathrate, *J. Chem. Phys.*, **96**, 9138-9143.

LEADBETTER AJ & LECHNER RE (1979) Neutron scattering studies. In: SHERWOOD JN, Ed., The Plastically Crystalline State, John Wiley & Sons, pp 285-320.

LINDLEY EJ & MAYERS J (1988) Experimental method and corrections to data. In: NEWPORT RJ, RAINFORD BD & CYWINSKI R, Eds., Neutron Scattering at a Pulsed Source, Adam Hilger, pp 155-173.

MEAKINS RJ (1955) The dielectric properties of urea occlusion compounds, *Trans. Faraday Soc.*, **51**, 953-961.

MEIROVITCH E & BELSKY I (1984) Hydrogen-2 nuclear magnetic resonance observations on conformation and dynamics of alkyl chains trapped within solid urea inclusion compounds, *J. Phys. Chem.*, **88**, 6407-6411.

PEMBERTON RC & PARSONAGE NG (1965) Thermodynamic properties of urea+hydrocarbon adducts: Part 1. Heat capacities of the adducts of *n*-$C_{10}H_{22}$, *n*-$C_{12}H_{26}$, *n*-$C_{16}H_{34}$ and *n*-$C_{20}H_{42}$ from 12-300 K, *Trans. Faraday Soc.*, **61**, 2112-2121.

PYNN R (Summer 1990) Neutron scattering: a primer, *Los Alamos Science*, 1-31.

RIEUTORD F (1990) INX program for time-of-flight data reduction: a users' guide, ILL Internal Report No. 90-RI-17-T, Institut Laue-Langevin (Grenoble).

SMART SP, GUILLAUME F, HARRIS KDM, SOURISSEAU C & DIANOUX AJ (1992) Dynamic properties of α,ω-dibromoalkane guest molecules constrained within urea inclusion compounds: a neutron scattering study, *Physica B*, **180/181**, 687-690.

SPRINGER T (1972) Quasielastic neutron scattering for the investigation of diffusive motions in solids and liquids, *Springer Tracts in Modern Physics*, **64**.

VAN HOVE L (1954) Correlations in space and time and Born approximation scattering in systems of interacting particles, *Phys. Rev.*, **95**, 249-262.

VON DREELE RB (Summer 1990) X-ray and neutron crystallography: a powerful combination, *Los Alamos Science*, 133-157.

WILLIS BTM, ALBINATI A, BOOTHROYD AT, CARLILE CJ, CHEETHAM AK, FORSYTH JB, LANDER GH, MCGREEVY RL (1991) Lectures given at the Oxford Summer School on Neutron Scattering.

WOOD KA, SNYDER RG & STRAUSS HL (1989) Analysis of the vibrational bandwidths of alkane-urea clathrates, *J. Chem. Phys.*, **91**, 5255-5267.

CHAPTER 5
DEUTERIUM NMR STUDIES

5.1 THE TECHNIQUE

5.1.1 INTRODUCTION

The phenomenon of nuclear magnetic resonance (NMR) was discovered in 1946 in the United States of America, by Bloch of Stanford University and simultaneously by Purcell of Harvard University. High resolution NMR spectroscopy has since become an invaluable technique which has many wide-ranging applications in physical, biological and medical science. The growth of this technique has benefited enormously from advances in both instrumentation and NMR theory, and notably from the development, pioneered by Ernst & Anderson [1966], of pulsed Fourier transform NMR.

NMR of the solid state is often the method of choice for probing molecular motions; it is also used to study structural properties in cases where single crystal x-ray diffraction is impractical or gives inconclusive results. The technique used here was solid state ^{2}H NMR for study of molecular dynamics. Compared with other spectroscopies such as Raman and infrared, the characteristic time-scale of ^{2}H NMR is relatively long: time-scales observable by ^{2}H NMR are in the range 10^{-3}-10^{-8} seconds.

This section outlines the general theory of NMR spectroscopy: it covers basic principles of NMR (§5.1.2) and NMR of the solid state (§5.1.3), and then focuses on solid state ^{2}H NMR (§5.1.4). Selected references covering general NMR theory are the following: Abragam [1961], Akitt [1983], Fukushima & Roeder [1981], Freeman [1988], Harris [1983], Jelinski [1984], Kemp [1986] and Riddell [1991]. Discussion of solid state NMR, in particular, may be found additionally in Fyfe [1983], and ^{2}H NMR of the solid state is also reviewed by Jelinski [1986].

5.1.2 BASIC THEORY OF NMR

5.1.2.1 Larmor Precession

When a nucleus with a non-zero spin I is subjected to an external magnetic field, the (2I+1) nuclear spin energy levels lose their degeneracy and a population difference is induced between these energy levels, in accordance with the Boltzmann distribution. This phenomenon, termed the Zeeman interaction, causes the nuclear dipoles to precess about the direction of the applied magnetic field with an angular frequency, ω, given by the Larmor equation:

$$\omega = \gamma H_0$$

where H_0 is the strength of the external magnetic field and γ is termed the magnetogyric ratio: this is constant for a given nucleus and is defined as follows (μ is the magnetic moment of the spinning nucleus and h is Planck's constant):

$$\gamma = \frac{2\pi\mu}{hI}$$

Since the angular frequency, ω, is equal to $2\pi\upsilon$, the Larmor equation may be rewritten:

$$\upsilon = \frac{\gamma H_0}{2\pi}$$

where υ is termed the Larmor frequency. For a given nucleus, each chemically distinct environment generally gives rise to a slightly different Larmor frequency.

5.1.2.2 Principles of the NMR Experiment

The theory of NMR makes use of the rotating frame of reference, in which the **z** axis is fixed in the direction of the applied magnetic field H_0, and the **x** and **y** axes rotate about **z** at the Larmor frequency. In this frame of reference, there exists at

equilibrium an excess net magnetisation, denoted M_0, along the **z** direction. An NMR experiment consists of disturbing this equilibrium by applying a pulsed radiofrequency (RF) wave, with magnetic field component H_1, in the x-y plane at the Larmor frequency, υ. Energy is absorbed from this RF field as it is in resonance with the precessing nuclear dipoles; this RF field thus rotates the nuclear magnetisation by an angle ϕ about the direction of H_1, where:

$$\phi = \omega_1 t_p$$
$$\omega_1 = \gamma H_1$$

and t_p is the duration of the applied RF pulse. The perturbed spin system then strives to return to equilibrium via relaxation of the nuclear dipoles. Two important categories of relaxation are longitudinal (spin-lattice) relaxation along the **z** axis and transverse (spin-spin) relaxation in the x-y plane. Eventually, equilibrium magnetisation is re-established and the cycle can be repeated.

During the return to equilibrium, the induced voltage in the x-y plane is recorded. This is termed the free induction decay (FID) and it comprises one decaying sinusoidal wave (representing the variation in magnetisation) for each nuclear environment. The envelope of the FID is exponential with respect to time. This time-domain signal is converted to the frequency domain using the Fourier transform (FT):

$$F(\omega) = \int_{-\infty}^{\infty} f(t) \exp(-i\omega t)\, dt$$

which may also be written:

$$F(\omega) = \int_{-\infty}^{\infty} f(t) (\cos \omega t - i \sin \omega t)\, dt$$

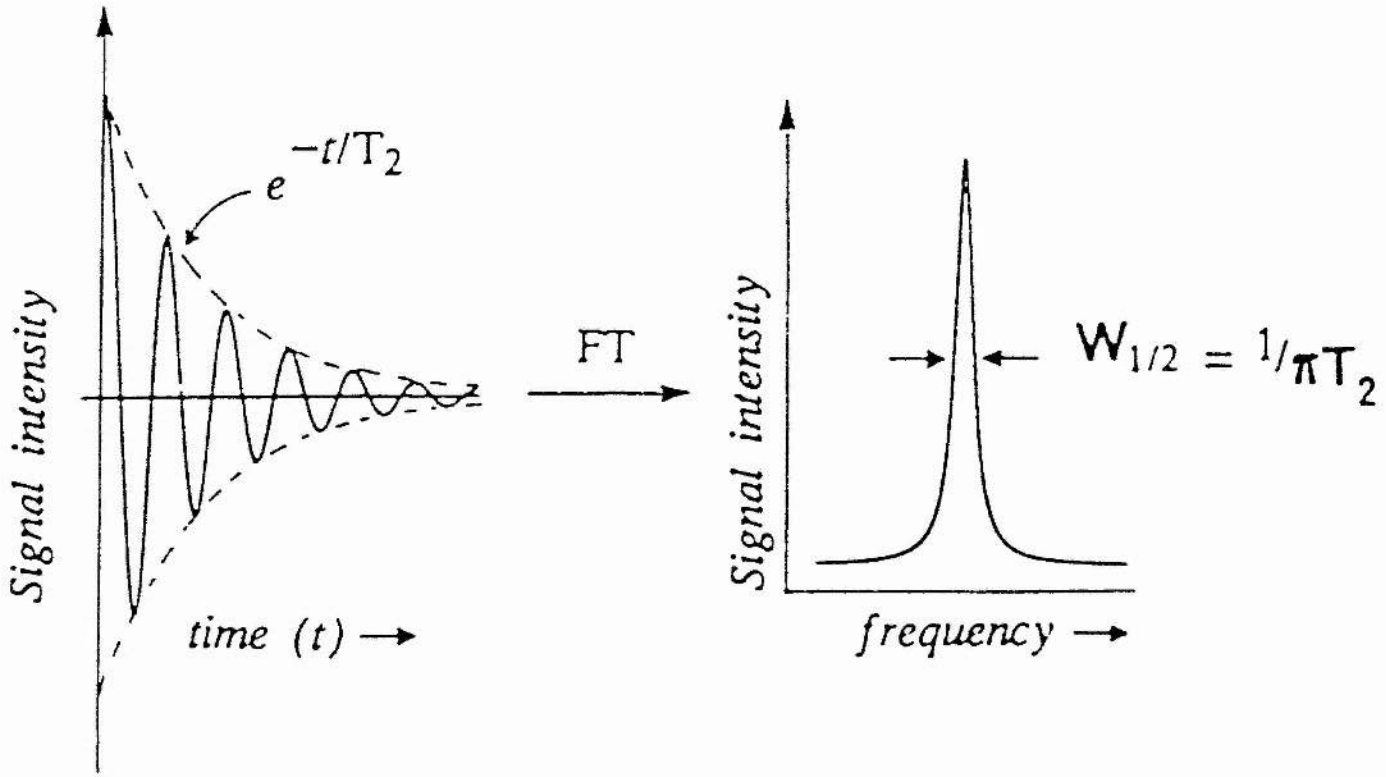

Fig. 5.1: The FID and frequency-domain spectrum for a single nuclear environment [from Field, 1989]

In this example the FID decays exponentially with time constant T_2 seconds, giving rise to a Lorentzian spectral lineshape whose width at half-height ($W_{1/2}$ in Hertz) is proportional to $1/T_2$.

Fig. 5.1 shows the idealised FID and frequency-domain spectrum for a single nuclear environment. The spectrum has a Lorentzian or Gaussian lineshape; the time constant for decay of the FID is related to the spectral linewidth (see below).

5.1.2.3 Nuclear Relaxation Processes

We now discuss in greater detail the two categories of nuclear relaxation.

(i) Spin-lattice relaxation involves the transfer of energy from the nuclear spins to their surroundings (loosely termed 'the lattice'). This process has a time constant T_1 which is known as the spin-lattice, or longitudinal, relaxation time. The rate of return of the longitudinal magnetisation M_z back to its equilibrium value M_0 is given by:

$$\frac{dM_z}{dt} = \frac{-(M_z-M_0)}{T_1}$$

(ii) Spin-spin relaxation leads to an increase in entropy of the spin system, but no energy change. The application of the RF pulse initially sets all nuclear spins to precess in phase at time zero, but this phase coherence is gradually lost due to small magnetic interactions between the nuclei which interfere with the exact nuclear precession frequencies. The transverse magnetisation thus spreads to a random distribution in the x-y plane. This loss of phase coherence occurs with decay constant T_2, known as the spin-spin, or transverse, relaxation time. The value of T_2 is the inverse of the natural linewidth (i.e. the width at half-height of the frequency-domain spectrum for a single nuclear environment).

In general $T_2 \leq T_1$; often the physical mechanisms which determine these time constants are the same and thus $T_2=T_1$. However, in solids $T_2 \ll T_1$ and for quadrupolar nuclei T_1 is short. Thus for solid state NMR of quadrupolar nuclei, such as ^2H, the natural linewidth (equal to $1/T_2$) is very large. In practice, the time constants derived

from NMR spectra, denoted T_1* and T_2*, often differ slightly from T_1 and T_2 due to instrumental shortcomings, such as inhomogeneity of the external magnetic field.

5.1.2.4 Mechanisms of Relaxation

The nuclear spins relax back to equilibrium via interactions with their local environment; the mechanisms available for this relaxation determine the values of T_1 and T_2. The most important of these processes for longitudinal (T_1) relaxation are outlined below; transverse (T_2) relaxation occurs via the same processes and may also make use of additional mechanisms, although these will not be discussed further.

(i) Dipole-dipole interactions: the nucleus experiences a fluctuating field due to the motion of dipoles from neighbouring magnetic nuclei (i.e. those with $I>0$). These interactions may be homonuclear or heteronuclear.
(ii) Electric quadrupolar interactions: these occur between a quadrupolar nucleus (i.e. one which has an electric quadrupole moment: $I\geq1$) and the electric field gradient tensor at the nucleus.
(iii) Indirect spin-spin coupling: this occurs indirectly between the nucleus and another magnetic nucleus, and is transmitted via the bonding electrons in the molecule. Again, these interactions may be homonuclear or heteronuclear.
(iv) Chemical shift anisotropy: electron shielding modifies the effective value of the applied magnetic field at the nucleus. The extent of this modification depends on both the orientation of the molecule with respect to the field direction and the magnitude of the field.

For spin-$^1/_2$ nuclei, dipole-dipole interactions are generally the dominant relaxation mechanism. For quadrupolar nuclei, the quadrupolar interaction is usually the most significant: this is discussed further in §5.1.4.

5.1.3 NMR OF SOLIDS

In solution, the solute molecules are isolated from each other, surrounded by solvent molecules, and are tumbling freely with respect to the magnetic field. All molecules are equivalent and interactions are averaged out. Dipole-dipole interactions and quadrupolar interactions are averaged to zero; spin-spin interactions and chemical shift anisotropy are averaged to isotropic values (denoted J and δ, respectively).

In contrast, in solids the molecules are trapped in a 'matrix' surrounded by similar molecules, and thus are held steady with respect to the magnetic field. Their nuclear spin energy levels depend on the orientation of the nucleus and its local environment with respect to the field: since averaging cannot occur, all nuclear interactions are anisotropic. Each of these anisotropic interactions may be described by a second rank tensor.

Due to this anisotropy, solid state spectra are characterised by very broad linewidths, often of the order of many kilohertz. Techniques used to narrow these linewidths include:

(i) magic angle spinning: the sample is rotated about an axis inclined at 54.7° to the applied magnetic field; this eliminates chemical shift anisotropy and dipole-dipole interactions by modifying the effective spatial coordinates
(ii) multiple pulse methods: these eliminate dipole-dipole and quadrupolar interactions by manipulation of the appropriate spin operators.

Other techniques used to improve spectral quality include high-power dipolar decoupling, cross-polarisation, non-quaternary suppression and suppression of spinning sidebands. However, since all of the above techniques are most commonly employed for spin-$^1/_2$ nuclei, such as ^{13}C, further discussion is outwith the scope of this chapter. We now discuss the theory of deuterium NMR of the solid state.

5.1.4 DEUTERIUM NMR IN THE SOLID STATE

5.1.4.1 Quadrupolar Nuclei

Deuterium is a quadrupolar nucleus with spin quantum number I=1. The solid state NMR spectra of quadrupolar nuclei are generally dominated by the nuclear quadrupolar interaction, such that the spin Hamiltonian may be approximated to:

$$\mathcal{H} = \mathcal{H}_{Zeeman} + \mathcal{H}_{Quadrupolar}$$

To a first approximation, dipolar interactions, chemical shift anisotropy and spin-spin couplings may be neglected. (Of these, dipolar interactions are the most significant and affect the spectra as a line-broadening.) For a single spin I, the quadrupolar interaction (denoted $\mathcal{H}_Q$ for brevity) is given by:

$$\mathcal{H}_Q = \frac{eQ}{2I(2I-1)\,h} \vec{I}.\,\vec{\vec{V}}.\,\vec{I}$$

where $Q =$ nuclear quadrupole moment

$\vec{I} =$ nuclear spin vector

$\vec{\vec{V}} =$ electric field gradient (EFG) tensor at the nucleus: this is a traceless tensor of the second rank, defined as:

$$\vec{\vec{V}} = \begin{bmatrix} V_{xx} & V_{xy} & V_{xz} \\ V_{yx} & V_{yy} & V_{yz} \\ V_{zx} & V_{zy} & V_{zz} \end{bmatrix}$$

An appropriate principal axis system (PAS) is chosen such that the off-diagonal elements of $\vec{\vec{V}}$ are zero and:

$$|V_{zz}| \geq |V_{yy}| \geq |V_{xx}|$$

The asymmetry parameter, η, and the quadrupolar coupling constant, A, are given by:

$$\eta = \left| \frac{V_{xx} - V_{yy}}{V_{zz}} \right|$$

$$A = \frac{e^2qQ}{h}$$

where $V_{zz} = eq$ (e being the charge on an electron) and $0 \leq \eta \leq 1$. Values of A and η are characteristic of a particular nucleus in a given chemical environment. For an EFG which is symmetric about the principal axis (i.e. the **z** axis of $\vec{\vec{V}}$ in the PAS), $V_{xx}=V_{yy}$, hence $\eta=0$, and the interaction is termed 'axially symmetric'. This is a good approximation for the ^2H nucleus when the principal axis is the C-D (or N-D in our case) bond vector, and the following discussion assumes that $\eta=0$ unless otherwise stated.

5.1.4.2 NMR Lineshape for Static Deuterons

In the high field approximation, which is applicable to deuterium, the Zeeman interaction is very much greater than the quadrupolar interaction. Thus, by first order perturbation theory, the energy shift ΔE_Q due to the quadrupolar interaction is given by equation ($\mathcal{A}$), where θ is the angle between the principal axis of the EFG tensor and the magnetic field vector:

$$\Delta E_Q = \frac{3}{8}\left[\frac{e^2qQ}{h}\right](3\cos^2\theta - 1) \qquad \text{- eqn } (\mathcal{A})$$

For a single ^2H nucleus, the two allowed spin energy level transitions are:

$$(m=-1) \leftrightarrow (m=0)$$

$$(m=0) \leftrightarrow (m=+1)$$

The solid state NMR spectrum is thus a doublet with peak separation, $\Delta\upsilon$, given by:

$$\Delta\upsilon = \frac{3}{4}\left[\frac{e^2qQ}{h}\right](3\cos^2\theta - 1) = 2\,\Delta E_Q \qquad \text{- eqn } (\mathcal{B})$$

Thus, each chemically distinct deuteron of a single crystal gives rise to two spectral lines (Fig. 5.2a), the frequencies of which depend on the orientation of the principal axis vector with respect to the external magnetic field. The linewidth is equal to $^1/_{T_2}$ and is termed the intrinsic, or natural, deuterium NMR linewidth. For a polycrystalline sample, equation ($\mathcal{A}$) is averaged over all possible crystal orientations, giving, for a single static deuteron, the spectrum shown in Fig. 5.2b. This is known as a Pake powder pattern. The separations of the central components ('horns') and of the outer components ('wings') are denoted $\Delta\upsilon_1$ and $\Delta\upsilon_2$ respectively (Fig. 5.2b). These correspond respectively to the perpendicular (θ=90°) and parallel (θ=0°) peak separations and thus are given by the expressions:

$$|\Delta\upsilon_1| = \frac{3}{4}\left[\frac{e^2qQ}{h}\right] = \frac{3}{4}A$$

$$|\Delta\upsilon_2| = \frac{3}{2}\left[\frac{e^2qQ}{h}\right] = \frac{3}{2}A$$

Fig. 5.2: Idealised ^2H NMR spectra for a static deuteron

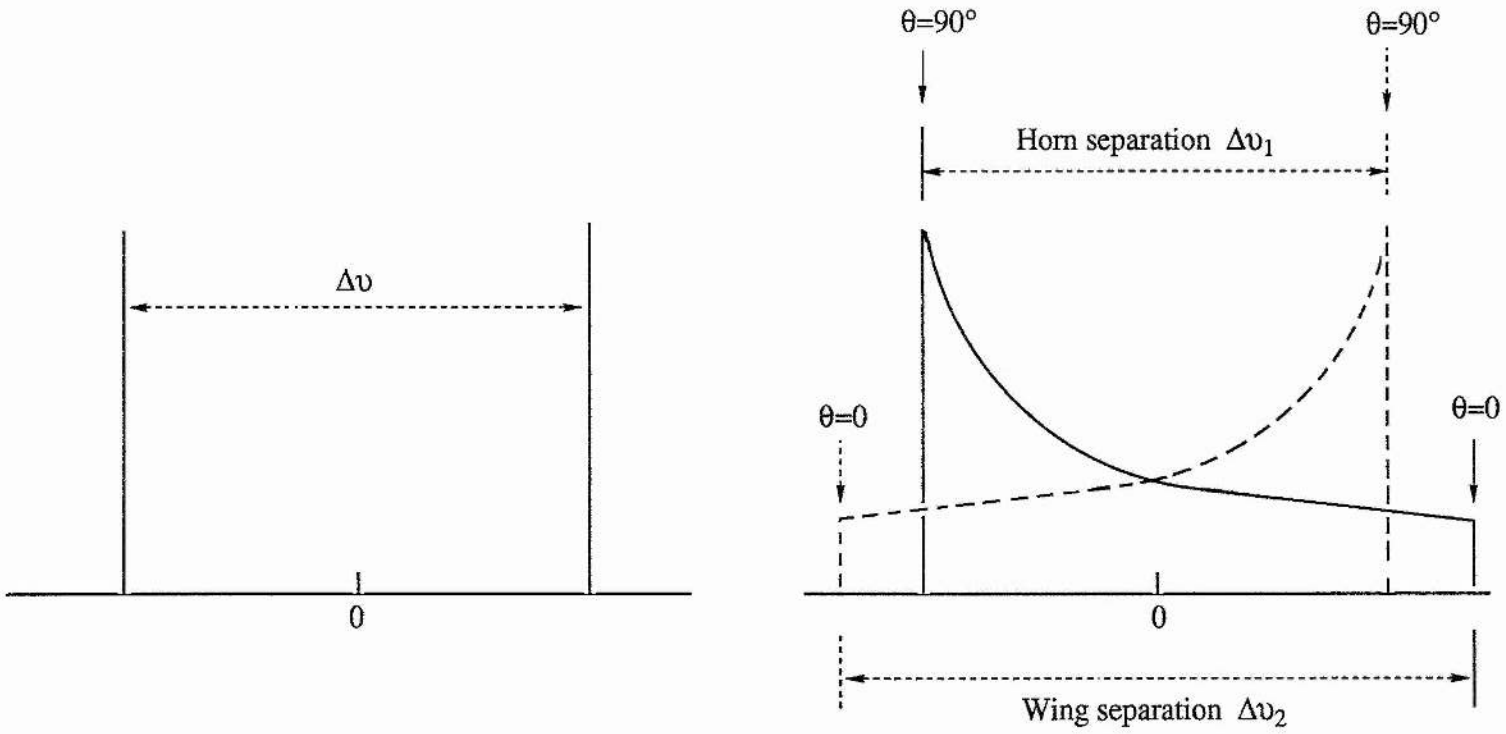

(a) For a single crystal

(b) For a polycrystalline sample

5.1.4.3 Mobile Deuterons

Any significant deviation from the Pake powder pattern indicates the presence of molecular motions. During a reorientational motion, such as molecular jumps, the EFG tensor for each deuteron samples a range of possible sites. The resultant powder lineshapes are thus characteristic of the exchange rate, the number of jump sites and the orientations of the EFG tensors for each site relative to the axis of rotation. Rigid deuterons have a relatively long longitudinal relaxation time, T_1, whereas more mobile deuterons have a shorter T_1: this difference is reflected in the spectral lineshapes.

A correlation time τ_c for the jump motion may be defined: this represents the mean residence time at each site (where the actual jump is assumed to be instantaneous). The exchange rate of a jump process is denoted κ, where $\kappa = 1/\tau_c$. Three motional regimes may be described in terms of the dimensionless constant $4\kappa/3A$:

slow motion:	$4\kappa/3A \ll 1$
intermediate motion:	$4\kappa/3A \approx 1$
rapid motion:	$4\kappa/3A \gg 1$

A* and η* denote, respectively, the effective (i.e. measured) values of the quadrupole coupling constant and the asymmetry parameter. Unlike A and η, the values of A* and η* are affected by the rate of motion. In the slow and rapid motion regimes, the spectral lineshapes are qualitatively similar to that for static deuterons. However, in the rapid regime, A*<A and η* may differ from zero. Thus, the measured values, $\Delta\upsilon_1$* and $\Delta\upsilon_2$*, respectively, of the separations of the central horns (θ=90°) and the outer wings (θ=0) are given by:

$$|\Delta\upsilon_1^*| = \frac{3}{4} A^* (1-\eta^*)$$

$$|\Delta\upsilon_2^*| = \frac{3}{2} A^*$$

In the intermediate motional regime, the lineshape is often broad and featureless [e.g. Meier *et al*, 1987].

5.1.4.4 Quadrupolar Spin-Echo Technique

Deuterium NMR spectra cover a very wide frequency range, typically several hundreds of kilohertz. The high-power pulses required to excite the full frequency range (and the additional effect of dipolar line broadening) lead to distorted spectra, especially in the region of the outer wings. Therefore, the quadrupolar spin-echo (QSE) technique is used in order to obtain undistorted spectra over wide frequency ranges. This technique was developed by Davis *et al* [1976] and comprises three stages, which are illustrated schematically in Fig. 5.3:

(i) application of a $\pi/2$ pulse

(ii) time delay τ

(iii) application of a second $\pi/2$ pulse, phase-shifted by $\pi/2$ radians (with respect to the first pulse)

The phase-shifted pulse refocuses the spin vectors at time 2τ to produce an echo of the original FID, this echo being well-removed in time from the first pulse. Fourier transformation begins at the echo maximum. This technique avoids loss of spectral data, especially at the beginning of the FID, which may occur as a result of receiver deadtime and pulse breakthrough.

Fig. 5.3: The quadrupole spin-echo technique

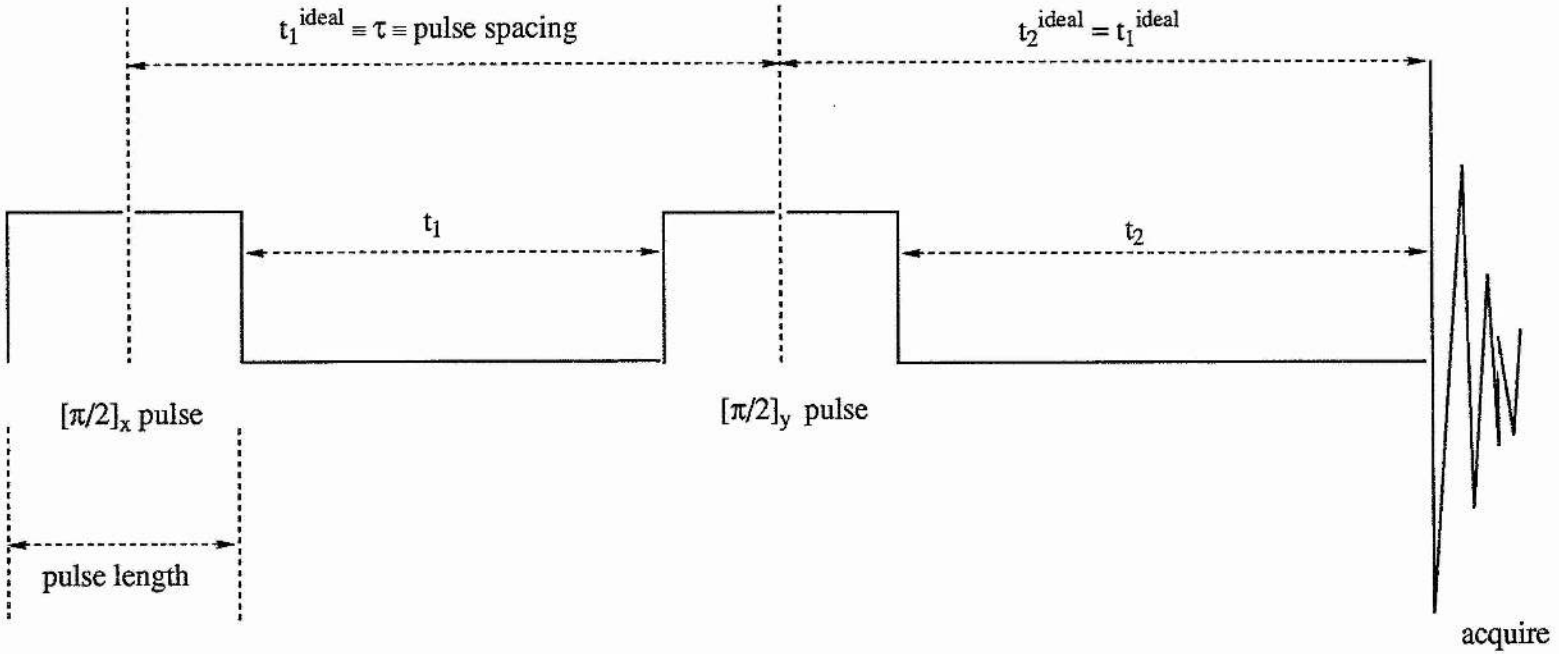

5.2. ^{2}H NMR INVESTIGATION OF UREA HOST MOTION

5.2.1 INTRODUCTION

Although many studies have been carried out on the motion of the guest molecules inside urea inclusion compounds, by both NMR and other techniques, the majority of these studies have assumed that the urea host remains an essentially rigid structure. It is also generally assumed that this host structure does not affect the motion of the guest molecules other than by imposing geometric restrictions. An exception to these assumptions is the early ^{1}H NMR work on various urea inclusion compounds of Bell & Richards [1969], who suggest that the motion of the urea molecules may affect the spin-lattice relaxation mechanisms of the guest molecules.

Although ^{2}H NMR studies of guest motions in urea inclusion compounds are discussed briefly in §5.3, the principal NMR investigations carried out here involve study of urea motion.

5.2.2 BACKGROUND

Heaton *et al* [1989a&b] have studied *n*-nonadecane/urea-d_4 in both its poly-crystalline [1989a] and single crystal [1989b] forms by ^{2}H NMR using the quadrupole spin-echo technique. They proposed that the urea molecules undergo 180° flips about their C=O axis, as illustrated in Fig. 5.4. There was no evidence for rotation of the NH_2 groups about the C-N bonds, although fast librational motion is not ruled out.

The difference in motional time-scales indicates that the host and guest motions in urea inclusion compounds are independent, these time-scales being of the order of 10^{-12} s for guest motions (see Chapter 4) and 10^{-6} s for urea flips. Nevertheless, the existence of such urea motion is rather surprising in view of the tight fit of the guest molecules within the urea channels (the channel diameter being *ca.* 5.1-5.9 Å). It suggests that the presence of the guest molecules may interfere in some way with the urea jump motion.

Fig. 5.4: 180° flip of the urea molecule about its C=O axis

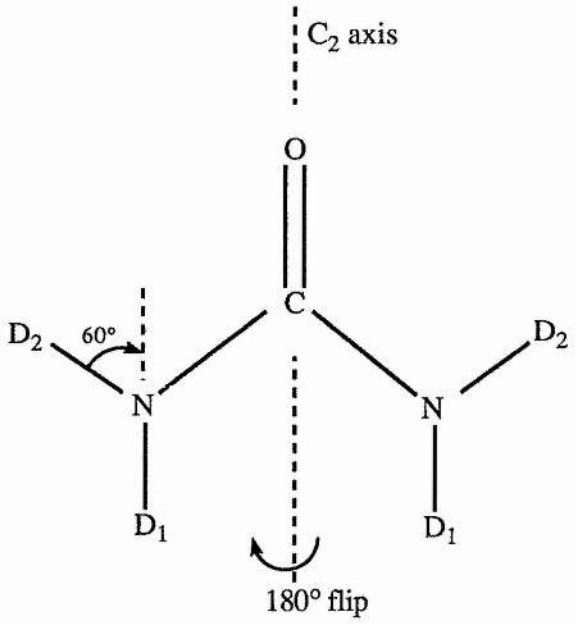

Heaton *et al* [1989a&b] found that the rate of this 180° flipping motion was dependent on temperature, showing Arrhenius behaviour with an activation energy of 23 (±2) $kJmol^{-1}$. At 303 K, the rate was $2x10^6$ s^{-1}. Further, it was shown that the rate of motion was also dependent on the pulse spacing, if this was greater than 40 μs. Values of A and η were evaluated as follows:

Sample: *n*-nonadecane/urea-d_4	A / kHz	η
Polycrystalline [Heaton *et al*, 1989a]	208 (±3)	0.155 (±0.005)
Single crystal [Heaton *et al*, 1989b]	208 (±1)	0.150 (±0.005)

In comparison, NMR studies on pure crystalline urea [Emsley & Smith, 1961; Chiba, 1965; Zussman, 1973; also Mantsch *et al*, 1977] have shown evidence for 180° rotation about the C=O axis above room temperature. It has been proposed that simultaneous rotation about the C-N bond may also occur [Das, 1957 & 1961; Emsley & Smith, 1961], especially at temperatures above 383 K [Chiba, 1965]. ^2H NMR

experiments carried out by Chiba [1965] and Heaton *et al* [1989a] have yielded the following values of A and η:

Sample: urea-d_4		A / kHz	η	temp./K
Polycrystalline	[Heaton *et al*, 1989a]	212 (±2)	0.145 (±0.005)	303
Single crystal	[Chiba, 1965]: D_1:	210.7 (±1.0)	0.146 (±0.010)	'room'
	D_2:	210.8 (±1.0)	0.139 (±0.010)	

Activation energies, E_a, for rotation about the C=O and C-N bonds in pure crystalline urea have also been determined. For the rotation about the C=O axis:

Reference	E_a/kJmol^{-1}	error / kJmol^{-1}	sample	technique
Emsley & Smith [1961]	38	'large'	urea-h_4	^{1}H NMR
Chiba [1965]	46	±8	urea-d_4	^{2}H NMR
Zussman [1973]	49	±8	urea-h_4	^{14}N NMR

and for the rotation about the C-N axis:

Reference	E_a/kJmol^{-1}	error / kJmol^{-1}	sample	technique
Das [1961]	51	not stated	urea-h_4	^{1}H NMR
Chiba [1965]	63	±13	urea-d_4	^{2}H NMR

These values compare with E_a=23 kJmol^{-1} [Heaton *et al*, 1989a] for rotation about C=O in the *n*-nonadecane/urea-d_4 inclusion compound. Thus, it appears that the activation barrier to rotation about the C=O axis is lower in the inclusion compound than in pure crystalline urea. This is rather surprising in view of the constraining nature of both the channel structure itself and the guest molecules in the channels. Rotation about C-N, which has the higher activation energy in pure urea, appears to be precluded completely in the inclusion compound (or, at least, is not apparent on the ^{2}H NMR time-scale).

5.2.3 OUTLINE AND AIMS OF OUR WORK

The α,ω-dibromoalkane/urea-d_4 family of inclusion compounds with n=7-10 was studied by quadrupole spin-echo ^2H NMR as a function of temperature and guest molecular length. Our objectives were to assess the occurrence of urea motion and to determine the mechanism of this motion. We also looked for change in deuteron mobility at the phase transition. We then compare our results with those of Heaton *et al* [1989a&b] in order to assess the effect on the urea motion of the relatively bulky Br substituents on the guest molecules.

In general, polycrystalline samples were used; however, room temperature spectra were also recorded of 1,10-dibromodecane/urea-d_4 single crystals oriented parallel and perpendicular to H_0. (It was impractical to record such spectra below room temperature due to experimental limitations.)

5.2.4 EXPERIMENTAL DETAILS

5.2.4.1 Materials

The polycrystalline samples used were α,ω-dibromoalkane/urea-d_4 inclusion compounds, $Br(CH_2)_nBr/D_2N(CO)ND_2$, where n=7-10. The single crystal spectra were obtained using $Br(CH_2)_{10}Br/D_2N(CO)ND_2$. For brevity, these compounds are denoted C7, C8, C9 and C10 as appropriate. All compounds were prepared as detailed in Appendix A.

(I) Polycrystalline samples

The compounds were ground thoroughly and packed into glass NMR tubes of outer diameter 5 mm and length *ca.* 45 mm. Teflon plugs were inserted at either end of each tube to constrain the powdered sample to the central section of the tube. A small Supa-seal cap covered by a winding of Teflon tape was used to seal the tube.

(II) Single crystal samples

(i) Channel axis oriented parallel to H_0: Ten single crystals, each of approximate dimensions 4x1x1 mm^3, were positioned, using inert vacuum grease, parallel to one another on a cut-away ledge of a glass rod of diameter 5 mm and length *ca.* 45 mm. The crystals (hexagonal needles) each had one of their flat faces in contact with the glass surface. This set-up is shown in Fig. 5.5a (which shows only three crystals as an example). This glass rod was aligned within the NMR probe in such a way that the channel axes of all the single crystals were oriented vertically (as assessed by eye) and their flat faces were approximately parallel to the magnetic field vector, H_0.

(ii) Channel axis oriented perpendicular to H_0: A single crystal, of approximate dimensions 20x1x1 mm^3, was mounted, using vacuum grease, inside the glass NMR tube described above (see Fig. 5.5b). The crystal (a hexagonal needle) was positioned with its channel axis parallel to the long axis of the tube (as assessed by eye) so that, when placed in the probe, it was oriented perpendicular to H_0. Insofar as was possible, we attempted to position the crystal in such a way that two of its flat faces (i.e. opposite faces of the crystal) were also perpendicular to H_0.

Fig. 5.5: Side-on view of experimental set-ups for recording ^2H NMR spectra of single crystals (not drawn to scale)

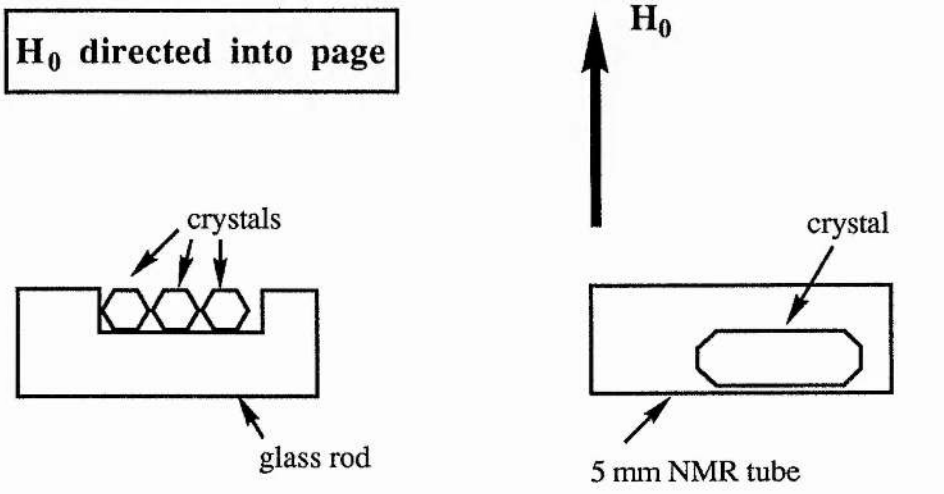

(a) Crystal bank parallel to H_0 (b) Crystal perpendicular to H_0

5.2.4.2 ^{2}H NMR Experiments

Spectra were recorded on a Bruker MSL-500 spectrometer, operating at 76.8 MHz in the high power mode. The field was shimmed when necessary using D_2O and the consistency of the $\pi/2$ pulse was checked regularly using a polycrystalline standard of fully deuterated poly(methyl methacrylate) at room temperature (293 K).

Ambient temperature was *ca.* 293 (±2) K. Below 293 K, the temperature was controlled to ±2 K using a Bruker BVT-1000 variable temperature unit with a nitrogen gas flow as the coolant. The temperature was monitored via a copper-constantan thermocouple inserted into the probe: this temperature was assumed to be the same as that of the sample.

The spectra were obtained using a standard QSE sequence (Fig. 5.3):

$$\left[\frac{\pi}{2}\right]_x - t_1 - \left[\frac{\pi}{2}\right]_y - t_2 - \text{acquire}$$

The length of each $\pi/2$ pulse was 2.4 μs, and values of t_1 and t_2 were: t_1=13.0 μs, t_2=10.0 μs, equivalent to a pulse spacing of 15.4 μs. A recycle delay of 60 s was used, chosen (after prior testing of many values) as being sufficiently long to allow full relaxation of all deuterons in the sample.

Spectra were recorded for all polycrystalline samples at 293 K. In addition, spectra were recorded for polycrystalline C7 in the temperature range 293-140 K at the following temperatures/K: 293, 240, 200, 160, 150 and 140. Smaller temperature increments were used in the 160-140 K range because the phase transition occurs in this temperature range (see Appendix B). Due to the limitations of the experimental set-up, it was possible to record spectra of the single crystal samples at room temperature only. A spectrum recorded at 293 K of undeuterated polycrystalline 1,10-dibromo-decane verified that any ^{2}H NMR signal due to natural abundance ^{2}H in the guest molecules in the α,ω-dibromoalkane/urea-d_4 inclusion compounds would be indistinguishable from the spectral noise. All samples were stationary.

In general, 180 acquisitions were required to give acceptable signal-to-noise. However, at very low temperatures (160-140 K) only 60 acquisitions were recorded: signal-to-noise was better and, moreover, experimental limitations precluded longer acquisition times at these temperatures. In cases of abnormally poor signal quality, more than 180 acquisitions were recorded where possible.

Before Fourier transformation, the FIDs were treated using zero-filling. Where necessary, left-shifting was also applied to ensure that the start of the FID was as close as possible to the echo maximum. However, no other 'correction techniques' were used and the spectra were not artificially symmetrised.

5.2.4.3 Lineshape Simulations

Spectral simulations were performed using a high field ^{2}H NMR program written by Dr M. Trecoske (as described by Meier *et al* [1987]) and modified by Drs P. Jonsen and K.D.M. Harris. This program simulates the ^{2}H NMR spectrum resulting from the application of a single pulse to deuterons undergoing exchange between specific sites. Before Fourier transformation, the program sums the FID data points across all crystal orientations to simulate polycrystalline spectra. Further details of the program and the input parameters are discussed in §5.2.5.1, part (II)(i).

Fig. 5.6: ^{2}H NMR spectra for the four samples at 293 K

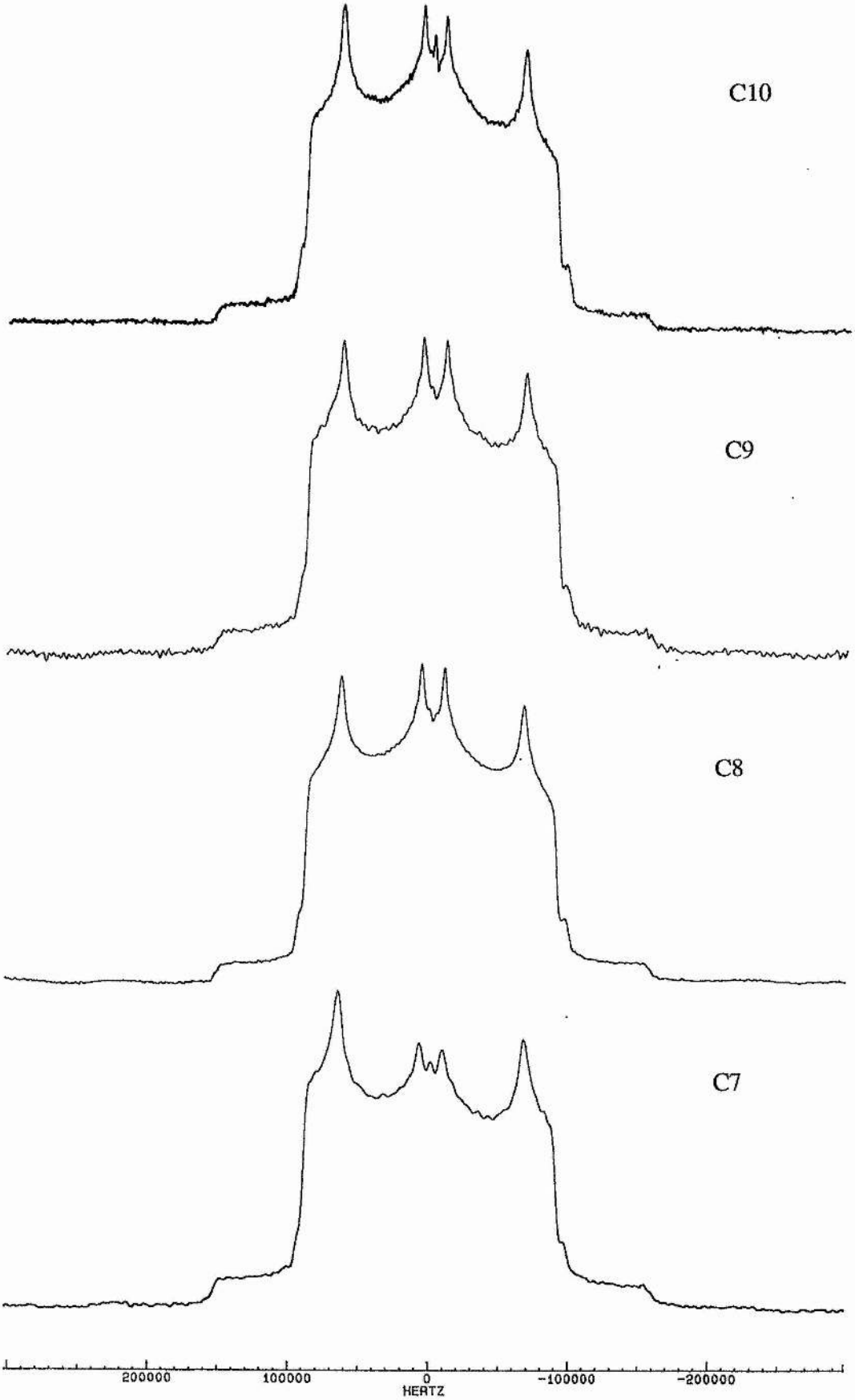

5.2.5 RESULTS AND DISCUSSION

5.2.5.1 Polycrystalline Samples

(I) Experimental spectra

(i) General comments

Spectra for all four samples at 293 K are shown in Fig. 5.6. The spectra are qualitatively identical for all samples, and we concentrate our dicussion on the case of C7. Fig. 5.7 shows the evolution of spectra for C7 over six temperatures: 293, 240, 200, 160, 150, 140 K (recorded from high to low temperature). Although, in theory, the spectra should be symmetric about zero frequency , in practice there is some discrepancy: this may be due to imperfections in the applied 90° pulses.

Above the static limit, spectral lineshapes are highly characteristic of the jump motion as they depend critically on jump rate and relative orientations of the exchange sites. The lineshapes shown in Fig. 5.7 are consistent with the existence, within a 180° jump model, of two distinct sets of urea deuterons, which we denote D_1 and D_2 (see Fig. 5.4). Although both sets of deuterons are necessarily undergoing the same 180° jump motion, the D_1 deuterons do not change their orientation significantly with respect to the applied magnetic field during the motion, because the N-D_1 vector is virtually parallel to the C=O vector (the axis of rotation). Thus, their contribution to the spectrum is almost indistinguishable from that of static deuterons. In contrast, the N-D_2 bond makes an angle of *ca.* 60° with the C=O vector, hence the orientation of the D_2 deuterons relative to the applied magnetic field changes appreciably during the motion and their mobility is reflected in the spectrum. Thus, in the fast motion regime, the D_1 deuterons give rise to the essentially static ('full-width') component of the spectrum, whereas the D_2 deuterons give rise to the features in the centre of the spectrum.

Fig. 5.7: ^{2}H NMR spectra for 1,7-dibromoheptane/urea-d_4

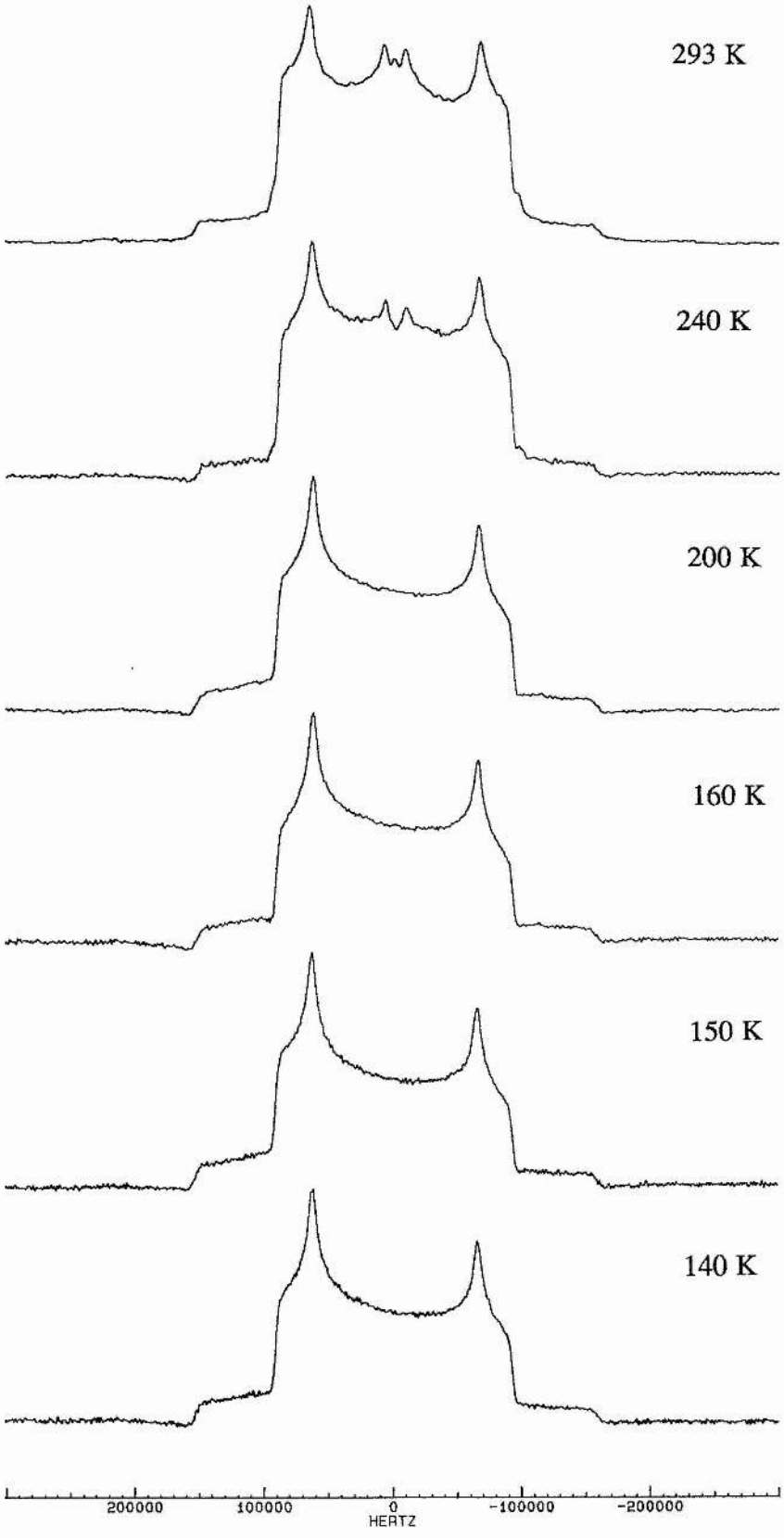

(ii) Discussion of phase transition

The spectrum at 140 K is assumed to represent that of the 'static' system. Fig. 5.7 shows that the spectra at 140 K, 150 K and 160 K are identical, within experimental error: there is no discernible change in lineshape with temperature, even though the phase transition is thought to occur within this temperature range (see Appendix B). There is thus no evidence for an intermediate motional regime. The reason for this is unclear (unless this regime occurs over a very narrow temperature range). It may be that the change in host structure does not, in itself, affect the motions of its constituent urea molecules (at least, not on a time-scale detectable by ^{2}H NMR). The intrinsic temperature-dependence of the rate of motion is not known: the rate of motion may indeed be changing with increasing temperature, but change in activation energy at the phase transition may be small. Furthermore, evidence for the intermediate regime may be difficult to discern, due to the presence of the spectrum of the D_1 deuterons. Alternatively, the possibility that the measured temperature does not correspond closely to that of the sample should not be discounted: this could mean that these three spectra all genuinely depict the low-temperature phase, and hence the slow motion regime. Even the spectrum recorded at 200 K is only just beginning to show evidence for a faster motion regime.

(iii) Evolution as function of temperature for C7

As the temperature increases to 240 K and 293 K (Fig. 5.7), 'inner horns' of splitting *ca.* 16 kHz, approximately symmetric about zero frequency, become evident in the centre of the spectrum. Such mid-spectral features reflect the mobility of the D_2 deuterons. A peak at zero frequency is also present at 293 K: this may be either an artefact of the spectrometer or isotropically mobile ^{2}H in the gas phase, arising from slight sublimation of the urea inclusion compound. At T≥240 K, a slight shoulder is visible at *ca.* -100 kHz: this occurs only on the negative frequency side of the spectra and is thus assumed to be an artefact. These spectra are (at least qualitatively) in good

agreement with those of Heaton *et al* [1989a] for *n*-nonadecane/ urea-d_4 at comparable temperatures.

In a given motional regime, changes in exchange rate (corresponding to changes in temperature) may be expected to affect the relative intensities of the different parts of the spectrum, but not their frequencies. Splitting frequencies and relative intensities for the C7 set of spectra are displayed in Table 5.1. There is no significant change in splitting frequency with temperature: the wings and outer horns arise predominantly from the D_1 deuterons (as their contribution to the spectrum is virtually equivalent to that of static deutrons, regardless of temperature), whereas the inner horns due to the 'mobile' D_2 deuterons are observed only at T>200 K (i.e. the faster motion regime). The central region of the spectrum and the inner horns increase in relative intensity with increasing temperature, reflecting the increased mobility of the D_2 deuterons.

Table 5.1: Splitting frequencies and relative intensities for C7 set of ^{2}H NMR spectra

TEMP. / K	SPLITTING FREQUENCY / kHz				RELATIVE INTENSITY	
	Wings	Full-width	O. Horns	I. Horns	Mid-point	Wings
140	~315	~182	127.1	-	0.54	0.10
150	~312	~182	128.3	-	0.54	0.11
160	~310	~182	127.6	-	0.57	0.09
200	~315	~182	128.2	-	0.56	0.10
240	~310	~180	129.1	15.8	0.68	0.07
293	~315	~180	132.4	16.3	0.67	0.09

Explanation of terms:

(i) Wings, full-width spectrum, outer horns, inner horns are defined on Fig. 5.8. (In the Table, 'outer horns' and 'inner horns' are abbreviated to 'O. Horns' and 'I. Horns', respectively).

(ii) Splitting frequency of wings and full-width spectrum were measured at half-height to ±2 kHz. Splitting frequency of outer horns and inner horns were measured at full-height to ±0.2 kHz.

(iii) Mid-point intensity is defined as the underlying intensity of the mid-point of the spectrum (i.e. discounting any zero-frequency peak or intensity due to the inner horns) relative to the average intensity of the outer horns. Wing intensity is defined as the average intensity of the wings at their mid-frequency point relative to the average intensity of the outer horns.

Fig. 5.8: Simulated ^{2}H NMR spectrum, defining the terms used in Table 5.1

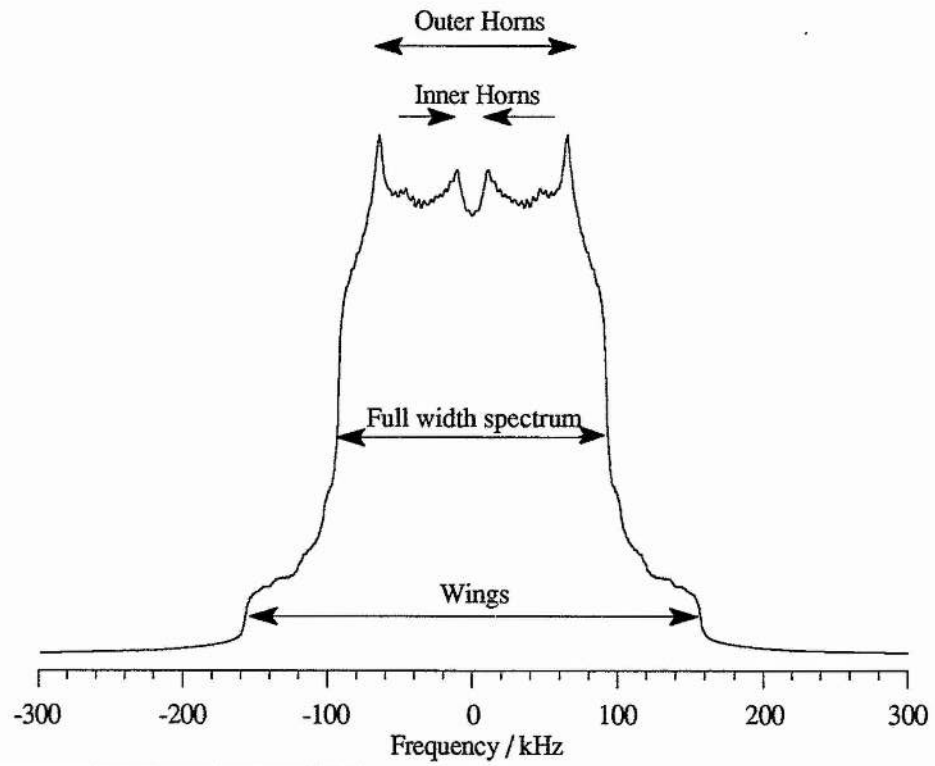

(iv) Evolution as function of length of guest molecule

As noted earlier, spectra for the four samples at 293 K are qualitatively similar. Listed in Table 5.2 are the splitting frequencies and relative intensities for the four spectra at 293 K; Table 5.3 shows the corresponding values of of A* and η*. The frequencies of the spectral features do not change significantly (within a few kHz) with change in length of the guest molecule. However, the spectra *do* differ in relative intensity of the inner horns compared to the outer horns: for C8, C9 and C10 the inner horns are approximately equivalent in intensity to the outer horns, whereas for C7 they have a significantly lower intensity than the outer horns. All four spectra have the unexplained shoulder at *ca.* -100 kHz, belived to be an artefact.

If the guest molecules *do* interfere significantly with the urea motion, we should expect guest molecular length to affect the rate of urea motion, and hence the spectral lineshapes. At shorter guest molecular length there is a higher proportion of bulky Br atoms per unit length of channel, so we should expect the motion of more of the urea molecules (those adjacent to the Br end-groups) to be hindered, and the ^{2}H NMR lineshape to reflect this decreased mobility. This appears not to be the case along the series C8, C9, C10; however, it is possible that for C7 the density of Br's along the channel is sufficient that this effect is noticeable, and is reflected in the relatively low intensity of the inner horns. This possibility is discussed in more detail in §5.2.5.1, part (II)(ii).

Table 5.2: Splitting frequencies and relative intensities for the four samples at 293 K

SAMPLE	SPLITTING FREQUENCY / kHz				RELATIVE INTENSITY	
	Wings	Full-width	O. Horns	I. Horns	Mid-point	Wings
C7	~315	~180	132.4	16.3	0.67	0.09
C8	~310	~180	130.3	16.4	0.74	0.07
C9	~310	~180	130.4	16.5	0.73	0.08
C10	~310	~180	130.0	15.8	0.72	0.06

Table 5.3: Values for A* and η^* at 293 K

SAMPLE	A* / kHz	η^*
C7	210	0.159
C8	207	0.159
C9	207	0.159
C10	207	0.161

(II) Simulations

(i) Description of simulation program

The simulation program makes use of a general form of equation ($\mathcal{B}$) (see §5.1.4.2) that gives the splitting frequency between the two lines observed for a single static deuteron under the high field approximation:

$$\Delta\upsilon = \frac{3}{4}\left[\frac{e^2qQ}{h}\right]\left[(3\cos^2\theta - 1) + (\eta \sin^2\theta \cos 2\phi)\right]$$

where θ and ϕ are the spherical Euler angles which describe the transformation of the deuteron vector from the PAS of the EFG tensor to the (fixed, but arbitrary) molecular axis system.

The simulation program requires the following input parameters:

1. The rate κ for the jump process. We assume that jumps are instantaneous; κ is defined as the inverse of the residence time in each site.
2. The number of sites available to the deuterons during the motion (i.e. four in total).
3. The relative orientation of the principal axis system for each deuteron site occupied during the motion. This gives a set of Euler angles for each site (see below).
4. The quadrupole coupling constant parameter, $^{3A}/_{4}$, for the static deuteron: this was set to 156 kHz (see below).

5. The asymmetry parameter, η, for the static deuteron: this was set to 0.183 (see below).
6. The natural linewidth, i.e. $^{1}/_{T_2}$. This was set to 1600 Hz (≡*ca.* 1% of $^{3A}/_{4}$).
7. The exchange matrix: this defines the sites between which the deuteron can and cannot jump.
8. The relative populations of the deuteron sites: these were all set to 1.
9. The polar angular increment, $\Delta\omega$, for the powder averaging: this was set to 1°.

180° flips of the urea molecules were modelled, with D_1 deuterons parallel to the jump axis (the C=O bond) and D_2 deuterons at 60° to the jump axis. Parameters 2, 3, 7 and 8 were invariant within this model; no other motions (such as rotation of the ND_2 groups) were considered.

The cartesian Euler angles ($\alpha\beta\gamma$) are those required to transform from each principal axis system ($X_PY_PZ_P$) to the fixed molecular axis system ($X_MY_MZ_M$) by rotating sequentially around the Z_P axis (giving $X'_PY'_PZ'_P$), then around the Y'_P axis (giving $X''_PY''_PZ''_P$) and finally around the Z''_P axis. For the urea molecule, two possibilities were considered:

(i) X_P in the plane of the urea molecule

(ii) X_P normal to the plane of the urea molecule

Case (i) was found to give simulations consistent with the experimental spectra. This corresponds to the axes systems shown in Fig. 5.9 and the Euler angles listed in Table 5.4. The Zp axes are assumed to make angles of 180° (for D_1 deuterons) and 60° (for D_2 deuterons) with the jump axis C=O. A positive turn is taken to be in the clockwise direction when viewed from the origin along the positive axis: this is equivalent to the Rose convention [Rose, 1957].

Fig. 5.9: The principal axis systems and the molecular reference frame

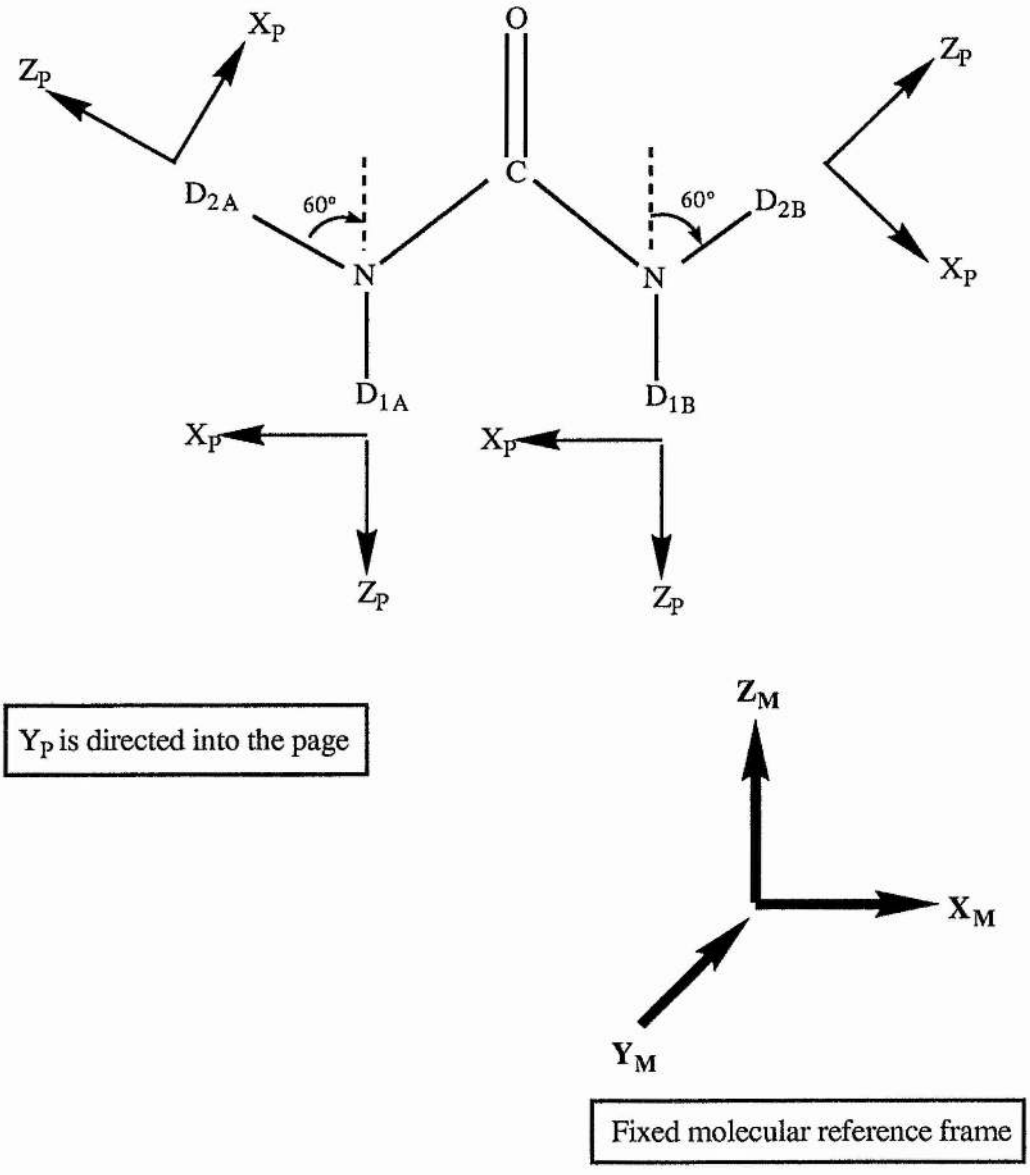

DEUTERON	EULER ANGLES		
	α	β	γ
D_{1A}	0_Z	$180°_{Y'}$	$0_{Z''}$
D_{1B}	0_Z	$180°_{Y'}$	$0_{Z''}$
D_{2A}	0_Z	$+60°_{Y'}$	$0_{Z''}$
D_{2B}	0_Z	$-60°_{Y'}$	$0_{Z''}$

Table 5.4: Euler angles for the four deuterons

Again, we concentrate our discussion on the C7 spectra. The experimental C7 spectrum at 140 K was assumed to represent the spectrum of a static system. As discussed earlier, the splitting frequencies of the full-width spectral components did not vary significantly with temperature in the 140-160 K range. Therefore, the measured values of A* and η* derived from the 140 K, 150 K and 160 K spectra were averaged: the resultant values were used in the simulation program as the static values, A and η (parameters 4 and 5). Thus A=208 kHz and η=0.183.** Both sets of deuterons were assumed to have the same A and η values.# The values for $^1/T_2$ and $\Delta\omega$ (parameters 6 and 9) were optimised by trial-and-error through visual comparison of simulated and experimental spectra at 140 K. The optimal values of those tested were $^1/T_2$=1600 Hz†† and $\Delta\omega$=1°. These parameters (4, 5, 6 and 9) were fixed at the above values for the complete set of simulations.

A change in temperature, T, can be modelled by an appropriate change in κ. The values of κ used are shown in Table 5.5: of the many κ values tested, these gave the best agreement between simulated and experimental spectra. We assume that, at T=140, 150 and 160 K, the system is in the static regime ($4\kappa/3A<\sim10^{-2}$), whereas

** This compares with the values used by Heaton *et al* [1989a] of A=208 kHz (±3 kHz) and η=0.155 (±0.005) for *n*-nonadecane/urea-d_4.

Although the D_1 and D_2 sets of deuterons may have intrinsically different A and η values, on the basis of the spectrum at 140 K, such differences must be small and may therefore be ignored.

†† The value for natural linewidth determined from the spectrum of a single crystal at 293 K (see §5.2.5.2, part (I)) was *ca.* 2 kHz.

T=200, 240 and 293 K correspond to a faster motional regime ($4\kappa/3A \geq \sim 10^{-2}$). The values of κ in this motional regime correspond (on the assumption of Arrhenius behaviour) to an activation energy, E_a, for the 180° flips of 36.2 (±0.5) $kJmol^{-1}$. This is in good agreement with E_a=38 $kJmol^{-1}$ [Emsley & Smith, 1961] for 'pure' urea-h_4 and compares with E_a=23 $kmol^{-1}$ for *n*-nonadecane/urea-d_4 [Heaton *et al*, 1989a].

T / K	κ / Hz	$4\kappa/3A$
140	$< 1.0 \times 10^3$	$< 6.4 \times 10^{-3}$
150	$< 1.0 \times 10^3$	$< 6.4 \times 10^{-3}$
160	$< 1.0 \times 10^3$	$< 6.4 \times 10^{-3}$
200	5.0×10^3	3.2×10^{-2}
240	2.0×10^5	1.3×10^0
293	5.0×10^6	3.2×10^1

Table 5.5: Values for exchange rate, κ, at the temperatures studied

(ii) Simulated spectra

The simulated spectra are shown as a function of temperature in Fig. 5.10. These spectra should be compared with the experimental spectra shown earlier (Fig. 5.7). The simulated spectra for 140 K, 150 K and 160 K were indistinguishable from each other and identical to that obtained using κ=0 (i.e. the static spectrum). The wings, outer horns and emergence of the inner horns are well-modelled by the simulations with regard to general lineshape and frequencies. This suggests that the parameters used were realistic. However, at T≥200 K, discrepancies occur between simulation and experimental spectra concerning the intensities, relative to the other spectral features, of both the underlying central region of the spectrum (*ca.* -50 Hz to

+50 Hz) and the inner horns (where present). The simulated relative intensity of these central features is consistently higher than in the experimental spectra. Although many other κ values were tested, no better agreement could be found. The relative intensity of the wings is also higher than in the experimental spectra, especially for $T \leq 200$ K. The simulated spectra also show a 'dip' in the lineshape of the wings which is not discernible in the experimental spectra.

One reason for the inconsistency in intensity simulation may be the following. We have assumed that, in the motional regime, the number of static deuterons is zero. However, if there *were* a proportion of deuterons that remained static, even at high temperatures (e.g. those corresponding to the ureas next to the bulky bromine atoms), they would contribute to the 'full-width' component of the spectrum. This would lead to an increase in the intensity of the outer horns and a corresponding decrease in the intensity of the central spectral features. This appears to be the case for C7, for which the relative intensity of the inner horns in the experimental spectrum is measurably less than that in the experimental spectra of the other compounds. Comparison of simulated with experimental spectra implies that this may also be the case for the other compounds, but that the effect is less marked.

Fig. 5.10: Simulated ^2H NMR spectra for 1,7-dibromoheptane/urea-d_4

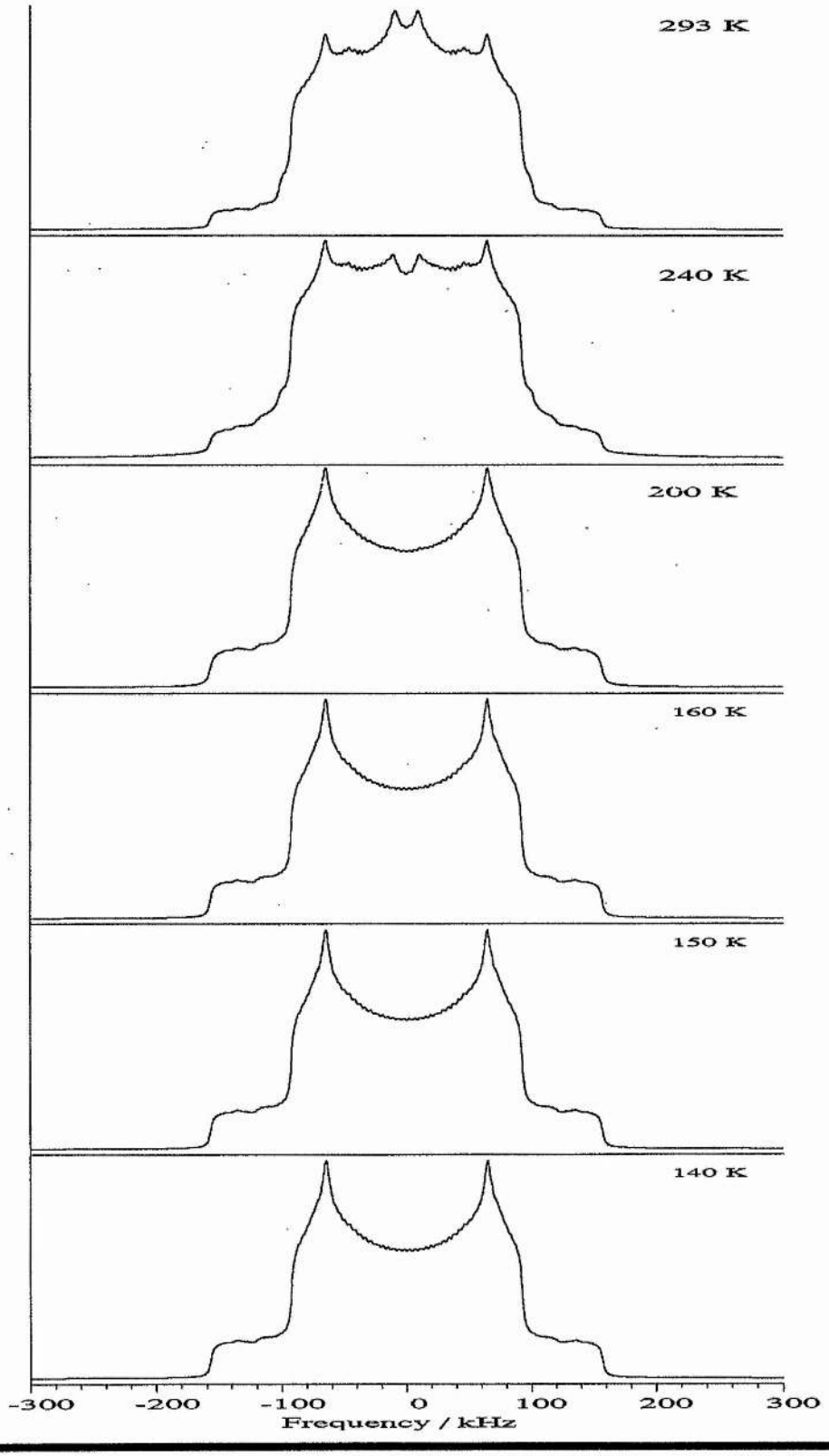

Fig. 5.11: ^2H NMR spectra for 1,10-dibromodecane/urea-d_4

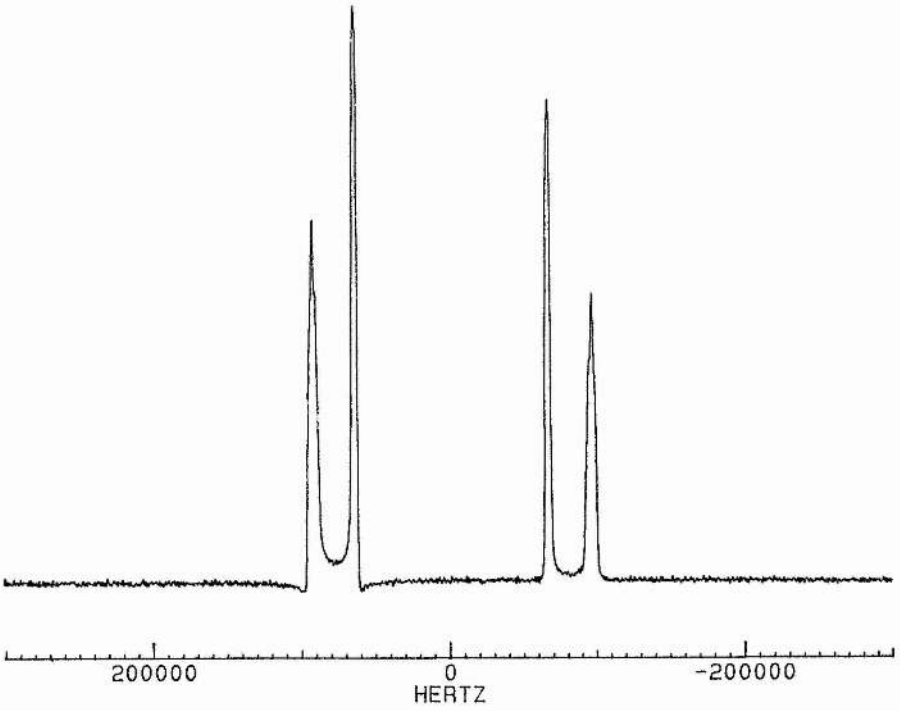

(a) Bank of single crystals oriented parallel to H_0

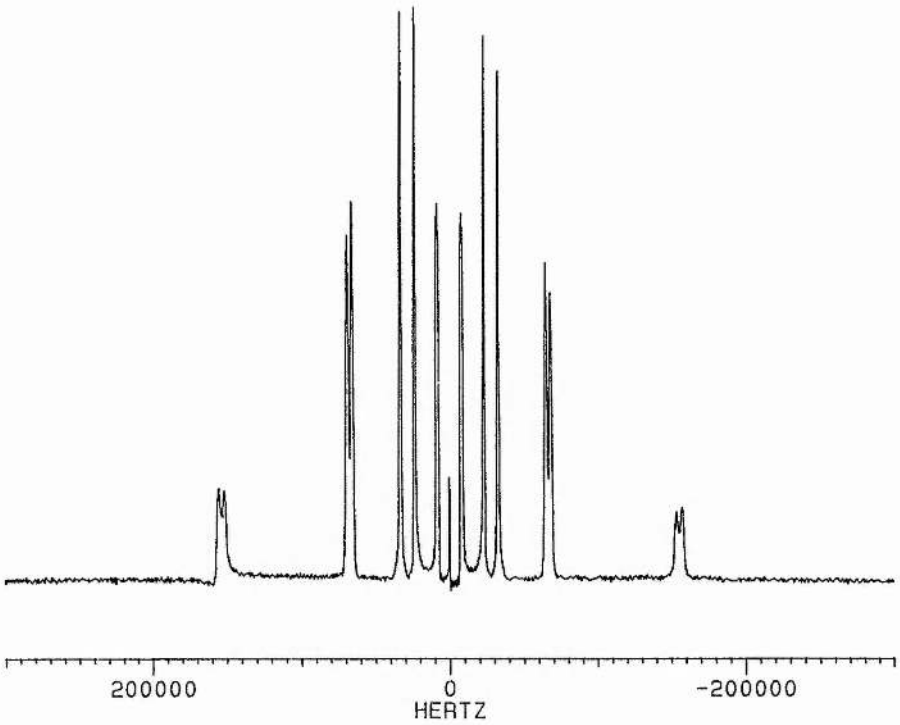

(b) Single crystal oriented perpendicular to H_0

5.2.5.2 Single Crystal Study of 1,10-Dibromodecane/Urea-d_4

(I) Experimental spectra

(i) Parallel to H_0

The room-temperature spectrum of the crystal bank oriented parallel to H_0 consists of two doublets (at frequencies symmetric about zero) of separation 131 kHz and 189 kHz, respectively (see Fig. 5.11a). The linewidth of each peak is 4.1 kHz, as measured at half-height. This value (at 293 K) compares with the value of 1.6 kHz used in the simulation program for C7, estimated to be the 'static' value (140 K). This suggests either that the single crystal spectrum actually consists of a number of underlying doublets, at slightly different frequencies, making up these two apparent doublets, or that the natural linewidth, $^1/_{T_2}$, is dependent on temperature.

(ii) Perpendicular to H_0

The room-temperature spectrum of the single crystal oriented perpendicular to H_0 is more complex (see Fig. 5.11b): it comprises five narrow doublets centred around zero frequency in the 100 kHz to -100 kHz range, and two overlapping doublets, of lower intensity, at *ca.* ±150 kHz. The linewidth, which is *ca.* 2 kHz at half-height, is less than that of the doublets in the spectrum of the crystal parallel to H_0, and presumably reflects the orientation-dependence of $^1/_{T_2}$.

(II) Discussion

As shown in Fig. 5.12, there are six different orientations of the urea molecule with respect to the channel axis, **c**. Hence, in general, there are six different orientations of the C=O rotation axis with respect to H_0; we define δ as the angle between the C=O axis and the H_0 direction. In the absence of motion, there would thus be a total of 24 doublets: 6 orientations of the C=O axis x 4 deuterons per urea-d_4 molecule.

Fig. 5.12: Representation of the six orientations of the C=O axis with respect to **c**

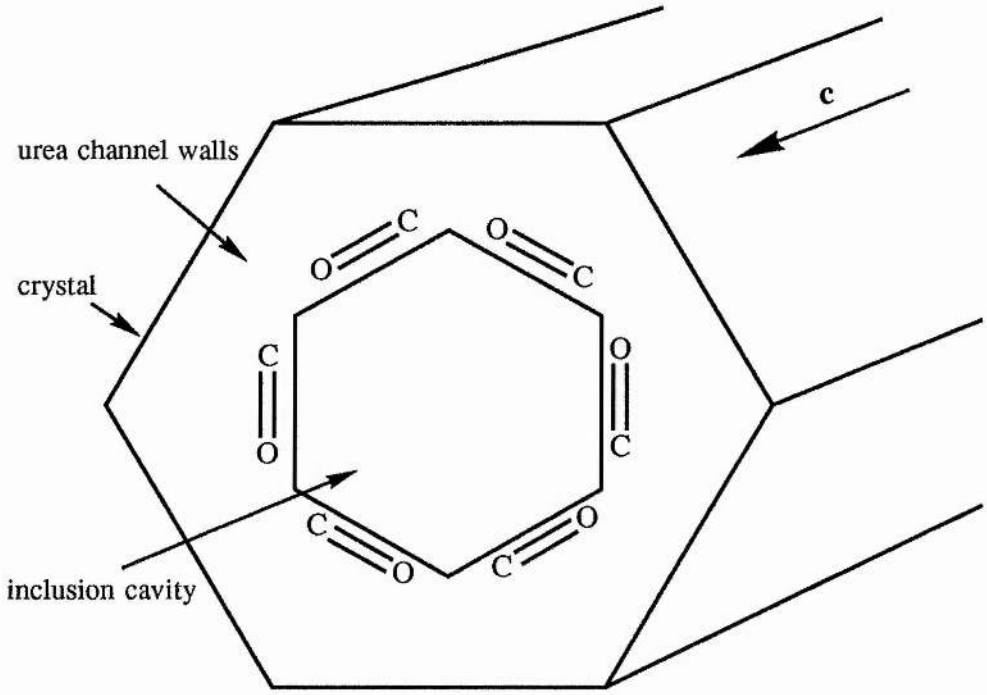

(i) Parallel to H_0

When the urea channel axis is oriented parallel to H_0, there is only one orientation of the C=O jump axes with respect to H_0 (i.e. δ=90°). Hence, in the absence of motion and for four non-equivalent deuterons, we should expect four doublets. That we see only two implies that we have only two non-equivalent deuteron environments: this is entirely consistent with 180° flips of the urea molecules about their C=O axes. Our spectrum is qualitatively and quantitatively similar to that recorded in the same crystal orientation at 303 K for *n*-nonadecane/urea-d_4 [Heaton *et al*, 1989b].

(ii) Perpendicular to H_0

In this orientation, the C=O axes make the following angles (δ) with H_0: 0, 60°, 120°, 180°, 240° and 300°. However, δ=60° ≡ δ=240° and δ=120° ≡ δ=300°, hence we expect 16 doublets, assuming no urea motion; eight doublets would accord with the proposed urea motion. Our spectrum shows a total of seven doublets: this is,

therefore, consistent with 180° flips of the urea molecules about their C=O axes (the eighth doublet is presumably too close in frequency to one of the others to be distinguishable).

Our spectrum is reasonably similar to the spectrum recorded at 303 K by Heaton *et al* [1989b] for an *n*-nonadecane/urea-d_4 crystal, oriented perpendicular to the channel axis and rotated by 2° about the **c** axis. This is consistent with the fact that we attempted to align our crystal so that two of its flat faces were as close as possible to being perpendicular to the field. (In saying this, we assume that the position of a 0° rotation about **c**, as designated by Heaton *et al* [1989b], corresponds to the flat face of the crystal being perpendicular to the field, although they do not state this explicitly.) However, although the agreement with relative intensities and relative doublet positions is generally good, Heaton *et al* [1989b] resolve only five doublets whereas we see a total of seven. This suggests that we have better resolution, reflecting the higher operating frequency at which we recorded the spectra (76.8 MHz, compared with 38.4 MHz used by Heaton *et al* [1989b]).

Due to limitations in our experimental set-up, we were not able to record single crystal spectra below 293 K, nor were we able to accurately assess the precise orientation of the crystal with respect to rotation about the channel axis. Further, our simulation program was not appropriate for simulating the spectra of single crystals. Hence this study was not developed further.

5.3 ^{2}H NMR INVESTIGATION OF GUEST MOTION

5.3.1 INTRODUCTION

Previous ^{2}H NMR studies of guest molecular motion in urea inclusion compounds have been carried out by many research groups. These include investigations of the following guest species: various fully deuterated *n*-alkanes [Cannarozzi *et al*, 1991; Vold *et al*, 1989]; *n*-nonadecane-d_{40} [Casal *et al*, 1984a; Greenfield *et al*, 1985 & 1989]; *n*-hexadecane-d_{34} [Harris, 1988; Harris & Jonsen, 1989; Harris & Thomas, 1990]; various deuterated derivatives of stearic acid [Casal *et al*, 1984b; Meirovitch & Belsky, 1984]; bromo-*n*-octane-α-d_2 [Meirovitch & Belsky, 1984]; and octanoyl peroxide-d_{30} [Harris, 1988].

These studies (some of which are discussed elsewhere in this thesis) have analysed various models for molecular motion. However, from our IQNS studies (Chapter 4), we already know that the guest molecules in the α,ω-dibromoalkane/urea inclusion compounds studied undergo uniaxial rotational diffusion on the picosecond time-scale. Our aim here is to study for 1,10-dibromodecane-d_{20}/ urea-h_4 the effect on the ^{2}H NMR spectral lineshape of change in temperature.

5.3.2 EXPERIMENTAL DETAILS

5.3.2.1 Materials

The sample of 1,10-dibromodecane-d_{20}/urea-h_4 was prepared as described in Appendix A. (Although visual inspection showed that the crystals produced were not of the highest quality, excess guest had been removed by washing with 2,2,4-trimethylpentane and any excess host that had not formed the inclusion compound was undeuterated, as was the solvent methanol. Hence any ^{2}H NMR signal resulted solely from the included guest molecules.) The sample was ground thoroughly and packed into glass NMR tubes in the manner described in §5.2.4.1, part (I).

5.3.2.2 NMR Spectra

General experimental details were as given in §5.2.4.2, and the same parameter values were used in the QSE sequence. Spectra were again recorded at temperatures: 140, 150, 160, 200, 240 and 293 K (from low to high temperature).

5.3.2.3 Simulations

We know from our IQNS studies (Chapter 4) that the dominant motion of the guest molecules is a uniaxial rotational diffusion about the channel axis. Our simulation program, designed to model jump processes, is not entirely appropriate, but development of a program to model rotational diffusion is difficult from a computational viewpoint. However, we carried out the simulation by approximating the rotational diffusion to a six-fold jump process of the CD_2 deuterons (as the difference between these motions is not readily distinguished by NMR). Details of the simulation are given in §5.3.3.2.

5.3.3 Results and Discussion

5.3.3.1 Features of the Spectra

Fig. 5.13 shows the evolution of the spectra as a function of temperature. At 140 K the spectral lineshape is that of a conventional static Pake powder pattern. Through the phase transitional range (160-150 K), the spectra comprise a single peak, which is very broad and featureless. At 200 K and 240 K the spectra progressively regain lineshape definition, and at 293 K the lineshape is again a Pake powder pattern. Note that the full-width frequency of the spectrum at 293 K (*ca.* 65 kHz) is very much narrower than that (*ca.* 130 kHz) in the static regime, at 140 K. Measured values for the quadrupole coupling constant, A*, and asymmetry parameter, η*, at 140 K and 293 K are:

A*=163 kHz and η*=0.016 at 140 K

A*=80 kHz and η*=0.065 at 293 K.

Fig. 5.13: ^2H NMR spectra for 1,10-dibromodecane-d_{20}/urea-h_4

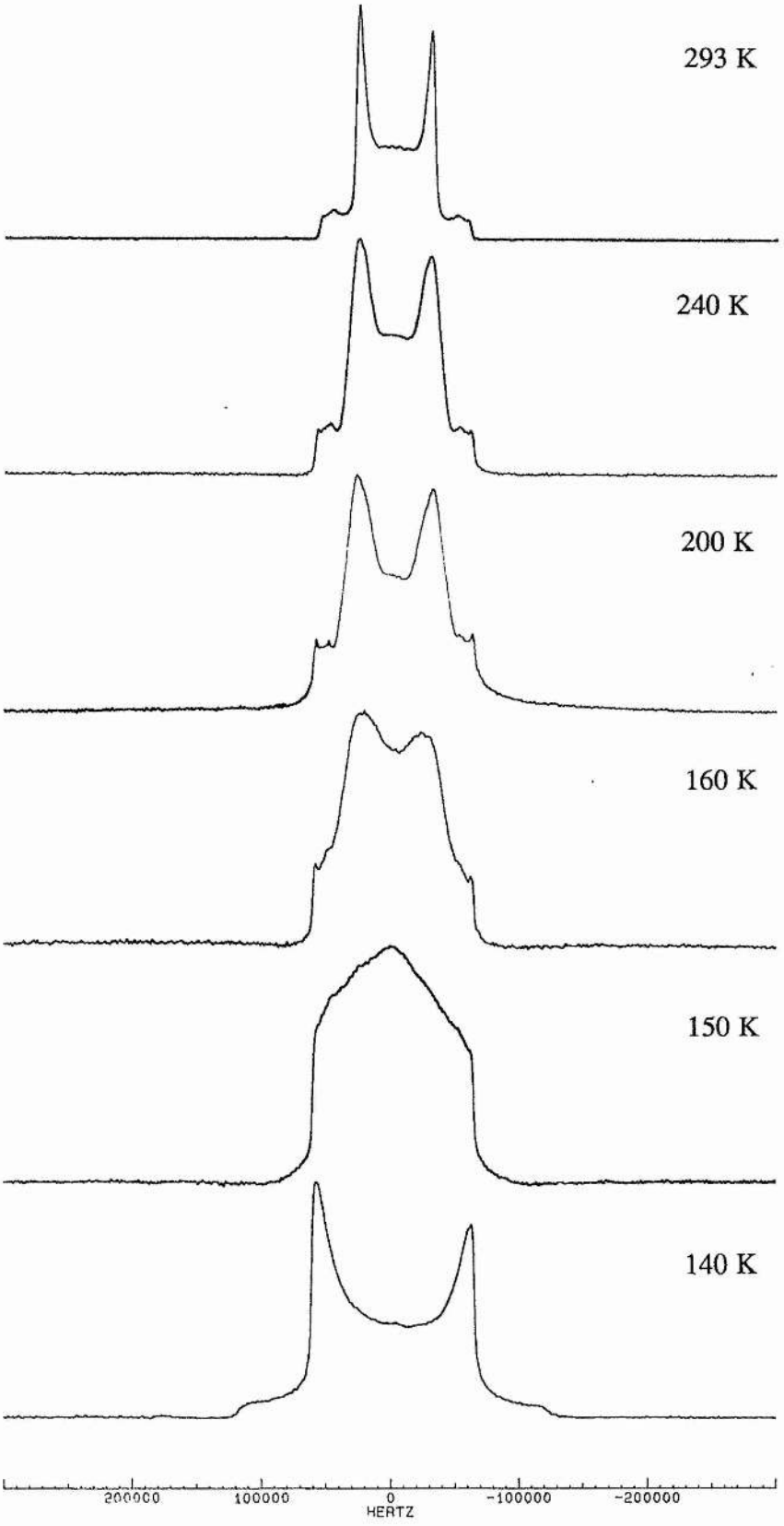

The broad and featureless character of the spectra at 150 K and 160 K indicates that the guest molecules have entered an intermediate motional regime. This suggests that the change in host structure occurring at the phase transition significantly affects the motional freedom of the guest molecules. These spectra may be contrasted with those for the deuterated host, which do not show evidence, at the phase transition, for any discontinuity in the temperature-dependence of κ (see §5.2.5.1, part (I)(ii)).

5.3.3.2 Simulations

The spectra were simulated using the program described previously (§5.2.5.1, part (II)(i)). A six-fold jump motion was modelled (see Fig. 5.14) using the Euler angles listed in Table 5.6. Other parameters were as follows:

$3A/4$=121 kHz (i.e. A=161 kHz)

η=0

$1/T_2$=2400 Hz for T≤240 K; $1/T_2$=1200 Hz for T=293 K

Relative populations of all deuteron sites = 1

$\Delta\omega$=1°.

DEUTERON	EULER ANGLES		
	α	β	γ
D_1	0_Z	$0_{Y'}$	$0_{Z''}$
D_2	0_Z	$-60°_{Y'}$	$0_{Z''}$
D_3	0_Z	$-120°_{Y'}$	$0_{Z''}$
D_4	0_Z	$180°_{Y'}$	$0_{Z''}$
D_5	0_Z	$120°_{Y'}$	$0_{Z''}$
D_6	0_Z	$60°_{Y'}$	$0_{Z''}$

Table 5.6: Euler angles for the six deuteron sites

Fig. 5.14: Six-fold jump model for the CD_2 deuterons, showing principal axis systems and molecular reference frame

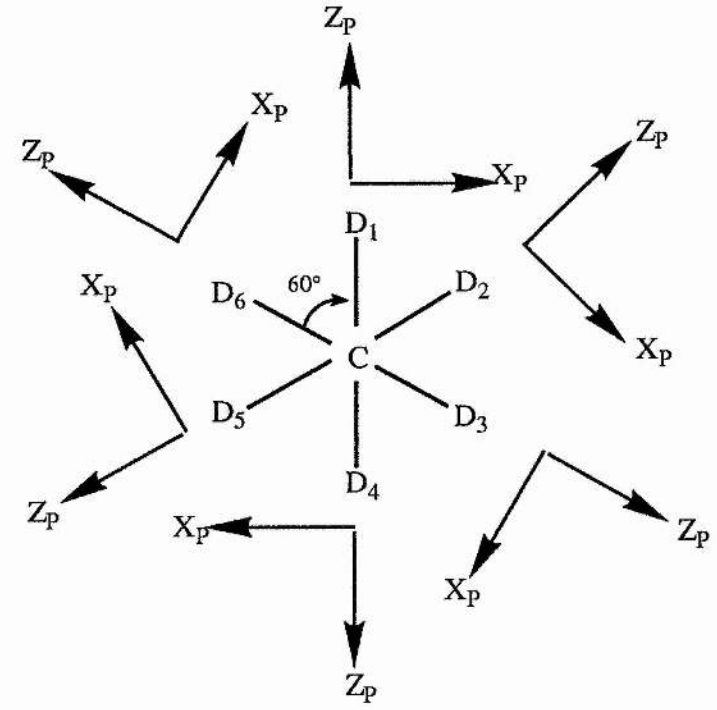

Y_P is directed into the page

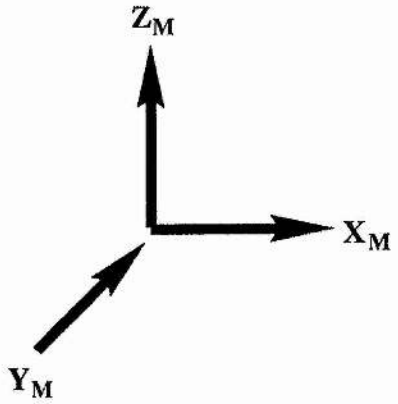

Fixed molecular reference frame

The values for κ and the corresponding temperatures are shown in Table 5.7. At 140 K, the system is in a static regime ($4\kappa/3A<10^{-1}$); between 150 K and 160 K it is in a slow-intermediate regime ($10^{0}\lesssim 4\kappa/3A\lesssim 10^{1}$); between 160 and 240 K it is in an intermediate-fast regime $10^{1}\lesssim 4\kappa/3A\lesssim 10^{3}$); and at 293 K, it has entered a fast motion regime ($4\kappa/3A>10^{3}$). Assuming Arrhenius behaviour for the temperature-dependence of κ, we can evaluate activation energies (E_a) for a single jump. Fig. 5.15 shows a plot of ln κ against $^{1}/T$, indicating an abrupt change in the value of E_a at *ca.* 160 K. This implies that the phase transition occurs at this temperature (although this value is somewhat higher than that (135-141 K) determined for this compound by differential scanning calorimetry (see Appendix B)). Calculated values for activation energy are E_a=56 (±9) kJmol^{-1} in the slow-intermediate regime and E_a=18 (±4) kJmol^{-1} in the intermediate-fast regime. The latter value is reasonably close to the range of values obtained in Chapter 4 for V_0, the potential energy barrier to uniaxial rotational diffusion of the guest molecules ($7<V_0<16$ kJmol^{-1}). However, as the two motions are different, numerical comparison of these values is not strictly valid.

T / K	κ / Hz	$4\kappa/3A$
140	2.5×10^{3}	2.1×10^{-2}
150	1.0×10^{5}	8.3×10^{-1}
160	1.0×10^{6}	8.3×10^{0}
200	1.0×10^{7}	8.3×10^{1}
240	1.0×10^{8}	8.3×10^{2}
293	1.0×10^{9}	8.3×10^{3}

Table 5.7: Values for exchange rate, κ, at the temperatures studied

Fig. 5.15: Plot of ln κ versus 1/T for the guest motion in 1,10-dibromodecane-d_{20}/urea

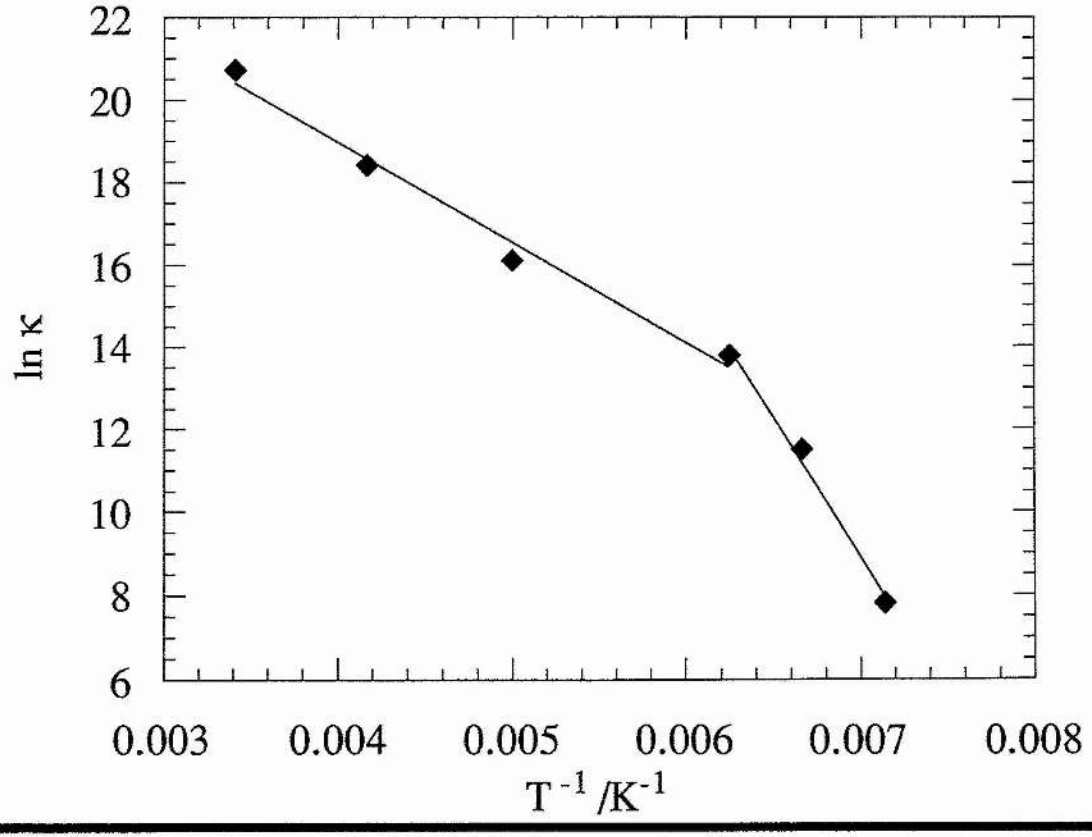

Fig. 5.16: Simulated ^2H NMR spectra for 1,10-dibromodecane-d_{20}/urea

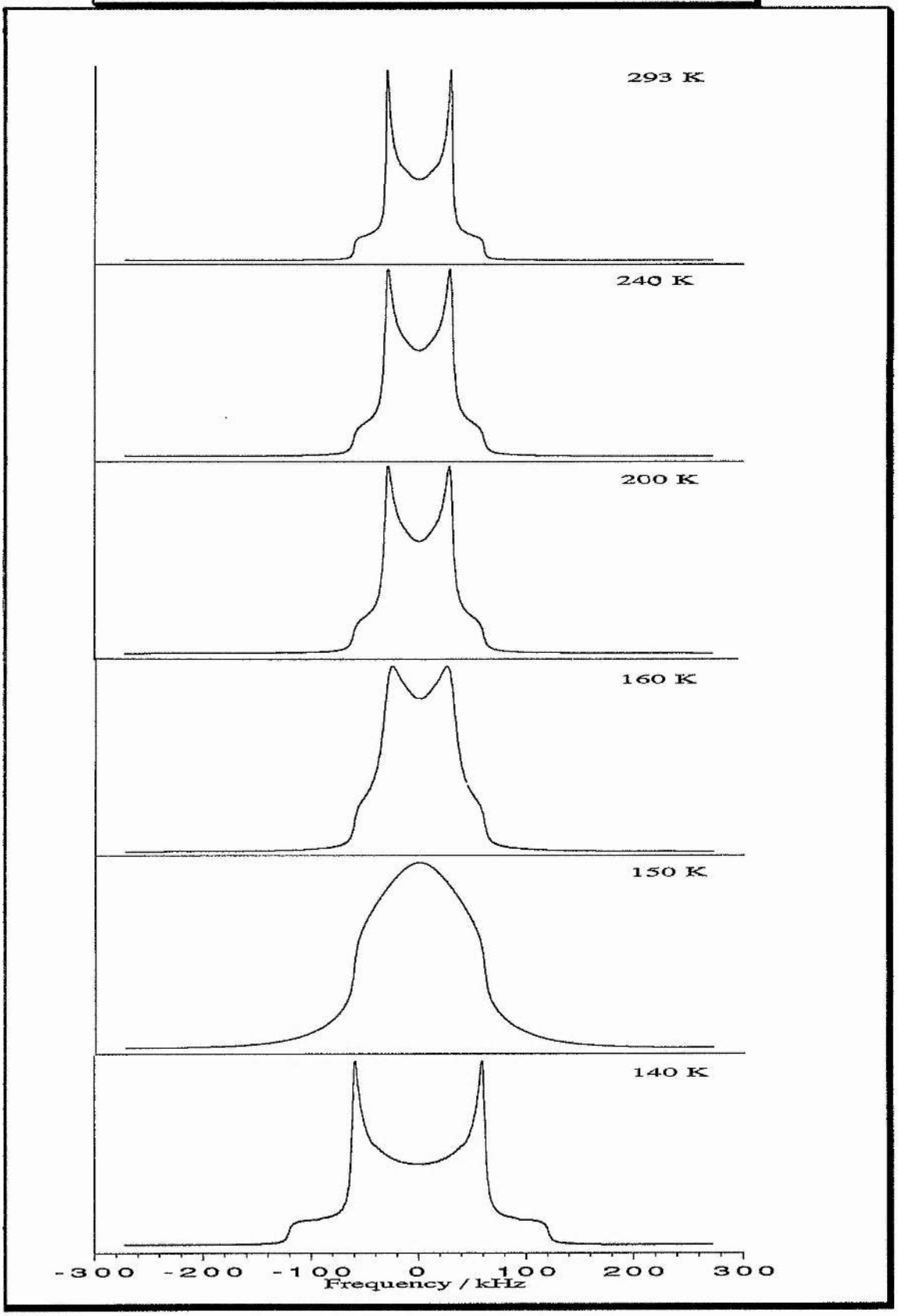

The simulated spectra (Fig. 5.16) are in reasonably good agreement with the experimental spectra (Fig. 5.13) throughout the temperature range, and indicate that the assumption of a six-fold jump is an acceptable approximation insofar as interpretation of the ^{2}H NMR lineshape is concerned.

5.3.3.3 Comparison with Previous Studies

Variable-temperature studies of polycrystalline *n*-nonadecane-d_{40}/urea-h_4 [Casal, 1984a], *n*-hexadecane-d_{34}/urea-h_4 [e.g. Harris & Jonsen, 1989] and various deuterated derivatives of stearic acid/urea-h_4 [Casal *et al*, 1984b; Meirovitch & Belsky, 1984] show evidence for phase transitions (at 160-170 K, *ca*. 147 K, and 234 K, respectively) from a high-temperature hexagonal phase to a low-temperature orthorhombic phase. In general, the ^{2}H NMR lineshapes close to the phase transition temperature are broad and featureless; our spectra are consistent with these observations.

However, our spectra show fewer distinguishable powder patterns than these and other spectra of polycrystalline fully deuterated *n*-alkane/urea-h_4 inclusion compounds [Cannarozzi *et al*, 1991]. Even when the powder pattern arising from the CD_3 groups is discounted, these literature spectra comprise many more powder patterns than our spectra. They indicate that there are various types of CD_2 groups, each type having a different relative motional freedom and each giving rise to a specific powder pattern. For example, due to torsional libration about the penultimate C-C bond in *n*-alkane guests, the powder patterns due to the 'end' CD_2 groups are distinguishable from those due to the 'bulk' CD_2 groups.

In contrast, our spectral evidence suggests that the 1,10-dibromodecane guest contains just one deuteron environment, all CD_2 groups thus undergoing the same motion, regardless of their position in the guest molecule. There is no evidence, on the ^{2}H NMR time-scale, for additional motions of the CD_2 groups near the chain ends. It is possible that the α,ω-dibromoalkanes are more restricted or 'locked-in' by virtue of

their spatial relationship $\Delta_g=c_g/3$ that exists between molecules in adjacent channels.† However, in view of the fact that we know that a measurable proportion of Br end-groups are in the *gauche* conformation (as discussed in Chapter 3), it is perhaps surprising that the motion of the CD_2 groups neighbouring such *gauche* Br's is indistinguishable from that of those neighbouring the *trans* Br's.

† In comparison, the dioctanoyl peroxide-d_{30} guest [Harris, 1988] is thought to be highly 'anchored' as a consequence of its constant offset (Δ_g=4.6 Å): variable-temperature ^2H NMR spectra of this compound show no evidence for reorientational motion on the ^2H NMR time-scale.

5.4 CONCLUSIONS

5.4.1 HOST MOTION

The ^2H NMR spectra of the four urea inclusion compounds studied, $Br(CH_2)_nBr/D_2N(CO)ND_2$ where n=7-10, were consistent with the hypothesis that the urea molecules undergo 180° flips about their C=O axes at a temperature, T, greater than 160 K and at rates observable on the ^2H NMR time-scale (10^3-10^8 s^{-1}). The activation energy for this 180° flipping motion was estimated, from simulations of the NMR spectra for 1,7-dibromoheptane/urea-d_4, to be 36.2 (±0.5) $kJmol^{-1}$. At T≤160 K, the spectra were consistent with the urea molecules being static on the ^2H NMR time-scale. There was no evidence from the spectra for an intermediate motional regime. Although change in chain length of the guest molecule did not *significantly* affect the ^2H NMR lineshapes, the room-temperature spectrum of 1,7-dibromoheptane/urea-d_4 differed from the room-temperature spectra of the other compounds in the relative intensity of the inner horns. This may reflect the fact that there is a higher proportion of Br end-groups to urea molecules in 1,7-dibromoheptane/urea-d_4: these Br end-groups may hinder the motion of adjacent urea molecules sufficiently to cause a detectable change in intensity in the ^2H NMR spectrum.

5.4.2 GUEST MOTION

The ^2H NMR spectra of $Br(CD_2)_{10}Br/H_2N(CO)NH_2$ indicate that the guest molecules have four motional regimes: a static regime at T=140 K, a slow-intermediate motional regime at 150 K≤T≤160 K, an intermediate-fast motional regime at 160 K≤T≤240 K, and a fast motional regime at T=293 K. The slow-intermediate regime is consistent with the compound passing through the phase transition. The spectra imply that all CD_2 groups are undergoing the same dynamic process, regardless of their position in the guest molecule. In Chapter 4 it was concluded that, at sufficiently high temperatures, the guest molecules undergo a uniaxial rotational diffusion about their long axes on the picosecond time-scale. Nevertheless, these ^2H NMR spectra were adequately simulated by approximating this motion to a six-fold

jump of the CD_2 deuterons. Activation energies for the two intermediate motional regimes were estimated, from these simulations, to be 56 (±9) $kJmol^{-1}$ (slow-intermediate) and 18 (±4) $kJmol^{-1}$ (intermediate-fast). This latter value is reasonably close to the range of values obtained in Chapter 4, over a comparable temperature range, for the potential energy barrier to uniaxial rotational diffusion.

5.5 REFERENCES

ABRAGAM A (1961) The Principles of Nuclear Magnetism, Oxford University Press.

AKITT JW (1983) NMR and Chemistry: An Introduction to the Fourier Transform-Multinuclear Era, 2nd Edition, Chapman and Hall.

BELL JD & RICHARDS RE (1969) Nuclear spin relaxation studies on urea+hydrocarbon clathrates, *Trans. Faraday Soc.*, **65**, 2529-2536.

CANNAROZZI GM, MERESI GH, VOLD RL & VOLD RR (1991) Conformation and stability of alkane/urea inclusion compounds: evidence from deuterium NMR spectroscopy, *J. Phys. Chem.*, **95**, 1525-1527.

CASAL HL, CAMERON DG & KELUSKY EC (1984a) A ^{2}H NMR study of molecular motions of nonadecane-d_{40} in a urea inclusion adduct, *J. Chem. Phys.*, **80**, 1407-1410.

CASAL HL, CAMERON DG, KELUSKY EC & TULLOCH AP (1984b) A spectroscopic study of the structure and dynamics of the urea inclusion adduct of stearic acid, *J. Chem. Phys.*, **81**, 4322-4327.

CHIBA T (1965) A deuteron magnetic resonance study of urea-d_4, *Bull. Chem. Soc. Japan*, **38**, 259-263.

DAS TP (1957) Tunneling through high periodic barriers: II. Application to nuclear magnetic resonance in solids, *J. Chem. Phys.*, **27**, 763-781.

DAS TP (1961) Erratum: Tunneling through high periodic barriers: II. Application to nuclear magnetic resonance in solids, *J. Chem. Phys.*, **35**, 1897-1898.

DAVIS JH, JEFFREY KR, BLOOM M, VALIC MI & HIGGS TP (1976) Quadrupolar echo deuteron magnetic resonance spectroscopy in ordered hydrocarbon chains, *Chem. Phys. Lett.*, **42**, 390-394.

EMSLEY JW & SMITH JAS (1961) Proton magnetic resonance studies of amides: Part 2. Molecular motion in urea and thiourea, *Trans. Faraday Soc.*, **57**, 1233-1247.

ERNST RR & ANDERSON WA (1966) Application of Fourier transform spectroscopy to magnetic resonance, *Rev. Sci. Instrum.*, **37**, 93-102.

FIELD LD (1989) Fundamental aspects of NMR spectroscopy. In: FIELD LD & STERNHELL S, Eds., Analytical NMR, John Wiley & Sons, pp 5-39.

FREEMAN R (1988) A Handbook of Nuclear Magnetic Resonance, Longman Scientific & Technical.

FUKUSHIMA E & ROEDER SBW (1981) Experimental Pulse NMR: A Nuts and Bolts Approach, Addison-Wesley.

FYFE CA (1983) Solid State NMR for Chemists, CFC Press, pp 73-137.

GREENFIELD MS, VOLD RL & VOLD RR (1985) Deuterium relaxation and vibrationally averaged quadrupole coupling in an alkane/urea clathrate, *J. Chem. Phys.*, **83**, 1440-1443.

GREENFIELD MS, VOLD RL & VOLD RR (1989) Deuterium spin relaxation and guest motion in the *n*-nonadecane/urea clathrate, *Mol. Phys.*, **66**, 269-298.

HARRIS RK (1983) Nuclear Magnetic Resonance Spectroscopy: A Physicochemical View, Pitman.

HARRIS KDM (1988) Studies of urea inclusion compounds and other solids, PhD Thesis, University of Cambridge.

HARRIS KDM & JONSEN P (1989) ^{2}H NMR investigation of the dynamic behaviour of *n*-hexadecane in its urea inclusion compound, *Chem. Phys. Lett.*, **154**, 593-598.

HARRIS KDM & THOMAS JM (1990) Probing the properties of urea inclusion compounds, *Mol. Cryst. Liq. Cryst.*, **180**, 177-184.

HEATON NJ, VOLD RL & VOLD RR (1989a) Deuterium quadrupole echo study of urea motion in urea/*n*-alkane inclusion compounds, *J. Am. Chem. Soc.*, **111**, 3211-3217.

HEATON NJ, VOLD RL & VOLD RR (1989b) Single-crystal deuterium NMR study of urea-d_4/*n*-nonadecane, *J. Magn. Reson.*, **84**, 333-343.

JELINSKI LW (1984) Modern NMR spectroscopy. New techniques and instruments help elucidate structures and dynamics in polymer studies and biochemistry, *Chem. Eng. News*, **62**(45), 26-47.

JELINSKI LW (1986) Deuterium NMR of solid polymers. In: KOMOROSKI RA, Ed., High-Resolution NMR Spectroscopy of Synthetic Polymers in Bulk, VCH Publishers, pp 335-364.

KEMP W (1986) NMR in Chemistry: A Multinuclear Introduction, Macmillan.

MANTSCH HH, SAITO H & SMITH ICP (1977) Deuterium magnetic resonance: applications in chemistry, physics and biology, *Prog. NMR Spectrosc.*, **11**, 211-272.

MEIER P, KOTHE G, JONSEN P, TRECOSKE M & PINES A (1987) Theory of line shapes for zero-field NMR in the presence of molecular motion, *J. Chem. Phys.*, **87**, 6867-6876.

MEIROVITCH E & BELSKY I (1984) Hydrogen-2 nuclear magnetic resonance observations on conformation and dynamics of alkyl chains trapped within solid urea inclusion compounds, *J. Phys. Chem.*, **88**, 6407-6411.

RIDDELL FG (1991) Advanced NMR, Postgraduate Lecture Course, University of St Andrews.

ROSE ME (1957) Elementary Theory of Angular Momentum, John Wiley & Sons, pp 48-75.

VOLD RL, VOLD RR & HEATON NJ (1989) Deuterium nuclear magnetic resonance and molecular dynamics in alkane/urea inclusion compounds, *Adv. Magn. Reson.*, **13**, 17-42.

ZUSSMAN A (1973) Effect of molecular reorientation in urea on the ^{14}N PNQR linewidth and relaxation time, *J. Chem. Phys.*, **58**, 1514-1522.

CHAPTER 6
SUMMARY AND GENERAL CONCLUSIONS

The complementary techniques of single crystal XRD, polarised Raman spectroscopy, IQNS and ^2H NMR spectroscopy have allowed us to study the structural and dynamic properties of some urea inclusion compounds. The main focus of this work has been $Br(CH_2)_nBr$/urea where n=7-10. Properties of both the host and guest species were investigated. A study of $Br(CH_2)_6Br$/urea was also carried out: this compound was found to have a totally different structure from the other compounds studied and is discussed in §6.3.

6.1 SUMMARY OF RESULTS FOR 'CONVENTIONAL' UICs

6.1.1 HOST PROPERTIES

Results from photographic single crystal XRD, at room temperature, were consistent with the known hexagonal structure of the urea host. Raman spectroscopic studies indicated (in agreement with previous work) that although the structure becomes orthorhombic in the low-temperature phase, the difference between these two structures is small. These Raman spectra showed evidence for lattice modes corresponding to a 'breathing' of the urea channel perpendicular to the **c** direction and a 'stretching' of the urea channel along the **c** direction. ^2H NMR studies were consistent with a 180° flipping motion of the urea molecules about their C=O axes (at sufficiently high temperature): this occurs on the microsecond time-scale at room temperature. From spectral simulations, the activation energy for this motion was evaluated to be 36.2 (±0.5) $kJmol^{-1}$ for 1,7-dibromoheptane/urea. The length of the guest molecule does not appear to have a significant effect on the properties of the host, with the possible exception that the $Br(CH_2)_7Br$ guest may have a greater hindering effect on the motion of the urea molecules than the other guests studied. IQNS spectra of *n*-hexadecane-d_{34}/urea were consistent with the proposed time-scale for these motions: there was no evidence for urea motion on the IQNS instrumental time-scale (10^{-10}-10^{-13} s).

6.1.2 GUEST PROPERTIES

6.1.2.1 α,ω-Dibromoalkane Guests (n=7-10)

The $Br(CH_2)_nBr$ guests, with n=7-10, were studied from the point of view of their structural, conformational and dynamic properties. There does not appear to be a significant change in guest properties with change in guest molecular length. Photographic single crystal XRD studies showed that, within each single crystal, there are *both* regions in which the guest molecules are one-dimensionally ordered (along the channel axis) *and* regions in which they are three-dimensionally ordered. In the latter regions, the guest molecules have a well-defined offset $\Delta_g=c_g/3$: this represents a new mode of interchannel guest ordering in urea inclusion compounds. There are two domains of the basic guest structure in these three-dimensionally ordered regions. The lattices defining the periodicities of these two domains differ by 180° rotation about the channel axis and have rhombohedral metric symmetry; the crystal symmetry of each domain is also rhombohedral.

Raman spectroscopic studies showed evidence for a LAM-1 mode, indicating that the conformation of the 'bulk' guest molecules is the linear, *trans*, extended form. However, there was evidence for '*gauche* defects' of the Br end-groups, as shown by the existence of the ν(C-Br) *gauche* band in the Raman spectra. Nevertheless, the percentage of these *gauche* defects was estimated to be relatively low, in the range *ca.* 4-15%. This percentage increases markedly with applied pressure but shows only a weak temperature-dependence.

IQNS studies showed evidence for extensive guest molecular motion at sufficiently high temperature: translations of the molecules *along* the channel axis (plus an oscillatory component which is overdamped at high temperature) and rotations of the molecules *about* the channel axis. These two motions both occur on the picosecond time-scale, and although they were modelled independently of one another, a screw-type motion is plausible. The translational motion was modelled as continuous linear diffusion between two impermeable boundaries and the rotational motion as uniaxial rotational diffusion in a one-fold cosine potential. The activation energy for the

translational motion was evaluated (on the assumption of Arrhenius behaviour) to be E_a=6 (±1) kJmol^{-1} and the effective potential barrier to rotations (which was correlated to temperature) was found to be *ca.* 7<V_0<16 kJmol^{-1} over the temperature range 280-160 K.

Simulations of ^{2}H NMR spectra for guest molecular motion were achieved using a 6-fold jump model; however, this motion is indistinguishable from rotational diffusion on the ^{2}H NMR time-scale (10^{-3}-10^{-8} s). This ^{2}H NMR study implied that all CH_2 groups in the guest molecule are undergoing the same motion, regardless of their position in the molecule. The significant change in guest motional freedom at the phase transition is reflected by values of activation energy for a single jump: 18 (±4) kJmol^{-1} just above and 56 (±9) kJmol^{-1} just below the phase transition temperature, for 1,10-dibromodecane/urea. (Phase transition temperatures for these compounds are in the range *ca.* 135-166 K as measured by DSC).

6.1.2.2 Other Guest Molecules

Other guest species were studied briefly. Photographic single crystal XRD indicated that whereas the I$(CH_2)_{10}$I guest exhibits the same mode of interchannel guest ordering as the Br$(CH_2)_n$Br guests, *viz* $\Delta_g=c_g/3$, the Cl$(CH_2)_{10}$Cl guest did not show any evidence for three-dimensional ordering. These XRD studies indicated that the Br$(CH_2)_n$Br guests with n=11-12 also lack three-dimensional ordering, as do the Br$(CH_2)_nCH_3$ guests with n=9-12 (although factors controlling packing of such asymmetric guest molecules are more complex).

Raman spectroscopic studies on I$(CH_2)_8$I and Cl$(CH_2)_8$Cl guests at room temperature indicated that the percentage of *gauche* defects decreases with the size of the terminal substituent: the spectra indicated *ca.* 51% for the Cl$(CH_2)_8$Cl guest and *ca.* 1% for the I$(CH_2)_8$I guest (compared with *ca.* 7% for the Br$(CH_2)_8$Br guest, measured under the same conditions).

6.2 DISCUSSION

This discussion concentrates on the results of the studies on the α,ω-dibromoalkane/urea inclusion compounds (studies of other guest molecules were not extensive enough to allow detailed discussion). The motion of the urea molecules about their C=O axes is rather surprising in view of the tight fit of the guest molecules in the channels, and invites the question of whether the motion of the urea molecules affects, or is affected by, the structure and dynamics of the guest molecules. For the $Br(CH_2)_7Br$ guest, it is possible that the higher relative proportion of Br in the channels may allow two Br end-groups in different channels to be adjacent to the same urea molecule, thus hindering its motion.

The mode of interchannel ordering of the guest molecules contrasts with those found for other families of urea inclusion compounds: *n*-alkane and most acid anhydride guests display Δ_g=0, whereas diacyl peroxides have Δ_g=4.6 Å. The factors dictating the mode of interchannel ordering have not been satisfactorily established. Nevertheless, in view of this difference in guest structures, it is surprising that the conformation and dynamics of the α,ω-dibromoalkane guests appear to be qualitatively similar to those of the *n*-alkane guests.

The urea and guest motions are probably uncorrelated: at room temperature, the former occur on the microsecond, and the latter on the picosecond, time-scale. There is no evidence for different types of motion in the one-dimensional and three-dimensional regions of guest ordering (although the relative proportions of guest molecules in each of these regions are not known). Regardless of region, the dense packing of the guest molecules along the channel implies that the translational motions of neighbouring guest molecules within a given channel are highly correlated. It is not known whether *gauche* defects are 'frozen in' at the crystal-growing stage, or whether there is a subsequent *trans*↔*gauche* interconversion. The translation of a guest molecule towards its neighbour in the same channel may be associated with the production of a *gauche* end-group: this would require the translation and the interconversion of the *trans*↔*gauche* end-groups to occur on the same time-scale. The repulsive intrachannel interaction

suggests that the reorientational motions of neighbouring guest molecules in the same channel should also be highly correlated. The fact that the offset Δ_g is well-defined, as probed by XRD, indicates that independent motions of greater than *ca.* 2 Å translational length cannot be occurring: this suggests that the motion of guest molecules in *adjacent* channels is correlated. The reorientational motion of guest molecules in adjacent channels may also be correlated, although this cannot be assessed from the available evidence. Finally, in view of the fact that the urea molecules making up the channel wall are arranged in a spiral, it is plausible that the guest rotations and translations are coupled in a screw-type motion: if associated with the host spiral, the form of coupling may be independent of the identity of the guest molecules for any 'conventional' urea inclusion compound, as the urea structure is invariant.

6.3 1,6-DIBROMOHEXANE/UREA

6.3.1 STRUCTURE AND CONFORMATION

This compound has a totally different structure from the 'conventional' urea inclusion compounds. The host structure was found to be monoclinic at room temperature. The host and guest structures are commensurate and the guest molecules have exclusively *gauche* end-groups, yet they still show a LAM-1 mode in the low-frequency Raman spectra at both room temperature and low temperature (90 K). The Raman spectra also suggest that the structure undergoes a phase transition at a temperature between 298 K and 90 K.

6.3.2 DISCUSSION

The reason for this uncharacteristic structure is unclear: it is possible that the relatively short length of the guest molecule is insufficient to stabilise the formation of a 'conventional' hexagonal urea host structure. The fact that the structure is commensurate suggests that some energetically favourable 'locking-in' occurs during its formation. Further studies are required to elucidate the nature of the low-temperature phase transition and to investigate the dynamics (if any) of the guest molecules.

APPENDIX A
PREPARATION OF UREA INCLUSION COMPOUNDS

A.1 SYNTHESIS

The general method of preparation for the urea inclusion compounds discussed in this thesis was as follows. All materials were standard laboratory reagent grade, unless otherwise stated, and were used as received from Aldrich or Lancaster. The guest species used were:

α,ω-dibromoalkanes:	$Br(CH_2)_nBr$	n=6-12
α,ω-diiodoalkanes:	$I(CH_2)_nI$	n=8&10
α,ω-dichloroalkanes:	$Cl(CH_2)_nCl$	n=8&10
1–bromoalkanes:	$Br(CH_2)_nCH_3$	n=9-12

A.1.1 GENERAL METHOD OF PREPARATION

An excess amount of the guest species (excess with respect to the expected molar guest/host ratio in the inclusion compound) was added to a saturated solution of urea in methanol in a conical flask at *ca.* 48°C. Extra solvent was then added, as required, to dissolve completely the guest and/or any crystals of inclusion compound which sometimes precipitated immediately upon adding the guest. The conical flask was then stoppered, immersed in a Dewar flask containing water at *ca.* 48°C, and left to cool to room temperature to allow crystallisation to occur. If necessary, the Dewar containing the conical flask in water was then placed in a refrigerator overnight at 5°C to allow further crystallisation. After the crystals had been collected by filtration, they were washed sparingly with 2,2,4-trimethylpentane* to remove any non-included (e.g. surface-adsorbed) guest species. (Non-included host urea, being very soluble in methanol, should have remained in solution.)

* Schlenk [1949] showed that 2,2,4-trimethylpentane does not form an inclusion compound with urea (its molecular diameter is too large to allow it to fit inside the urea channel).

A.1.2 MODIFICATIONS

(i) For 1,11-dibromoundecane and 1,12-dibromododecane guests, which are only sparingly soluble in methanol, the solvent used was ethanol.

(ii) The α,ω-diiodoalkane/urea inclusion compounds were prepared in the dark to prevent oxidation of the guests to iodine (the conical flasks were, therefore, covered in foil throughout the preparation).

(iii) The preparation of deuterated compounds for neutron scattering and ^2H NMR studies (α,ω-dibromoalkane/urea-d_4 compounds: n=7-10) required use of deuterated urea, $D_2N.CO.ND_2$, as supplied by Aldrich (≥99% purity), and deuterated methanol, CH_3OD (Aldrich: ≥99.5% purity). The sample preparation was conducted under a nitrogen hood, in order to minimise exchange of ^2H and ^1H.

(iv) $Br(CD_2)_{10}Br$/urea-h_4 was prepared for ^2H NMR studies. The general method of preparation was followed and no special precautions were necessary.

A.2 CHARACTERISATION OF PRODUCTS

With the exception of 1,6-dibromohexane/urea, all UIC crystals obtained were long, white hexagonal needles (unlike the crystal morphology of 'pure' urea). As expected, these crystals extinguished under cross-polars of the polarising microscope. The structural integrity of these inclusion compounds was verified by powder x-ray diffraction and their chemical composition was confirmed by solution state ^1H NMR spectroscopy (with d_6-dimethylsulphoxide as solvent). All compounds showed the expected hexagonal urea host structure (with the exception of 1,6-dibromohexane/urea) and, in all cases, the amount of solvent included within the urea channels was found to be negligible (as assessed from the ^1H NMR spectra).

A.3 REFERENCE

SCHLENK W (1949) Die Harnstoff-Addition der aliphatischen Verbindungen, *Liebigs Ann. Chem.*, **565**, 204-240.

APPENDIX B
PHASE TRANSITION TEMPERATURES

B.1 DSC RESULTS

Differential scanning calorimetry (DSC) was used in an attempt to determine the phase transition temperatures of the $Br(CH_2)_nBr$/urea-h_4 inclusion compounds, for n=7-11. The calorimeter used was a Perkin-Elmer 7 Series Thermal Analysis System; this was calibrated prior to use with a cyclohexane standard. Values for the phase transition temperatures are quoted in the table below. However, in some cases, the onset of the phase transition could not be determined precisely, because the DSC spectra showed a wide band rather than a sharp peak. The reason for this is unclear. In these cases, marked * in the table below, a temperature range is quoted.

COMPOUND	PHASE TRANSITION TEMPERATURE / K
$Br(CH_2)_7Br$/urea-h_4	166-153 *
$Br(CH_2)_8Br$/urea-h_4	156.5 (±0.5 K)
$Br(CH_2)_9Br$/urea-h_4	148-141 *
$Br(CH_2)_{10}Br$/urea-h_4	141-135 *
$Br(CH_2)_{11}Br$/urea-h_4	165.5 (±0.5 K)

B.2 COMMENT

One would expect, in keeping with the work of Parsonage & Pemberton [1967] on *n*-alkane/urea inclusion compounds, that the phase transition temperature would increase with the length of the guest molecule. This is indeed the case for the two relatively reliable values above (those for n=8 and n=11). The remaining values should be treated with extreme caution.

B.3 REFERENCE

PARSONAGE NG & PEMBERTON RC (1967) Thermal anomalies in the adducts of urea with *n*-paraffins: a theoretical treatment, *Trans. Faraday Soc.*, **63**, 311-328.